



HAL
open science

Conditioning and enhanced sampling schemes for simulating thermodynamic and kinetic properties of condensed matter

Manuel Athènes

► **To cite this version:**

Manuel Athènes. Conditioning and enhanced sampling schemes for simulating thermodynamic and kinetic properties of condensed matter. Materials Science [cond-mat.mtrl-sci]. Université Paris Saclay; Université paris sud, 2018. tel-01851686

HAL Id: tel-01851686

<https://cea.hal.science/tel-01851686v1>

Submitted on 30 Jul 2018

HAL is a multi-disciplinary open access archive for the deposit and dissemination of scientific research documents, whether they are published or not. The documents may come from teaching and research institutions in France or abroad, or from public or private research centers.

L'archive ouverte pluridisciplinaire **HAL**, est destinée au dépôt et à la diffusion de documents scientifiques de niveau recherche, publiés ou non, émanant des établissements d'enseignement et de recherche français ou étrangers, des laboratoires publics ou privés.



Conditioning and enhanced sampling schemes for simulating thermodynamic and kinetic properties of condensed matter

Manuel Athènes

CEA Saclay, Service de Recherches de Métallurgie Physique
Université Paris Saclay

Scientific report

Habilitation à diriger des recherches, Université Paris Sud

January 31, 2018

Abstract

The Monte Carlo method is a stochastic simulation approach essentially used to estimate multi-dimensional integrals. This is traditionally achieved by generating a sample of points, i.e. a Markov chain of states, configurations, states, trajectories or even more abstract and structured objects, and then implementing an estimator. In this context, conditioning is a trick consisting of doing part of the job in closed form or through numerical quadrature so as to reduce the statistical variance associated with the estimator. This variance reduction technique has found limited applications in molecular simulation so far. In this thesis, several enhanced sampling and conditioning schemes are presented in order to improve the algorithmic efficiency of Monte Carlo and molecular dynamics simulations of condensed-matter systems. We specifically show how to sample multi-particle systems more ergodically, to estimate ensemble averages of physical quantities more accurately and to solve a first passage problem that is associated with the discrete master equation governing the evolution of lattice-based models for alloys and glasses. Illustrative applications are chosen in the field of materials science: structural transitions in clusters, calculations of solubility limits in alloys and of the migration barrier associated with a point defect.

Acknowledgements

This scientific report has been prepared to fulfill a requirement of Université Paris Sud for obtaining the grade of *habilitation à diriger des recherches*. I am much indebted to Sophie Guéron for supervising the entire habilitation process and for advising me on the formation of the jury in particular. I thank Fabienne Berthier and Daan Frenkel for their involvement during the reviewing procedure, Daniel Borgis, Florent Calvo, Jérôme Creuze and Benjamin Jourdain for their interventions during the oral examination and finally Nicolas Combe and Normand Mousseau for their participation to both the reviewing and oral examination.

As for the scientific content presented in the document, I would like to thank my coauthors, Gilles Adjanor, Vasily Bulatov, Lingling Cao, Florent Calvo, Tony Lelièvre, Mihai-Cosmin Marinica, Gabriel Stoltz and Pierre Terrier with whom I collaborated over the years and interacted on multidisciplinary domains such as materials science, algorithmics, statistical mechanics and probability theory. Besides, the trajectory followed by my research activities was noticeably influenced by Daan Frenkel from whom I discovered the waste-recycling Monte Carlo algorithm and Benjamin Jourdain who draw my attention on the conditioning techniques employed in probability theory.

Outline

Molecular simulation

An important task of molecular simulation is to compute the thermodynamic and transport properties of multi-particle model systems. The former properties are often equilibrium quantities such as energy, specific heat, pressure/volume, while the latter ones encompass rate constants and first-passage statistics associated with the thermally activated events that are responsible for defect migration, atomic transport and microstructure evolution.

Equilibrium simulations are always performed in a well-defined thermodynamic ensemble characterized by a set A of values of some external parameters λ and by a phase space \mathcal{X} , the set of the states x accessible to the system. A state x corresponds to the particle momenta and particle coordinates (positions). The external parameters may be intensive quantities such as *temperature*, *pressure* and the *chemical potentials* of the species present in the system. These external parameters couple linearly to some extensive conjugate quantities which are *energy*, *volume* and *the numbers of particles of the involved species*, respectively, for the three aforementioned examples. The external parameter usually corresponds to a thermodynamic force restraining the particle system and imposing the mean value of the conjugate quantity. Fluctuations around the average account for exchanges of energy, volume or particles with a virtual reservoir.

The external parameter can also be an extensive quantity, such as volume in periodic systems or the number of particles of any species, or may alternatively be used to artificially restrain or confine the positions of the system in a particular region of the position space. This is usually achieved by mechanically constraining the value of some collective variable ξ , a function taking input values in the position space and whose output is a real or integer number or a low-dimensional vector. At variance with external parameters, the collective variable (CV) corresponds to internal degrees of freedom and is often called reaction coordinate (RC) or order parameter depending on whether it is used to describe a reaction pathway in particular or to merely discriminate molecular or crystal structures. Harmonic forces acting on the CV are often used to mechanically restrain the system in a portion of the phase space via the external parameter. In practice, a restraining harmonic potential is included in the mechanical energy of the particle system (the Hamiltonian). In this situation, the coupling between the external parameter and the system contains quadratic terms in λ and the collective variable.

Motivations and objectives

In this habilitation thesis, one will be particularly interested in characterizing the conditions of phase transition or coexistence and in measuring the activation barrier associated with thermally activated events. These two practical tasks of molecular simulations reflect the aforementioned linear or quadratic coupling of external parameters to molecular or atomic systems, and requires estimating thermodynamic quantities with varying the values of the external parameters in some (hopefully narrow) intervals A . Unless otherwise specified, the external parameter will be considered to be a one-dimensional additional coordinate included in the Hamiltonian $\mathcal{H}(\lambda, x)$. After reviewing the commonly used Monte Carlo techniques and their applications in **Chapter 1**, a systematic way of improvement based on conditioning technique is developed throughout this thesis. Conditioning¹ is a variance reduction technique that stems from an elementary property of probability theory, namely the law of total cumulance [1]. It was introduced relatively recently in the field of molecular simulation with the waste-recycling Monte Carlo method [2] wherein conditioning is done on the proposals. The sampling techniques to be addressed are listed below.

¹ *Conditioning* relates to the *Rao-Blackwellization* procedure in mathematical statistics.

Enhanced sampling and λ -conditioning Considering the extended Hamiltonian framework in which λ is an additional coordinate, the canonical thermodynamic ensemble average of any physical observable $\mathcal{O}(\lambda, x)$ corresponds to a conditional expectation given λ which will be similarly written as $\mathbb{E}[\mathcal{O}(\lambda, \cdot)|\lambda]$. When one is interested in thermodynamic averages with the external parameter in the range Λ , the experience tells us that making the external parameter an additional simulation parameter, denoted by ζ , is often advantageous, in the sense that enhanced sampling is achieved. In this framework, the conditional expectation is traditionally evaluated based on the expectation ratio $\mathbb{E}[\mathcal{O}(\lambda, \cdot)|\lambda] = \mathbb{E}[\mathbf{1}_\lambda \mathcal{O}(\lambda, \cdot)] / \mathbb{E}[\mathbf{1}_\lambda]$, where $\mathbf{1}_\lambda(\zeta)$ is the indicator function taking output value 1 if input value ζ is λ , and output value 0 otherwise. In practice, we will show that the conditional expectation is always more efficiently evaluated based on the following identity

$$\mathbb{E}[\mathcal{O}(\lambda, \cdot)|\lambda] = \frac{\mathbb{E}[\mathbb{E}[\mathbf{1}_\lambda|x] \mathcal{O}(\lambda, x)]}{\mathbb{E}[\mathbb{E}[\mathbf{1}_\lambda|x]]}, \quad (1)$$

obtained by resorting to the law of total probability twice, in the numerator and denominator. The outer expectation is estimated from a Monte Carlo sample owing to the ergodic theorem, while the inner conditional expectation will be evaluated by integrating the integrand $\mathbf{1}_\lambda(\zeta)$ with external parameter $\zeta \in \Lambda$ through numerical quadrature for each sampled state. This procedure is precisely the one referred to as *conditioning* in probability theory [3]. Conditioning should always be implemented whenever its cost is modest and the overall computational efficiency is improved. We show that this is the case in most situations involving equilibrium Monte Carlo simulations. In supplement to conditioning, simulations will be performed more efficiently if an auxiliary potential $\alpha(\lambda)$ is added to the system so as to increase the marginal probability $p^\Lambda(\lambda) = \mathbb{E}[\mathbf{1}_\lambda]$ in the denominator of Eq. (1). In practice, a uniform sampling along the external parameter is looked for, which can be achieved by setting the auxiliary biasing potential equal to the free energy, which corresponds to the co-logarithm of the marginal probability of λ . Various ways of calculating the free energy and adapting the auxiliary potential are discussed in **Chapter 2** and **Chapter 3**, respectively.

Nonequilibrium path sampling and conditioning Conditioning can also be used to retrieve equilibrium information contained in a sample of nonequilibrium dynamics, which allows recovering any equilibrium thermodynamic average. Path-sampling may be used as a last resort when sampling with an auxiliary biasing potential fails to achieve numerical ergodicity. The path-sampling approach will be discussed in **Chapter 4**. It will lead us to define the concept of path ensemble and path average. A traditional prescription is that any trajectory is a sequence of states $z = \{\lambda_\ell, x_\ell\}_{0 \leq \ell \leq L}$ initiated from an equilibrium distribution of states and propagated out of equilibrium through the action of some external forces. This way of proceeding enables one to (i) assign a weight to nonequilibrium states based on the weight of the initial equilibrium state and the probability to generate the subsequent trajectory, (ii) explore regions that would be otherwise rarely explored without external forcing. The second feature is usually achieved through pulling upon an external parameter that itself couples to the particle system via a reaction coordinate or order parameter. To enable conditioning in path ensembles, the path expectation, denoted by $\mathbb{E}^Z[\mathcal{O}]$, is defined as the expectation of $\mathcal{O}(\lambda_\ell, x_\ell)$ where x_ℓ refers to the equilibrium state included in the considered path. The standard state expectation $\mathbb{E}[\mathcal{O}]$ coinciding with the path expectation $\mathbb{E}^Z[\mathcal{O}]$, the law of total expectation on the path distribution yields the following relation

$$\mathbb{E}[\mathcal{O}] = \mathbb{E}^Z[\mathbb{E}^Z[\mathcal{O}|z]].$$

Conditioning therefore consists of evaluating the inner conditional expectation analytically for each sampled path. This task amounts to assigning equilibrium weighting factors to the nonequilibrium states included in the path based on Crook's nonequilibrium ratio [4, 5]. The outer expectation is eventually estimated from a path sample owing to the ergodic theorem. A conditional expectation given the value λ of the external parameter can also be constructed based on a generalized conditioning scheme. This approach is discussed in **Chapter 4**.

Transition path sampling and conditioning An important field of application of molecular simulation is the calculation of transport properties. Atomic transport is usually mediated by the migration of point defects. For instance, atomic diffusion in α -Fe proceeds through the exchange of vacancies with their neighboring atoms. The difficulty is that it takes a substantial amount of computer time to observe a single jump of an atom into a vacancy. In other words, vacancy migration is a rare event at the computer time scale. To alleviate the ubiquitous problem of rare events in molecular simulation, one may implement the transition path sampling technique (TPS). TPS consists of preferentially sampling the rare events (the transition paths) owing to the

introduction of a biasing path functional [6, 7]. In TPS, the rate of rare events is then evaluated from the time derivative of state-to-state correlation functions. By introducing an external parameter λ that couples to the biasing path functional, conditioning can be used in TPS method at two levels [8]; first when estimating the conditional expectation given that the simulation bias is switched off ($\lambda = 0$), and second to evaluate state-to-state correlation functions along trial trajectories (waste-recycling point of view). The example is illustrated with the migration of a single vacancy in α -iron. As shown in **Chapter 4**, this conditioning results in dramatic variance reduction and enables us to compute the time correlation function in a single simulation, a task that could only be achieved through stage simulations so far.

Waste recycling Monte Carlo and further conditioning The conditioning approach that is implemented in the various path sampling schemes can be seen as a particular example of waste-recycling Monte Carlo (WRMC). Briefly, in WRMC technique, the information about the trial states that have been generated but rejected by the Metropolis test is included in the ensemble average. The weight of the trial state may be seen as the outcome of a conditioning scheme. The connection is discussed at the end of **Chapter 4**. The focus of **Chapter 5** will be on the control variate formulation introduced by Delmas and Jourdain [9] and on the estimation of the optimal control variate through conditioning. The obtained optimal waste-recycling estimator is implemented in calculations of Cr solubility limits in α -iron. A comparison to alternative approaches is eventually made [10].

Kinetic path sampling and deconditioning Another field of application of conditioning is kinetic Monte Carlo (KMC). Statistically equivalent to the (most often unknown) solution of the underlying master equation, KMC calculations find a growing number of applications in natural and engineering sciences. However still wider applicability of KMC simulations is severely limited by the notorious kinetic trapping where the stochastic trajectory repeatedly visits a subset of states, a trapping basin, connected to each other by high-rate transitions while transitions out of the trapping basin are infrequent and take a great many of KMC steps to observe. In **Chapter 6** we present the kinetic path sampling (kPS) method for alleviating the trapping issue. Unlike the transition path sampling method that focuses on short portions of the full kinetic path directly leading to the escapes, the kPS method does not assume any quasi-equilibrium distribution of the initial states and is statistically equivalent to the master equation. The new algorithm constructs an entire stochastic trajectory within the trapping basin, including the typically large numbers of repeated visits to each trapping state. It entails (i) iterative factorization of paths inside a trapping basin, which formally amounts to conditioning, (ii) sampling a single exit state within the basin's perimeter, and (iii) generating a first-passage path and an exit time to the selected perimeter state through an exact randomization procedure which formally amounts to a deconditioning procedure. We demonstrate the accuracy and efficiency of the KPS algorithm on two models: (1) diffusion on a random energy landscape specifically designed to yield a wide and continuous spectrum of time scales and (2) kinetics of phase separation in supersaturated solid solutions of copper in iron. We will show that the proposed method is immune to kinetic trapping and performs well under physical conditions where the standard KMC simulations slow down to a crawl. In particular, simulations are able to reach later stages of phase separation in the Fe-Cu system and captures a qualitatively new kinetics and mechanism of copper precipitation.

Avenue for future research

To further benefit from the conditioning approach, future attention should be focused on optimizing the auxiliary biasing potentials that control the allocation of computational resources along the external parameters within the sampling process.

Contents

Outline	v
1 Conditioning in computational statistical mechanics	1
1.1 Thermodynamic ensembles and expectations	1
1.2 Ergodic theorem and quasi-ergodicity	2
1.3 Metastability	4
1.4 Poor sampling of distribution tails	4
1.5 Achieving ergodicity through <i>Umbrella sampling</i>	5
1.6 Enhanced sampling through <i>replica exchange simulations</i>	7
1.7 Two standard setups for the extended potential energy	7
1.8 Restrained sampling and <i>stratification</i>	8
1.9 Enhanced sampling through <i>expanded ensemble simulations</i>	9
1.10 Generic estimator for conditional expectations	13
1.11 Conditioning and variance reduction	14
1.12 Summary	20
2 From free energies to probabilities and expectations	21
2.1 On the relativity of free energies	21
2.2 Conditioning and variance reduction	22
2.3 Estimating rare-event probabilities	29
2.4 Assessment of variance reduction	32
2.5 Summary	34
3 Advanced Monte Carlo and adaptively biased sampling	37
3.1 Biased sampling along external and internal coordinates: similarities and differences	37
3.2 Hidden metastabilities and advanced Monte Carlo	38
3.3 Adaptively biased sampling	41
3.4 Estimation of the free energy along a reaction coordinate	43
3.5 Characterization of structural transition	48
3.6 Summary	49
4 Path sampling and conditioning	51
4.1 Equilibrium out of nonequilibrium	51
4.2 Dynamical forcing	52
4.3 Nonequilibrium path ensemble	57
4.4 Expanded path ensemble	63
4.5 Calculating rates of thermally activated events	69
4.6 Expanded transition path ensemble	69
4.7 Summary	75
5 Waste recycling and conditioning	77
5.1 Conditioning on Monte Carlo proposals	77
5.2 Control variate approach to waste-recycling Monte Carlo	77
5.3 Work-biased path ensemble	83
5.4 Applications	84

5.5	Summary	90
6	A matter of time evolution: kinetic pathways and deconditioning	91
6.1	Kinetic Monte Carlo and master equation	91
6.2	Conditioning and deconditioning	91
6.3	Application to diffusion in a disordered substrate	93
6.4	Application to phase separation kinetics in FeCu	94
6.5	Summary	96
	Conclusion and perspectives	97
A	Asymptotic variances of estimators	107
A.1	Elementary laws of probability theory and statistics	107
A.2	Delta method	108
A.3	Estimation of conditional expectations	109
A.4	Estimation of total expectations	109
A.5	Estimation of free energies along λ	110
A.6	Variance reduction through conditioning of self-consistent reweighting	110
B	Algorithms	113
B.1	Metropolis algorithms	113
B.2	Adaptively biased sampling algorithms	114
B.3	Harmonic superposition approximation	117
C	Perspectives	119
C.1	Optimal biasing potential for estimating conditional expectation through standard binning . . .	119
C.2	Optimal biasing potential for the thermodynamic occupation method	120
C.3	Optimal biasing potential with conditioned estimators	121

1 | Conditioning in computational statistical mechanics

1.1 Thermodynamic ensembles and expectations

One important goal of statistical mechanics is to explain the thermodynamic behavior of condensed matter systems at equilibrium. Statistical mechanics connects thermodynamic quantities, such as temperature or heat capacity, to mechanical laws governing the molecular, atomic or electronic motions. Statistical mechanics also makes it possible to extend the laws of thermodynamics to cases which are not considered in classical thermodynamics, such as microscopic systems and other mechanical systems with few degrees of freedom.

Prior to performing any simulation, an appropriate thermodynamic ensemble must be defined. This one is usually characterized by a phase space \mathcal{X} , the set of the states x accessible to the system, and a given set Λ of values of some external parameters λ . The energetics of the particle system is also to be defined and will be described throughout this report by an extended Hamiltonian $\mathcal{H}(\lambda, x)$ where $\lambda \in \Lambda$ and $x \in \mathcal{X}$. Even though Λ will be considered to be a discrete set, we assume that the Hamiltonian $\mathcal{H}(\lambda, x)$ can always be extended within a dense domain $\bar{\Lambda} \times \mathcal{X}$ containing $\Lambda \times \mathcal{X}$ and that the partial derivative of $\mathcal{H}(\lambda, x)$ with respect to $\lambda \in \bar{\Lambda}$, denoted by $\partial_\lambda \mathcal{H}(\lambda, x)$, always exists. In anticipation of the developments to come, canonical ensemble averages are written as conditional expectations given the value of the external parameter(s). The reason for adopting this probabilistic formalism will be justified later in Sec. 1.8 where the stratified sampling approach of probability theory is described. The use of conditional probabilities will also prove to be convenient throughout this report about conditioning. Hence, the occurrence probability of state x in the considered thermodynamic ensemble, a quantity often referred to as Boltzmann weight, is equal to the conditional probability of $x \in \mathcal{X}$ given the value of the external parameter

$$x \mapsto \pi(x|\lambda) = \exp[\mathfrak{F}_{\text{mech}}(\lambda) - \mathcal{H}(\lambda, x)],$$

where dimensionless units are used for the Hamiltonian and the log-normalizing constant reads

$$\mathfrak{F}_{\text{mech}}(\lambda) = -\ln \int_{x \in \mathcal{X}} \exp[-\mathcal{H}(\lambda, x)] dx \triangleq -\Psi^{\{\lambda\}}. \quad (1.1)$$

The quantity $\mathfrak{F}_{\text{mech}}(\lambda)$ will be referred to as *absolute* free energy. Its negative, quantity $\Psi^{\{\lambda\}}$, is sometimes referred to as Massieu function or entropic potential because it is the logarithm of a partition function. The subscript “mech” stands for *mechanical*. In this thesis, we consider that the Hamiltonian is separable, meaning that the kinetic and potential parts of the mechanical energy exclusively depend on momenta p and positions q , respectively

$$\mathcal{H}(\lambda, x) = \mathcal{K}(p) + \mathcal{U}(\lambda, q), \quad \lambda \in \Lambda, \quad x = (p, q) \in \mathcal{X},$$

where $\mathcal{K}(p)$ is the kinetic energy and $\mathcal{U}(\lambda, q)$ the extended potential energy. Note that it is standard practice to decouple the temperature β associated with the kinetic energy to the one associated with the potential energy that may possibly be controlled by λ . The reason is that contributions to thermodynamic properties of the system coming from the kinetic energy can be integrated analytically, hence there is no need to vary any external parameter associated with the kinetic energy. The absolute free energy may be decomposed into the sum of kinetic and potential contributions

$$\mathfrak{F}_{\text{mech}}(\lambda) = \mathfrak{F}_{\text{kin}} + \mathfrak{F}_{\text{pot}}(\lambda).$$

Writing the kinetic energy as $\mathcal{K}(p) = \beta \frac{1}{2} p^T M^{-1} p$ with M the mass matrix, the kinetic part of the absolute free energy may be evaluated analytically by integrating the multidimensional normal distributions over the

momentum space

$$\mathfrak{F}_{\text{kin}} = \frac{1}{2} \ln \left| \frac{2\pi}{\beta} \mathbf{M} \right|$$

where $|\cdot|$ denotes the determinant of a matrix. The potential part reads

$$\mathfrak{F}_{\text{pot}}(\lambda) = -\ln \int_{q \in \mathcal{Q}} \exp[-\mathcal{U}(\lambda, q)] dq.$$

Besides, the effect of the quantum statistics is assumed to be included in the potential energy. Hence, the potential part of the absolute free energy of an ideal gas of noninteracting particles obeying Bose-Einstein statistics is

$$\mathfrak{F}_{\text{pot}}^{\text{id}} = \sum_s [\ln(N_s!) - N_s \ln(V/h^3)]$$

where N_s corresponds to the number of particle of species s , h is Planck's constant and V is the position space volume. The factorial terms reflect the fact that particles of same species are indiscernible. This quantity is connected to the Helmholtz free energy of an ideal boson gas that is $\mathbf{F}^{\text{id}} = (\mathfrak{F}_{\text{kin}} + \mathfrak{F}_{\text{pot}}^{\text{id}})/\beta$. In physics and chemistry, the excess Helmholtz free energy, defined by $\mathbf{F}^{\text{ex}} = \mathfrak{F}_{\text{m}}/\beta - \mathbf{F}^{\text{id}}$, contains the crucial contributions arising from the particle interactions and determining the thermodynamic properties of the involved particle system. The ideal gas contribution to the Helmholtz free energy will be crucial when calculating solubility limits because the numbers of particles vary. An illustration, we refer the reader to Chapter 5 where the solubility of a minor alloying element of α -iron is calculated.

The ensemble average of a physical observable $\mathcal{O}(\lambda, x)$, where $\lambda \in \Lambda$ and $x \in \mathcal{X}$, is given by the conditional expectation of $\mathcal{O}(\lambda, \cdot)$ given $\lambda \in \Lambda$

$$\mathbb{E}(\mathcal{O}(\lambda, \cdot) | \lambda) = \int_{\mathcal{X}} \mathcal{O}(\lambda, x) \pi(x | \lambda) dx.$$

When the observable $(\lambda, q) \mapsto \mathcal{O}(\lambda, q)$ depend on λ and the coordinate positions $q \in \mathcal{Q}$ exclusively, we have

$$\mathbb{E}[\mathcal{O}(\lambda, \cdot) | \lambda] = \int_{\mathcal{X}} \mathcal{O}(\lambda, q) \exp[\mathfrak{F}_{\text{mech}}(\lambda) - \mathcal{H}(\lambda, x)] dx = \int_{\mathcal{Q}} \mathcal{O}(\lambda, q) \exp[\mathfrak{F}_{\text{pot}}(\lambda) - \mathcal{U}(\lambda, q)] dq,$$

where \mathcal{Q} is the configuration or position space. The conditional expectation in the configuration space thus writes

$$\mathbb{E}[\mathcal{O}(\lambda, \cdot)] = \int_{\mathcal{Q}} \mathcal{O}(\lambda, q) \pi(q | \lambda) dq,$$

where the conditional probability of q given λ is defined as

$$\pi(q | \lambda) = \exp[\mathfrak{F}_{\text{pot}}(\lambda) - \mathcal{U}(\lambda, q)].$$

To simplify the notations in the following, absolute free energies $\mathfrak{F}_{\text{mech}}(\lambda)$ and $\mathfrak{F}_{\text{pot}}(\lambda)$ will be denoted by $\mathfrak{F}(\lambda)$, regardless of which sampled space is involved. We have

$$\mathfrak{F}(\lambda) = \tilde{\mathfrak{F}}_{\text{kin}} - \ln \int_{q \in \mathcal{Q}} \exp[-\mathcal{U}(\lambda, q)] dq, \quad (1.2)$$

where $\tilde{\mathfrak{F}}_{\text{kin}}$ is equal to $\mathfrak{F}_{\text{kin}}$ if momenta are considered, otherwise it is 0.

1.2 Ergodic theorem and quasi-ergodicity

The cornerstone of molecular simulation is the ergodic theorem which states the equivalence between ensemble and time averages. Concerning time averages, the term *time* refers to the physical time along a molecular dynamics (MD) trajectory or to the indexes labeling the states of a Markov chain generated using a Monte Carlo (MC) algorithm. When stochastic algorithms such as Langevin dynamics and Monte Carlo schemes are involved, the ergodic theorem relates to the law of large number. For instance, the thermodynamic quantity corresponding to the ensemble average of $\mathcal{O}(\lambda, x)$ for $x \in \mathcal{X}$ can be estimated from the information contained

in a generated Markov chain of states $\{x_m\}_{1 \leq m \leq M}$ using the following arithmetic mean:

$$\mathbb{I}^M(\mathcal{O}|\lambda) = \frac{1}{M} \sum_{m=1}^M \mathcal{O}(\lambda, x_m). \quad (1.3)$$

The condition λ inside the estimator indicate that both the sampling and the observation are performed at the constant value λ of the external parameter. Besides, the sample size M must be large enough otherwise inaccurate estimates will be obtained. The ergodic theorem states that in the limit $M \rightarrow +\infty$, the estimate given by (1.3) converges to $\mathbb{E}[\mathcal{O}(\lambda, \cdot)|\lambda]$, the conditionally expected value of \mathcal{O} given λ , a standard ensemble average. The averaging scheme associated with a given MC algorithm or MD scheme is referred to as ‘‘estimator’’. Because ideal gas contributions are known, simulations essentially focus on excess contributions arising from the interactions between the particles. It is thus simpler to restrict the sampling to the position space, as often done in the following, and to apply estimator (1.3) to a Markov chain of configurations:

$$\mathbb{I}^M(\mathcal{O}|\lambda) = \frac{1}{M} \sum_{m=1}^M \mathcal{O}(\lambda, q_m).$$

However, from the viewpoint of numerical ergodicity, simulations achieve better efficiency with momenta. This observed tendency is attributed to inertial effects that facilitate barrier crossings each time the system reaches a saddle region of the high-dimensional potential energy surface.

For any sampling of the configuration space \mathcal{Q} , one denotes by $P(q_0, q_1)$ the probability to transition from q_0 to q_1 , then the Monte Carlo algorithm must satisfy the detailed balance condition with respect to the probability distribution $\pi(q|\lambda)$ involved in the corresponding ensemble average. For Monte Carlo algorithms, this condition states that the equality of the forward and backward probability fluxes

$$\pi(q_0|\lambda)P(q_0, q_1) = \pi(q_1|\lambda)P(q_1, q_0),$$

where $P(q_1, q_0)$ is the probability of the reverse transition. For stochastic molecular dynamics such as Langevin dynamics, another form of detailed balance is obeyed and will be discussed in greater details in Chapter 4. The reverse transition involves reversed momenta:

$$\pi(x_0|\lambda)P(x_0, x_1) = \pi(\bar{x}_1|\lambda)P(\bar{x}_1, \bar{x}_0),$$

where $\bar{x} = (-p, q)$ if $x = (p, q)$ and $\pi(x|\lambda) = \pi(\bar{x}|\lambda)$ since $\mathcal{H}(\lambda, x) = \mathcal{H}(\lambda, \bar{x})$.

From the law of large number and the central limit theorem [11], it can be shown that, when the sample size M tends to infinity, the statistical variance of $\mathbb{I}^M(\mathcal{O}|\lambda)$ multiplied by M converges towards a finite value, traditionally referred to as asymptotic variance of the estimator. This means that the accuracy (standard deviation) of the estimates evaluated with estimator $\mathbb{I}^M(\mathcal{O}|\lambda)$ in Eq. (1.3) scales as $1/\sqrt{M}$. Moreover, if \mathcal{P} denotes the functional such that $\mathcal{P}\mathcal{O}(\lambda, x) = \int_{\mathcal{X}} P(x, dy)\mathcal{O}(\lambda, y)$ for $x \in \mathcal{X}$ and whatever observable \mathcal{O} , then the value of the asymptotic variance is formally

$$\lim_{M \rightarrow +\infty} M\mathbb{V}[\mathbb{I}^M(\mathcal{O}|\lambda)] = \mathbb{E}[\widehat{\mathcal{O}}(\lambda, \cdot)^2|\lambda] - \mathbb{E}[\mathcal{P}\widehat{\mathcal{O}}(\lambda, \cdot)^2|\lambda],$$

where $x \mapsto \widehat{\mathcal{O}}(\lambda, x)$ is the unique solution up to an additive constant of the Poisson equation [11]:

$$\widehat{\mathcal{O}}(\lambda, x) - \mathcal{P}\widehat{\mathcal{O}}(\lambda, x) = \mathcal{O}(\lambda, x) - \mathbb{E}[\mathcal{O}(\lambda, \cdot)|\lambda].$$

Solving the Poisson equation is more difficult than calculating the expectation itself, except in particular cases, for instance if the sampled states are identically and independently distributed (iid). In this situation, the transition matrix $P(x, y)$ is independent of x and we have $\mathcal{P}\mathcal{O}(\lambda, x) = \mathbb{E}[\mathcal{O}(\lambda, x)|\lambda]$. This in turn implies that an admissible solution of the Poisson equation is $\widehat{\mathcal{O}}(\lambda, x) = \mathcal{O}(\lambda, x)$ and that the asymptotic variance of the estimator is the variance of the observable. This result is simply obtained through the variance decomposition of the sum of independent random variables

$$\mathbb{V}\left[\frac{1}{M} \sum_{m=1}^M \mathcal{O}(\lambda, x_m)\right] = \frac{1}{M} \mathbb{V}[\mathcal{O}(\lambda, x)].$$

The asymptotic variance of the estimator is generally (but not always) larger than the variance of the observable, due to positive correlations between the sampled states, which may result in quasi-ergodicity or nonergodic sampling. This is the main difficulty encountered by molecular simulation for estimating observable averages. It has two distinct causes.

1.3 Metastability

The first cause of nonergodic sampling is due to the presence of metastability. Metastability manifests itself when many distinct basins of attraction substantially contribute to the Boltzmann distribution and the sampling algorithm does not allow to explore these separate regions in sufficient number. This kind of issue occurs when the energy surface is rugged and consists of energy minima separated by energetic and/or entropic barriers. Metastability arises at many different scales in materials science or condensed matter. To give an example, let consider a phase separation process occurring in an alloy initially quenched from a disordered solid solution at high temperature down to a temperature at which the solute concentration is moderately supersaturated. The atomic transport process that is responsible for the nucleation, growth and coarsening of solute precipitates occurs via the exchange of solute and solvent atoms with point defects located on the crystal lattice. The mediating defects may be interstitial atoms and/or vacancies, which is more often the case in alloys. Each location of a migrating defect within the crystal structure corresponds to a metastable basin of attraction, the hopping rates of defects on its underlying lattice being several orders of magnitude lower than the vibration frequency of that lattice (see illustration in Chapter 4). As a result, it takes a great many of MD steps to observe a defect transitioning from one site (basin) to another in molecular dynamics. Another type of metastability happens at the next scale when nucleation of the second phase proceeds through an incubation stage. This one may, for instance, result from the time lag associated with the repeated re-dissolution of subcritical nuclei prior to reaching the critical size. Time scales for incubation are typically many orders of magnitude larger than those involved in the migration of point defects, as shown in Chapter 6.

The degree of correlation of the states along a long MC or MD trajectory yields a measure of metastability. In practice, an appropriate observable \mathcal{O} must be defined, and the correlation time as the integral of the following time autocorrelation function must be defined

$$\text{Corr}_{\mathcal{O}\mathcal{O}}(L) = \lim_{M \rightarrow +\infty} \frac{\sum_{m=1}^M \mathcal{O}(\lambda, x_m) \mathcal{O}(\lambda, x_{m+L}) - \left[\sum_{m=1}^M \mathcal{O}(\lambda, x_m) \right]^2}{\sum_{m=1}^M \mathcal{O}(\lambda, x_m) \mathcal{O}(\lambda, x_m) - \left[\sum_{m=1}^M \mathcal{O}(\lambda, x_m) \right]^2}.$$

If a substantial number of simulation steps is needed to uncorrelate consecutive measurements, there is metastability on the investigated time scale. However, the apparent absence of long-time correlations does not entail that ergodic sampling is achieved. There might be a hidden metastability that can not be detected by monitoring the available observable \mathcal{O} . Estimating the time autocorrelation function requires being able to correctly estimate the mean and variance of the observable, a non trivial task in strongly metastable systems. The autocorrelation time approach is nevertheless useful to compare the efficiency of different sampling algorithms on testbed models.

1.4 Poor sampling of distribution tails

Numerical ergodicity can also be broken when the phase space regions that substantially contribute to the ensemble average have an extremely small Boltzmann weights. This means that the region of interest is in the tail of the Boltzmann distribution. A substantial amount of computer time will be required to harvest a significant statistics. This type of broken ergodicity occurs for instance when estimating the high-order moments of the energy distribution, which correspond to standard ensemble averages. To show this, let consider a particle $q = (q_1, q_2, q_3)$ in a harmonic potential with inverse temperature λ . For a three-dimensional harmonic system, the energy density $g(E)$ is proportional to the energy E . Any algorithm sampling the Boltzmann distribution therefore constructs a Markov chain of states whose energies are distributed according to the energy distribution $E \rightarrow g(E) \exp(\mathfrak{F}(\lambda) - \lambda E)$ where the absolute free energy is $\mathfrak{F}(\lambda) = -\ln \int_{\mathbb{R}^+} e^{-\lambda E} g(E) dE$. Figure 1.1 displays the contributions of energy E to the n th moment of the sampled Boltzmann distribution for n equal to 2, 4 and 6 at reduced temperature one. Estimating the moments of the energy becomes problematic as the moment order is increased because the range of contributing energies shift towards the (poorly sampled) tail of the

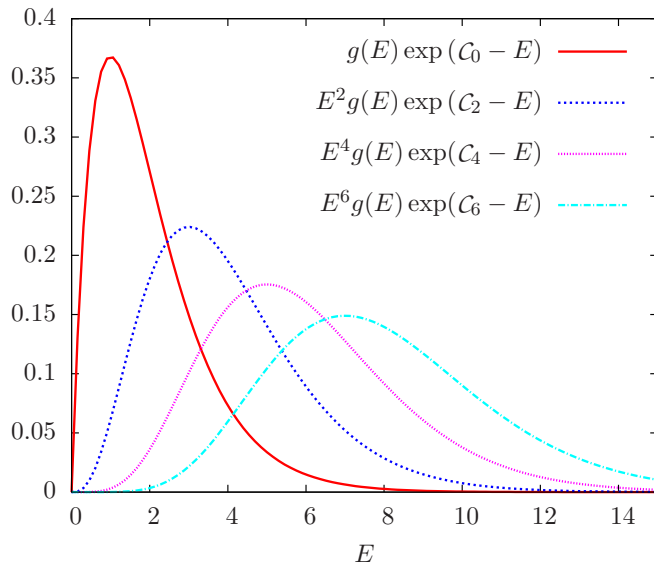


Figure 1.1: The functions $E^n g(E) \exp(C_n - E)$ represents the contribution of energy E to the n th moment of the Boltzmann distribution at $\lambda = 1$, C_n being the associated normalizing constant [$C_0 = \mathfrak{F}(1)$].

exponential distribution, as illustrated in Fig. 1.1. Nonergodic sampling is commonly met in calculations of free energy differences. This issue will be discussed quite extensively in Chapters 2 and 3.

1.5 Achieving ergodicity through *Umbrella sampling*

A major methodological advance for overcoming ergodicity issues is umbrella sampling (US). This Monte Carlo approach [12] is referred to as importance sampling or preferential sampling in the mathematical literature. It consists of adding a biasing potential $\mathcal{B}(q)$ to the reference potential energy $\mathcal{U}(0, q)$ and of using the so-modified potential energy $\mathcal{U}(1, q) = \mathcal{U}(0, q) + \mathcal{B}(q)$ in MC or MD simulations so as to artificially enhance the exploration of phase space regions contributing substantially to the expected value of $\mathcal{O}(0, q)$. By doing so, numerical ergodicity is achieved much faster. In the following, the estimator used in combination with umbrella sampling is referred to as standard reweighting.

1.5.1 Standard reweighting estimator

Since the system with potential energy $\mathcal{U}(1, q)$ is sampled, then the effect of the biasing potential $\mathcal{B}(q)$ must be corrected when evaluating the estimates, which can be done by resorting to the following standard reweighting (R) estimator

$$\mathbb{I}_R^M(\mathcal{O}|\lambda = 0; \pi|\zeta = 1) = \frac{\frac{1}{M} \sum_{m=1}^M \mathcal{O}(0, q^m) \exp[\mathcal{B}(q_m)]}{\frac{1}{M} \sum_{m=1}^M \exp[\mathcal{B}(q_m)]}. \quad (1.4)$$

In the estimators of (1.4), the condition $\zeta = 1$ means that the sampling is performed with respect to thermodynamic state \mathcal{S}_1 (biased measurements) and the condition $\lambda = 0$ corresponds to the conditional expectation that is estimated. This estimator follows from the relation

$$\mathbb{E}[\mathcal{O}(0, q)|0] = \mathbb{E}\left[\mathcal{O}(0, q) \frac{\pi(q|0)}{\pi(q|1)} \Big| 1\right] = \mathbb{E}\left[\mathcal{O}(0, q) \exp(\mathfrak{F}(0) - \mathfrak{F}(1) + \mathcal{B}(q)) \Big| 1\right],$$

where the free energy difference satisfies the particular relation obtained by setting the observable to the constant value 1:

$$\mathbb{E}[1|0] = \mathbb{E}\left[1 \times \exp(\mathfrak{F}(0) - \mathfrak{F}(1) + \mathcal{B}(q)) \Big| 1\right] = 1.$$

The logarithm of the denominator is therefore an estimate of the free energy difference $\mathfrak{F}(1) - \mathfrak{F}(0)$ between the biased (perturbed) thermodynamic state \mathcal{S}_1 (which is sampled) and the reference thermodynamic state \mathcal{S}_0 (which corresponds to the ensemble of interest). Accurately estimating a free energy difference between two thermodynamic states of potential energy $\mathcal{U}(0, q)$ and $\mathcal{U}(1, q) = \mathcal{U}(0, q) + \mathcal{B}(q)$ amounts to accurately estimating

the first moments of the distribution $B \rightarrow P(B) = \mathbb{E}[\delta_B(\mathcal{B}(q)) | \lambda = 1]$, the conditional expectation of Dirac δ -function with respect to the biased thermodynamic state \mathcal{S}_1 . This feature stems from the equality

$$\exp(\mathfrak{F}(1) - \mathfrak{F}(0)) = \mathbb{E}[\exp(\mathcal{B}(q)) | 1] = \sum_{n=1}^{+\infty} \frac{(-1)^n}{n!} \mathbb{E}[\mathcal{B}(q)^n | 1].$$

The tail of the distribution $P(B)$, may have a considerable contribution to the free energy difference, as illustrated previously in Fig. 1.1 for a simple harmonic oscillator. The way the free energy difference is estimated in the denominator of (1.4) corresponds to the free energy perturbation method [13, 14, 15]. Free energy methods are discussed in detail in Chapter 2.

Umbrella sampling is also called *non-Boltzmann sampling* [14] because it can be formalized with respect to any couple of thermodynamic states \mathcal{S}_λ and \mathcal{S}_ζ by replacing the biasing potential $\mathcal{B}(q)$ by $\mathcal{U}(\zeta, q) - \mathcal{U}(\lambda, q)$. It is then possible to estimate an ensemble average with respect to thermodynamic states \mathcal{S}_λ from a sample generated in thermodynamic state \mathcal{S}_ζ using the more general form for the standard reweighting estimator:

$$\mathbb{I}_R^M(\mathcal{O} | \lambda; \pi | \zeta) = \frac{\frac{1}{M} \sum_{m=1}^M \mathcal{O}(\lambda, q_m) \exp[\mathcal{U}(\zeta, q_m) - \mathcal{U}(\lambda, q_m)]}{\frac{1}{M} \sum_{m=1}^M \exp[\mathcal{U}(\zeta, q_m) - \mathcal{U}(\lambda, q_m)]}. \quad (1.5)$$

It is instructive to recast the standard reweighting estimator (1.5) into the following form

$$\mathbb{I}_R^M(\mathcal{O} | \lambda; \pi | \zeta) = \sum_{m=1}^M \mathcal{O}(\lambda, q_m) \frac{\exp[\widehat{\mathfrak{F}}(\lambda) - \mathcal{U}(\lambda, q_m)]}{M \exp[\widehat{\mathfrak{F}}(\zeta) - \mathcal{U}(\zeta, q_m)]}, \quad (1.6)$$

where the quantities $\widehat{\mathfrak{F}}(\lambda)$ and $\widehat{\mathfrak{F}}(\zeta)$ correspond to an estimate of the free energies $\mathfrak{F}(\lambda)$ and $\mathfrak{F}(\zeta)$, up to a common additive constant. Their difference $\widehat{\mathfrak{F}}(\lambda) - \widehat{\mathfrak{F}}(\zeta)$ is solution of the following equation

$$\mathbb{I}_R^M(1 | \lambda; \pi | \zeta) = 1.$$

In practice, in order to obtain accurate estimates based on the standard reweighting estimator (1.4), the biased sample must contain typical data of the unbiased distribution in a significant proportion. Stated differently, the perturbed and unperturbed distribution should substantially overlap. If this condition is not met, then the associated free-energy difference is usually overestimated [16, 14, 15]. For instance, choosing the biasing potential equal to the potential energy amounts to estimating the ensemble average from an unbiased random walk in the multi-dimensional phase space, an approach obviously doomed to fail! From a mathematical point of view, umbrella sampling is a variance reduction technique that does not guarantee variance reduction. The question of how to alleviate convergence issues in umbrella sampling simulations arose naturally and motivated the methodological developments to be discussed next.

1.5.2 Self-consistent reweighting estimators

When the overlapping conditions are not satisfied in practice, it is possible to evaluate the ensemble average through staged transformations [17, 18]. The biasing potential is gradually switched on resorting to the external parameter λ and to the extended potential energy $\mathcal{U}(\lambda, q)$, where $\mathcal{U}(0, q)$ possibly denotes the potential energy of the reference system. Then, a simulation is performed at each stage of the switching protocol. A self-consistent estimator is eventually implemented to combine the data from the multiple simulations and, based on accurate estimates of the successive free-energy differences, to eventually extract a reliable estimate of the desired observable [14, 15]. This postprocessing procedure is known under various names such as the *Bennett acceptance ratio* (BAR) method [16], the *weighted histogram analysis method* [19, 17] (WHAM), the reverse logistic regression [20], bridge sampling [21], the multi-state BAR method [18], binless WHAM [22] and the global likelihood method [23, 24]. These various methods are equivalent in the sense that they involve first harvesting data from a number of independent simulations carried out for a predetermined set of external parameter values and second solving a set of nonlinear equations.

The self-consistent (SC) estimator aims at minimizing the statistical variances associated with a series of simulations performed with distinct values $\zeta \in \Lambda$ of the control parameter λ . The simulation performed at ζ

provides one with a Markov chain consisting of M_ζ points. Pooling all the data $\mathcal{O}(\zeta, q_m)$ of the observable into a single chain of size $M = \sum_{\zeta \in A} M_\zeta$, the SC estimate of the conditional expectation of observable \mathcal{O} given λ writes¹

$$\Upsilon_{\text{SC}}^M(\mathcal{O}|\lambda) = \sum_{m=1}^M \mathcal{O}(\lambda, q_m) \frac{\exp[\widehat{\mathfrak{F}}(\lambda) - \mathcal{U}(\lambda, q_m)]}{\sum_{\zeta} M_\zeta \exp[\widehat{\mathfrak{F}}(\zeta) - \mathcal{U}(\zeta, q_m)]}. \quad (1.7)$$

The free energy estimates $\{\widehat{\mathfrak{F}}(\lambda)\}_{\lambda \in A}$ are obtained by solving the set of nonlinear equations

$$\Upsilon^M(1|\lambda) = 1, \quad \lambda \in A,$$

using an appropriate solver.² The obtained free energy estimates $\widehat{\mathfrak{F}}(\lambda^i)$ are optimal from the point of view of statistical inference [18]. Note that the (standard) reweighting estimator (1.6) that is used for non-Boltzmann sampling is recovered when a single thermodynamic state \mathcal{S}_1 is employed. MBAR also reduces to Bennett acceptance ratio method [16] when two thermodynamic states are sampled, which explains the name given to MBAR method in the physics and chemistry literature. The BAR method is known as the bridge sampling method in the statistical literature wherein a rigorous mathematical foundation can be found [24]. The MBAR method is described in detail in Ref. [15].

Next, we briefly mention an important sampling technique with which a multi-state estimator is most often employed.

1.6 Enhanced sampling through *replica exchange simulations*

In practice, self-consistent estimators are applied to data harvested using replica exchange Monte Carlo (REMC) [19] or replica exchange molecular dynamics (REMD) [25] simulations. This sampling approach propagates several independent MD or MC trajectories (the replicas), each one performed at different and constant value of the external parameter, and occasionally attempts swapping the λ values of two adjacent replicas. The exchange is accepted with a probability that is essentially the ratio of the Boltzmann weights after and before the exchange. Mixing trajectories propagated at different values of the external parameter increases the overall numerical ergodicity and thus the sampling efficiency of simulations. For instance, if the energy surface is rugged, then choosing inverse temperature as the external parameter allows crossing the energy barriers separating the basins of attraction at the higher temperatures and detailed sampling of the visited basins at low temperatures owing to temperature exchanges. Much shorter correlation times are observed in practice in simulations performed with replica exchanges than without.

1.7 Two standard setups for the extended potential energy

At this point, it is instructive to give examples of extended potential energies that are commonly employed in enhanced sampling techniques, such as umbrella sampling and replica exchange methods. We depict two important setups in which the external parameter couples either linearly to a potential energy or harmonically to a reaction coordinate $\xi(q)$. Note that nonlinear couplings between the external parameter and the potential energy can possibly be employed, for instance to achieve improved efficiency through functional minimization [26].

With linear coupling, the extended system evolves between a reference system \mathcal{S}_0 and a target system \mathcal{S}_1 . In practice, it is convenient to write the extended potential as

$$\mathcal{U}(\lambda, q) = (1 - \lambda)\mathcal{U}_0(q) + \lambda\mathcal{U}_1(q), \quad (1.8)$$

where λ takes values in the interval $[0, 1]$. In Eq. (1.8), $\mathcal{U}_0(q)$ and $\mathcal{U}_1(q)$ are the potentials of the reference and target systems, respectively. This parameterization covers situations where the external parameter is used to vary an intensive thermodynamic force like inverse temperature or pressure. For instance, when the reference and target systems correspond to a system of identical potential energy $\mathcal{V}(q)$ held at two distinct temperatures β_{\min} and β_{\max} , we simply set $\mathcal{U}_0 = \beta_{\min}\mathcal{V}$ and $\mathcal{U}_1 = \beta_{\max}\mathcal{V}$. An important task is to estimate conditional expectations given some values of the external parameter λ [see Eq. (1.25)]. Estimating the average internal

¹A noticeable feature of the self-consistent estimator is that the subsample origin of q_m is an irrelevant information.

²The solver provided online at <https://simtk.org/home/pymbar>, uses a fixed-point iterative method first and switch to Newton-Raphson method close to the solution.

energy at a given inverse temperature is a typical example that will be illustrated in Section 3.5 for icosahedral and octahedral atomic clusters. The present linear setup is also used in Section 2.4 to illustrate the estimation of total expectations, free energies and rare-event probabilities in a simple model using various estimators.

With harmonic coupling of the external parameter to a reaction coordinate $\xi : q \in \mathcal{Q} \mapsto \xi(q)$, the extended potential exhibits the following form

$$\mathcal{U}(\lambda, q) = \mathcal{U}_0(q) + \mathcal{R}(\lambda, \xi(q)), \quad (1.9)$$

with $\mathcal{U}_0(q) = \beta_{\text{ref}} \mathcal{V}(q)$ wherein $\mathcal{V}(q)$ and β_{ref} are the potential and the inverse temperature of the reference system, respectively. Here, the restraining potential $\mathcal{R}(\lambda, \xi(q))$ is harmonic and centered on the value of the reaction coordinate $\xi(q)$, denoted by ξ^* below

$$\mathcal{R}(\lambda, \xi^*) = \frac{1}{2} \beta_{\text{ref}} \kappa \|\lambda - \xi^*\|^2 + \varepsilon(\xi^*), \quad (1.10)$$

where κ is the spring stiffness and $\varepsilon(\xi^*)$ is a small correcting potential defined by

$$\varepsilon(\xi^*) = \sum_{\zeta \in \Lambda} \exp \left[-\frac{1}{2} \beta_{\text{ref}} \kappa \|\zeta - \xi^*\|^2 \right].$$

This term is included to ensure that the artificial restraining potential does not affect the reference distribution in which restraints are absent. In this setup, the reference probability is cast in the form of a marginal probability of q defined from the conditional probabilities of q given λ , resorting to the law of total probability. This approach is referred to as stratification and is detailed in Sec. 1.8 below.

1.8 Restrained sampling and *stratification*

Here, we specifically consider the harmonic setup with the reaction coordinate $\xi(q)$. We wish to construct the histograms of the reaction coordinate by averaging the indicator function associated with the histogram bins. The function for bin ξ^* is denoted by $\mathbf{1}_{\xi^*} \circ \xi(q)$ where the empty circle symbolizes the functional composition. Let further assume that a replica exchange simulation with $\zeta \in \Lambda$ has been performed and that the conditional expectations $\mathbb{E}[\mathbf{1}_{\xi^*} \circ \xi | \zeta]$ have been estimated for $\zeta \in \Lambda$ using the self-consistent estimator (1.38). The simulation biases associated with the additional harmonic restraining potential $\mathcal{R}(\lambda, \xi^*)$ are to be removed. The stratification approach does this job automatically.

The trick consists of resorting to the law of total expectation with respect to ζ :

$$\mathbb{E}^{\mathcal{Q}}[\mathbf{1}_{\xi^*} \circ \xi] = \mathbb{E}^{\Lambda}[\mathbb{E}[\mathbf{1}_{\xi^*} \circ \xi | \zeta]].$$

The meaning of the two involved expectations $\mathbb{E}^{\mathcal{Q}}[\cdot]$ and $\mathbb{E}^{\Lambda}[\cdot]$ needs being clarified.

The first expectation $\mathbb{E}^{\mathcal{Q}}[\cdot]$ is defined with respect to the marginal probability of q with respect to $\zeta \in \Lambda$

$$p^{\mathcal{Q}}(q) = \sum_{\zeta \in \Lambda} p(\zeta, q),$$

where the joint probability, defined over the extended phase space $\{\Lambda, \mathcal{Q}\}$, writes $p(\zeta, q) = \exp[-\mathcal{U}(\zeta, q) - \Psi_0^{\Lambda}]$ wherein the log-normalizing constant for general setups reads

$$\Psi_0^{\Lambda} = \ln \left[\sum_{\zeta \in \Lambda} \int_{\mathcal{Q}} \exp[-\mathcal{U}(\zeta, q)] dq \right] = \ln \left[\sum_{\zeta \in \Lambda} \exp[-\mathfrak{F}(\zeta)] \right].$$

For the harmonic setup, we have specifically

$$p^{\mathcal{Q}}(q) = \sum_{\zeta \in \Lambda} \exp[-\mathcal{U}_0(q) - \mathcal{R}(\zeta, q) - \Psi_0^{\Lambda}] = \exp[-\mathcal{U}_0(q) - \Psi_0]$$

where the log-normalizing constant is $\Psi_0 = \ln \int_{\mathcal{Q}} \exp[-\mathcal{U}_0(q)] dq$.³

³Note that the quantities Ψ_0^{Λ} and Ψ_0 are equal to each other for the particular harmonic setup (1.10).

The second expectation $\mathbb{E}^A[\cdot]$ is associated with the marginal probability of $\lambda \in A$ and writes

$$p^A(\lambda) = \int_{\mathcal{Q}} p(\lambda, q) dq = \exp[-\mathfrak{F}(\lambda) - \Psi_0^A] = \frac{\exp[-\mathfrak{F}(\lambda)]}{\sum_{\zeta \in A} \exp[-\mathfrak{F}(\zeta)]}. \quad (1.11)$$

A third expectation can be defined with respect to the joint probability, which writes for a general observable $\mathcal{O}(\zeta, q)$:

$$\mathbb{E}[\mathcal{O}] = \sum_{\zeta \in \mathcal{A}} \int_{\mathcal{Q}} \mathcal{O}(\zeta, q) p(\zeta, q) dq. \quad (1.12)$$

The laws of total expectation (LTE) on ζ and q are expressed as:

$$\mathbb{E}[\mathcal{O}] = \begin{cases} \mathbb{E}^{\mathcal{Q}} [\mathbb{E}[\mathcal{O}(\cdot, q)|q]] = \int_{\mathcal{Q}} \mathbb{E}[\mathcal{O}(\cdot, q)|q] p^{\mathcal{Q}}(q) dq, \\ \mathbb{E}^A [\mathbb{E}[\mathcal{O}(\zeta, \cdot)|\zeta]] = \sum_{\zeta \in A} \mathbb{E}[\mathcal{O}(\zeta, \cdot)|\zeta] p^A(\zeta). \end{cases}$$

Since observable $\mathbf{1}_{\xi^*} \circ \xi$ does not depend on the external parameter, its expectation with respect to the marginal distribution can be defined and is equal to the expectation with respect to the joint distribution (see LTE on q in first case above). Owing to the LTE above and to expression (1.11), we obtain

$$\mathbb{E}^{\mathcal{Q}} [\mathbf{1}_{\xi^*} \circ \xi] = \mathbb{E} [\mathbf{1}_{\xi^*} \circ \xi] = \frac{\sum_{\zeta \in A} \mathbb{E} [\mathbf{1}_{\xi^*} \circ \xi | \zeta] \exp[-\mathfrak{F}(\zeta)]}{\sum_{\zeta \in A} \exp[-\mathfrak{F}(\zeta)]}.$$

This relation entails that if the quantities $\mathbb{E} [\mathbf{1}_{\xi^*} \circ \xi | \zeta]$ and $\mathfrak{F}(\zeta)$ have been estimated for $\zeta \in A$, then an estimate of $\mathbb{E}^{\mathcal{Q}} [\mathbf{1}_{\xi^*} \circ \xi]$ can be immediately deduced. Stratification is a standard implementation of MBAR [18].

1.9 Enhanced sampling through *expanded ensemble simulations*

When estimating a series of thermodynamic expectations along an external parameter λ , another way of improving numerical ergodicity consists in considering that the external parameter is an additional coordinate and sampling the extended space $A \times \mathcal{Q}$. This is the principle of the method of *expanded ensemble* (EE). In practice, an auxiliary biasing potential $\alpha(\zeta)$ is subtracted from the potential energy. The extended potential energy [27] that is actually sampled exhibits the following form

$$\mathcal{U}_\alpha(\zeta, q) = \mathcal{U}(\zeta, q) - \alpha(\zeta).$$

In the EE method, the set A of possible values for the external parameter is discrete and finite. The expanded ensemble is thus an union of sub-ensembles: $\cup_{\lambda \in A} \mathcal{S}_\lambda$. In the expanded ensemble, the joint probability of extended state (ζ, q) writes

$$p_\alpha(\zeta, q) = \exp[-\Psi_\alpha^A + \alpha(\zeta) - \mathcal{U}(\zeta, q)], \quad (1.13)$$

where the log-normalizing constant Ψ_α^A depends on the auxiliary potential.

In Monte Carlo schemes, some moves occasionally attempt to modify the current value of the dynamical external parameter, entailing that a Markov chain $\{\zeta_m, q_m\}_{1 \leq m \leq M}$ is generated in the extended phase space. The method of expanded ensemble achieves improved ergodicity for the same reason replica exchange method does. The difference is that the subsample sizes M_λ are not predetermined but are outputs of EE simulations. The size M_λ corresponds to the number of visits of the sub-ensemble within the generated sample of extended states:

$$M_\lambda = \sum_{m=1}^M \mathbf{1}_\lambda(\zeta_m) \equiv M \Gamma^M(\mathbf{1}_\lambda), \quad (1.14)$$

where the function $\mathbf{1}_\lambda$ is the indicator function taking value 1 when input value is λ and 0 otherwise. In (1.14), Γ^M denotes the arithmetic mean estimator. In practice, all the subsample sizes should be large enough otherwise inaccurate estimates will be obtained. To ensure that the sampled values ζ_m are distributed uniformly enough along the λ coordinate, an (additional) auxiliary biasing potential $\alpha(\lambda)$ is subtracted from the potential energy $\mathcal{U}(\lambda, q)$. The action of the auxiliary biasing potential is crucial not only in the linear setup but also in the harmonic setup with which the restraining potential alone does not affect the thermodynamic expectations of observable $\mathbf{1}_{\xi^*} \circ \xi$. Subtracting an adequate biasing potential $\alpha(\zeta)$ to the extended system enables one to drive

the external parameter that in turn will pull the particle system towards regions of interests. This setup aims at mechanically steering the sampled values of the reaction coordinate ξ owing to $\alpha(\zeta)$. We show how this task can be efficiently done in Sec. 3.4. In the considered example, $\xi(q)$ is a bond orientational order parameter [28] able to monitor structural transitions in small atomic clusters.

In EE simulations, the biased probability density $p_a(\zeta, \bar{q})$ is sampled, but expectations should be evaluated with respect to the unbiased probability density $p_0(\zeta, \bar{q})$. The simulation biases are straightforwardly removed when evaluating thermodynamic averages by employing a binning estimator whose formal expression is independent of the auxiliary biasing potential, as explained next.

1.9.1 Binning estimator

The conditional probability of observing q given the external parameter λ is

$$\pi(q|\lambda) = \exp[\mathfrak{F}(\lambda) - \mathcal{U}(\lambda, q)] = \frac{p_a(\lambda, q)}{\int_{\mathcal{Q}} p_a(\lambda, q) dq} = \frac{\sum_{\zeta \in A} \mathbf{1}_\lambda(\zeta) p_a(\zeta, q)}{\sum_{\zeta \in A} \int_{\mathcal{Q}} \mathbf{1}_\lambda(\zeta) p_a(\zeta, q) dq}$$

where the normalizing quantity $\mathfrak{F}(\lambda)$ is the free energy introduced in (1.2). A thermodynamic average at $\lambda \in A$ corresponds to a conditional expectation of an observable \mathcal{O} and writes

$$\mathbb{E}(\mathcal{O}|\lambda) = \int_{\mathcal{Q}} \mathcal{O}(\lambda, q) \pi(dq|\lambda) = \frac{\sum_{\zeta \in A} \int_{\mathcal{Q}} \mathbf{1}_\lambda(\zeta) \mathcal{O}(\lambda, q) p_a(\zeta, dq)}{\sum_{\zeta \in A} \int_{\mathcal{Q}} \mathbf{1}_\lambda(\zeta) p_a(\zeta, dq)}.$$

The conditional expectations in the EE can be estimated using the following standard binning estimator

$$\Upsilon_{\text{H}}^M(\mathcal{O}|\lambda) = \frac{\frac{1}{M} \sum_{m=1}^M \mathbf{1}_\lambda(\zeta_m) \mathcal{O}(\lambda, q_m)}{\frac{1}{M} \sum_{m=1}^M \mathbf{1}_\lambda(\zeta_m)}, \quad \lambda \in A, \quad (1.15)$$

where the subscript H stands for histogram. The standard binning estimator corresponds to a ratio involving arithmetic-mean estimators

$$\Upsilon_{\text{H}}^M(\mathcal{O}|\lambda) = \frac{\mathbf{I}^M(\mathbf{1}_\lambda \mathcal{O})}{\mathbf{I}^M(\mathbf{1}_\lambda)}, \quad \lambda \in A. \quad (1.16)$$

As an example of application, the derivative of the free energy with respect to λ [which is the conditional expectation of $\partial_\lambda \mathcal{U}(\lambda, q)$ given λ as shown in (1.2)] can be estimated after setting $\mathcal{O}(\lambda, q)$ to $\partial_\lambda \mathcal{U}(\lambda, q)$ in (1.15) or (1.16):

$$\widehat{\mathfrak{F}}'(\lambda) = \frac{\sum_{m=1}^M \mathbf{1}_\lambda(\zeta_m) \partial_\lambda \mathcal{U}(\lambda, q_m)}{\sum_{m=1}^M \mathbf{1}_\lambda(\zeta_m)}.$$

Note that, from a thermodynamic viewpoint, the external parameter is usually referred to as the thermodynamic force when it is an intensive quantity. Herein, we rather adopt a mechanical viewpoint and assume that λ is an additional coordinate. The dynamics of λ is determined by the variation of both the biasing potential and the potential energy with respect to λ . From a mechanical point of view, $\partial_\lambda \mathcal{U}$ and its conditionally expected value given λ corresponds to a *local mean force* and a *mean force*, respectively. Since $\widehat{\mathfrak{F}}'(\lambda)$ is the mean force along λ , the free energy $\mathfrak{F}(\lambda)$ defined in (1.2) can be referred to as a potential of mean force.

1.9.2 Adaptive biasing force in expanded ensembles

The bias is traditionally chosen in such a way that uniform sampling is achieved along λ . This entails that the average effective forces along λ vanish during simulations for all λ values in the interval of interest. The requested biasing force therefore corresponds to the mean force defined as the conditional expectation of $\partial_\lambda \mathcal{U}(\lambda, q)$ given λ in (1.2). It was proposed [29] to adapt the biasing force during a preliminary simulation on the current estimate

of the mean force.⁴ In the expanded ensemble, this is achieved as follows

$$\alpha'_M(\lambda) = \frac{\sum_{m=1}^M \mathbf{1}_\lambda(\zeta_m) \partial_\lambda \mathcal{U}(\lambda, q_m)}{\sum_{m=1}^M \mathbf{1}_\lambda(\zeta_m)}. \quad (1.17)$$

The denominator of the fraction indicates the size of the corresponding subsample. The present way of constructing the biasing potential from its gradient corresponds to a technique referred to as *adaptive biasing force* (ABF) in the literature [15]. In the long term, the adaptive biasing force in (1.17) converges to the mean force [32]: $\lim_{M \rightarrow +\infty} \alpha_M = \mathfrak{F}$, up to a common additive constant. More details about the ABF method will be given in Chapter 3.

1.9.3 Adaptive biasing potential in expanded ensembles

As an alternative to ABF, it is possible to adapt the auxiliary biasing potential during the course of a simulation based on the size of each subsample, i.e., the numbers of visits of each subensemble [33]. This alternative way of proceeding corresponds to a technique referred to as adaptive biasing potential (ABP) in the literature [15]. Numerous variant schemes based on the ABP idea have been proposed for the more general reaction coordinate case [15]. The main difficulty in implementing an ABP scheme involves tuning the update frequency of the biasing potential in order to ensure efficient convergence of the simulations. If the update frequency is too low, then the rate of convergence will be small. If the update frequency is too high, then the biasing potential will oscillate around a mean value. A trade-off minimizing these two adverse scenarios should therefore be found. Details and examples of ABP algorithms are given in Chapter 3 for the reaction coordinate case.

⁴The biasing forces in the original ABF method [30, 31] are along a reaction coordinate $\xi(q)$. The original ABF algorithm is depicted in Chapter 3

1.9.4 Adiabatic reweighting

The *adiabatic reweighting* estimator [34, 8] is an estimator specifically dedicated to expanded ensemble simulations. This estimator is based on Bayes formula [34] and requires that the associated Markov chain of states is sampled from the marginal probability of q , which is defined by

$$p_a^{\mathcal{Q}}(q) = \sum_{\lambda \in \Lambda} p_a(\lambda, q) = \sum_{\lambda \in \Lambda} \exp[\alpha(\lambda) - \mathcal{U}(\lambda, q) - \Psi_a^A].$$

This means that, for any state q sampled according to the marginal probability distribution, the reweighting factor used in the estimator of a conditional expectation given λ is the conditional probability of λ given q . This quantity depends on the auxiliary potential and is defined by

$$\pi_a(\lambda|q) = \frac{p_a(\lambda, q)}{p_a^{\mathcal{Q}}(q)} = \frac{\exp[\alpha(\lambda) - \mathcal{U}(\lambda, q)]}{\sum_{\zeta \in \Lambda} \exp[\alpha(\zeta) - \mathcal{U}(\zeta, q)]}.$$

The expression relating the target distribution $\pi(q|\lambda)$ and the normalized reweighting factor $\pi_a(\lambda|q)/p_a^A(\lambda)$ to the sampled distribution $p_a^{\mathcal{Q}}(q)$ corresponds to the well-known Bayes formula, which writes

$$\pi(q|\lambda) = \frac{\pi_a(\lambda|q)p_a^{\mathcal{Q}}(q)}{p_a^A(\lambda)}. \quad (1.18)$$

The estimator is directly constructed upon the expectation form of Bayes formula (1.18). This alternative form is obtained by multiplying both sides of (1.18) by $\mathcal{O}(\lambda, q)$, integrating over $q \in \mathcal{Q}$ and then expressing the marginal probability of λ in (1.18) using the law of total expectation:

$$p_a^A(\lambda) = \int_{\mathcal{Z}} \pi_a(\lambda|q)p_a^{\mathcal{Q}}(dq) \triangleq \mathbb{E}_a^{\mathcal{Q}}[\pi_a(\lambda|q)].$$

These manipulations eventually enable one to cast the conditional expectation of the observable value $\mathcal{O}(\lambda, q)$ given λ in its Bayesian form

$$\mathbb{E}[\mathcal{O}|\lambda] = \frac{\mathbb{E}_a^{\mathcal{Q}}[\pi_a(\lambda|q)\mathcal{O}(\lambda, q)]}{\mathbb{E}_a^{\mathcal{Q}}[\pi_a(\lambda|q)]}.$$

Owing to the ergodic theorem, the resulting estimator is eventually

$$\Upsilon_{\Pi}^M(\mathcal{O}|\lambda) = \frac{\frac{1}{M} \sum_{m=1}^M \mathcal{O}(\lambda, q_m) \pi_a(\lambda|q_m)}{\frac{1}{M} \sum_{m=1}^M \pi_a(\lambda|q_m)}, \quad (1.19)$$

where the sampled states $\{q_m\}_{1 \leq m \leq M}$ are distributed according to $p_a^{\mathcal{Q}}(dq)$.

The term *adiabatic* was introduced in reference to the virtual dynamical decoupling that is involved when the method is implemented within MD simulations [34]. When the position coordinates q evolve very slowly compared to λ , the latter variable has enough time to fully explore its space Λ and visits any value of λ according to the corresponding equilibrium probability $\pi_a(\lambda|q)$. With this picture in mind, the force exerted upon q is $-\mathbb{E}_a^{\mathcal{Q}}[\nabla_q \mathcal{U}(\zeta, q)|q]$, the average of minus the gradient of $\mathcal{U}(\lambda, q)$ with respect to q and over the current equilibrium distribution of λ given q . This force is precisely equal to the logarithmic gradient of the equilibrium marginal probability distribution:

$$\nabla_q \ln p_a^{\mathcal{Q}}(q) = -\frac{\sum_{\zeta \in \Lambda} \nabla_q \mathcal{U}(\zeta, q) \exp[\alpha(\zeta) - \mathcal{U}(\zeta, q)]}{\sum_{\zeta \in \Lambda} \exp[\alpha(\zeta) - \mathcal{U}(\zeta, q)]} = -\mathbb{E}_a[\nabla_q \mathcal{U}(\zeta, q)|q].$$

Hence, the conditionally expected force acting on q can be employed as a forcefield in MD simulations to sample states according to the marginal probability distribution, provided the dynamics is coupled to a thermostat as shown in Ref [34].

In MC simulations, it seems that a new scheme is required to sample the marginal distribution $p_a^{\mathcal{Q}}(q)$. But, we have already that scheme since we know how to sample the joint probability $p_a(\zeta, q)$. In fact, estimator (1.19) could have been equally implemented using a sample $\{\zeta_m, q_m\}_{1 \leq m \leq M}$ by application of the ergodic theorem to

the following expectation ratio

$$\mathbb{E}[\mathcal{O}|\lambda] = \frac{\mathbb{E}_a[\pi_a(\lambda|q)\mathcal{O}(\lambda, q)]}{\mathbb{E}_a[\pi_a(\lambda|q)]}, \quad (1.20)$$

where the expectation \mathbb{E}_a is defined with respect to any function $(\zeta, q) \mapsto \mathcal{G}(\zeta, q)$ as follows

$$\mathbb{E}_a[\mathcal{G}(\cdot, \cdot)] \triangleq \sum_{\zeta \in \Lambda} \int_{\mathcal{Q}} \mathcal{G}(\zeta, q) p_a(\zeta, dq) = \sum_{\zeta \in \Lambda} \int_{\mathcal{Q}} \pi_a(\zeta|q) \mathcal{G}(\zeta, q) p_a^{\mathcal{Q}}(dq) = \mathbb{E}_a^{\mathcal{Q}} \left[\sum_{\zeta \in \Lambda} \pi_a(\zeta|q) \mathcal{G}(\zeta, q) \right].$$

Setting the function $\mathcal{G}(\zeta, q)$ to $\pi_a(\lambda|q)\mathcal{O}(\lambda, q)$ and $\pi_a(\lambda|q)$ yields the two following relations

$$\mathbb{E}_a[\pi_a(\lambda|\cdot)\mathcal{O}(\lambda, \cdot)] = \mathbb{E}_a^{\mathcal{Q}}[\pi_a(\lambda|\cdot)\mathcal{O}(\lambda, \cdot)] \quad \text{and} \quad \mathbb{E}_a[\pi_a(\lambda|\cdot)] = \mathbb{E}_a^{\mathcal{Q}}[\pi_a(\lambda|\cdot)],$$

obtained noticing that the observables do not depend on ζ and plugging $\sum_{\zeta \in \Lambda} \pi_a(\zeta|q) = 1$. The ratio given in (1.20) immediately follows. It is instructive to establish the connection with umbrella sampling method in which $\mathcal{U}(\lambda, q) = \mathcal{U}(0, q) + \lambda \mathcal{B}(q)$. The estimator with respect to the reference system ($\lambda = 0$) becomes

$$\Upsilon_{\text{H}}^M(\mathcal{O}|0) = \frac{\frac{1}{M} \sum_{m=1}^M \mathcal{O}(\lambda, q_m) \exp \mathcal{B}_a(q_m)}{\frac{1}{M} \sum_{m=1}^M \exp \mathcal{B}_a(q_m)}. \quad (1.21)$$

where we have introduced

$$\mathcal{B}_a(q) = \ln \pi_a(0|q) = \ln \frac{p_a(0, q)}{\sum_{\zeta \in \Lambda} p_a(\zeta, q)} = \mathbf{a}(0) - \ln \sum_{\zeta \in \Lambda} \exp[\mathbf{a}(\zeta) - \zeta \mathcal{B}(q_m)].$$

Adiabatic reweighting thus exhibits similarities with standard reweighting (1.4). The standard reweighting estimator in the expanded ensemble would be transposed as

$$\Upsilon_{\text{R}}^M(\mathcal{O}|0) = \frac{\frac{1}{M} \sum_{m=1}^M \mathcal{O}(0, q_m) \exp[\mathbf{a}(0) - \mathbf{a}(\zeta_m) + \zeta_m \mathcal{B}(q_m) - \ln \|A\|]}{\frac{1}{M} \sum_{m=1}^M \exp[\mathbf{a}(0) - \mathbf{a}(\zeta_m) + \zeta_m \mathcal{B}(q_m) - \ln \|A\|]}, \quad (1.22)$$

where $\|A\| = \sum_{\zeta \in \Lambda} 1$ is the cardinal of Λ . With the inclusion of this quantity, the denominator in (1.22) yields an estimate of the marginal probability $p_a^A(0)$, like the denominator of estimator (1.21).

The behavior of standard reweighting with that of adiabatic reweighting on a practical rare-event problem will be compared in subsection 2.3.3. We will observe that the former estimator is much more efficient than the latter estimator, by several orders of magnitude in the rare event context, due to improved overlapping properties of the marginal probability distribution when the auxiliary potential is adequately chosen. The question naturally arises as to which of the estimators described heretofore is the most accurate for any given auxiliary biasing potential from a statistical viewpoint.

To address this question, we first introduce a generic weighing function allowing us to define a large class of estimators which the conditioning approach will apply to. The standard binning and reweighting estimators will be two particular instances of this class of estimators.

1.10 Generic estimator for conditional expectations

The generic estimator of the conditional expectation of observable $\mathcal{O}(\lambda, \bar{q})$ given λ is based on the following generic weighing function

$$g_a^\lambda(\zeta, \bar{q}) = \frac{p_a(\lambda, \bar{q})}{p_a(\zeta, \bar{q})} K_{\lambda\zeta},$$

where the matrix $K_{\lambda\zeta}$ satisfies the condition

$$\sum_{\zeta \in \Lambda} K_{\lambda\zeta} = 1, \quad \forall \lambda \in \Lambda. \quad (1.23)$$

Owing to normalization (1.23), the expectation of g_a^λ is always equal to the marginal probability of the external parameter:

$$\mathbb{E}_a [g_a^\lambda] = \sum_{\zeta \in A} \int_{\mathcal{Q}} g_a^\lambda(\zeta, \bar{q}) p_a(\zeta, \bar{q}) d\bar{q} = p_a^A(\lambda). \quad (1.24)$$

Similarly, the following relation holds whatever the generic function:

$$\begin{aligned} \mathbb{E}_a [g_a^\lambda(\cdot, \cdot) \mathcal{O}(\lambda, \cdot)] &= \int_{\mathcal{Q}} \mathcal{O}(\lambda, \bar{q}) p_a(\lambda, \bar{q}) d\bar{q} \\ &= \mathbb{E}[\mathcal{O}(\lambda, \cdot) | \lambda] \times p_a^A(\lambda). \end{aligned}$$

This relation together with Eq. (1.24) allows to express the conditional expectation of \mathcal{O} given λ as a function of g_a^λ

$$\mathbb{E}[\mathcal{O} | \lambda] = \frac{\mathbb{E}_a [g_a^\lambda(\cdot, \cdot) \mathcal{O}(\lambda, \cdot)]}{\mathbb{E}_a [g_a^\lambda]}, \quad (1.25)$$

and to obtain the generic estimators by application of the ergodic theorem

$$\Upsilon_G^M(\mathcal{O} | \lambda) = \frac{\frac{1}{M} \sum_{m=1}^M g_a^\lambda(\zeta_m, \bar{q}_m) \mathcal{O}(\lambda, \bar{q}_m)}{\frac{1}{M} \sum_{m=1}^M g_a^\lambda(\zeta_m, \bar{q}_m)}, \quad (1.26)$$

where we considered a Markov chain $\{\zeta_m, \bar{q}_m\}_{1 \leq m \leq M}$ ergodic with respect to $p_a(\zeta, \bar{q})$.

The generic weighing estimator generalizes the binning estimator [27] and the standard reweighting estimator [8]. The binning estimator is obtained by setting the kernel matrix $K_{\lambda\zeta}$ to the identity matrix. The function $g_a^\lambda(\zeta, \bar{q})$ then reads

$$h_a^\lambda(\zeta, \bar{q}) \triangleq \mathbf{1}_\lambda(\zeta)$$

and we denote the corresponding estimator by $\Upsilon_H^M(\mathcal{O} | \lambda)$. The standard reweighting estimator of $\mathbb{E}[\mathcal{O} | \lambda]$, denoted by $\Upsilon_R^M(\mathcal{O} | \lambda)$, is obtained by setting the entries of the kernel matrix to the inverse of $\|A\| = \sum_{\zeta \in A} 1$, the cardinal of the discrete set A . Unlike the binning estimator $\Upsilon_H^M(\mathcal{O} | \lambda)$, the standard reweighting estimator $\Upsilon_R^M(\mathcal{O} | \lambda)$ includes information from all the sampled subensembles ($\zeta \in A$) owing to the standard reweighting function,

$$r_a^\lambda(\zeta, \bar{q}) = \frac{1}{\|A\|} \frac{\exp[\mathbf{a}(\lambda) - \mathbf{u}(\lambda, \bar{q})]}{\exp[\mathbf{a}(\zeta) - \mathbf{u}(\zeta, \bar{q})]}.$$

Thus, the factors $r_a^\lambda(\zeta_m, \bar{q}_m)$ must be used in place of the generic weighing factors $g_a^\lambda(\zeta_m, \bar{q}_m)$ in (1.26). This standard reweighting function with $\|A\| = 1$ is commonly used in umbrella sampling (see Sec. 1.5) or free energy perturbation techniques [13, 12, 14, 15] to rescale the contribution of states sampled with probability $\bar{q} \mapsto \pi(\bar{q} | \zeta)$ with respect to target probability $\bar{q} \mapsto \pi(\bar{q} | \lambda)$ inside the estimator. The forthcoming derivations involving the generic estimator will cover binning and standard reweighting as two particular remarkable cases. We show in Subsection 1.11.3 that the adiabatic reweighting estimator can be constructed from the generic estimator through the *conditioning* procedure of probability theory and that this guarantees a reduction of the asymptotic variance. We complete the study by proving variance reduction with respect to STWHAM [35], a self-consistent estimator dedicated to expanded ensemble simulations. Prior to showing how *conditioning* is done within the generic and self-consistent reweighting estimator, we first describe in Subsection 1.11.1 a simple conditioning scheme and prove variance reduction in the estimation of the marginal probability of λ .

1.11 Conditioning and variance reduction

1.11.1 Estimating the marginal probability of λ

Let consider a sample $\{\zeta_m, \bar{q}_m\}_{1 \leq m \leq M}$ drawn from the distribution of probability mass $p_a(\zeta, \bar{q})$ using a Metropolis Monte Carlo algorithm or a Langevin process. The generic estimator for estimating $p_a^A(\lambda)$ consists of evaluating the arithmetic mean of g_a , denoted by

$$\mathbb{I}^M(g_a^\lambda) = \frac{1}{M} \sum_{m=1}^M g_a^\lambda(\zeta_m, \bar{q}_m), \quad (1.27)$$

where we applied the ergodic theorem to relation (1.24). Let also simplify the notation of the conditional probability of λ given q by using

$$\pi_a^\lambda(q) = \frac{\exp[\alpha(\lambda) - \mathcal{U}(\lambda, q)]}{\sum_{\zeta \in \Lambda} \exp[\alpha(\zeta) - \mathcal{U}(\zeta, q)]}$$

instead of $\pi_a(\lambda|q)$. The conditionally expected value of g_a^λ given q is the conditional probability of λ given q

$$\mathbb{E}_a[g_a^\lambda(\cdot, q)|q] = \pi_a^\lambda(q). \quad (1.28)$$

Besides, the expected value of g_a^λ is the expected value of π_a^λ (law of total expectation)

$$\mathbb{E}_a[g_a^\lambda] = \mathbb{E}_a^\mathcal{Q}[\mathbb{E}_a[g_a^\lambda(\cdot, q)|q]] = \mathbb{E}_a^\mathcal{Q}[\pi_a^\lambda] = \mathbb{E}_a[\pi_a^\lambda],$$

where we first resorted to Eq. (A.1) with $\mathcal{O}(\cdot, q)$ set to $\mathbb{E}_a[g_a^\lambda(\cdot, q)|q]$. Interestingly, the last term in the sequence of equalities above means that for estimating $\mathbb{E}_a[g_a^\lambda]$, it is possible to replace $g_a^\lambda(\zeta_m, \bar{q}_m)$ in Eq. (1.27) by $\pi_a^\lambda(\bar{q}_m)$. It is precisely this replacement scheme that is referred to as *conditioning*. Estimating the marginal probability of λ with the conditioning scheme therefore consists of evaluating the following quantity

$$\mathbf{I}^M(\pi_a^\lambda) = \frac{1}{M} \sum_{m=1}^M \pi_a^\lambda(\bar{q}_m).$$

The equality between expectations $\mathbb{E}_a^\mathcal{Q}[\pi_a^\lambda]$ and $\mathbb{E}_a[\pi_a^\lambda]$ indicates that the arithmetic estimator can still be employed using a configuration chain $Q^T = \{\bar{q}_m\}_{1 \leq m \leq M}$ distributed according to the marginal probability $p_a^\mathcal{Q}(q)$. Superscript T stands for transposition so that Q is a column stochastic vector.

In general, the sampled configurations are *identically* but *not independently* distributed. This implies that the covariance matrix of Q is non diagonal in general (see Lemma A.2.1 for the definition of the covariance matrix of a random vector). Denoting the vector encompassing the sampled factors by $G = \{g_a^\lambda(\zeta_m, \bar{q}_m)\}_{1 \leq m \leq M}^T$ and the M -dimensional vector whose components are equal to M^{-1} by e_M , the quantities $\mathbf{I}^M(g_a^\lambda)$ and $\mathbf{I}^M(\pi_a^\lambda)$ can be re-written as $e_M^T G$ and $\mathbb{E}_a(e_M^T G|Q)$, respectively. The statistical variances of estimators $\mathbf{I}^M(g_a^\lambda)$ and $\mathbf{I}^M(\pi_a^\lambda)$ are then

$$\mathbb{V}_a[\mathbf{I}^M(g_a^\lambda)] = \mathbb{V}_a[e_M^T G], \quad (1.29)$$

$$\mathbb{V}_a[\mathbf{I}^M(\pi_a^\lambda)] = \mathbb{V}_a^\mathcal{Q}[\mathbb{E}_a(e_M^T G|Q)], \quad (1.30)$$

where the variance \mathbb{V}_a is defined in Eq. A.3 of the Appendix. The reduction of the variance through conditioning stems from the law of total variance (A.2). Setting \mathcal{O} to $e_M^T G$, the law writes

$$\mathbb{V}_a[e_M^T G] = \mathbb{E}_a^\mathcal{Q}[\mathbb{V}_a[e_M^T G|Q]] + \mathbb{V}_a^\mathcal{Q}[\mathbb{E}_a(e_M^T G|Q)]. \quad (1.31)$$

The variance reduction is thus equal to the expected conditional variance, a strictly positive quantity in practical applications:

$$\mathbb{E}_a^\mathcal{Q}[\mathbb{V}_a[e_M^T G|Q]] > 0. \quad (1.32)$$

The equality is reached when, for any given sample Q , $e_M^T G$ is constant. This is assumed to be never the case, otherwise a sampling strategy would no be justified. Equality (1.31) and inequality (1.32) thus imply the following strict inequality between the variance of the two estimators in (1.29) and (1.30)

$$\mathbb{V}_a[\mathbf{I}^M(g_a^\lambda)] > \mathbb{V}_a[\mathbf{I}^M(\pi_a^\lambda)].$$

Hence, the statistical variance associated with the arithmetic mean of the generic function is always larger than that associated with arithmetic mean of the conditional probabilities of λ , whatever the value of the biasing potential. It is therefore always preferable to use an estimator obtained through conditioning, provided that the overhead associated with the evaluation of the conditional expectation given the sampled states is small enough. The cost of conditioning becomes substantial in practice when the dimension of Λ exceeds two or three. In this situation, the reduction of the variance may not be important enough to justify implementing a conditioning

scheme. In the following, we always assume that performing the numerical quadrature integration within the conditioning scheme has a negligible cost compared to the one of evaluating the potential energy and its gradient. Assuming that the sampled configurations are *identically* and *independently distributed* (i.i.d) entails that the covariance matrix of G is diagonal. The statistical variances of the considered estimators therefore take the following simple forms

$$\begin{aligned}\mathbb{V}_a [\mathbf{I}^M(g_a^\lambda)] &= \frac{1}{M} \mathbb{V}_a [g_a^\lambda], \\ \mathbb{V}_a [\mathbf{I}^M(\pi_a^\lambda)] &= \frac{1}{M} \mathbb{V}_a [\pi_a^\lambda].\end{aligned}$$

The i.i.d. assumption is made from now so as to facilitate the comparison of the estimator variances in the asymptotic limit of large sample sizes. It will not modify the various inequalities which will be derived to compare the asymptotic variances of the generic and conditioned estimators.

1.11.2 Visualization of the expected conditional variance

Conditioning can be applied to the estimation of any quantity, like for instance the expected value of the external parameter in the expanded ensemble. Let $\{(\zeta_m, q_m)\}_{1 \leq m \leq M}$ be a iid sample of extended states drawn from $p_a(\zeta, q)$ distribution in which the extended potential energy has the form $\mathcal{U}_a(\zeta, q) = \omega q^2 + \frac{\kappa}{2} (\zeta - \alpha q)^2$ with α set to 0. This entails that each extended state $\{\zeta_m, q_m\}$ corresponds to a pair of two correlated normal variables. The variance of the standard estimator writes

$$\mathbb{V}_a [\mathbf{I}^M(\zeta)] = \mathbb{V}_a \left[\frac{1}{M} \sum_{m=1}^M \zeta_m \right] = \frac{1}{M} \mathbb{V}_a [\zeta]$$

while the variance of the conditioned estimator is

$$\mathbb{V}_a [\mathbf{I}^M(\mathbb{E}_a[\zeta|q])] = \left[\frac{1}{M} \sum_{m=1}^M \mathbb{E}_a[\zeta|q_m] \right] = \frac{1}{M} \mathbb{V}_a [\mathbb{E}_a[\zeta|q]].$$

The reduction of variance through conditioning can be visualized in figure 1.2 in which the sampled states have been displayed. Variance reduction is guaranteed by the law of total variance

$$\mathbb{V}_a[\zeta] = \mathbb{V}_a[\mathbb{E}_a[\zeta|q]] + \mathbb{E}_a[\mathbb{V}_a[\zeta|q]].$$

The two variances and the expected conditional variance above are equal to the areas of the three central squares in figure 1.2, as indicated by the legend. The lengths of the square edges thus correspond to standard deviations. The expected value of the ζ -component of the blue arrows is equal to $\mathbb{E}_a[\zeta - \mathbb{E}_a[\zeta|q]]$ which is 0. The variance of the arrow component is thus equal to the expected value of the conditional variance

$$\mathbb{V}_a[\zeta - \mathbb{E}_a[\zeta|q]] = \mathbb{E}_a \left[\mathbb{E}_a \left[(\zeta - \mathbb{E}_a[\zeta|q])^2 | q \right] \right] = \mathbb{E}_a[\mathbb{V}_a[\zeta|q]],$$

which is precisely the area of the blue square in figure 1.2. The variance reduction is $\frac{1}{M} \mathbb{E}_a[\mathbb{V}_a[\zeta|q]]$.

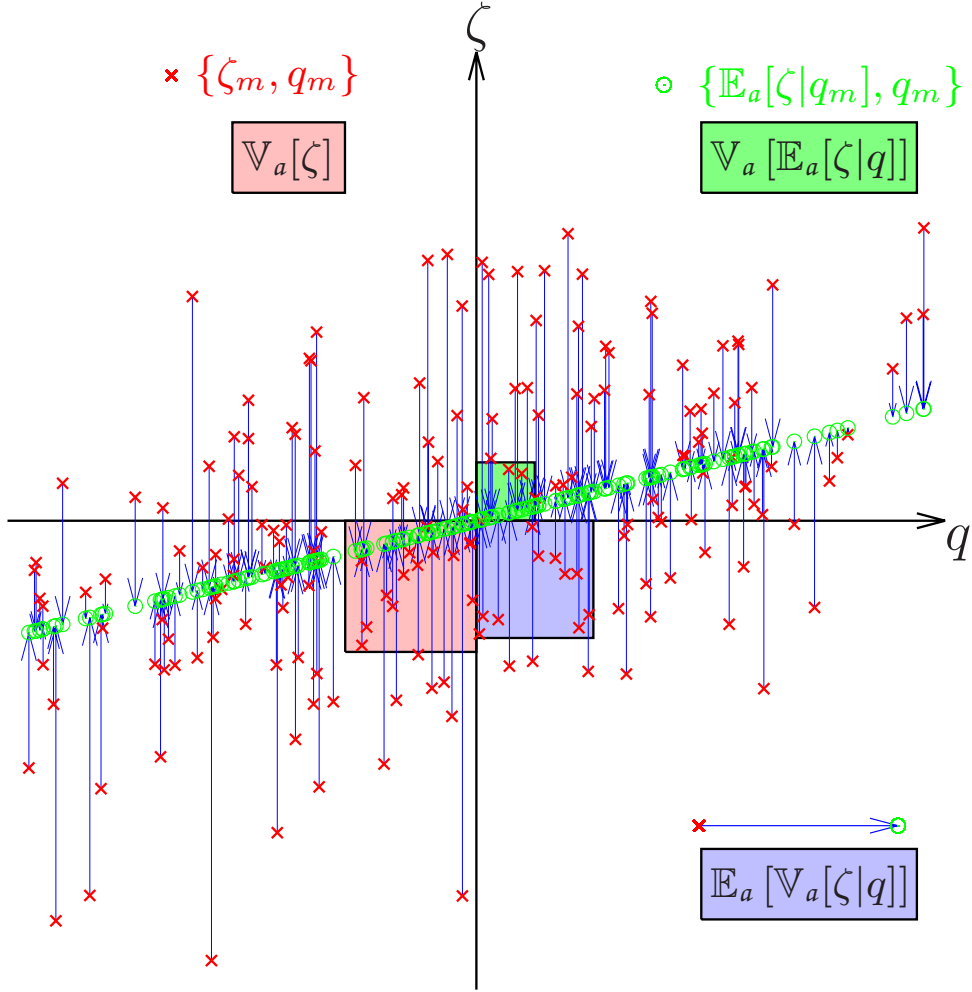


Figure 1.2: Illustration of variance reduction through conditioning for estimating the expected value of ζ . The \times symbols represent the sampled points.

1.11.3 Estimation of conditional expectations

Standard reweighting, binning and generic weighing

Conditioning for estimating the conditional expectations of \mathcal{O} given λ consists in substituting the conditional expectation given the sampled states for the sampled values of the generic function in the generic estimator of Eq. 1.26. Thus, substituting $\pi_a^\lambda(\bar{q}_m)$ for $g_a^\lambda(\zeta_m, \bar{q}_m)$ yields the adiabatic reweighting estimator of $\mathbb{E}[\mathcal{O}|\lambda]$:

$$\Upsilon_{\text{II}}^M(\mathcal{O}|\lambda) = \frac{\frac{1}{M} \sum_{m=1}^M \pi_a^\lambda(\bar{q}_m) \mathcal{O}(\lambda, \bar{q}_m)}{\frac{1}{M} \sum_{m=1}^M \pi_a^\lambda(\bar{q}_m)}, \quad (1.33)$$

where we used a Markov chain $\{\zeta_m, \bar{q}_m\}_{1 \leq m \leq M}$ distributed according to $p_a(\zeta, \bar{q})$, or a configuration chain $\{\bar{q}_m\}_{1 \leq m \leq M}$ distributed according to the marginal $p_a^\mathcal{Q}(\bar{q})$. The substitution that is done amounts to plugging the law of total expectation both in the numerator and the denominator of Eq. (1.25),

$$\mathbb{E}[\mathcal{O}|\lambda] = \frac{\mathbb{E}_a^\mathcal{Q} [\mathbb{E}_a [g_a^\lambda(\cdot, q) \mathcal{O}(\lambda, q) | q]]}{\mathbb{E}_a^\mathcal{Q} [\mathbb{E}_a [g_a^\lambda(\cdot, q) | q]]} = \frac{\mathbb{E}_a [\pi_a^\lambda(\cdot) \mathcal{O}(\lambda, \cdot)]}{\mathbb{E}_a [\pi_a^\lambda]}.$$

The AR estimator can alternatively be viewed as an instance of waste-recycling Monte Carlo [2, 9] when the ζ_m are sampled directly from the conditional probabilities $\zeta \mapsto \pi_a^\zeta(\bar{q}_m)$ at each given \bar{q}_m as suggested in Ref. [36]: the wasted information relative to rejected trial moves for $\zeta \in \Lambda$ is recycled in the estimator. However, resorting to such a Gibbs sampler [37] is not a necessary prescription and any sampler satisfying the detailed balance condition can possibly be used. In fact, adiabatic reweighting amounts to performing virtual Monte Carlo moves

and can be viewed as a particular instance of the virtual-move Monte Carlo method proposed in Ref. [38].

The present conditioning scheme entails variance reduction in the asymptotic limit of large sample sizes. To prove this property, we will compare the asymptotic variance of the adiabatic reweighting estimator (Eq. (1.33)) to that of the generic estimator (Eq. (1.26)). The present situation differs from that of subsection 1.11.1 wherein reduction was guaranteed for any sample sizes. The difficulty is due to the presence of a denominator in Eqs. (1.26) and (1.33). Let us assume that the function $q \mapsto \mathcal{O}(\lambda, q)$ is non-constant (otherwise sampling would not be necessary) and introduce the centered observable $\mathcal{O}^\lambda(q) = \mathcal{O}(\lambda, q) - \mathbb{E}[\mathcal{O}|\lambda]$, a quantity centered on the value of the conditional expectation given λ . Then, the quantity $\mathcal{O}^\lambda g_a^\lambda$ is centered with respect to the total expectation. We have

$$\mathbb{E}_a[g_a^\lambda \mathcal{O}^\lambda] = \mathbb{E}_a^\mathcal{Q} \left[\mathbb{E}_a[g_a^\lambda(\cdot, q) \mathcal{O}^\lambda(q)|q] \right] = \mathbb{E}_a^\mathcal{Q} [\pi_a^\lambda(\cdot) \mathcal{O}(\lambda, \cdot)] - \mathbb{E}(\mathcal{O}|\lambda) p_a^A(\lambda) = 0.$$

Let us now assume that the generated Markov chains $\{\zeta_m, \bar{q}_m\}_{1 \leq m \leq M}$ consist of a sequences of random variables that are i.i.d. according to $p_a(\zeta, \bar{q})$. Then, the variance of the arithmetic mean of $g_a^\lambda(\zeta_m, \bar{q}_m) \mathcal{O}^\lambda(\bar{q}_m)$ multiplied by M decomposes into the variance of $g_a^\lambda(\zeta, \bar{q}) \mathcal{O}^\lambda(\bar{q})$:

$$M \mathbb{V}_a \left[\frac{1}{M} \sum_{m=1}^M g_a^\lambda(\zeta_m, \bar{q}_m) \mathcal{O}^\lambda(\bar{q}_m) \right] = \mathbb{V}_a [g_a^\lambda \mathcal{O}^\lambda].$$

In the limit of large sample sizes, the variance of the $\sqrt{M} \Upsilon_G^M(\mathcal{O}|\lambda)$ quantity becomes equivalent to the following variance

$$M \mathbb{V}_a [\Upsilon_G^M(\mathcal{O}|\lambda)] \underset{M \rightarrow +\infty}{\sim} \mathbb{V}_a \left[\frac{g_a^\lambda \mathcal{O}^\lambda}{\mathbb{E}_a[g_a^\lambda]} \right]. \quad (1.34)$$

The limit of the left-hand side term of Eq. (1.34) as M tends to infinity is called the asymptotic variance of the $\Upsilon_G^M(\mathcal{O}|\lambda)$ estimator. The square-root of the asymptotic variance corresponds to the asymptotic standard error and writes

$$\sigma_a [\Upsilon_G^\infty(\mathcal{O}|\lambda)] = \frac{1}{p_a^A(\lambda)} \sqrt{\mathbb{V}_a [g_a^\lambda \mathcal{O}^\lambda]}, \quad (1.35)$$

where we have substituted $p_a^A(\lambda)$ for $\mathbb{E}_a(g_a^\lambda)$. This mathematical result is a consequence of the delta method (see Appendix A). More precisely, the delta method states that the following convergence in law holds

$$\frac{\frac{1}{M} \sum_{m=1}^M g_a^\lambda(\zeta_m, \bar{q}_m) \mathcal{O}^\lambda(\bar{q}_m)}{\frac{1}{M} \sum_{m=1}^M g_a^\lambda(\zeta_m, \bar{q}_m)} \underset{M \rightarrow +\infty}{\xrightarrow{\mathcal{L}}} \mathcal{N}(\mathbb{E}[\mathcal{O}|\lambda], \sigma_a^2 [\Upsilon_G^\infty(\mathcal{O}|\lambda)]),$$

where $\mathcal{N}(\mu, \varsigma)$ denotes the normal law of mean μ and variance ς . Similarly, the asymptotic error of the adiabatic reweighting estimator is, with i.i.d. assumption again,

$$\sigma_a [\Upsilon_\Pi^\infty(\mathcal{O}|\lambda)] = \frac{1}{p_a^A(\lambda)} \sqrt{\mathbb{V}_a [\pi_a^\lambda \mathcal{O}^\lambda]}. \quad (1.36)$$

To compare the two asymptotic errors, we resort to the law of total variance as in subsection 1.11.1, but with respect to $\mathcal{O}^\lambda g_a^\lambda$ quantity in place of g_a^λ . The law states that the total variance is equal to the sum of the expectation of the conditional variances given q and the variance of the conditional expected values given q :

$$\mathbb{V}_a(g_a^\lambda \mathcal{O}^\lambda) = \mathbb{E}_a^\mathcal{Q} [\mathbb{V}_a(g_a^\lambda(\cdot, q) \mathcal{O}^\lambda(q)|q)] + \mathbb{V}_a^\mathcal{Q} [\mathbb{E}_a(g_a^\lambda(\cdot, q) \mathcal{O}^\lambda(q)|q)].$$

Plugging Eq. (1.28) into the law of total variance leads to

$$\mathbb{V}_a [\pi_a^\lambda \mathcal{O}^\lambda] = \mathbb{V}_a [g_a^\lambda \mathcal{O}^\lambda] - \mathbb{E}_a^\mathcal{Q} [\mathbb{V}_a [g_a^\lambda \mathcal{O}^\lambda|q]]. \quad (1.37)$$

The function $q \mapsto \mathcal{O}^\lambda(q)$ being non-constant and the conditional variance of g_a^λ being strictly positive for all q , the last expectation above is strictly positive. Thus, $\mathbb{V}_a(\pi_a^\lambda \mathcal{O}^\lambda)$ is strictly lower than $\mathbb{V}_a(g_a^\lambda \mathcal{O}^\lambda)$. From identities (1.35), (1.36) and (1.37), we deduce the following strict inequality between the asymptotic errors of the estimators

$$\sigma_a [\Upsilon_\Pi^\infty(\mathcal{O}|\lambda)] < \sigma_a [\Upsilon_G^\infty(\mathcal{O}|\lambda)].$$

It is therefore always preferable to use the adiabatic reweighting estimator rather than the binning, standard reweighting or generic estimators. We now go on by discussing the relevance of implementing self-consistent reweighting estimators in combination with expanded ensemble simulations.

Self-consistent reweighting

To estimate conditional expectations in expanded ensemble simulations with high accuracy, it has been suggested by Chodera *et al.* [35] to implement the self-consistent reweighting estimator WHAM. The original WHAM approach consists of performing a number of independent simulations for each $\lambda \in \Lambda$ and pooling the generated samples into a single sample whose total size is $M = \sum_{\lambda \in \Lambda} M_\lambda$. The M_λ quantities are the sizes of the λ -samples, the original samples generated at constant λ using the independent simulations. These sizes are crucial input parameters in self-consistent reweighting estimators together with the pooled sample. Since a single simulation is performed in the expanded ensemble, it has been proposed to estimate the λ -sample sizes through standard histogram binning (see Eq. 1.27)

$$M_\lambda = \sum_{m=1}^M \mathbf{1}_\lambda(\zeta_m) = M \mathbf{I}^M(\mathbf{1}_\lambda), \quad \lambda \in \Lambda.$$

The collected data are then postprocessed using WHAM. The overall procedure [35] is referred to as *simulated tempering WHAM* (STWHAM). Resorting to the bin-less formulation [18, 22] of WHAM, the self-consistent reweighting estimator of $\mathbb{E}[\mathcal{O}|\lambda]$ can be cast into the following form

$$\Upsilon_{\text{SC}}^M(\mathcal{O}|\lambda) = \sum_{m=1}^M \frac{\mathcal{O}(\lambda, \bar{q}_m) \exp[\widehat{\mathfrak{F}}(\lambda) - \mathbf{u}(\lambda, \bar{q}_m)]}{\sum_{\zeta \in \Lambda} M_\zeta \exp[\widehat{\mathfrak{F}}(\zeta) - \mathbf{u}(\zeta, \bar{q}_m)]}, \quad (1.38)$$

where the quantities $\widehat{\mathfrak{F}}(\zeta)$ for $\zeta \in \Lambda$ are the estimated free energies. They are given by the solutions (up to a common constant) to the following set of nonlinear equations:

$$\Upsilon_{\text{SC}}^M(\mathbf{1}|\lambda) = 1, \quad \lambda \in \Lambda. \quad (1.39)$$

System (1.39) is equivalent to

$$\mathbf{I}^M(\pi_{\widehat{\mathbf{a}}}^\lambda) = \mathbf{I}^M(\mathbf{1}_\lambda), \quad \lambda \in \Lambda. \quad (1.40)$$

where the unknown function $\widehat{\mathbf{a}}(\lambda)$ stands for the quantity $\widehat{\mathfrak{F}}(\lambda) + \ln M_\lambda$ in Eq (1.38). Since the λ -sample sizes M_λ are stochastic quantities in the STWHAM estimator (1.38), it is legitimate to do some conditioning on them and to use as input data

$$\widehat{M}_\lambda = \sum_{m=1}^M \frac{\exp[\mathbf{a}(\lambda) - \mathbf{u}(\lambda, \bar{q}_m)]}{\sum_{\zeta \in \Lambda} \exp[\mathbf{a}(\zeta) - \mathbf{u}(\zeta, \bar{q}_m)]} = M \mathbf{I}^M(\pi_{\widehat{\mathbf{a}}}^\lambda),$$

instead of M_λ for $\lambda \in \Lambda$. We show in Appendix A.6 that conditioning the self-consistent reweighting estimator further reduces its asymptotic statistical variance. Besides, conditioning amounts to substituting $\mathbf{I}^M(\pi_{\widehat{\mathbf{a}}}^\lambda)$ for $\mathbf{I}^M(\mathbf{1}_\lambda)$ in system (1.40). This entails that the self-consistent solutions $\widehat{\mathbf{a}}(\lambda)$ become equal to $\mathbf{a}(\lambda)$ (up to a common additive constant). The conditioned self-consistent reweighting estimator is therefore obtained by substituting $\mathbf{a}(\lambda) - \ln \widehat{M}_\lambda$ for $\widehat{\mathfrak{F}}(\lambda)$ and \widehat{M}_λ for M_λ in the unconditioned self-consistent reweighting estimator (1.38). These two substitutions enable one to recover the AR estimator (1.33) as shown below:

$$\begin{aligned} \Upsilon_{\text{SC}}^{\widehat{M}}(\mathcal{O}|\lambda) &= \sum_{m=1}^M \frac{\mathcal{O}(\lambda, \bar{q}_m) \exp[\mathbf{a}(\lambda) - \ln \widehat{M}_\lambda - \mathbf{u}(\lambda, \bar{q}_m)]}{\sum_{\zeta \in \Lambda} \widehat{M}_\zeta \exp[\mathbf{a}(\zeta) - \ln \widehat{M}_\zeta - \mathbf{u}(\zeta, \bar{q}_m)]} = \\ &= \frac{\frac{1}{M} \sum_{m=1}^M \mathcal{O}(\lambda, \bar{q}_m) \frac{\exp[\mathbf{a}(\lambda) - \mathbf{u}(\lambda, \bar{q}_m)]}{\sum_{\zeta \in \Lambda} \exp[\mathbf{a}(\zeta) - \mathbf{u}(\zeta, \bar{q}_m)]}}{\frac{1}{M} \sum_{m=1}^M \frac{\exp[\mathbf{a}(\lambda) - \mathbf{u}(\lambda, \bar{q}_m)]}{\sum_{\zeta \in \Lambda} \exp[\mathbf{a}(\zeta) - \mathbf{u}(\zeta, \bar{q}_m)]}} = \frac{\frac{1}{M} \sum_{m=1}^M \pi_{\widehat{\mathbf{a}}}^\lambda(\bar{q}_m) \mathcal{O}(\lambda, \bar{q}_m)}{\frac{1}{M} \sum_{m=1}^M \pi_{\widehat{\mathbf{a}}}^\lambda(\bar{q}_m)} = \Upsilon_{\text{II}}^M(\mathcal{O}|\lambda). \end{aligned}$$

To summarize, the use of the conditioned λ -sample sizes in STWHAM provides a reduction of the statistical variance (see Appendix A.6), and, concomitantly, the task of solving a large set of nonlinear equations is avoided because the self-consistent reweighting with conditioning amounts to adiabatic reweighting. More generally, *conditioning* the expectations associated with the binning, standard reweighting and self-consistent reweighting estimators reduces the statistical variances in the analysis of *expanded ensemble simulations* and leads to the formulation of the identical adiabatic reweighting estimator. Adiabatic reweighting is thus asymptotically optimal among the large class of considered estimators.

1.12 Summary

Molecular simulations such as MD or MC are often plagued by ergodicity issues making the estimation of thermodynamic averages unreliable. The two main causes of broken ergodicity are metastability and small distribution tails. This results in the rare occurrence of the physically interesting events. Enhanced sampling algorithms in combination with efficient estimators are often employed to speedup the convergence of simulations. The principle is often the following: some biased or perturbed systems are sampled so as to achieve ergodicity artificially and then an accurate estimate of the desired thermodynamic average is recovered using an unbiasing procedure. In difficult problems, an external parameter is used to tune the strength of the bias perturbing the system. This naturally leads to defining an extended potential energy framework in which two simulation approaches can be envisaged:

- performing replica exchange simulations to sample the thermodynamic states corresponding to a set of values for the external parameter and implementing a self-consistent estimator (MBAR or WHAM) to compute the desired thermodynamic averages through post-processing of the information contained in the sampled states;
- performing simulations in an expanded ensemble wherein the external parameter is an additional coordinate and estimating the conditional expectations online using a conditioning scheme.

Because thermodynamic estimates are obtained straightforwardly with the conditioning procedure, the second approach obviates the need of post-processing the collected data. However, an auxiliary biasing potential allowing homogeneous sampling along the external parameter needs instead to be constructed with the help of a preliminary run (preprocessing). In practice, the biasing potential is adapted on the current estimate of the free energy or of its gradient, as briefly mentioned in subsections 1.9.2 and 1.9.3. We show in Chapter 2 how to efficiently compute free energies using the conditioning technique and in Chapter 3 how to construct an adequate biasing potential using adaptively biased sampling techniques.

2 | From free energies to probabilities and expectations

2.1 On the relativity of free energies

In this Chapter, we discuss the possible ways of calculating the free energies along λ within the expanded ensemble. We assume that the auxiliary biasing potential is constant, i.e. that it does not vary in the course of the simulation. We have shown in Chapter 1 that the absolute free energies $\mathfrak{F}(\lambda)$, up to an undetermined and unimportant constant, can be estimated for $\lambda \in \Lambda$ by solving self-consistent system. The common additive constant remains undetermined because the absolute free energy defined in can not conveniently be cast in the form of an expectation within the expanded ensemble framework. Fortunately, this indetermination is armless in practice because one is essentially interested in differences of free energies between two or several thermodynamic states. In order to rationally review the various free energy techniques of the literature, we found it more judicious and convenient to adopt Landau's viewpoint [39, 14] and to define the free energy as the cologarithm of the expected indicator value:

$$\mathcal{A}(\lambda) = -\ln \mathbb{E}[\mathbf{1}_\lambda], \quad (2.1)$$

reminding that the indicator function takes output value 1 if input value ζ is equal to λ and 0 otherwise. The total expectation denoted by \mathbb{E} is defined in (1.12). It coincides with the total expectation \mathbb{E}_α when $\alpha(\lambda)$ is set to 0. The joint probabilities $p(\lambda, q)$ and $p_0(\lambda, q)$ are identical. Noticing that the expected value of $\mathbf{1}_\lambda(\zeta)$ is the marginal probability of λ whose expression is given in (1.11) yields

$$\mathcal{A}(\lambda) = -\ln p^A(\lambda) = \mathfrak{F}(\lambda) - \ln \sum_{\zeta \in \Lambda} \exp[-\mathfrak{F}(\zeta)].$$

Differences of free energies are not affected by the logarithmic term and can be estimated considering the absolute or relative viewpoint:

$$\mathcal{A}(\lambda) - \mathcal{A}(\zeta) = \mathfrak{F}(\lambda) - \mathfrak{F}(\zeta).$$

However, due to the finiteness of Λ , the derivative of the relative free energy is not strictly equal to the derivative of the absolute free energy which corresponds to a mean force along λ :

$$\mathcal{A}'(\lambda) = \mathfrak{F}'(\lambda) [1 - p^A(\lambda)] \approx \mathfrak{F}'(\lambda) = \mathbb{E}[\partial_\lambda \mathcal{U}(\lambda, q) | \lambda].$$

In practice, we assume that the set $\|A\|$ is large enough so that the marginal probability of λ is negligible and the derivative of the absolute and relative free energies will be considered to be each other equal.

It is worth mentioning that the Landau free energy along a reaction coordinate $\xi(q)$ exhibits a form similar to (2.1) and writes:

$$\mathcal{F}(\xi^*) = -\ln \mathbb{E}[\mathbf{1}_{\xi^*} \circ \xi].$$

Calculations of the free energy along a bond-orientational order parameter are described in Chapter 3 using the expanded ensemble method with harmonic coupling setup.

The concept of relative free energy is universal. It similarly applies to state-to-state time correlations in dynamical processes. This is because the time correlations between let say state $A \subset \mathcal{Q}$ and state $B \subset \mathcal{Q}$ correspond to the probabilities of observing a transition from A to B during the considered elapsed time t . To formalize this probability, let $t \in \mathbb{R} \mapsto q_t \in \mathcal{Q}$ denote the dynamical process, \mathcal{S} denote a subset of the

configuration space ($\mathbf{S} \subset \mathcal{Q}$) and $\chi_{\mathbf{S}}(q)$ be the characteristic function that takes value 1 if $q \in \mathbf{S}$ and 0 otherwise. Then, the free energy associated with the A-to-B time correlation function is defined by

$$\mathcal{F}(\mathbf{B}, t, \mathbf{A}, 0) = -\ln \mathbb{E}^* [\chi_{\mathbf{B}}(q_t)\chi_{\mathbf{A}}(q_0)] \quad (2.2)$$

where expectation \mathbb{E}^* refers to a time average over the involved dynamical process. By assigning a free energy to a rare-event probability (2.2), the idea of applying standard free energy techniques to the calculations of time correlation functions comes naturally [6]. This approach is referred to as the *transition path sampling* (TPS) method, introduced by Bolhuis, Chandler, Dellago and Geissler and reviewed by these authors in Ref. [7]. The TPS approach is useful when the available reaction coordinates are not reliable. In this situation, restraining or constraining the system using a bad reaction coordinate (BRC) on a multidimensional potential energy surface often breaks numerical ergodicity. An illustration of this issue will be given in Sec. 3.2. A free energy barrier computed along a BRC usually underestimates the activation free energy, i.e. the true free energy barrier yielding the rate of thermally activated reactive events. We show in Sec. 2.3 how to straightforwardly estimate a state-to-state time correlation function based on a conditioning procedure. This is achieved by casting this function in the form of a conditional expectation of the characteristic function $\chi_{\mathbf{B}}$ within an appropriate expanded transition path ensemble. The main difficulty of the proposed approach lies in the construction of a biasing path functional that sufficiently increases the fraction of paths ending in the product state, for which $\chi_{\mathbf{B}}(q_t)$ is 1. An expanded transition path sampling method fulfilling this requirement will be presented in Chapter 4 together with an application to the migration of a vacancy in α -iron and a comparison with the transition rates obtained using transition state theory, which is discussed in Sec. 4.5.

Outline of the Chapter We show first how to construct conditioned estimators for computing total expectations, relative free energies (2.1) and rare-event probabilities (2.2). We then assess the performance of the estimators on a toy model, and explain the efficiency of the conditioning procedure by resorting to a fluctuation theorem of statistical mechanics.

2.2 Conditioning and variance reduction

2.2.1 Estimation of total expectations

We consider first the estimation of total expectations of the form given in Eq. (1.12) using expanded ensemble simulations. The involved observable may for instance be some indicator functions when occupation probabilities need being calculated along an external parameter or an internal reaction coordinate. The questions then arise as to (i) how to transpose the generic estimator, (ii) how to condition the transposed estimator and (iii) whether conditioning achieves variance reduction.

To answer question (i), we decompose the total expectation of \mathcal{O} resorting to the law of total expectation (1.12) on $\lambda \equiv \zeta$, as in the stratification approach detailed in Sec. 1.8, but we plug instead the expectation ratio (1.25) that involves the weighing function g_a^λ . This yields

$$\mathbb{E}[\mathcal{O}] = \sum_{\lambda \in \Lambda} \frac{\mathbb{E}_a [g_a^\lambda(\cdot, \cdot)\mathcal{O}(\lambda, \cdot)]}{\mathbb{E}_a [g_a^\lambda]} p_0^A(\lambda). \quad (2.3)$$

The unbiased marginal probability of λ that appears in the right-hand side (rhs) term is now expressed as a function of the marginal probability of λ with the biasing potential switched on

$$p_0^A(\lambda) = \frac{e^{-a(\lambda)} p_a^A(\lambda)}{\sum_{\lambda^* \in \Lambda} e^{-a(\lambda^*)} p_a^A(\lambda^*)} = \frac{e^{-a(\lambda)} \mathbb{E}_a [g_a^\lambda]}{\mathbb{E}_a [\sum_{\lambda^* \in \Lambda} e^{-a(\lambda^*)} g_a^{\lambda^*}]}.$$

Inserting the last term above into the rhs term of equation (2.3) and eventually permuting the expectation \mathbb{E}_a and the sum $\sum_{\lambda \in \Lambda}$ yields

$$\mathbb{E}[\mathcal{O}] = \frac{\mathbb{E}_a [\sum_{\lambda \in \Lambda} \mathcal{O}(\lambda, \cdot) e^{-a(\lambda)} g_a^\lambda(\cdot, \cdot)]}{\mathbb{E}_a [\sum_{\lambda \in \Lambda} e^{-a(\lambda)} g_a^\lambda]}. \quad (2.4)$$

To manipulate such total expectations, it is more convenient to multiply the previously employed weighing

functions $(\mathbf{1}_\lambda, r_a^\lambda, g_a^\lambda$ and $\pi_a^\lambda)$ by $\exp[-\mathbf{a}(\lambda)]$. The modified weighing functions are denoted by $h_a^\lambda, r_a^\lambda, g_a^\lambda$ and π_a^λ , respectively. The employed notations with their definitions are compiled in Table 2.1. Inserting the functions $g_a^\lambda(\zeta, \bar{q}) = e^{-\mathbf{a}(\lambda)} g_a^\lambda(\zeta, \bar{q})$ and $g_a(\zeta, \bar{q}) = \sum_{\lambda \in \Lambda} g_a^\lambda(\zeta, \bar{q})$ into equation (2.4) yields

$$\mathbb{E}[\mathcal{O}] = \frac{\mathbb{E}_a \left[\sum_{\lambda \in \Lambda} \mathcal{O}(\lambda, \cdot) g_a^\lambda(\cdot, \cdot) \right]}{\mathbb{E}_a [g_a]}. \quad (2.5)$$

We are now in a position to formulate the estimator of the total expectation based on relation (2.5):

$$\Upsilon_G^M(\mathcal{O}) = \frac{\frac{1}{M} \sum_{m=1}^M \sum_{\lambda \in \Lambda} \mathcal{O}(\lambda, \bar{q}_m) g_a^\lambda(\zeta_m, \bar{q}_m)}{\frac{1}{M} \sum_{m=1}^M g_a(\zeta_m, \bar{q}_m)}, \quad (2.6)$$

where $\{\zeta_m, \bar{q}_m\}_{1 \leq m \leq M}$ is a Markov chain generated according to the probability distribution $p_a(\zeta, \bar{q})$.

We have in particular for the binning estimator of $\mathbb{E}[\mathcal{O}]$

$$\Upsilon_H^M(\mathcal{O}) = \frac{\frac{1}{M} \sum_{m=1}^M \mathcal{O}(\zeta_m, \bar{q}_m) \exp[-\mathbf{a}(\zeta_m)]}{\frac{1}{M} \sum_{m=1}^M \exp[-\mathbf{a}(\zeta_m)]},$$

where we replaced g_a^λ and g_a in Eq. (2.5) by h_a^λ and h_a . With *harmonic coupling*, the standard reweighting estimator of $\mathbb{E}[\mathbf{1}_{\xi^*}]$ writes

$$\Upsilon_R^M(\mathbf{1}_{\xi^*}) = \frac{\frac{1}{M} \sum_{m=1}^M \mathbf{1}_{\xi^*}(\xi_m) \exp[-\mathbf{a}(\zeta_m) + \mathcal{R}(\zeta_m, \xi_m)]}{\frac{1}{M} \sum_{m=1}^M \exp[-\mathbf{a}(\zeta_m) + \mathcal{R}(\zeta_m, \xi_m)]},$$

where we replaced g_a^λ and g_a in Eq. (2.5) by r_a^λ and r_a and ξ_m stands for $\xi(\bar{q}_m)$. This relation shows that it is in principle possible to remove the biasing and harmonic potentials simultaneously. However, this way of proceeding is not efficient. Instead, integration of the averaged restraint $\mathbb{E}_a[\partial_{\xi^*} \mathcal{R}(\cdot, \xi^*) | \xi^*]$ along ξ^* is preferred in practice [40]. This approach, referred to as CZAR method, exploits the fact that the restraint can be differentiated with respect to ξ^* . It will be further described in Sec. 3.4 and compared to adiabatic reweighting.

With regards to question (ii), conditioning consists in replacing the $g_a^\lambda(\zeta_m, \bar{q}_m)$ and $g_a(\zeta_m, \bar{q}_m)$ terms by their expected values given \bar{q}_m , which are respectively ($q \equiv \bar{q}_m$)

$$\mathbb{E}_a [g_a^\lambda(\cdot, q) | q] = \exp[-\mathbf{a}(\lambda)] \mathbb{E}_a [g_a^\lambda(\cdot, q) | q] = \pi_a^\lambda(q),$$

and

$$\mathbb{E}_a [g_a(\cdot, q) | q] = \sum_{\lambda \in \Lambda} \pi_a^\lambda(q) = \pi_a(q).$$

Next, we write the law of total expectation in the rhs ratio of Eq. 2.4 and plug the expected value of $g_a(\zeta, q)$ given q

$$\mathbb{E}[\mathcal{O}] = \frac{\mathbb{E}_a^Q \left[\mathbb{E}_a \left[\sum_{\lambda \in \Lambda} g_a^\lambda(\cdot, q) \mathcal{O}(\lambda, q) | q \right] \right]}{\mathbb{E}_a^Q \left[\mathbb{E}_a [g_a(\cdot, q) | q] \right]} = \frac{\mathbb{E}_a \left[\sum_{\lambda \in \Lambda} \pi_a^\lambda(\cdot) \mathcal{O}(\lambda, \cdot) \right]}{\mathbb{E}_a [\pi_a]}.$$

From the rhs expectation ratio of Eq. 2.2.1 and by application of the ergodic theorem, the adiabatic reweighting estimator of $\mathbb{E}[\mathcal{O}]$ below is deduced:

$$\Upsilon_{II}^M(\mathcal{O}) = \frac{\frac{1}{M} \sum_{m=1}^M \sum_{\lambda \in \Lambda} \pi_a^\lambda(\bar{q}_m) \mathcal{O}(\lambda, \bar{q}_m)}{\frac{1}{M} \sum_{m=1}^M \pi_a(\bar{q}_m)}, \quad (2.7)$$

where $\{\bar{q}_m\}_{1 \leq m \leq M}$ is a Markov chain of states distributed according to probability distribution $p_a^Q(q)$. This one can possibly be extracted from an expanded Markov chain $\{\zeta_m, \bar{q}_m\}_{1 \leq m \leq M}$ generated according to $p_a(\zeta, \bar{q})$ probability density. We have compiled in Table 2.1 the relations between total expectations and weighing

functions which are useful for the construction of the estimators.

We answer question (iii) in the affirmative: conditioning for estimating total expectations achieves variance reduction. As for estimations of conditional expectations in section 1.11, this property is a consequence of the law of total variance. The proof follows the same reasoning, but requires replacing the conditionally centered variable $\mathcal{O}^\lambda(q) = \mathcal{O}(\lambda, q) - \mathbb{E}[\mathcal{O}|\lambda]$ by the totally centered variable

$$\mathcal{O}^A(\zeta, \bar{q}) = \mathcal{O}(\zeta, \bar{q}) - \mathbb{E}[\mathcal{O}],$$

and the weighing factor g_a^λ by a sum over $\lambda \in \Lambda$ involving the \mathfrak{g}_a^λ factors. The asymptotic variance of the $\Upsilon_{\text{R}}^M(\mathcal{O})$ estimator writes (see Appendix A)

$$\sigma_a^2[\Upsilon_{\text{G}}^\infty(\mathcal{O})] = \mathbb{V}_a \left[\sum_{\lambda \in \Lambda} \mathcal{O}^A(\lambda, \cdot) \frac{\mathfrak{g}_a^\lambda(\cdot, \cdot)}{\mathbb{E}_a(\mathfrak{g}_a)} \right],$$

where the quantity inside the variance is also centered. The asymptotic variance of the $\Upsilon_{\text{H}}^M(\mathcal{O})$ estimator is obtained from the one of the $\Upsilon_{\text{H}}^M(\mathcal{O}|\lambda)$ estimator by replacing the conditional probabilities $\pi_a^\lambda(q)$ by sums involving $\mathfrak{n}_a^\lambda(q)$ over $\lambda \in \Lambda$. One obtains

$$\sigma_a^2[\Upsilon_{\text{H}}^\infty(\mathcal{O})] = \mathbb{V}_a \left[\sum_{\lambda \in \Lambda} \mathcal{O}^A(\lambda, \cdot) \frac{\mathfrak{n}_a^\lambda(\cdot)}{\mathbb{E}_a(\mathfrak{n}_a)} \right] = \mathbb{V}_a^{\mathcal{Q}} \left[\mathbb{E}_a \left[\sum_{\lambda \in \Lambda} \mathcal{O}^A(\lambda, q) \frac{\mathfrak{g}_a^\lambda(\cdot, q)}{\mathbb{E}_a(\mathfrak{g}_a)} \middle| q \right] \right],$$

where $\mathfrak{n}_a = \sum_{\lambda \in \Lambda} \mathfrak{n}_a^\lambda$. Plugging the law of total variance into the right-hand side variance enables one to conclude that the asymptotic variance of the $\Upsilon_{\text{H}}^M(\mathcal{O})$ estimator is smaller than that of the $\Upsilon_{\text{G}}^M(\mathcal{O})$ estimator

$$\sigma_a^2[\Upsilon_{\text{H}}^\infty(\mathcal{O})] = \mathbb{V}_a \left[\sum_{\lambda \in \Lambda} \mathcal{O}^A(\lambda, \cdot) \frac{\mathfrak{g}_a^\lambda(\cdot, \cdot)}{\mathbb{E}_a(\mathfrak{g}_a)} \right] - \mathbb{E}_a^{\mathcal{Q}} \left[\mathbb{V}_a \left[\sum_{\lambda \in \Lambda} \mathcal{O}^A(\lambda, q) \frac{\mathfrak{g}_a^\lambda(\cdot, q)}{\mathbb{E}_a(\mathfrak{g}_a)} \middle| q \right] \right] < \sigma_a^2[\Upsilon_{\text{G}}^\infty(\mathcal{O})].$$

We will illustrate the estimation of total expectations by setting the observable to the indicator functions $\mathbf{1}_\lambda(\zeta)$ or $\mathbf{1}_{\xi^*}(\xi(\bar{q}))$ where $\xi(\bar{q})$ is an internal reaction coordinate. The co-logarithms of the expected values of the two indicator functions yield the free energies along the external and internal coordinate, respectively. Various ways of estimating free energies, the primary goal of expanded ensemble simulations, are discussed next in subsection 2.2.2 and also later in Sec. 3.4, for the external and internal coordinate cases, respectively.

2.2.2 Estimation of the free energy along an external parameter

As defined in Eq. 2.1, the free energy $\mathcal{A}(\lambda)$ is the co-logarithm of the total expectation of the indicator function $\mathbf{1}_\lambda(\zeta)$ for $\lambda \in \Lambda$. Its derivative is a conditional expectation of the λ -derivative of the extended potential given λ :

$$\mathcal{A}'(\lambda) = \mathbb{E}[\partial_\lambda \mathcal{U}(\lambda, \cdot) | \lambda].$$

This quantity can be estimated and then integrated to obtain the free energy. Table 2.2 illustrates the various ways of estimating the corresponding total and conditional expectations using the generic weighing functions and a time-independent auxiliary biasing potential.

Let denote the binning, standard reweighting and adiabatic reweighting estimators by Υ_{H}^M , Υ_{R}^M and Υ_{H}^M respectively. Considering these three important estimators potentially makes 6 direct methods of computing the free energy or its derivative, while direct free energy methods are usually classified into three *overlapping* categories in the literature: thermodynamic occupation [41, 14, 42] (TO), thermodynamic integration [43] (TI), free energy perturbation [13] (FEP). We next analyze the correspondence between estimators and free energy methods.

As for methods belonging to the first category, estimating the free energy from the log-probability of λ is

Table 2.1: Notations and definitions of weighing functions and relations to conditional and total expectations.

Definitions		
$\mathfrak{h}_a^\lambda(\zeta, \bar{q}) = \exp[-\mathbf{a}(\lambda)] h_a^\lambda(\zeta, \bar{q}) = \exp[-\mathbf{a}(\lambda)] \mathbf{1}_\lambda(\zeta)$		$\mathfrak{h}_a = \sum_{\lambda \in \Lambda} \mathfrak{h}_a^\lambda,$
$\mathfrak{r}_a^\lambda(\zeta, \bar{q}) = \exp[-\mathbf{a}(\lambda)] r_a^\lambda(\zeta, \bar{q}) = \frac{1}{\ \Lambda\ } \frac{\exp[-\mathbf{u}(\lambda, \bar{q})]}{\exp[\mathbf{a}(\zeta, \bar{q}) - \mathbf{u}(\zeta, \bar{q})]}$		$\mathfrak{r}_a = \sum_{\lambda \in \Lambda} \mathfrak{r}_a^\lambda,$
$\mathfrak{g}_a^\lambda(\zeta, \bar{q}) = \exp[-\mathbf{a}(\lambda)] g_a(\zeta, \bar{q}) = \begin{cases} \mathfrak{h}_a^\lambda(\zeta, \bar{q}) & \text{if binning,} \\ \mathfrak{r}_a^\lambda(\zeta, \bar{q}) & \text{if standard reweighting,} \end{cases}$		$\mathfrak{g}_a = \sum_{\lambda \in \Lambda} \mathfrak{g}_a^\lambda,$
$\mathfrak{n}_a^\lambda(\bar{q}) = \exp[-\mathbf{a}(\lambda)] \pi_a^\lambda(\bar{q}) = \frac{\exp[-\mathbf{u}(\lambda, \bar{q})]}{\sum_{\zeta \in \Lambda} \exp[\mathbf{a}(\zeta, \bar{q}) - \mathbf{u}(\zeta, \bar{q})]},$		$\mathfrak{n}_a = \sum_{\lambda \in \Lambda} \mathfrak{n}_a^\lambda.$
Expressions for total expectations		
$\mathbb{E}[\mathcal{O}] = \frac{\mathbb{E}_a[\sum_{\lambda \in \Lambda} \mathfrak{g}_a^\lambda(\cdot, \cdot) \mathcal{O}(\lambda, \cdot)]}{\mathbb{E}_a[\mathfrak{g}_a]}$	\implies	$\mathbb{E}[\mathbf{1}_\lambda] = \frac{\mathbb{E}_a[\mathfrak{g}_a^\lambda]}{\mathbb{E}_a[\mathfrak{g}_a]}$
$\mathbb{E}[\mathcal{O}] = \frac{\mathbb{E}_a[\sum_{\lambda \in \Lambda} \mathfrak{n}_a^\lambda(\cdot) \mathcal{O}(\lambda, \cdot)]}{\mathbb{E}_a[\mathfrak{n}_a]}$	\implies	$\mathbb{E}[\mathbf{1}_\lambda] = \frac{\mathbb{E}_a[\mathfrak{n}_a^\lambda]}{\mathbb{E}_a[\mathfrak{n}_a]}$
Expressions for conditional expectations		
$\mathbb{E}_a[\mathfrak{g}_a^\lambda(\cdot, q) q] = \pi_a^\lambda(q)$	\iff	$\mathbb{E}_a[g_a^\lambda(\cdot, q) q] = \pi_a^\lambda(q),$
$\mathbb{E}[\partial_\lambda \mathbf{u}(\lambda, \cdot) \lambda] = -\partial^\lambda \ln \mathbb{E}_a[\mathfrak{r}_a^\lambda]$	\iff	$\partial^\lambda \mathfrak{r}_a^\lambda(\cdot, \cdot) = -\partial_\lambda \mathbf{u}(\lambda, \cdot) \mathfrak{r}_a^\lambda(\cdot, \cdot),$
$\mathbb{E}[\partial_\lambda \mathbf{u}(\lambda, \cdot) \lambda] = -\partial^\lambda \ln \mathbb{E}_a[\mathfrak{n}_a^\lambda]$	\iff	$\partial^\lambda \mathfrak{n}_a^\lambda(\cdot) = -\partial_\lambda \mathbf{u}(\lambda, \cdot) \mathfrak{n}_a^\lambda(\cdot).$

done resorting to the binning estimator as follows

$$\widehat{\mathcal{A}}(\lambda)_{\text{TO}}^M = -\ln \left[\frac{\frac{1}{M} \sum_{m=1}^M \mathbf{1}_\lambda(\zeta_m) \exp[-\mathbf{a}(\zeta_m)]}{\frac{1}{M} \sum_{m=1}^M \exp[-\mathbf{a}(\zeta_m)]} \right] = -\ln \frac{\mathbf{I}^M(\mathfrak{h}_a^\lambda)}{\mathbf{I}^M(\mathfrak{h}_a)} = -\ln \Upsilon_{\text{H}}^M(\mathbf{1}_\lambda).$$

Methods of the second category consists in estimating the free energy derivative and evaluating the free energy through numerical integration. This is what is actually done in the extended ABF technique [34, 40]. From an expanded ensemble simulation, a simple way of obtaining an estimate $\widehat{\mathcal{A}}'(\lambda)$ of the mean force involves the binning estimator Υ_{H}^M

$$\widehat{\mathcal{A}}'(\lambda)_{\text{TI}}^M = \frac{\frac{1}{M} \sum_{m=1}^M \partial_\lambda \mathbf{u}(\lambda, \bar{q}_m) \mathbf{1}_\lambda(\zeta_m)}{\frac{1}{M} \sum_{m=1}^M \mathbf{1}_\lambda(\zeta_m)} = \frac{\mathbf{I}^M(\partial_\lambda \mathbf{u} \mathfrak{h}_a^\lambda)}{\mathbf{I}^M(\mathfrak{h}_a^\lambda)} = \Upsilon_{\text{H}}^M[\partial_\lambda \mathbf{u} | \lambda].$$

It may be suggested to estimate the free energy derivative resorting instead to the standard reweighting estimator as it is done in umbrella sampling [12]. Using the standard reweighting function introduced in Table 2.1 together with the property $\partial_\lambda \mathfrak{r}_a^\lambda(\zeta, \bar{q}) = -\partial_\lambda \mathbf{u}(\lambda, \bar{q}) \mathfrak{r}_a^\lambda(\zeta, \bar{q})$, we have

$$\widehat{\mathcal{A}}'(\lambda)_{\text{FEP}}^M = \Upsilon_{\text{R}}^M(\partial_\lambda \mathbf{u} | \lambda) = -\partial^\lambda \ln \left[\frac{1}{M} \sum_{m=1}^M \mathfrak{r}_a^\lambda(\zeta_m, \bar{q}_m) \right].$$

The fact that the estimator can be written has a logarithmic derivative of another standard reweighting estimator indicates that it is not necessary to integrate the mean force to obtain the free energy. The standard reweighting approach pertains to the second category of free energy methods (FEP), which aim at directly evaluating the

Table 2.2: Expectation ratios based on which the various free energy estimators of Table 2.3 are constructed.

$$\begin{aligned}
 \mathcal{A}(\lambda) &= \begin{cases} -\ln \frac{\mathbb{E}_a[\mathfrak{g}_a^\lambda]}{\mathbb{E}_a[\mathfrak{g}_a]} & \text{with generic weighing,} \\ -\ln \frac{\mathbb{E}_a^\mathcal{Q}[\mathbb{E}_a[\mathfrak{g}_a^\lambda(\cdot, q)|q]]}{\mathbb{E}_a^\mathcal{Q}[\mathbb{E}_a[\mathfrak{g}_a(\cdot, q)|q]]} = -\ln \frac{\mathbb{E}_a[\mathfrak{r}_a^\lambda]}{\mathbb{E}_a[\mathfrak{r}_a]} & \text{with conditioning,} \end{cases} \\
 \mathcal{A}'(\lambda) &= \begin{cases} \frac{\mathbb{E}_a[\mathfrak{g}_a^\lambda \partial_\lambda \mathcal{U}(\lambda, \cdot)]}{\mathbb{E}_a[\mathfrak{g}_a^\lambda]} & \text{with generic weighing,} \\ \frac{\mathbb{E}_a^\mathcal{Q}[\mathbb{E}_a[\partial_\lambda \mathcal{U}(\lambda, q) \mathfrak{g}_a^\lambda(\cdot, q)|q]]}{\mathbb{E}_a^\mathcal{Q}[\mathbb{E}_a[\mathfrak{g}_a^\lambda(\cdot, q)|q]]} = -\frac{\mathbb{E}_a[\partial^\lambda \mathfrak{r}_a^\lambda]}{\mathbb{E}_a[\mathfrak{r}_a^\lambda]} & \text{with conditioning.} \end{cases}
 \end{aligned}$$

free energy by estimating a partition function ratio and then taking its co-logarithm

$$\widehat{\mathcal{A}(\lambda)}_{\text{FEP}}^M = -\ln \left[\frac{\frac{1}{M} \sum_{m=1}^M \mathfrak{r}_a^\lambda(\zeta_m, \bar{q}_m)}{\frac{1}{M} \sum_{m=1}^M \mathfrak{r}_a(\zeta_m, \bar{q}_m)} \right] = -\ln \Upsilon_{\text{R}}^M(\mathbf{1}_\lambda).$$

To perform a conditioning with respect to the FEP and TO method above, one must replace the weighing factors \mathfrak{h}_a^λ and \mathfrak{r}_a^λ by their conditional expected values given q , which happens to be given by $\mathfrak{r}_a^\lambda(q)$. Similarly, \mathfrak{h}_a and \mathfrak{r}_a must also be replaced by $\mathfrak{r}_a(q)$. One thus obtains the following estimator

$$\widehat{\mathcal{A}(\lambda)}_{\text{AR}}^M = -\ln \left[\frac{\frac{1}{M} \sum_{m=1}^M \mathfrak{r}_a^\lambda(\bar{q}_m)}{\frac{1}{M} \sum_{m=1}^M \mathfrak{r}_a(\bar{q}_m)} \right].$$

Differentiating the free energy estimate with respect to λ yields

$$\frac{d\widehat{\mathcal{A}(\lambda)}_{\text{AR}}^M}{d\lambda} = -\partial^\lambda \ln \left[\frac{\sum_{m=1}^M \mathfrak{r}_a^\lambda(\bar{q}_m)}{\sum_{m=1}^M \mathfrak{r}_a(\bar{q}_m)} \right] = -\frac{\sum_{m=1}^M \partial^\lambda \mathfrak{r}_a^\lambda(\bar{q}_m)}{\sum_{m=1}^M \mathfrak{r}_a^\lambda(\bar{q}_m)} = \Upsilon_{\text{II}}^M(\partial_\lambda \mathcal{U}|\lambda) = \widehat{\mathcal{A}'(\lambda)}_{\text{AR}}^M,$$

where we substituted $-\partial_\lambda \mathcal{U}(\lambda, \bar{q}_m) \mathfrak{r}_a^\lambda(\bar{q}_m)$ for $\partial^\lambda \mathfrak{r}_a^\lambda(\bar{q}_m)$ in the second line and eventually identify with the AR estimate of $\mathbb{E}[\partial_\lambda \mathcal{U}|\lambda]$. The consistency between the estimated mean force and the derivative of the estimated free energy in the AR method is a property inherited from the FEP method. However, unlike FEP method, the adiabatic reweighting approach is directly related to thermodynamic integration, since the estimated mean force can also be constructed from the following conditioning scheme

$$\widehat{\mathcal{A}'(\lambda)}_{\text{AR}}^M = \frac{\frac{1}{M} \sum_{m=1}^M \partial_\lambda \mathcal{U}(\lambda, \bar{q}_m) \mathbb{E}_a[\mathfrak{h}_a^\lambda(\zeta)|\bar{q}_m]}{\frac{1}{M} \sum_{m=1}^M \mathbb{E}_a[\mathfrak{h}_a^\lambda(\zeta)|\bar{q}_m]}.$$

This means in particular that each sampled point \bar{q}_m with $1 \leq m \leq M$ contributes to the estimated mean force with an integrated weight over Λ that is equal to one. This property is inherited from the TI method and does not hold for the FEP method. This explains why the latter method may yield completely inaccurate results in some circumstances. This point is illustrated in Section 2.4. The four ways of estimating the free energy and its derivative are summarized in Table 2.3.

Next, we compare the variances of the TI, FEP and TO methods to the one of the AR method. The asymptotic variance for the TO/FEP method can be cast in the following form using the generic functions \mathfrak{g}_a^λ and \mathfrak{g}_a (see Appendix A, Eq. (A.5))

$$\sigma_a^2 \left[\widehat{\mathcal{A}(\lambda)}_{\text{FEP/TO}}^\infty \right] = \mathbb{V}_a \left[\frac{\mathfrak{g}_a^\lambda(\zeta, q)}{\mathbb{E}_a[\mathfrak{g}_a^\lambda]} - \frac{\mathfrak{g}_a(\zeta, q)}{\mathbb{E}_a[\mathfrak{g}_a]} \right].$$

The asymptotic variance of the AR method can be cast in the similar form (see Appendix A, Eq. (A.6))

$$\sigma_a^2 \left[\widehat{\mathcal{A}}(\lambda)_{\text{AR}}^\infty \right] = \mathbb{V}_a^{\mathcal{Q}} \left[\mathbb{E}_a \left[\frac{\mathfrak{g}_a^\lambda(\cdot, q)}{\mathbb{E}_a[\mathfrak{g}_a^\lambda]} - \frac{\mathfrak{g}_a(\cdot, q)}{\mathbb{E}_a[\mathfrak{g}_a]} \middle| q \right] \right] = \mathbb{V}_a \left[\frac{\mathbb{P}_a^\lambda}{\mathbb{E}_a[\mathbb{P}_a^\lambda]} - \frac{\mathbb{P}_a}{\mathbb{E}_a[\mathbb{P}_a]} \right].$$

The law of total variance then entails the following strict inequality

$$\mathbb{V}_a \left[\frac{\mathfrak{g}_a^\lambda}{\mathbb{E}_a[\mathfrak{g}_a^\lambda]} - \frac{\mathfrak{g}_a}{\mathbb{E}_a[\mathfrak{g}_a]} \right] - \mathbb{V}_a \left[\frac{\mathbb{P}_a^\lambda}{\mathbb{E}_a[\mathbb{P}_a^\lambda]} - \frac{\mathbb{P}_a}{\mathbb{E}_a[\mathbb{P}_a]} \right] = \mathbb{E}_a \left\{ \mathbb{V}_a \left[\frac{\mathfrak{g}_a^\lambda(\cdot, q)}{\mathbb{E}_a[\mathfrak{g}_a^\lambda]} - \frac{\mathfrak{g}_a(\cdot, q)}{\mathbb{E}_a[\mathfrak{g}_a]} \middle| q \right] \right\} > 0.$$

It results the following strict inequality for the asymptotic variances

$$\sigma_a^2 \left[\widehat{\mathcal{A}}(\lambda)_{\text{AR}}^\infty \right] < \min \left\{ \sigma_a^2 \left[\widehat{\mathcal{A}}(\lambda)_{\text{TO}}^\infty \right], \sigma_a^2 \left[\widehat{\mathcal{A}}(\lambda)_{\text{FEP}}^\infty \right] \right\}.$$

With regards to the TI method, the efficiencies of the adiabatic reweighting and histogram binning estimators are more easily compared considering the derivative of the free energy. The asymptotic variances associated with the $\Upsilon_{\text{H}}^M(\partial_\lambda \mathcal{U}|\lambda)$ and $\Upsilon_{\text{H}}^M(\partial_\lambda \mathcal{U}|\lambda)$ estimators satisfy the relation $\sigma_a^2 [\Upsilon_{\text{H}}^M(\partial_\lambda \mathcal{U}|\lambda)] < \sigma_a^2 [\Upsilon_{\text{H}}^M(\partial_\lambda \mathcal{U}|\lambda)]$. It is therefore always preferable to estimate free energies in combination with a conditioning scheme when the auxiliary biasing potential is time-independent. Remarkably, whatever the standard free energy method (TO, FEP, TI) that is chosen, conditioning with respect to the external parameter provides the same AR estimator, as illustrated in Table 2.3.

Prior to assessing the performance of the various estimators considered so far, we show how to implement a conditioning procedure in the transition path sampling method briefly mentioned in Sec. 2.1 and further described in Subsec. 2.3.1 below. We refer to Chapter 4 and Section 4.4.2 in particular for a general description of path sampling algorithms.

Table 2.3: Standard (TI, FEP, TO) and conditioning (AR) estimators for computing mean forces and free energies. Note that, unlike \mathfrak{r}_a^λ and \mathfrak{v}_a^λ weighing functions, the function \mathfrak{h}_a^λ can not be differentiated with respect to λ . It results that two distinct methods (TO and TI) are based on binning.

Estimation of free energy $\widehat{\mathcal{A}}(\lambda)_X^M$		Corresponding mean force $\widehat{\mathcal{A}'(\lambda)}_X^M$
$\widehat{\mathcal{A}}(\lambda)_{\text{TO}}^M = -\ln \Upsilon_{\text{H}}^M(\mathbf{1}_\lambda) = -\ln \frac{\mathbb{I}^M(\mathfrak{h}_a^\lambda)}{\mathbb{I}^M(\mathfrak{h}_a)}$	\rightarrow	derivative by finite difference $\rightarrow \widehat{\mathcal{A}'(\lambda)}_{\text{TO}}^M$
$\widehat{\mathcal{A}}(\lambda)_{\text{TI}}^M \leftarrow$ numerical quadrature	\leftarrow	$\frac{\mathbb{I}^M(\mathfrak{h}_a^\lambda \partial_\lambda \mathfrak{u})}{\mathbb{I}^M(\mathfrak{h}_a^\lambda)} = \Upsilon_{\text{H}}^M(\partial_\lambda \mathfrak{u} \lambda)$
$\widehat{\mathcal{A}}(\lambda)_{\text{FEP}}^M = -\ln \Upsilon_{\text{R}}^M(\mathbf{1}_\lambda) = -\ln \frac{\mathbb{I}^M(\mathfrak{r}_a^\lambda)}{\mathbb{I}^M(\mathfrak{r}_a)}$	\Leftrightarrow	$-\partial^\lambda \ln \frac{\mathbb{I}^M(\mathfrak{r}_a^\lambda)}{\mathbb{I}^M(\mathfrak{r}_a)} = \frac{\mathbb{I}^M(-\partial^\lambda \mathfrak{r}_a^\lambda)}{\mathbb{I}^M(\mathfrak{r}_a^\lambda)} = \Upsilon_{\text{R}}^M(\partial_\lambda \mathfrak{u} \lambda)$
$\widehat{\mathcal{A}}(\lambda)_{\text{AR}}^M = -\ln \Upsilon_{\text{H}}^M(\mathbf{1}_\lambda) = -\ln \frac{\mathbb{I}^M(\mathfrak{v}_a^\lambda)}{\mathbb{I}^M(\mathfrak{v}_a)}$	\Leftrightarrow	$-\partial^\lambda \ln \frac{\mathbb{I}^M(\mathfrak{v}_a^\lambda)}{\mathbb{I}^M(\mathfrak{v}_a)} = \frac{\mathbb{I}^M(-\partial^\lambda \mathfrak{v}_a^\lambda)}{\mathbb{I}^M(\mathfrak{v}_a^\lambda)} = \Upsilon_{\text{H}}^M(\partial_\lambda \mathfrak{u} \lambda)$

2.3 Estimating rare-event probabilities

2.3.1 Conditional correlation function

The crucial task in TPS is to compute the free energy difference

$$\mathcal{F}(\mathbf{B}, t, \mathbf{A}, 0) - \mathcal{F}(\mathcal{Q}, t, \mathbf{A}, 0) = -\ln \frac{\mathbb{E}^* [\chi_{\mathbf{B}}(q_t) \chi_{\mathbf{A}}(q_0)]}{\mathbb{E}^* [\chi_{\mathbf{A}}(q_0)]} \triangleq -\ln \mathcal{C}(t),$$

that is the difference between the free energy of the space of transition paths (of duration t) and the free energy of the space of paths initiated from state \mathbf{A} and ending anywhere at t . Note that the latter quantity simplifies into the relative free energy of the reactant state \mathbf{A} , $\mathcal{F}(\mathbf{A}) = -\ln \mathbb{E}^* [\chi_{\mathbf{A}}]$, because $\chi_{\mathcal{Q}}(q) = 1$ for any q and because of the translational time invariance. The two introduced characteristic functions $\chi_{\mathbf{A}}$ and $\chi_{\mathbf{B}}$ merely serve to distinguish the final product states \mathbf{B} from the initial reactant states \mathbf{A} without providing any relevant information on the reaction mechanism. In TPS, short trajectories of duration t and initiated from \mathbf{A} are sampled from a biased distribution controlled by an external parameter (denoted by λ or θ). This parameter is used to gradually switch on a biasing path functional favoring the sampling of transition paths. Path ensembles and path functionals being later introduced in Chapter 4, we rather consider a biasing potential of form $\lambda \mathcal{B}(q_t)$, linear in λ and acting on the path ending point q_t . The transition paths favored by the biased sampling have a higher probability to commit to the product state, in which case $\chi_{\mathbf{B}}(q_t) = 1$. This setup is adopted in the transition path sampling method of Chapter 4 where the path functional $\theta \mathcal{L}(z)$ replaces $\lambda \mathcal{B}(q_t)$.

In standard TPS, a series of umbrella sampling simulations is performed and a self-consistent estimator (WHAM or MBAR) is used to calculate the time correlation function. These tasks can be done directly and simultaneously in a single simulation through conditioning. For this purpose, we formalize an *expanded transition path ensemble* in Subsection 2.3.2. In this framework, the \mathbf{A} -to- \mathbf{B} time correlation function is then given by the following expectation

$$\mathcal{C}(L\tau) = \mathbb{E} [\chi_{\mathbf{B}}(q_{L\tau}) | \chi_{\mathbf{A}}(q_0) = 1, \lambda = 0], \quad (2.8)$$

where we considered a discretized dynamics of timestep τ and L steps. We derive the conditioned estimator in Subsection 2.3.3 and assess its performance on the estimation of rare-event probabilities on a simple model.

2.3.2 Expanded transition path ensemble

We illustrate the rare-event problem using an analytically tractable model to make it possible to compare the obtained Monte Carlo estimates with exact reference data. We consider a generic Brownian motion model in which a one-dimensional single particle evolves on a flat potential energy profile. The position of the particle is obtained by integrating the corresponding overdamped Langevin equation: we have $q_{\ell\tau+\tau} = q_{\ell\tau} + \sqrt{2\tau D} B_\ell$ where D a diffusion coefficient and B_ℓ is a random variate drawn in the normal distribution of zero mean and unit variance. We next set \mathbf{A} to $\{0\}$ and \mathbf{B} to $[1, +\infty[$. This implies that q_0 is equal to 0 and that $q_{L\tau}$ is distributed according to the normal distribution

$$\pi(q|0) = \sqrt{\omega/\pi} \exp(-\omega q^2) \triangleq \exp[\mathfrak{F}(0) - \mathcal{U}_0(q)],$$

where $\omega = (4DL\tau)^{-1}$ and $\mathcal{U}_0(q) \equiv \mathcal{U}(0, q)$ stands for ωq^2 . Integrating this distribution from 1 to ∞ yields $\mathcal{C}(L\tau) = \text{erfc}(\sqrt{\omega})/2$, the probability that a path ends at a position larger than 1.

Dropping the subscript L , we simply denote the path endpoints by q and omit the condition $\chi_{\mathbf{A}}(q_0) = 1$ in the involved expectations. We introduce the biasing potential $\mathcal{B}(q) = -2\omega q$ so as to softly and partially restrain the trajectory endpoints with the overall biasing potential

$$\mathcal{U}(\lambda, q) - \mathcal{U}_0(q) = -2\lambda\omega q,$$

so as to gradually increase the fraction of trajectories ending in the product basin $q \geq 1$ with increasing λ value. This way of proceeding corresponds to the so-called tilting protocol that is used in path sampling simulations to sample rare trajectories from a path distribution [44, 45, 46, 8]. In the expanded ensemble with auxiliary potential $\alpha(\lambda)$, the biased probability of (λ, q) is

$$p_\alpha(\lambda, q) = \exp[\alpha(\lambda) - \mathcal{U}_0(q) - \lambda \mathcal{B}(q) - \Psi_\alpha^A].$$

The conditional probability of q given λ is then

$$\pi(q|\lambda) = \sqrt{\omega/\pi} \exp[-\omega(q - \lambda)^2]. \quad (2.9)$$

The reference distribution is obtained by setting λ to 0 in (2.9) and is represented as a function of q by the green curve delimiting the red area in Fig. 2.1. We set $\Lambda = \{\lambda^j\}_{0 \leq j \leq J}$ with $\lambda^j = j/J$ and $J = 10^3$. The conditional distributions with various biases, obtained by setting λ to $\frac{1}{4}$, $\frac{1}{2}$, $\frac{3}{4}$ and 1 in (2.9) are displayed in Fig. 2.1 for the two values of the ω parameter. The two selected values correspond to a fast Brownian motion for which $\omega = 5$ and to a slow one for which $\omega = 100$. For $\omega = 5$, we observe that the biased distributions $q \rightarrow \pi(q|1)$ substantially overlap with both the target region ($q \geq 1$) and the reference distribution $q \rightarrow \pi(q|0)$ (areas displayed in red and green respectively). For $\omega = 100$, none of the biased distribution ($\lambda = \frac{1}{4}$, $\frac{1}{2}$ and $\frac{3}{4}$) substantially overlaps with both the reference distribution and the target region. At variance, the marginal distribution of q obtained for $\lambda_{\max} = 1$ and both values of ω (curves displayed in blue) overlap with the unbiased distribution. In brief, for small values of ω , the various conditional probabilities substantially overlap with each other. The degree of overlap decreases with increasing ω . The state-to-state time correlation function (2.8)

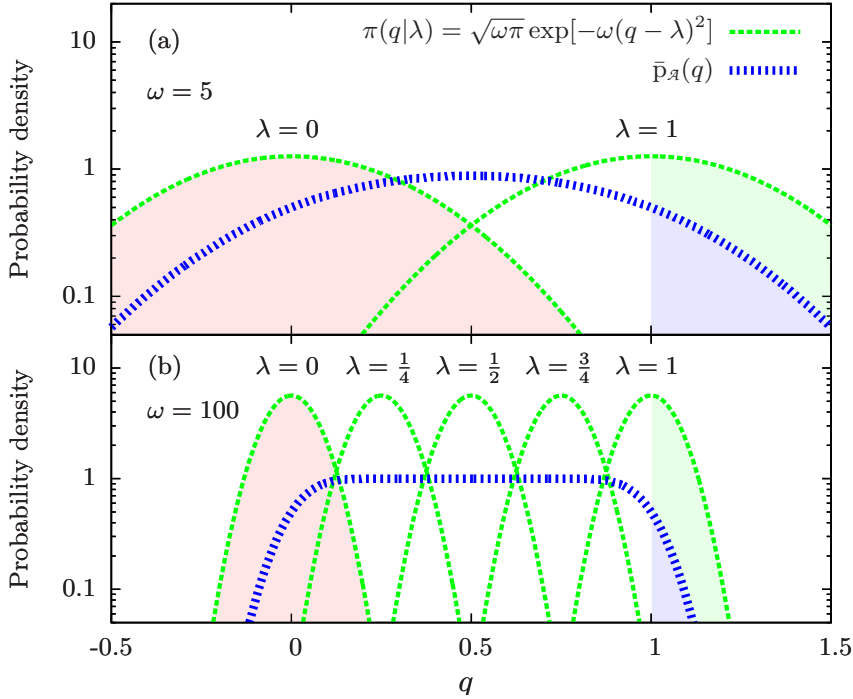


Figure 2.1: Conditional distributions $\pi(q|\lambda)$ for the indicated values of λ (green curves) and the marginal probability of q (blue curves) for $\omega = 5$ in pannel (a) and $\omega = 100$ in pannel (b). The target region corresponds to $q \geq 1$ and the unbiased distribution of q is filled in red.

transposed in the expanded (path) ensemble becomes

$$\mathcal{C} = \frac{\mathbb{E}_a [\chi_B(q) \pi_a(0|q)]}{\mathbb{E}_a [\pi_a(0|q)]} = \frac{\mathbb{E}_a [\chi_B \pi_a^0]}{\mathbb{E}_a [\pi_a^0]}.$$

The dependence of \mathcal{C} on the final time $L\tau$ is also omitted from now. This ratio can be seen as a conditioned version of the expectation ratio involving the standard reweighting function:

$$\mathcal{C} = \frac{\mathbb{E}_a [\chi_B r^0]}{\mathbb{E}_a [r^0]}.$$

Next, we emphasize the importance of conditioning for estimating probabilities of rare-events [8]. We show in Sec. 2.3.3 below that, when the auxiliary potential is set to free energy $\mathcal{A}(\lambda)$, it is possible to accurately

compute \mathcal{C} through the biased sampling of trajectory endpoints, even for very slow diffusion processes in which the value of ω is large and the probability to reach $q \geq 1$ is very small. The auxiliary biasing potential can be constructed adaptively using one of the techniques reviewed in Chapter 3 and is assumed to have correctly converged to the free energy.

2.3.3 Estimation of rare-event probabilities

The probability $\mathcal{C} = \text{erfc}(\sqrt{\omega})/2$ to observe a point at a position larger than 1 from the reference distribution (2.9) with λ equal to 0 is computed through biased sampling of $p_{\mathcal{A}}(\zeta, \bar{q})$. The conditional expectation is estimated using the adiabatic reweighting estimator and standard reweighting estimator respectively given by

$$\Upsilon_{\text{R}}^M(\chi_{\text{B}}|0) = \frac{\frac{1}{M} \sum_{m=1}^M \chi_{\text{B}}(\bar{q}_m) \pi_{\mathcal{A}}^0(\bar{q}_m)}{\frac{1}{M} \sum_{m=1}^M \pi_{\mathcal{A}}^0(\bar{q}_m)}, \quad (2.10)$$

$$\Upsilon_{\text{R}}^M(\chi_{\text{B}}|0) = \frac{\frac{1}{M} \sum_{m=1}^M \chi_{\text{B}}(\bar{q}_m) r_{\mathcal{A}}^0(\zeta_m, \bar{q}_m)}{\frac{1}{M} \sum_{m=1}^M r_{\mathcal{A}}^0(\zeta_m, \bar{q}_m)}, \quad (2.11)$$

as obtained by replacing the observable $q \mapsto \mathcal{O}(0, q)$ by the indicator function. Here, we did not consider the binning estimator as it is obviously not suited to the present rare event problem. The goal is to retrieve statistics from configurations exhibiting large \bar{q}_m values which are observed concomitantly with large ζ_m sampled values. The marginal probability of λ at 0 is first estimated from the denominator of (2.10) and (2.11). Each generated

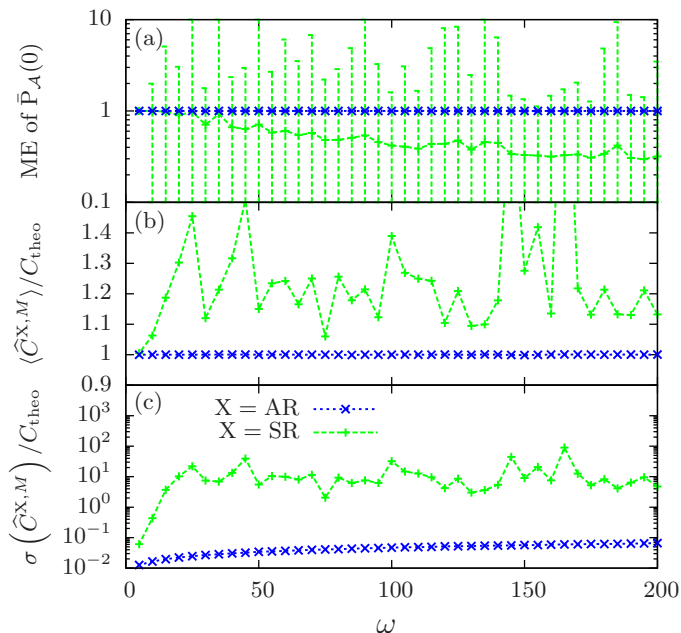


Figure 2.2: Comparison between the adiabatic reweighting estimator (2.10) and standard reweighting estimator (2.11): (a) mean estimate (ME) of the marginal probability of λ at 0 as a function of ω , (b) averaged estimates of the probability $\mathcal{C} = \mathcal{C}(L\tau)$ normalized to the exact probability and (c) its normalized standard error. All averages are obtained from 10^5 estimates and each estimate is obtained using $M = 10^4$ points.

Markov chain $\{\zeta_m, q_m\}_{1 \leq m \leq M}$ is used twice, first to obtain a AR estimate based on (2.10) and then to get a SR estimate based on (2.11). The m th state of the chain is generated as follows: ζ_m is drawn randomly and uniformly in $\Lambda = [0, 1]$ interval and q_m is drawn in the Gaussian distribution of $(2\omega)^{-1}$ variance and ζ_m mean. Displayed in Fig. (2.2) are the means and standard errors of 10^5 independent estimates, obtained using both estimators. We observe that, with increasing ω parameter, only the AR estimator yields an accurate estimation of the marginal probability of λ at 0 (Fig. 2.2.a) and of the correlation function (2.2.b). The computational speed-up of convergence that is achieved by using AR estimator rather than SR estimator can be assessed from their respective standard errors plotted as a function of ω in Fig. 2.2.c. As soon as ω becomes larger than 20, the standard error associated with AR estimator is two orders of magnitude lower than the one obtained using the SR estimator. The conditioning procedure accelerates the simulations by about four orders of magnitude. With conditioning, accurate estimates of the probability \mathcal{C} are always obtained, even for very narrow conditional distributions $\pi(\bar{q}|\lambda)$ for which the value of ω is large and \mathcal{C} is very small. For rare-event problems, available

alternatives [7, 47] to conditioning consists of post-processing the harvested information by implementing a self-consistent reweighting estimator.

2.4 Assessment of variance reduction

We consider the extended potential $\mathcal{U}(\zeta, \bar{q}) = \omega (\bar{q}^2 - 2\bar{q}\zeta)$ of the two-dimensional system of Sec. 2.3 and assess the numerical performance of the aforementioned methods of estimating the free energy $\mathcal{A}(\lambda)$ by computing the reduction of the statistical variances in Subsection 2.4.1 and explain the origin of this reduction in Subsection 2.4.2. Here, we still consider that the biasing potential is equal to the free energy. It is shown in Appendix C that this choice is optimal in term of overall variance reduction for the thermodynamic occupation method when the number of bins is large.

2.4.1 Free energy estimations

We generate a series of free energy estimates $\hat{\mathcal{A}}_X^M(\lambda; k)$ wherein $k \in \llbracket 1, K \rrbracket$ is the simulation index, using $K = 2 \cdot 10^3$ simulations, employing method $X = \text{TI, FEP, TO or AR}$ and setting the biasing potential equal to the true free energy $\mathcal{A}(\lambda)$. Each simulation consists of up to $M_{\max} = 10^5$ sampled states. The sampled distribution is $p_{\mathcal{A}}(\zeta, \bar{q}) \propto \exp[\mathcal{A}(\zeta) - \omega\bar{q}^2 + 2\omega\zeta\bar{q}]$, which is proportional to $\exp[-\omega(\zeta - \bar{q})^2]$. We compute the variance of the generated estimates using the following variance estimator

$$\text{var}^K \left(\hat{\mathcal{A}}_X^M \right) = \frac{1}{\|\Lambda\|} \sum_{\lambda \in \Lambda} \frac{1}{K} \sum_{k=1}^K \left(\frac{\hat{\mathcal{P}}_X^M(\lambda; k)}{\frac{1}{K} \sum_{h=1}^K \hat{\mathcal{P}}_X^M(\lambda; h)} - \frac{\sum_{\zeta \in \Lambda} \hat{\mathcal{P}}_X^M(\zeta; k)}{\sum_{\zeta \in \Lambda} \frac{1}{K} \sum_{h=1}^K \hat{\mathcal{P}}_X^M(\zeta; h)} \right)^2, \quad (2.12)$$

where M ranges from $5 \cdot 10^2$ to M_{\max} and

$$\hat{\mathcal{P}}_X^M(\lambda; k) = \frac{\exp \left[-\hat{\mathcal{A}}_X^M(\lambda; k) \right]}{\sum_{\zeta \in \Lambda} \exp \left[\mathcal{A}(\zeta) - \hat{\mathcal{A}}_X^M(\zeta; k) \right]}.$$

This quantity arises from the generic expression of the asymptotic variances of $\hat{\mathcal{A}}_X^M$ and corresponds to the k th estimate of the quantity $\exp[-\mathcal{A}(\lambda)] \times p_{\mathcal{A}}^{\Lambda}(\lambda)$. Note that when the bin of $\mathbf{1}_{\lambda}$ remains unvisited during the entire k th simulation, $\hat{\mathcal{A}}_{\text{TO}}^M(\lambda; k)$ is infinite and $\hat{\mathcal{P}}_{\text{TO}}^M(\lambda; k)$ is zero. However, the sums $\sum_{h=1}^K \hat{\mathcal{P}}_{\text{TO}}^M(\lambda; h)$ over the $2 \cdot 10^3$ simulations never canceled, so that the variance estimator (2.12) was always defined.

We display in Fig. 2.3 the estimated variances multiplied by the sample size M as a function of M in order to observe the convergence towards the asymptotic limit for the given number K of independent simulations. We observe that a considerable variance reduction is achieved in practice owing to the conditioning scheme. Furthermore, the asymptotic regime is obtained faster and the estimated variances are also less fluctuating with conditioning.

While fluctuations decrease with increasing K , it is extremely costly to obtain accurate estimates of the asymptotic variance for large sample sizes M for the FEP method when ω is large. The observed inefficiency of the FEP method results from the fact that the simulation samples non-overlapping distributions.¹

2.4.2 Fluctuation relations

To explain why adiabatic and standard reweighting estimators behave so differently, we resort to fluctuation relations [16, 48] in order to analyse how the quantity $p_{\mathcal{A}}(0)$ is evaluated in both approaches. This probability corresponds to the denominator of ratio (2.10) for the AR estimator, and of ratio (2.11) for the SR estimator, when $\alpha(\lambda)$ is set to $\mathcal{A}(\lambda)$. The marginal probability is $(1 + J)^{-1}$ when Λ contains $1 + J$ points. This probability is computed from two different ensemble averages, entailing two distinct types of fluctuation relations. For the BF approach, the following single relation must hold

$$\langle e^{-\Delta(q)} \rangle = \int_{\mathbb{R}} e^{-\Delta \bar{\mathcal{P}}(d\Delta)} = e^0 \quad (2.13)$$

¹In real FEP computations, the reaction path is usually divided into a number of small pieces and the standard reweighting estimator is applied for each of them.

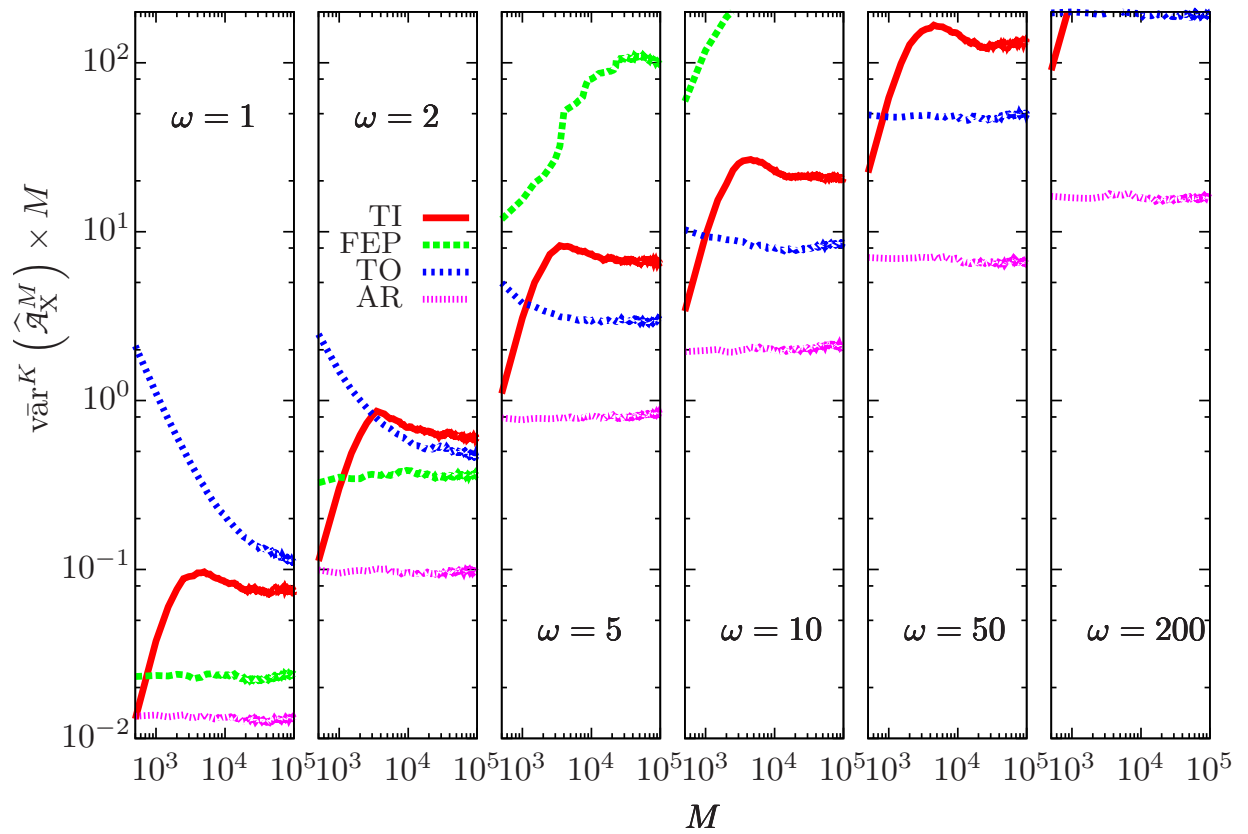


Figure 2.3: Evolution of the estimated variances as a function of the sample size M for the four free energy method ($X=TI, FEP, TO, AR$) and using $K = 2000$ simulations.

where $\Delta(q) = -\ln [p_{\mathcal{A}}(0, q)/\bar{p}_{\mathcal{A}}(q)]$ and $\bar{P}(\Delta)$ denotes the probability that $\Delta(q)$ takes the particular value Δ . As for the SR approach, a whole family of detailed fluctuation relations must be satisfied by the quantity $\Delta(\zeta, q) = -\ln [p_{\mathcal{A}}(0, q)/p_{\mathcal{A}}(\zeta, q)]$

$$\langle e^{-\Delta(\lambda, q)} \rangle_{\lambda} = \int_{\mathbb{R}} e^{-\Delta} P_{\lambda}(d\Delta) = e^0, \quad (2.14a)$$

$$\langle e^{-\Delta(\zeta, q)} \rangle = \sum_{\lambda \in \Lambda} \langle e^{-\Delta(\lambda, q)} \rangle_{\lambda} p_{\mathcal{A}}(\lambda) = e^0 \quad (2.14b)$$

where $P_{\lambda}(\Delta)$ denotes the probability that $\Delta(\lambda, q)$ takes the particular value Δ . The uniform average over $\lambda \in \Lambda$ yields an additional overall fluctuation relation (2.14b) corresponding to (2.13). Because the exponential function is strictly increasing, the negative values of Δ and the strictly positive ones have similar statistical weight in (2.13) or (2.14a), in the sense that the sum of the two contributions are equal to one (except for the case $\lambda = 0$). Hence, excessively small fractions of negative Δ values will result in large statistical variance and in slow numerical convergence of the estimates as a function of simulation time [16]. The probabilities $P_{\lambda}(\Delta)$ with $\lambda \in \{0, \frac{1}{4}, \frac{1}{2}, \frac{3}{4}, 1\}$ and $\bar{P}(\Delta)$ have been plotted as a function of Δ for $\omega = 5$ in Fig. 2.4.a and for $\omega = 100$ in Fig. 2.4.b. From the distributions at $\omega = 100$, we observe that the probability to have $\Delta(\zeta_m, q_m) \leq 0$ is negligible when $\zeta_m > \frac{1}{2}$. Given the fact that the ζ_m 's are sampled uniformly in $[0, 1]$, substantial deviations from fluctuation relations (2.14a) will inevitably be measured in typical (finite-length) simulations, resulting in inaccurate SR estimates. At variance, the AR approach does not suffer from this limitation, as the fluctuation relation that must be satisfied is global. We indeed observe that the fraction of the negative values of Δ is always substantial, making the AR estimator particularly efficient for large ω values.

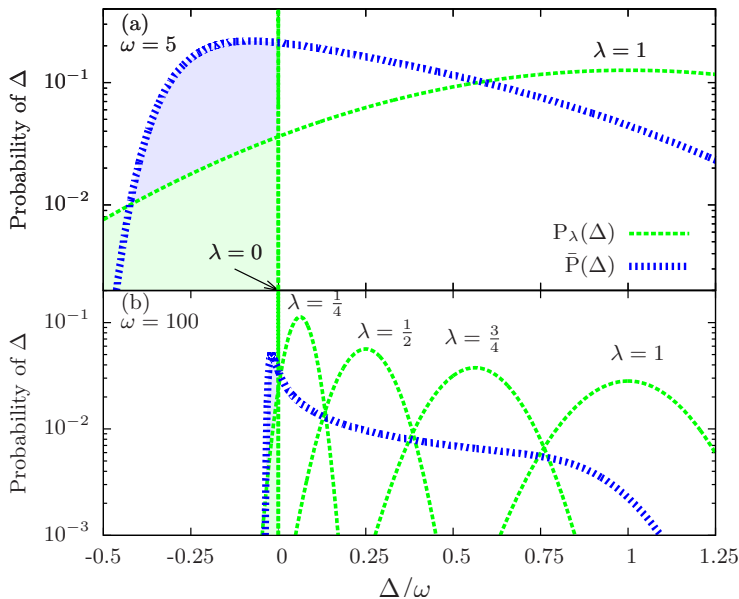


Figure 2.4: Probability distribution of Δ as a function of the Δ , blue curve for AR estimator and green curves for SR estimator with various values of $\lambda \equiv \theta$.

2.5 Summary

Estimating relative free energies and free energy differences are two important tasks of expanded ensemble simulations and of molecular simulation in general. When a conditioning scheme is implemented for estimating the free energy in an expanded ensemble, the three standard approaches (thermodynamic integration, thermodynamic occupation and free energy perturbation) merge into the adiabatic reweighting method that inherits the appealing features of each parent method. Conditioning should always be implemented since it ensures variance reduction compared to any of the three standard approaches.

When, in addition to conditioning, the biasing potential is equal to the free energy, the marginal distribution that is sampled exhibits excellent overlapping properties, making it possible to retrieve the relevant information in rare event problems. This makes the conditioning approach particularly suited to free-energy and rare-events

calculations. Besides, it does not require any postprocessing, unlike with self-consistent estimators.

In Chapter 3, we proceed further with the description of algorithms achieving homogeneous sampling along the external parameter or the reaction coordinate.

3 | Advanced Monte Carlo and adaptively biased sampling

In this Chapter, we focus on two enhanced sampling techniques, advanced Monte Carlo and adaptively biased sampling. The former technique aims at enabling non-local Monte Carlo moves ideally crossing free energy barriers. The second technique aims at flattening the free energy surface with the help of an auxiliary biasing potential adapted during the course of the simulation.

Outline of the Chapter After recalling the principle of biased sampling along some internal or external coordinates, we show its limitation for overcoming free energy barriers and outline the advantage of advanced Monte Carlo. We eventually discuss various schemes of adapting the auxiliary biasing potential or its gradient and show how to apply such a scheme to the characterization of the transition temperature in a small Lennard-Jones cluster.

3.1 Biased sampling along external and internal coordinates: similarities and differences

Because ergodicity issues along a reaction coordinate are similar to those occurring along an external parameter, adaptive techniques allowing to construct an appropriate biasing potential are the same in both situations. It is instructive to make a parallel between the external parameter and reaction coordinate using the same extended potential framework of probability $p_0(\zeta, \bar{q})$, with unbiased expectations \mathbb{E}_0 denoted by \mathbb{E} for simplicity.

Problems arise whenever the sampling along a coordinate, either external or internal, is confined into a small portion of the range of interest, here Λ or Ξ . It becomes particularly problematic to compute the relative free energy along the associated coordinate, because it is equal to the cologarithm of the probability to observe the desired coordinate value

$$\mathcal{A}(\lambda) = -\ln \mathbb{E} [\mathbf{1}_\lambda(\zeta)], \quad \lambda \in \Lambda, \quad (3.1a)$$

$$\mathcal{F}(\xi^*) = -\ln \mathbb{E} [\mathbf{1}_{\xi^*} \circ \xi(q)], \quad \xi^* \in \Xi, \quad (3.1b)$$

where Λ in (3.1a) and Ξ in (3.1b) are two discrete sets. The indicator function along the reaction coordinate is used to approximate the Dirac distribution $\delta_{\xi(q)-\xi^*}(dq)$ associated with $\xi(x)$ and centered on ξ^* . We consider that the external parameter λ couples quadratically to $\xi(q)$. We show later that this coupling is practically useful in the advanced Monte Carlo scheme described in Sec. 3.2. Biased sampling consists of subtracting a biasing potential so as to achieve a more homogeneous sampling along the desired coordinate. This is what was done in chapter 1 with the additional auxiliary biasing potential $\alpha(\lambda)$. We can similarly introduce a biasing the biasing potential $q \mapsto f \circ \xi(q) = f[\xi(q)]$ with respect to the reaction coordinate. The resulting biased probabilities are

$$p_\alpha(\lambda, q) = \frac{\exp[\alpha(\lambda) - \mathcal{U}(\lambda, q)]}{\sum_{\zeta \in \Lambda} \int_{\mathcal{Q}} \exp[\alpha(\zeta) - \mathcal{U}(\zeta, q)] dq},$$

$$p_f(\lambda, q) = \frac{\exp[f \circ \xi(q) - \mathcal{U}(\lambda, q)]}{\sum_{\zeta \in \Lambda} \int_{\mathcal{Q}} \exp[f \circ \xi(q) - \mathcal{U}(\zeta, q)] dq}.$$

The unbiased probability can also be written as a function of the biased probabilities

$$p_0(\zeta, \bar{q}) = \frac{\exp[-\alpha(\zeta)]p_a(\zeta, \bar{q})}{\sum_{\zeta \in \Lambda} \int_{\mathcal{Q}} \exp[-\alpha(\zeta)]p_a(\zeta, d\bar{q})} = \frac{\exp[-\alpha(\zeta)]p_a(\zeta, \bar{q})}{\mathbb{E}_a[\exp[-\alpha(\zeta)]]} = \frac{\mathfrak{h}_a(\zeta)p_a(\zeta, \bar{q})}{\mathbb{E}_a[\mathfrak{h}_a(\zeta)]} \quad (3.2a)$$

$$p_0(\zeta, \bar{q}) = \frac{\exp[-f \circ \xi(\bar{q})]p_f(\zeta, \bar{q})}{\sum_{\zeta \in \Lambda} \int_{\mathcal{Q}} \exp[-f \circ \xi(\bar{q})]p_f(\zeta, d\bar{q})} = \frac{\exp[-f \circ \xi(\bar{q})]p_f(\zeta, \bar{q})}{\mathbb{E}_f[\exp[-f \circ \xi(\bar{q})]]} = \frac{\mathfrak{h}_f \circ \xi(\bar{q})p_f(\zeta, \bar{q})}{\mathbb{E}_f[\mathfrak{h}_f \circ \xi(\bar{q})]}, \quad (3.2b)$$

where \mathbb{E}_a in (3.2a) and \mathbb{E}_f in (3.2b) denote the biased expectations associated with probabilities $p_a(\zeta, \bar{q})$ and $p_f(\zeta, \bar{q})$, respectively. The quantity $\mathfrak{h}_a(\zeta)$ is defined in Table 2.1 and $\mathfrak{h}_f(\xi^*) = \exp[-f(\xi^*)]$ is defined by extension. In this formulation (3.2), the way of removing the bias is a generalization of the histogram binning method considered in Chapter 2 for conditional expectations. The following pair of similar relations between the unbiased and biased expectations of observable $\mathcal{O}(\zeta, q)$ are thus obtained

$$\mathbb{E}[\mathcal{O}(\zeta, q)] = \frac{\mathbb{E}_a[\mathcal{O}(\zeta, q) \exp[-\alpha(\zeta)]]}{\mathbb{E}_a[\exp[-\alpha(\zeta)]]}; \quad \mathbb{E}[\mathcal{O}(\zeta, q)] = \frac{\mathbb{E}_f[\mathcal{O}(\zeta, q) \exp[-f \circ \xi(q)]]}{\mathbb{E}_f[\exp[-f \circ \xi(q)]]}. \quad (3.3a,b)$$

Replacing $\mathcal{O}(\zeta, q)$ by $\mathbf{1}_\lambda$ and $\mathbf{1}_{\xi^*} \circ \xi$ in (3.3a,b) yields a pair of identities expressing the free energies

$$\mathcal{A}(\lambda) = \alpha(\lambda) - \ln \mathbb{E}_a[\mathbf{1}_\lambda(\zeta)] + \ln \mathbb{E}_a[\exp[-\alpha(\zeta)]], \quad (3.4a)$$

$$\mathcal{F}(\xi^*) = f(\xi^*) - \ln \mathbb{E}_f[\mathbf{1}_{\xi^*} \circ \xi(q)] + \ln \mathbb{E}_f[\exp[-f \circ \xi(q)]]. \quad (3.4b)$$

The right-hand side terms in (3.4a) and (3.4b) are constants and independent of λ or ξ^* .

Biasing along an internal coordinate $\xi(q)$ differs from biasing along λ in that resorting to conditioning is not practical in general, as it would require evaluating the potential energy of all the particle positions inside a high-dimensional hypersurface. Another difference is that the free energy along a generalized internal coordinate can not always be differentiated. This is the case of the free energy along the orientation-bond order parameter of Steinhardt, Nelson, and Ronchetti [28]. This order parameter is not continuous and the associated mean force, the free energy derivative, cannot be averaged. This issue is discussed in Sec. 3.4. At variance, the free energy $\mathcal{A}(\lambda)$ is differentiable for the usual setups coupling the external parameter λ and the internal coordinate ($\xi(q)$ or $\mathcal{U}(q)$). A remarkable similarity shared by both biasing approaches is eventually worth noticing. Setting α and f to their respective free energies entails that the respective functions $\lambda \mapsto \mathbb{E}_a[\mathbf{1}_\lambda(\zeta)]$ and $\xi^* \mapsto \mathbb{E}_f[\mathbf{1}_{\xi^*} \circ \xi(q)]$ are both constant on Λ and Ξ . This in turn implies that uniform sampling is normally achieved along the corresponding coordinate, unless there exist hidden metastabilities in some hyper-surface orthogonal to the coordinate gradient. The subsequent limitation of biased sampling is illustrated with the help of simple simulations in a problematic two-dimensional system.

3.2 Hidden metastabilities and advanced Monte Carlo

Hidden metastabilities may occur when the chosen internal coordinate is an inappropriate reaction coordinate. In this situation, biased simulations may fail to achieve ergodic sampling. We illustrate this issue on a simple model, a two-dimensional system with periodic boundary conditions along the first coordinate q_1 . The phase space is denoted by $\mathbb{T} \times \mathbb{R}$ where $\mathbb{T} = [-3, 3]$ is the centered period. The potential energy and the extended potential energy are respectively

$$\mathcal{U}_0(q_1, q_2) = \omega(q_2)^2 + \mathcal{U}_{hc}(q_1, q_2), \quad \mathcal{U}(\lambda, q_1, q_2) = \frac{\kappa}{2}(\lambda - q_1)^2 + \mathcal{U}_0(q_1, q_2).$$

The harmonic potential $\omega(q_2)^2$ is introduced to restrain the large deviation of $|q_2|$ absolute values from its origin in simulations. The hard-core potential \mathcal{U}_{hc} describes the action of an impassable quadrangle obstacle centered on $(0, 0)$. It is infinite if (q_1, q_2) lies inside the periodically replicated quadrangle of vertexes $(1, 0) - (h, 1) - (-1, 0) - (-h, -1)$, otherwise the particle lies outside the obstacle and the hard-core potential is equal to 0. The horizontal locations of the top and bottom vertexes are determined by the value of h , initially set to 0. The period of the potential along q_1 is half the spatial period, so that the system presents exactly 2 basins of attraction. Contours of the potential energy surface are plotted in Fig. 3.1. The selected internal coordinate is

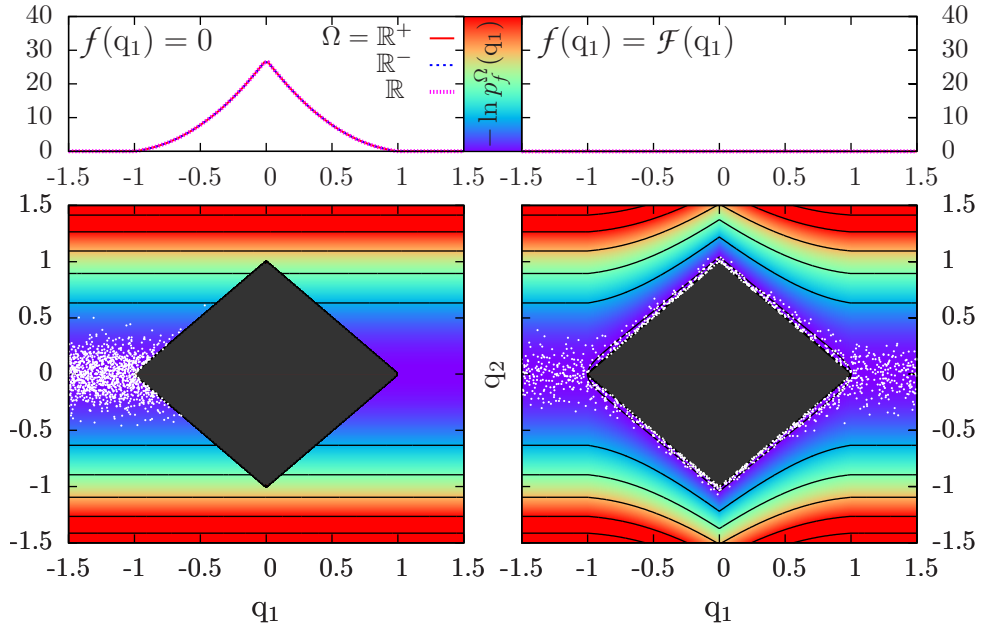


Figure 3.1: MC simulations of the two-dimensional toy model with symmetric hard-core obstacle ($h = 0$). Contours of the biased potential energy surface $(q_1, q_2) \mapsto \mathcal{U}_0(q_1, q_2) - f(q_1)$ are plotted in the two bottom panels, with $f(q_1)$ set to 0 (left panel) or to the free energy $\mathcal{F}(q_1)$ (right panel). The biased free energy barriers $-\ln p_f^\Omega(q_1)$ are shifted to their minimum value and plotted as a function of q_1 in the two top panels for Ω set to \mathbb{R}^+ , \mathbb{R}^- and \mathbb{R} . Some sampled configurations are materialized by the small white dots. The obstacle prevents the trajectory from escaping its basin of attraction (bottom left panel). The biased MC trajectories is able to bypass the obstacle either by transitioning through the up or down channels.

q_1 and the harmonic potential that couples λ to q_1 is introduced in anticipation of later use.

We first consider the sampling of the biased marginal probability $\bar{p}_f(q_1, q_2) \propto \exp[f(q_1) - \mathcal{U}_0(q_1, q_2)]$ in which biasing potential $f(q_1)$ is subtracted from the potential energy so as to enhance the sampling along the internal coordinate. The probability to observe the system at q_1 with $q_2 \in \Omega$ is

$$p_f^\Omega(q_1) = \frac{\int_{\Omega} \exp[f(q_1) - \mathcal{U}_0(q_1, q_2)] dq_2}{\int_{\mathbb{T} \times \mathbb{R}} \exp[f(q_1) - \mathcal{U}_0(q_1, q_2)] dq_1 dq_2}.$$

The free energy along q_1 is therefore

$$\mathcal{F}(q_1) = -\ln \frac{\int_{\mathbb{R}} \exp[-\mathcal{U}_0(q_1, q_2)] dq_2}{\int_{\mathbb{T} \times \mathbb{R}} \exp[-\mathcal{U}_0(q_1, q_2)] dq_1 dq_2} = f(q_1) - \ln p_{\mathbb{R}}(q_1) + \text{Constant}.$$

The system can escape its trapping basin by circumventing the impenetrable obstacle through the top or bottom channels. This event is extremely rare in unbiased simulations when ω is large enough. We study this situation by setting ω to 50. Two Monte Carlo simulations are performed using the Metropolis algorithm 1 described p. 113. The biasing potential $f(q_1)$ is set to zero in the first simulation and to $\mathcal{F}(q_1)$ in the second simulation. The latter setup flattens the apparent free energy, $-\ln p_{\mathbb{R}}^{\mathbb{R}}(q_1)$, as shown in Fig. 3.1. Some of the sampled configurations are shown on the contour plots of the potential energy surface by the small white dots. In simulations with the biasing potential switched on, the sampling becomes ergodic and completely homogeneous along q_1 . In this situation, q_1 is said to be a good reaction coordinate, despite the fact that the reaction can follow two distinct pathways.

When the obstacle shape is made asymmetrical, the internal coordinate q_1 becomes an inappropriate RC, in the sense that it can not be used anymore to correctly monitor the transitions between the two metastable basins. We illustrate the reaction coordinate issue by setting h to $2/3$ and performing the two previous shorts simulations again, with the biasing potential first switched off and then set equal to the free energy. The contour

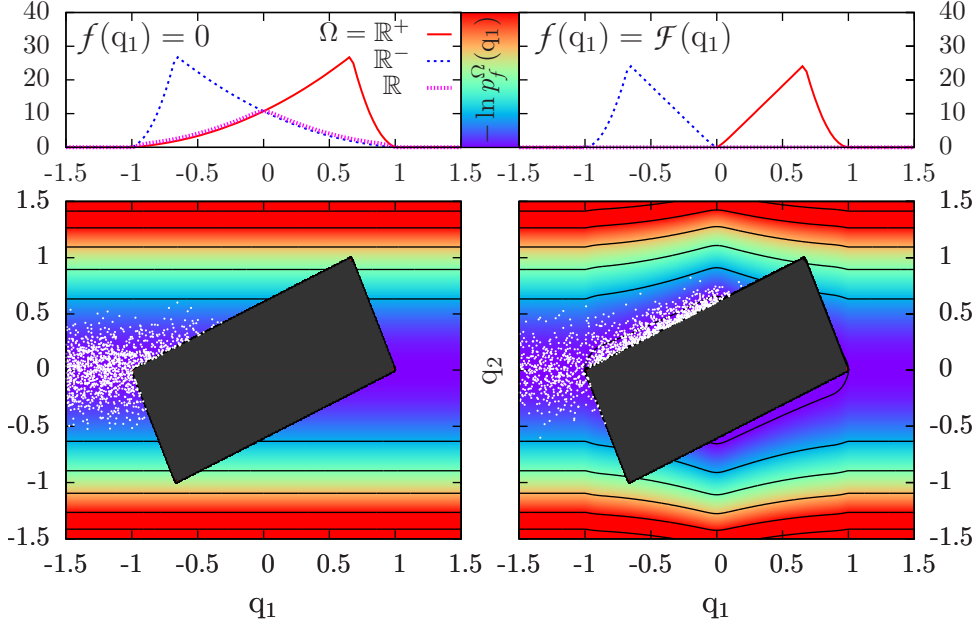


Figure 3.2: Identical set-up as in Fig. 3.1, except that the obstacle shape is now asymmetrical ($h = 2/3$). Left column panels: the bias is switched off. Right column panels: the bias switched on and set to $f(q_1)$. The displayed curves $-\ln p_f^{\mathbb{R}^+}(q_1)$ and $-\ln p_f^{\mathbb{R}^-}(q_1)$ correspond to the effective free energy along the two possible transition channels. The residual free energy barriers in each channel prevent the evolving system from transitioning even though uniform sampling is expected asymptotically (since $\Omega = \mathbb{R}$ and $p_f^{\mathbb{R}}(q_1)$ is constant).

plots of the potential energy surfaces and the simulation results are displayed in Fig. 3.2. We observe that the simulated trajectory can never escape its trapping basin, even when the biasing potential is switched on and homogeneous sampling is expected along q_1 . The reason is that to circumvent the asymmetrical obstacle, one of the two free energy barriers displayed in top right panels in Fig. 3.2 must be crossed. Biasing along q_1 does not allow to guide the system inside either of the two possible transition paths, at variance with the previous symmetrical set-up. Note that biasing with the free energy profile based on either of the 2 channels confines the system to the opposite channel.

The natural way of achieving sampling ergodicity would be to bias the simulations along more appropriate reaction coordinates. Identifying good reaction coordinates is indeed an active field of research [49]. However, there exist many systems presenting multiple transition pathways that we don't know how to describe by means of a one- or two-dimensional reaction coordinates. Another way to achieve improved ergodicity is to resort to advanced Monte Carlo techniques [14]. We describe and implement such a technique [44] below. The technique, termed “work-bias Monte Carlo” (WBMC), need not be able to discriminate the multiple transitioning channels to sample them.

Work-bias Monte Carlo scheme

The WBMC scheme [44] consists of generating the trial configurations in the Metropolis algorithm through nonequilibrium paths so as to allow for non-local or global Monte Carlo moves jumping across free energy barriers. WBMC employs an external parameter coupled to the system to guide the system from one basin to another one. The algorithmic structure is presented in Algorithm 2 of Appendix B. The variation of energy along a trajectory starting in (λ^0, q^0) and ending in (λ^L, q^L) is sketched in figure 3.3 and satisfies the conservation equation

$$\mathcal{U}_f(\lambda^L, q^L) - \mathcal{U}_f(\lambda^0, q^0) = \sum_{\ell=0}^{L-1} \mathcal{W}_f^{\ell \rightarrow \ell+1} + \sum_{\ell=0}^{L-1} \mathcal{Q}_f^{\ell \rightarrow \ell+1} = \mathcal{W}_f^{0 \rightarrow L} + \mathcal{Q}_f^{0 \rightarrow L}$$

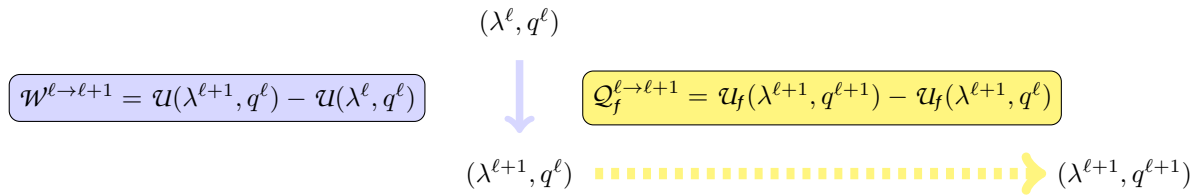


Figure 3.3: The quantity $\mathcal{W}^{\ell \rightarrow \ell+1}$ represents the work done on the system when switching the external parameter from λ^ℓ to $\lambda^{\ell+1}$ (plain arrows). The quantity $\mathcal{Q}_f^{\ell \rightarrow \ell+1}$ represents the heat exchanged with the thermostat during the subsequent relaxation of the system (dashed arrow).

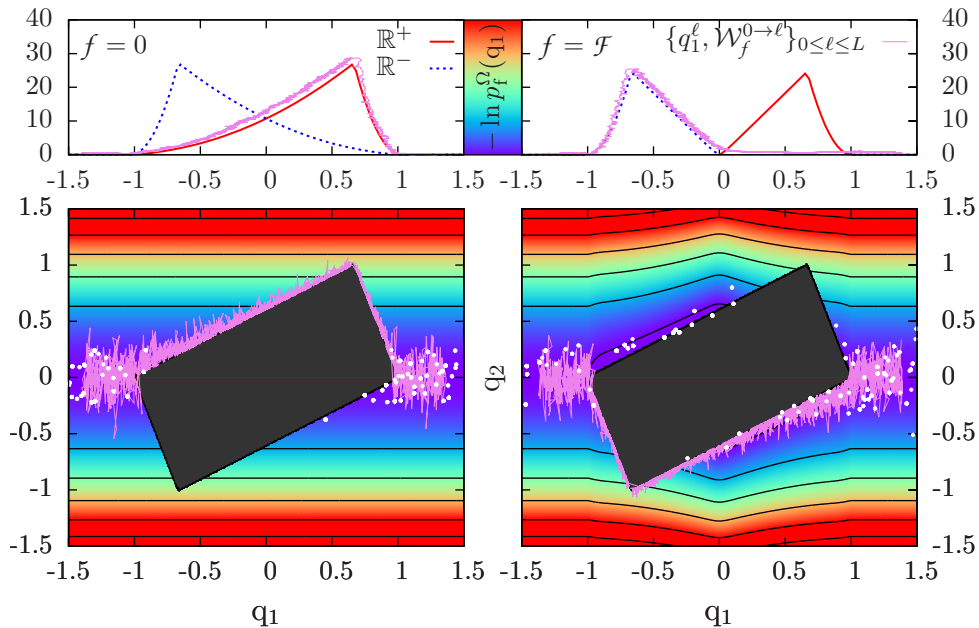


Figure 3.4: The WBMC scheme generates global moves based on the trajectories displayed in purple. The work along the paths approximates the free energy profile in the corresponding channel, a feature enabling the system to cross the barrier with a high probability. The auxiliary biasing potential f has been set to 0 (left panels) or to the free energy \mathcal{F} (right panels). White circles are the points sampled by a few WBMC moves.

where each $\mathcal{Q}_f^{\ell \rightarrow \ell+1}$ is the energy variation after a local Monte Carlo move and $\mathcal{W}^{0 \rightarrow L}$ is the effective work associated with a global trial Monte Carlo move, the acceptance probability being $\min[1, \exp(-\mathcal{W}^{0 \rightarrow L})]$.

The algorithm samples the marginal probability $p_f^Q(q)$ because it satisfies the detailed balance condition with respect to this distribution. The general proof that the detailed balance is obeyed by work-bias Monte Carlo moves is given in the Appendix of Ref [44]. In figure 3.4, it is shown that both basins of the toy model are sampled owing to the fact that some WBMC moves cross the local free energy barriers. The WBMC scheme has been used in [44] to insert/delete particles in a Lennard-Jones liquid. In this application, the external parameter is the particle number which allows particles to be gradually deleted or added to the dense fluid. Direct insertions and deletions using the standard Metropolis algorithm fail in dense fluids due to the high rejection rate.

3.3 Adaptively biased sampling

Here, we described adaptively biased sampling methods that construct the biasing potential on the fly during the simulation using the current estimate of the free energy so as to ensure uniform sampling. We thus consider that the internal or external coordinate on which the biasing potential applies correctly capture the transformation along this coordinate.

Many schemes have been proposed in the literature, but they can easily be classified into only two categories, depending on whether it is the biasing potential that is adapted or its gradient [32].

3.3.1 Adaptive biasing potential method

The biasing potential is adapted resorting to identities (3.4a) and (3.4b). The approach was proposed in Ref. [33] in the expanded ensemble framework based on identity (3.4), which relates the biasing potential, the logarithm of the measured probability and the free energy. It was proposed to construct the ideal biasing potential iteratively through a series of I static simulations. This corresponds to the concept of adaptation. The i th simulation ($i \in \llbracket 1 ; I \rrbracket$) consists of performing μ_i MC steps with biasing potential \mathbf{a}_i or \mathbf{f}_i so as to estimate next \mathbf{a}_{i+1} or \mathbf{f}_{i+1} . The successive sample sizes $\{\mu_i\}_{1 \leq i \leq I}$ are the crucial parameters of the iterative algorithm, as they determine the updating frequency of the biasing potential. Typically, the μ_i 's are much larger than one and moderate in the first iterations and increases in the last iterations when sampling becomes homogeneous along ξ coordinate. For the production simulation based on \mathbf{a}_I or \mathbf{f}_I , μ_I is usually the largest. The iterative biasing potential algorithm is obtained by setting $\gamma_i = \mu_i$ in Algorithm 3 page 114. The inner-loop on m corresponds to the static estimation associated with the next biasing potential, the outer-loop on i corresponding to the iterative construction. The limitation of this iterative algorithm is that a reliable estimate of the free energy must be obtained in a larger subrange of Ξ at each iteration because $\gamma_i = \mu_i$, implying a series of relatively long simulations: $\mu_i \gg 1$. This issue can be alleviated by updating the biasing potential continuously ($\mu_i = 1$), i.e., each time a configuration is sampled, and by a small amount. To satisfy the second criterion, one sets $\gamma_i \ll 1$, this factor controlling the amplitude of the adaptations. Because $\mu_i = 1$, the positive weights γ_i must additionally decrease to 0 as i tends to infinity so as to ensure that the adaptive biasing potential converges towards the free energy in this limit. This way of proceeding corresponds to the Wang-Landau algorithm described in Algorithm 4 of Appendix B. Note that in both ABP algorithms, the right-hand side logarithms in each updating rule stem from (3.4) and serve to ensure that the adaptive biasing potential is normalized:

$$\int_{\Xi} \exp[-f_0(\xi^*)] d\xi^* = 1 \quad \implies \quad \int_{\Xi} \exp[-f_i(\xi^*)] d\xi^* = 1.$$

Other variant ABP algorithms have been proposed in the literature, such as self-healing umbrella sampling [50] and metadynamics [51]. A review can be found in [15]. A detailed proof of convergence is given in [52] for a linearized version of algorithm 3. The proof is then extended to the original Wang-Landau version assuming $\gamma_i \ll 1$.

The common limitation of all ABP algorithms involves the optimal choice of the updating sequence $\{\gamma_i/\mu_i\}_{1 \leq i \leq I}$, which controls the rate of convergence. If the ratio γ_i/μ_i converges to 0 too fast, then the adaptation amplitude will be very small. The biasing potential will subsequently converge slowly to the free energy. At variance, if the ratios converge to 0 too slowly, then the biasing potential will fluctuate for a long period prior to stabilizing. Finding a good trade-off between these two adverse situations requires judiciously tuning the updating parameters, not an easy task in general.

The adapting biasing force method discussed below is (almost) free of such updating parameters.

3.3.2 Adaptive biasing force method along internal coordinate

The adaptive biasing force method constructs the biasing potential $\mathcal{A}(\lambda)$ or $\mathcal{F}(\xi^*)$ by adapting its derivative from the current estimate of the mean force. Estimating the mean force $\mathcal{F}'(\xi^*)$ is more complicated than estimating the mean force $\mathcal{A}(\lambda)$ in general. This is because the function $q \mapsto \xi(q)$ involves a non trivial dependence on the positions. The assumptions in the following developments are that the function $\xi(q)$ is smooth over \mathcal{Q} and that the $[\nabla \xi^T(q) \nabla \xi(q)]^{-1}$ is bounded. Here, one considers that the reaction coordinate can be differentiated twice and that its dimension is d . For a d -dimensional column vector $f(q)$, the divergence $\text{div } f$ is the d -dimensional column vector defined component-wise as $[\text{div } f(q)]_{\alpha} = \sum_{i=1}^d \partial_{q_i} f_{\alpha}(q)$. Resorting to the co-area formula and integrating by parts enable one to differentiate (3.4b) and to obtain the following identity

$$\mathcal{F}'(\xi^*) = - \frac{\int_{\mathcal{Q}} \text{div} \left[\exp[-\mathcal{U}_0(q)] [(\nabla \xi(q))^T \nabla \xi(q)]^{-1} \nabla \xi(q) \right] \delta_{\xi^* - \xi(q)}(dq)}{\int_{\mathcal{Q}} \exp[-\mathcal{U}_0(q)] \delta_{\xi^* - \xi(q)}(dq)}, \quad (3.5)$$

where $\nabla\xi$ is a $N \times d$ matrix, $(\nabla\xi)^T\xi$ is a $d \times d$ matrix whose inverse matrix is precisely $[(\nabla\xi)^T\xi]^{-1}$ in (3.5). The derivation of this relation being quite involved, the reader is referred to [15] for details. We can rewrite the mean force (3.5) as a conditional expectation given $\xi(q) = \xi^*$

$$\mathcal{F}'(\xi^*) = \mathbb{E} \left[\frac{d\mathcal{U}_0}{d\xi}(q) \middle| \xi(q) = \xi^* \right],$$

where we defined the local mean force by

$$\begin{aligned} \frac{d\mathcal{U}_0}{d\xi}(q) &= -\exp[\mathcal{U}_0(q)] \operatorname{div} \left[\exp[-\mathcal{U}_0(q)] [(\nabla\xi(q))^T \nabla\xi(q)]^{-1} \nabla\xi(q) \right] \\ &= \left[[(\nabla\xi)^T \nabla\xi]^{-1} \nabla\xi \right]^T \nabla_q \mathcal{U}_0(q) - \operatorname{div} \left[[(\nabla\xi)^T \nabla\xi]^{-1} \nabla\xi(q) \right] \end{aligned} \quad (3.6)$$

where ∇_q denotes the gradient with respect to q and where the dependence of ξ on q in the second line was dropped for clarity. Formula (3.6) applies to a d -dimensional reaction coordinate. For a one dimensional reaction coordinate, we have $(\nabla\xi)^T \nabla\xi = \nabla\xi \cdot \nabla\xi$ and $\frac{d\mathcal{U}_0}{d\xi} = (\nabla\xi \cdot \nabla_q \mathcal{U}_0) / (\nabla\xi \cdot \nabla\xi) - \operatorname{div} [\nabla\xi / (\nabla\xi \cdot \nabla\xi)]$. Since the free energy corresponds to the integral of the mean force with respect to ξ , this one is also referred to as *potential of mean force* in the chemical or biophysical literature. This one can also be cast as a ratio of two biased averages, i.e. in a form similar to (3.3a,b)

$$\mathcal{F}'(\xi^*) = \frac{\int_{\mathcal{Q}} \frac{d\mathcal{U}_0}{d\xi}(q) \exp[\mathbf{f} \circ \xi(q) - \mathcal{U}(q)] \delta_{\xi^* - \xi(q)}(dq)}{\int_{\mathcal{Q}} \exp[\mathbf{f} \circ \xi(q) - \mathcal{U}(q)] \delta_{\xi^* - \xi(q)}(dq)} = \frac{\mathbb{E}_{\mathbf{f}} \left[\frac{d\mathcal{U}_0}{d\xi}(q) \delta_{\xi^* - \xi(q)}(q) \right]}{\mathbb{E}_{\mathbf{f}} \left[\delta_{\xi^* - \xi(q)}(q) \right]}. \quad (3.7)$$

Based on (3.7), Darve and Pohorille proposed to adapt the biasing force \mathbf{f} using the current estimate of the mean force, as done in Algorithm 5 page 115 of Appendix B with K replicas of the system $\{q_m^k\}_{1 \leq k \leq K}$ evolving in parallel and guided using the common adaptive biasing force $\mathbf{f}_m \circ \xi$. After completion algorithm 5, the adaptive biasing force is equal to

$$\mathbf{f}'_M(\xi^*) = \frac{\sum_{m=1}^M \sum_{k=1}^K \frac{d\mathcal{U}_0}{d\xi}(q_m^k) \mathbf{1}_{\xi^*}[\xi(q_m^k)]}{\sum_{m=1}^M \sum_{k=1}^K \mathbf{1}_{\xi^*}[\xi(q_m^k)]}, \quad \xi^* \in \Xi,$$

which yields an estimate of the mean force $\mathcal{F}'(\xi^*)$ within the interval Ξ . The proof that the biasing force converges to \mathcal{F} within Ξ in the large sample limit ($M \rightarrow +\infty$) can be found in Ref [32]. After convergence, the $\xi(q_m^k)$ variables will freely explore Ξ .

The ABF approach assumes the existence of the mean local force and the ability to evaluate it. In particular, the mean local force should be defined for all configurations with non zero probability. With the hard-core potential used to illustrate the concept of biased sampling in Section 3.2, the mean local force $\mathcal{U}_\xi(\lambda, q)$ is not defined on the perimeter of the hard-obstacle. As a result, the mean force should include a contribution arising from the dependence of the obstacle boundary on the reaction coordinate. The ABF method, as based on algorithm 5, cannot be implemented.

A solution to the problem consists of implementing ABF with respect to an external parameter that is harmonically coupled to the reaction coordinate, resorting to algorithm 6. In this context, the extended potential should exhibit the form given in (1.9) and (1.10). The present harmonic setting is not only used in extended ABF [34], but also in unified free energy dynamics [53] and extended Lagrangian metadynamics [54, 55]. The last formulation of metadynamics differs from the (currently) most widely implemented formulation [51] in which a biasing potential similar to α acts directly on the reaction coordinate, $\xi(q)$. Once the biasing force has been adapted using algorithm 6, the expected value of any observable can be estimated using the adiabatic reweighting estimator described in algorithm 7 of Appendix B.

3.4 Estimation of the free energy along a reaction coordinate

3.4.1 ξ -AR estimator

Here, we show how to estimate the free energy along an internal reaction coordinate $\xi(q)$ with a biasing potential acting upon the external parameter in the *harmonic setup*. In practice, the quantity that is directly estimated is

the total expectation of the characteristic function $\mathbf{1}_{\xi^*} \circ \xi$, i.e. the probability to observe the reaction coordinate taking value ξ^* . Substituting $\mathbf{1}_{\xi^*} \circ \xi(q)$ for the observable $\mathcal{O}(\lambda, q)$ in Eq. (2.7), one obtains the AR estimator of total expectation $\mathbb{E}[\mathbf{1}_{\xi^*}]$

$$\Upsilon_{\text{H}}^M(\mathbf{1}_{\xi^*}) = \frac{\frac{1}{M} \sum_{m=1}^M \mathbf{1}_{\xi^*} \circ \xi(\bar{q}_m) \mathbb{P}_a(\bar{q}_m)}{\frac{1}{M} \sum_{m=1}^M \mathbb{P}_a(\bar{q}_m)}.$$

The corresponding asymptotic variance is given in Eq. A.4 in Appendix A. The free energy estimate is obtained by taking the co-logarithm of the estimated probability.

To write the function \mathbb{P}_a explicitly, let introduce the following effective restraining potential

$$\bar{\mathcal{R}}_a(\xi^*) = \ln \sum_{\zeta \in \Lambda} \exp[a(\zeta) - \mathcal{R}(\zeta, \xi^*)].$$

The marginal probability of q therefore writes $p_a^{\mathcal{Q}}(q) = \exp[-\mathcal{U}_0(q) + \bar{\mathcal{R}}_a \circ \xi(q) - \Psi_a^A]$. Thanks to the potential ε , the identity $\bar{\mathcal{R}}_0 \circ \xi(q) = 0$ holds whatever $q \in \mathcal{Q}$ and we have

$$\mathbb{P}_a(q) = \frac{p_a^{\mathcal{Q}}(q)}{p_a^{\mathcal{Q}}(q)} = \exp[-\bar{\mathcal{R}}_a \circ \xi(q)].$$

Hence, the AR estimator further simplifies into

$$\Upsilon_{\text{H}}^M(\mathbf{1}_{\xi^*}) = \exp[-\bar{\mathcal{R}}_a(\xi^*)] \frac{\frac{1}{M} \sum_{m=1}^M \mathbf{1}_{\xi^*}(\xi_m)}{\frac{1}{M} \sum_{m=1}^M \exp[-\bar{\mathcal{R}}_a(\xi_m)]},$$

where $\xi_m = \xi(\bar{q}_m)$. The estimator of the free energy is eventually obtained by taking the co-logarithm

$$\widehat{\mathcal{F}}(\xi^*)_{\text{AR}}^M = \bar{\mathcal{R}}_a(\xi^*) - \ln \Gamma^M(\mathbf{1}_{\xi^*} \circ \xi) + \ln \Gamma^M(\exp[-\bar{\mathcal{R}}_a \circ \xi]). \quad (3.8)$$

This specific estimator, denoted ξ -AR estimator in the following, has been applied to free energy calculations associated with vacancy migration in α -iron [34] and molecular folding [56]. Recently, it has been proposed to evaluate the free energy $\mathcal{F}(\xi^*)$ using an alternative estimator [40] referred to as *corrected z-average restraint* (CZAR) wherein $\xi^* \equiv z$. The CZAR estimator only differs from the ξ -AR estimator in the way the effective restraining potential is evaluated in (3.8). In CZAR, $\bar{\mathcal{R}}_a(\xi^*)$ is evaluated through thermodynamic integration, i.e. by integrating estimates of its derivative $\bar{\mathcal{R}}_a'(\xi^*)$. This is done by casting the effective restraining gradient in the form of a conditional expectation

$$\bar{\mathcal{R}}_a'(\xi^*) = \partial_{\xi^*} \ln \sum_{\lambda \in \Lambda} \exp[a(\lambda) - \mathcal{R}(\lambda, \xi^*)] = - \sum_{\lambda \in \Lambda} \partial_{\xi^*} \mathcal{R}(\lambda, \xi^*) \pi_a^\lambda(\xi^*) = -\mathbb{E}_a[\partial_{\xi^*} \mathcal{R}(\cdot, \xi^*) | \xi^*], \quad (3.9)$$

where the conditional probability given ξ^* reads

$$\pi_a^\lambda(\xi^*) = \exp[a(\lambda) - \mathcal{R}(\lambda, \xi^*) - \bar{\mathcal{R}}_a(\xi^*)]. \quad (3.10)$$

The effective restraining gradient in CZAR is estimated using the Υ_{H}^M estimator in which binning is performed using indicator function $\mathbf{1}_{\xi^*}$ instead of $\mathbf{1}_\lambda$:

$$\Upsilon_{\text{H}}^M(\partial_{\xi^*} \mathcal{R} | \xi = \xi^*) = \beta \kappa \left\{ \frac{\sum_{m=1}^M \zeta_m \mathbf{1}_{\xi^*}(\xi_m)}{\sum_{m=1}^M \mathbf{1}_{\xi^*}(\xi_m)} - \xi^* \right\}, \quad (3.11)$$

where we resorted to $\partial_{\xi^*} \mathcal{R}(\zeta, \xi^*) = \beta \kappa(\xi^* - \zeta)$, omitting the correcting force $\varepsilon'(\xi^*)$. Conditioning the binning estimator in Eq. (3.11) yields

$$\Upsilon_{\text{H}}^M(\partial_{\xi^*} \mathcal{R} | \xi^*) = \beta \kappa \left\{ \frac{\sum_{m=1}^M \mathbb{E}_a[\zeta | \xi^*] \mathbf{1}_{\xi^*}(\xi_m)}{\sum_{m=1}^M \mathbf{1}_{\xi^*}(\xi_m)} - \xi^* \right\} = -\bar{\mathcal{R}}_a'(\xi^*), \quad (3.12)$$

which, once integrated, leads to the formulation of the ξ -AR estimator. Because the asymptotic variance of

$\Upsilon_{\text{H}}^M(\partial_{\xi^*} \mathcal{R}|\xi^*)$ in Eq. (3.12) is zero, one concludes, owing to the delta method, that the CZAR estimator exhibits a larger asymptotic variance than the ξ -AR estimator (3.8).

To quantify the cumulated error in the estimation of $\Delta \bar{\mathcal{R}}_a = \bar{\mathcal{R}}_a(\xi_{\max}) - \bar{\mathcal{R}}_a(\xi_{\min})$ with CZAR method, let first write down the asymptotic variance of estimator $\Upsilon_{\text{H}}^M(\partial_{\xi^*} \mathcal{R}|\xi^*)$:

$$\sigma_a^2(\Upsilon_{\text{H}}^\infty(\partial_{\xi^*} \mathcal{R}|\xi^*)) = \frac{\mathbb{V}_a[\partial_{\xi^*} \mathcal{R}|\xi^*]}{\mathbb{E}_a[\mathbf{1}_{\xi^*}]},$$

where the variance is conditional on ξ^* . Next, we assume that $\bar{\mathcal{R}}_a$ is integrated over Ξ , a discrete set of evenly spaced values along $\Delta\xi = \xi_{\max} - \xi_{\min}$ interval. Let $\|\Xi\|$ be the cardinal of Ξ . Then, $\Delta\xi/\|\Xi\|$ is the constant spacing between consecutive values and the cumulated asymptotic error writes

$$\sigma(\Delta \bar{\mathcal{R}}_a) = \frac{\Delta\xi\beta\kappa}{\|\Xi\|} \sqrt{\sum_{\xi^* \in \Xi} \frac{\mathbb{V}_a[\zeta|\xi^*]}{\mathbb{E}_a[\mathbf{1}_{\xi^*}]}}, \quad (3.13)$$

The ζ variable in each conditional variance is assumed to be i.i.d. This assumption is verified when a Gibbs sampler directly generates the ζ values from the conditional probability (3.10). In contrast, residual metastability usually persists along ξ and the sampled values $\xi(q)$ will be highly correlated. The dominating contribution to the asymptotic variance of the CZAR estimator is expected to arise from the $\mathbb{I}^M(\mathbf{1}_{\xi^*} \circ \xi)$ term. Thus, the cumulated error (3.13) should not be significant in practical applications. We illustrate this point in next subsection.

3.4.2 The 38-atom Lennard-Jones cluster and Q_4 bond-orientational order parameter

We consider the problem of calculating the free energy along the Q_4 bond-orientational order parameter [28] in the 38-atom Lennard-Jones (LJ) cluster. The LJ potential reads

$$\mathcal{V}_{\text{LJ}}(q) = 4\epsilon \sum_{i>j} [r_{ij}^{-12} - r_{ij}^{-6}],$$

where $r_{ij} = \|\mathbf{q}_j - \mathbf{q}_i\|/\sigma$ is the reduced distance separating atoms \mathbf{q}_i and \mathbf{q}_j . LJ reduced units of length, energy and mass ($\sigma = 1$, $\epsilon = 1$, $m = 1$) will be used in the following. LJ₃₈ undergoes a two-stage phase change with increasing temperature. [57, 58] A solid-solid transition between the truncated octahedral funnel and the icosahedral funnel occurs near $T_{\text{ss}}=0.12$, melting follows near $T_{\text{s1}}= 0.17$. As in other finite size systems, [42] the transitions are not sharp but gradual. The most stable octahedral and icosahedral structures of the 38-atom cluster are a truncated octahedron with energy $E_0 = -173.9284$ (global minimum) and an incomplete icosahedron with energy $E_1 = -173.2524$, respectively. The order parameter Q_4 is a convenient collective variable to distinguish between the cubic structure favored at low temperatures and the icosahedral isomers above T_{ss} . The values of Q_4 typically range from 0.002 – 0.06 (icosahedral structures) to 0.19 (octahedral structures). The ABF method is implemented in the harmonic expanded ensemble resorting to the AR estimator in order to compute the free energy along the external parameter λ coupled harmonically to Q_4 . The standard ABF method [30, 31, 59] cannot be performed directly along Q_4 because the second derivatives of the Q_4 are not available. The restraining potential is set to $\frac{\kappa}{2T_{\text{ref}}}\|Q_4(q) - \lambda\|^2$ and the extended potential exhibits the form given in Eq. (1.9), so that the free energy derivative $\mathcal{A}'(\lambda)$ is constructed from the following identity

$$\mathbb{E}[\partial_\lambda u|\lambda] = \frac{\kappa}{T_{\text{ref}}} \left[\lambda - \frac{\mathbb{E}_a^Q[\pi_a^\lambda Q_4]}{\mathbb{E}_a^Q[\pi_a^\lambda]} \right].$$

We set $\kappa = 10^4$ and $T_{\text{ref}} = 0.15$. At this temperature, spontaneous structural transitions cannot be observed on the simulation timescale when $\alpha(\lambda)$ is set to 0 (no bias). The implemented ABF method, described in Algorithm 6 of Appendix B, adapt the bias $\alpha(\lambda)$ on the free energy $\mathcal{A}(\lambda)$ via the running estimate of its gradient. One collateral advantage of conditioning is to facilitate the sampling process, as it needs not propagating the external parameter. Twelve replicas of the system are propagated using Langevin dynamics [34] (a Metropolis algorithm is also implementable) to sample the marginal probability of q directly. The force acting on a replica

is the gradient of the involved marginal probability (see Eq. 1.9)

$$\nabla_q \ln p_a^Q(q) = -\nabla_q \mathcal{U}_0(q) + \nabla_q Q_4(q) \bar{\mathcal{R}}_a' \circ Q_4(q),$$

where $\mathcal{U}_0 = \mathcal{V}_{\text{LJ}}/T_{\text{ref}}$ and $\bar{\mathcal{R}}_a'$ is detailed in Eq. (3.9). The time-step $\tau = 5 \cdot 10^{-5}$ (lju) is chosen very small so as to keep discretization errors negligible. The simulation length $M = 10^8$ and replica number $K = 12$ enable the auxiliary biasing force to converge. Replicas are handled in parallel using a multi-core processor. They share the same biasing force during both the learning and subsequent production runs. We next freeze the biasing potential to the converged free energy $A(\lambda) = a_M(\lambda)$ and implement Algorithm 7 of Appendix B to check that the sampling is homogeneous along Q_4 parameter despite the persistence of strong correlations, as shown in Fig. 3.5. With Algorithm 2, we also construct 40 (biased) histograms of Q_4^* , using estimates $\mathbb{I}^{KM}(\mathbf{1}_{Q_4^*})$ of $\mathbb{E}_A[\mathbf{1}_{Q_4^*}]$ with $K = 12$, $M = 10^8$, a bin size of $2 \cdot 10^{-4}$ and Q_4^* ranging from 0 to 0.2. The free energy along Q_4 order parameter is then estimated using the ξ -AR estimator and the 40 harvested histograms denoted by $P_A(Q_4^*)$. The obtained results are plotted in the three panels of Fig. 3.6. The brackets $\langle \rangle$ indicate averaging over the series of 40 independent simulations. Thus, the displayed quantity $\langle B_A(Q_4) \rangle$ in Fig. 3.6.a represents the (averaged and scaled) effective biasing potential, $\beta^{-1} \bar{\mathcal{R}}_a(Q_4)$. The displayed histogram of Q_4 in Fig. 3.6.b represents the averaged of the $P_A(Q_4^*)$ estimates of $\mathbb{E}_A[\mathbf{1}_{Q_4^*}]$. The free energies displayed in Fig. 3.6.c are estimated from $F(Q_4^*) = B_{\hat{A}}(Q_4^*) - \beta^{-1} \ln P_A(Q_4^*)$. They correspond to the unreduced free energies $\beta^{-1} \mathcal{F}(Q_4^*)$.

The variance reduction compared to CZAR method is too small to be measurable from 40 simulations. Instead, we estimate the order of magnitude of the error that is made in the estimation of $\Delta \bar{\mathcal{R}}_a$ with the CZAR method. Neglecting the variations of the biasing forces along λ , which are much smaller than the value of κ/T_{ref} , the conditional variance in Eq. (3.13) simplifies into $\mathbb{V}_0(\zeta|Q_4^*)$ which is equal to T_{ref}/κ . If we additionally neglect the variations of the histogram $P_A(Q_4^*)$ and assume that $\mathbb{E}_A(\mathbf{1}_{Q_4^*}) = \|\Xi\|^{-1}$ between the icosahedral and octahedral structures in Eq. (3.13), then the integrated error between the two structures simplifies into $\Delta Q_4/\sqrt{T_{\text{ref}}\kappa}$. The expected standard deviation on $\Delta B_A = T_{\text{ref}}\Delta \mathcal{B}_A$ is therefore $\Delta Q_4\sqrt{T_{\text{ref}}/(\kappa MK)} = 2.0 \cdot 10^{-4}$ wherein $MK = 1.2 \cdot 10^9$ is the total number of sampled points. This is less than two orders of magnitude than $6.1 \cdot 10^{-2}$, the standard deviation that is obtained from the 40 estimates of the free energy difference ΔF .

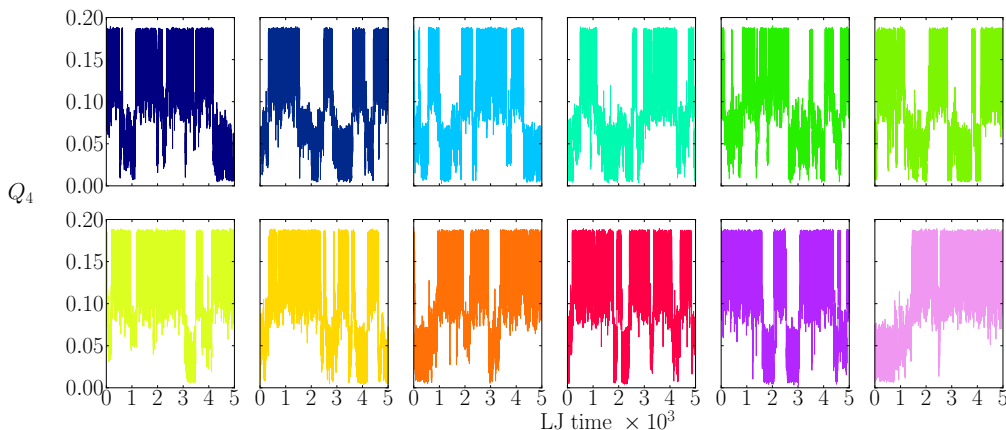


Figure 3.5: Evolution of the Q_4 order parameter during the production run for each replica. Each panel corresponds to a distinct replica.

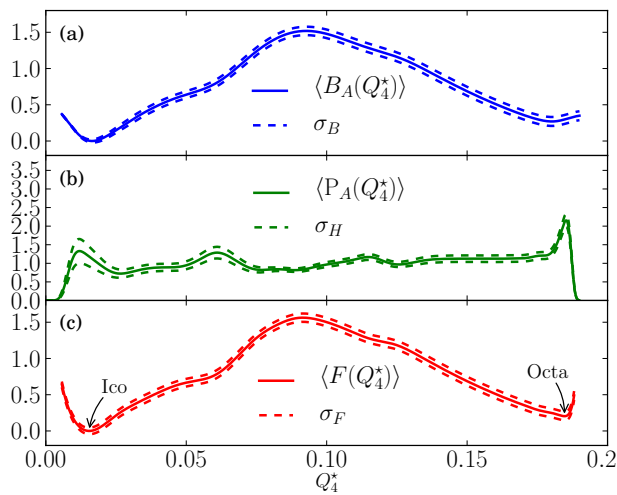


Figure 3.6: (a) mean effective biasing potential $\langle B_A(Q_4^*) \rangle$ shifted by its minimum value; (b) $\langle P_A(Q_4^*) \rangle$ is the mean estimate of $\mathbb{E}_A[\mathbf{1}_{Q_4^*}]$ histogram; (c) mean estimate of free energy $\langle F(Q_4^*) = B_A(Q_4^*) - \beta^{-1} \ln P_A(Q_4^*) \rangle$ shifted by its minimum value. Means and displayed standard deviations σ_B , σ_H and σ_F (for 68%-confidence intervals) are evaluated from 40 simulations.

3.5 Characterization of structural transition

From the free energy profile along Q_4 , the occurrence probabilities of the icosahedral and octahedral structures can be evaluated. For these two structures, the Landau free energies $A(\text{ico}|T_{\text{ref}}^{-1})$ and $A(\text{octa}|T_{\text{ref}}^{-1})$, defined as minus the logarithm of their respective occurrence probabilities, can be directly evaluated. We now wish to compute the two Landau free energies at other temperatures so as to characterize T_{ss} , the *solid-solid* structural transition temperature for which $A(\text{ico}|T_{\text{ss}}^{-1}) = A(\text{octa}|T_{\text{ss}}^{-1})$. Unfortunately, ABF simulations along Q_4 do not converge at temperature lower than 0.13, meaning that Q_4 becomes a bad reaction coordinate and that T_{ss} can not be determined this way.

The problem is solved by evaluating $A(\mathbf{x}|T^{-1})$ as a function of inverse temperature separately for the two structures \mathbf{x} of set $X \triangleq \{\text{ico}, \text{octa}\}$ from the knowledge of $\mathcal{A}(T^{-1}|\text{ico})$ and $\mathcal{A}(T^{-1}|\text{octa})$, the free energies along the inverse temperature given the structure. The identity connecting the two kinds of free energies corresponds to Bayes formula expressed in log-space

$$A(\mathbf{x}|T^{-1}) = \mathcal{A}(T^{-1}|\mathbf{x}) + A(\mathbf{x}) - \mathcal{A}(T^{-1}), \quad (3.14)$$

where $A(\mathbf{x})$ is the marginal colog-probability of structure \mathbf{x} in the expanded ensemble. Subtracting Bayes formula at T_{ref}^{-1} in log-space from Eq. (3.14) cancels the marginal colog-probability of \mathbf{x} , which leads to the desired Landau free energy

$$A(\mathbf{x}|T^{-1}) = \mathcal{A}(T^{-1}|\mathbf{x}) - \mathcal{A}(T_{\text{ref}}^{-1}|\mathbf{x}) + A(\mathbf{x}|T_{\text{ref}}^{-1}) + \mathcal{A}(T_{\text{ref}}^{-1}) - \mathcal{A}(T^{-1}).$$

The free energy difference $\mathcal{A}(T_{\text{ref}}^{-1}) - \mathcal{A}(T^{-1})$ is a common contribution to all structures. It does not affect phase equilibrium properties and merely serves as a normalizing constant. It may be calculated from the relation

$$\mathcal{A}(T_{\text{ref}}^{-1}) - \mathcal{A}(T^{-1}) = \ln \sum_{\tilde{\mathbf{x}} \in X} \exp [-\mathcal{A}(T^{-1}|\tilde{\mathbf{x}}) + \mathcal{A}(T_{\text{ref}}^{-1}|\tilde{\mathbf{x}}) - A(\tilde{\mathbf{x}}|T_{\text{ref}}^{-1})].$$

In our case study, phase equilibrium is reached when the two structures are equi-probable:

$$A(\text{ico}|T_{\text{ss}}^{-1}) = A(\text{octa}|T_{\text{ss}}^{-1}).$$

We proceed as follows: after setting the external parameter to the inverse temperature $\lambda = T^{-1}$, we perform two supplementary simulations to compute $\mathcal{A}(T^{-1}|\text{ico})$ and $\mathcal{A}(T^{-1}|\text{octa})$ with the AR estimator and the external parameter ranging from $\lambda_{\text{min}} = 6.25$ to $\lambda_{\text{max}} = 14$, taking advantage of the fact that structural transitions do not occur spontaneously in the range of involved temperatures. The transition temperature is characterized by the intersection point of our two Landau free energies as a function of inverse temperature, as shown in Fig. ?? . The error that is made in the estimation of the transition temperature essentially arises from the uncertainty in the evaluation of ΔF at T_{ref} .

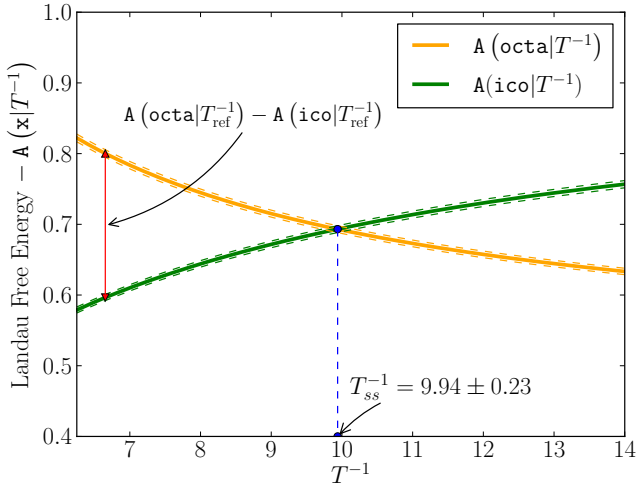


Figure 3.7: Estimation of the free energies of the icosahedral and octahedral structures as a function of inverse temperature.

3.6 Summary

In this Chapter, we practically show how to perform simulations adaptively in the expanded ensemble using adaptive biasing potential and adaptive biasing force methods. We advocate to resort to the ABF rather than ABP in order to set the biasing potential $\alpha(\lambda)$ equal to the free energy $\mathcal{A}(\lambda)$. A difficulty with ABP algorithms is that the updating rate of the biasing potential must be chosen adequately. If the rate rapidly converges to zero, then the biasing potential will evolve extremely slowly and likely not converge during the simulation. In contrast, if the rate slowly converges to zero, then the biasing potential will fluctuate for a long period prior to stabilizing. Finding a good trade-off between these two adverse situations requires judiciously tuning the updating parameters, a difficult task in general. ABF methods are (almost) free of such updating parameters. The advantage of extended ABF is that it is still applicable when the reaction coordinate is discrete or discontinuous. In contrast, standard ABF requires differentiating the reaction coordinate twice and can not be implemented to compute the free energy along the widely used bond orientational order parameters of Steinhardt et al. [28] for instance.

An open question concerns the usefulness of the conditioning procedure during the adaptive regime. Conditioned ABP exhibits accelerated convergence compared to unconditioned ABP, which seems to be mathematically justifiable [60]. However, mitigated numerical results are reported for ABF expanded ensemble simulations employing a linear coupling aimed at characterizing the melting temperature [34]. Once the adaptive procedure has been completed, we naturally advocate to implement the conditioning procedure in order to systematically reduce statistical variance associated with the estimation of the expected observable value.

Problems arise when the available collective variables incorrectly capture the involved reaction or transition paths. In this situation, spurious metastability may still be observed along the order parameter and biased Monte Carlo or MD simulation may fail to achieve ergodic sampling, as illustrated on a simple system exhibiting two transitioning channels with shifted barriers along the employed one-dimensional RC. Ergodic sampling can nevertheless be recovered by performing nonlocal moves using the work-bias Monte Carlo scheme. However, this is achieved at the expense of statistical accuracy. The reason is that the information associated with intermediate states that have been generated in the construction of the trial states are excluded from the estimator. For a given amount of computational resource, the sample size M scales as the inverse of the path length L that is used to construct the trial states. As a result, the amount of information that is actually included in the estimator is considerably reduced. In Chapter 4, we introduce another type of conditioning that makes it possible to retrieve all the information contained in the generated trial trajectories.

4 | Path sampling and conditioning

Path sampling schemes are becoming increasingly important tools in molecular simulations for estimating free energy differences through the fluctuations of entropy production [61] and for extracting rates of rare-events from state-to-state time correlation functions [7]. In this Chapter, we review techniques for conditioning on the states contained in a sample of harvested trajectories. The described techniques are exact instances of the more general waste-recycling Monte Carlo (WRMC) method in which conditioning is performed on proposals. The WRMC technique was briefly mentioned in Chapter 2 and will only be discussed in greater details in Chapter 5. For the ease of exposition, we first emphasize the path-sampling and path-ensemble concepts so as to establish connections with methods based on entropy fluctuations.

4.1 Equilibrium out of nonequilibrium

So far, we advocated so far to enhance the sampling along an internal collective coordinate or an external parameter with the help of an auxiliary biasing potential. While the sampling efficiency is improved in many situations, as illustrated on several testbed problems in Chapters 2 and 3, there are cases for which the approach is unable to achieve ergodic sampling along the specified coordinate. This happens when reactive events occur via separate transition channels along which the free energy barriers are located at distinct values of the order parameter.¹

Constructing a multi-dimensional order parameter faithfully capturing the degree of advancement of the reaction being a difficult task, an alternative approach was suggested in Chapter 2. The work-bias Monte Carlo (WBMC) technique described page 40 was shown to considerably enhance the sampling efficiency in this situation. Trial states are generated by driving the system out of equilibrium using an external mechanical force and are eventually accepted or rejected using the Metropolis acceptance rule. In a wider perspective, the WBMC [44] technique relates to Jarzynski’s identity [62] which makes it possible to estimate free energy differences from samples of transient nonequilibrium trajectories. Jarzynski’s approach [62] can be used to estimate any thermodynamic expectations [5, 63]. Besides, it can be derived from the entropy production fluctuation theorem [4], like the Metropolis acceptance rate in the WBMC technique.

A drawback of the aforementioned path-based approaches is that they are costly. A considerable amount of configurations are generated while generating the paths, but the information associated with all the propagated configurations is only partially included in the estimators. A first question that naturally arises is how to retrieve this nonequilibrium information more efficiently. We show hereafter how to do it by performing a pathwise conditioning, i.e within the sampled path ensemble. A second question to address is whether improved estimates of the state-to-state time correlation functions can be obtained through this additional pathwise conditioning. The objective is to further improve the efficiency of transition path sampling (TPS) simulations conducted in a tilted path ensemble² and with conditioning with respect to the (external) tilting parameter.

Outline of the Chapter The nonequilibrium Langevin dynamics and its time discretization [45, 46, 63] are first described in Section 4.2. The path ensemble concept and path reweighting technique are then introduced in Section 4.3. We then generalize the path ensemble concept and define the expanded path ensemble in Section 4.4. We show how conditioning can be done and establish the connection with waste-recycling. We show in Section 4.6 how to implement the conditioning approach within TPS to calculate the rate constant of rare thermally activated events. Path-reweighting and pathwise conditioning are illustrated with free energy

¹This limitation was also illustrated in Section 3.2 on a purposely designed model.

²wherein small occurrence probabilities of reactive trajectories are artificially increased using a biasing path functional

calculations of various LJ₃₈ structures at low temperatures and with calculations of the vacancy hopping rate in α -iron.

4.2 Dynamical forcing

4.2.1 Langevin dynamics

The Langevin dynamics is a phenomenological model of a Hamiltonian system coupled to a thermostat, which is an infinite reservoir of energy. Langevin dynamics has the ability to explore the various energy levels of a canonical distribution unlike Hamiltonian dynamics that preserves the total mechanical energy of the system. The Hamiltonian is considered to be separable and equal to the sum of the kinetic energy $K(p) = \frac{1}{2}p^T M^{-1}p$ and of a parameterized potential energy $U_\lambda(q)$. The mass matrix M is positive semidefinite. The parameterized Hamiltonian exhibits the form

$$H_\lambda(p, q) = K(p) + U_\lambda(q) = \beta^{-1} \mathcal{H}(\lambda, x),$$

where $\nabla_p K(p) = M^{-1}p$. The Langevin dynamics thus writes

$$\begin{cases} dp_t &= -\nabla_q H_\lambda(q_t, p_t) dt - \frac{1}{2} \beta \sigma^2 \nabla_p K(p_t) dt + \sigma dB_t \\ dq_t &= \nabla_p H_\lambda(q_t, p_t) dt, \end{cases} \quad (4.1)$$

where σ denotes a symmetric positive definite matrix and $t \mapsto B_t = \int_0^t dB_s$ is a $3N$ -dimensional standard Brownian motion.³ Each component of B_t has zero mean and t variance. The term $dB(t)$ describes an infinitesimal random fluctuation, while the term $-\frac{1}{2} \beta \sigma^2 \nabla_p K(p_t) dt$ describes the dissipation. The exchange of heat with the reservoir is the work done by the fluctuating and dissipative forces along the trajectory. In more general setups like dissipative particle dynamics [14, 15], σ depends on q . The quantity σ^2 characterizes the coupling strength between the particle coordinates and the thermostat held at temperature β^{-1} . The Hamiltonian dynamics is recovered by setting σ to 0 in (4.1). The probability density $\rho_t(\lambda, q, p)$ associated with the Hamiltonian dynamics evolves according to the following Liouville equation

$$\partial_t \rho_t = \{\rho_t, H_\lambda\} = \nabla_q \rho_t \cdot \nabla_p H_\lambda - \nabla_p \rho_t \cdot \nabla_q H_\lambda.$$

where $\{\cdot\}$ denotes Poisson brackets. The evolution operators associated with the kinetic and potential energy are respectively

$$\mathcal{L}^K = \{\cdot, K\}, \quad \mathcal{L}^U = \{\cdot, U_\lambda\}.$$

When the system is coupled to the thermostat, the probability density associated with the Langevin dynamics evolves according to the following forward Kolmogorov equation

$$\partial_t \rho_t = \{\rho_t, H_\lambda\} + \frac{1}{2} e^{\beta K(p)} \operatorname{div}_p \left(e^{-\beta K(p)} \sigma^2 \nabla_p \rho_t \right) \triangleq (\mathcal{L}^K + \mathcal{L}^U + \mathcal{L}^{\operatorname{div}}) \rho_t \quad (4.2)$$

where the additional evolution operator $\mathcal{L}^{\operatorname{div}}$ is associated with the momentum divergence and describes the fluctuation-dissipation contribution. The stationary distribution of (4.2) is the canonical distribution $\pi(x|\lambda) = \exp[\mathfrak{F}(\lambda) - \mathcal{H}(\lambda, x)]$ where $x = (p, q)$ and the absolute free energy is defined in (1.1). This distribution is indeed solution of the following equation

$$(\mathcal{L}^K + \mathcal{L}^U + \mathcal{L}^{\operatorname{div}}) \pi(x|\lambda) = 0. \quad (4.3)$$

In set-up (4.3), the external parameter is hold at the constant value λ . In the following, we shall consider situations for which the external parameter evolves with time.

4.2.2 External forcing

At equilibrium, the external parameter is usually viewed as a constant thermodynamic force acting upon the coordinates of the particle system. This viewpoint is used to construct the various thermodynamic ensembles considering that this force is a Lagrange multiplier acting on some macro-state variables, like for instance the total mechanical energy. This viewpoint is the one adopted by Jarzynski [62, 64] for describing trajectories driven out of equilibrium starting from an equilibrium macro-state. In this nonequilibrium context, the external

³also referred to as a Wiener process in the mathematical literature.

force λ_t is varied through an imposed scheduling protocol. As a result, the effective Hamiltonian is modified in the course of the simulation. The particle system undergoes an alchemical transformation by applying a Hamiltonian-switching protocol.

For our conditioning purpose, it is more convenient to assume that λ is an additional variable evolving according to the following Langevin equation

$$d\lambda_t = \phi_t dt - \frac{1}{2} \bar{\beta} \bar{\sigma}^2 \partial_\lambda U(\lambda_t, q_t) dt + \bar{\sigma} d\tilde{B}_t \quad (4.4)$$

where ϕ_t is the action of the external forcing and $\bar{\sigma}$ the coupling strength between the coordinate λ and the thermal reservoir at inverse temperature $\bar{\beta}$. This dynamics is valid if λ is not bounded. An example of such dynamics is given in Refs. [65] and [66] wherein λ is harmonically coupled to a reaction coordinate of the particle system. Denoting the evolution operator associated with λ -variable by \mathcal{L}^λ , the formal expression of the probability density at time $t_1 = \tau$ knowing the probability density at initial time $t_0 = 0$ writes

$$\rho_\tau = \exp\left(\int_0^\tau [\mathcal{L}^\lambda + \mathcal{L}^K + \mathcal{L}^U + \mathcal{L}^{\text{div}}] dt\right) \rho_0 = \exp\left(\int_0^\tau \mathcal{L}^{\text{tot}} dt\right) \rho_0,$$

where \mathcal{L}^{tot} is the total evolution operator.

4.2.3 Factorization of the evolution operator

In general, the evolution operators \mathcal{L}^K , \mathcal{L}^U , \mathcal{L}^{div} do not commute with each others, but \mathcal{L}^λ commutes with \mathcal{L}^K and \mathcal{L}^{div} . Let denote the operator integral $\int_0^\tau \mathcal{L}^X dt$ by \mathcal{L}_τ^X . The steered Langevin dynamics will be discretized by splitting the operator as follows:

$$\exp\left(\int_0^\tau \mathcal{L}^{\text{tot}} dt\right) \approx \exp\left(\mathcal{L}_{\tau/2}^{\text{div}}\right) \exp\left(\mathcal{L}_{\tau/2}^U\right) \exp\left(\int_0^\tau [\mathcal{L}^\lambda + \mathcal{L}^K] dt\right) \exp\left(\mathcal{L}_{\tau/2}^U\right) \exp\left(\mathcal{L}_{\tau/2}^{\text{div}}\right). \quad (4.5)$$

where τ will be the time-step. This (Trotter-Strang) splitting is symmetric with respect to a time reversal and valid to second order [45, 63, 63, 66]. A similar splitting can be applied to the evolution operator in the middle. Henceforth, we assume that the thermal bath is at an infinite temperature, i.e. $\bar{\beta}^{-1} = 0$ and that ϕ_t is independent of q_t in (4.4). It results that \mathcal{L}^λ and \mathcal{L}^K operators commutes

$$\exp\left(\int_0^\tau [\mathcal{L}^\lambda + \mathcal{L}^K] dt\right) = \exp\left(\mathcal{L}_\tau^\lambda\right) \exp\left(\mathcal{L}_\tau^K\right).$$

When time-stepping the dynamics, the coordinates at time $t = \ell\tau$ are denoted by λ_ℓ and $x_\ell = (q_\ell, p_\ell)$ with $\ell \in \llbracket 0, L \rrbracket$. We further assume that the discretized dynamics of λ evolves inside the finite set Λ and is reflected on the boundary of Λ . To achieve this, we assume that Λ contains evenly spaced points (along each direction when λ is a multi-dimensional parameter) and define $\bar{\Lambda}$ as the infinite lattice encompassing Λ . We first propagate an unbounded dynamics ζ_ℓ on lattice $\bar{\Lambda}$ as follows

$$\zeta_{\ell+1} = \zeta_\ell + \tau\phi + R, \quad R \sim \mathcal{N}_d(0, \tau\bar{\sigma}^2),$$

where the external forcing ϕ is assumed to be constant and $\mathcal{N}_d(0, \tau\bar{\sigma}^2)$ stands for a discretized form of the normal law of zero mean and $\tau\bar{\sigma}^2$ variance. The random vector is thus located on the infinite lattice $\bar{\Lambda}$ and so for the constant transition vector $\tau\phi$. We next reconstruct the actual positions $\lambda_{\ell+1} \in \Lambda$ from $\zeta_{\ell+1} \in \bar{\Lambda}$ resorting to Cell function defined as

$$\lambda_{\ell+1} = \lambda_{\min} + \min_{k \in \mathbb{Z}} (|\zeta_{\ell+1} - \lambda_{\min} + 2k(\lambda_{\max} - \lambda_{\min})|) \triangleq \text{Cell}(\zeta_{\ell+1}),$$

and used in the following to denote the resulting reflection on the Λ boundaries. The forced transition $\tau\phi$ is to be reversed under time-reversal like a velocity or a momentum. Whatever the current location on the lattice, the forward and reverse transition probabilities are therefore given by the probabilities to generate R and $-R$, respectively, which both equal each other. The symmetry of the transition probabilities associated with λ under time-reversal,

$$\mathcal{T}(\lambda_\ell \rightarrow \lambda_{\ell+1}) = \mathcal{T}(\lambda_\ell \leftarrow \lambda_{\ell+1}),$$

reflects the fact that λ is coupled to an infinite temperature reservoir. Further setting $\bar{\sigma}$ to zero amounts to uncoupling λ to the heat bath and to imposing the sequence $(\lambda_1, \dots, \lambda_\ell, \dots)$ in advance, as is done in Hamiltonian switching protocols introduced by Jarynski [62].

4.2.4 Ornstein-Uhlenbeck process in momentum space

The operator $\exp(\mathcal{L}^{\text{div}} \frac{\tau}{2})$ exhibits a closed form solution. This entails that the momenta $p_{\tau/2}$ at time $t = \tau/2$ can be exactly simulated from the knowledge of the momenta p_0 at time $t = 0$. This operator describes the evolution of an Ornstein-Uhlenbeck (OU) process in momentum space for a duration $\frac{\tau}{2}$. Introducing the positive friction matrix $\gamma = \frac{1}{2}\beta\sigma^2 M^{-1}$, the OU process writes

$$dp_t = -\gamma dp_t + \sqrt{2\gamma M/\beta} dB_t.$$

This particular stochastic differential equation can be integrated analytically [15], which yields

$$p_t = p_0 \exp[-\gamma t] + \Sigma_t B_1$$

where Σ_t is the principal square root of matrix $\Sigma_t^2 = [I - \exp(-2\gamma t)] M/\beta$ and $B_1 \propto \mathcal{N}(0, I)$, i.e. B_1 is normally distributed and each component has zero mean and unit variance. The OU process at time t is simulated by drawing $p_t = p_0 \exp(-\gamma t) + G$ where G is a normal noise of zero mean and Σ_t^2 variance. We write $G \sim \mathcal{N}(0, \Sigma_t^2)$. This stochastic move obeys a form of detailed balance with respect to the Maxwell-Boltzmann distribution (for the kinetic energy). This form states that the probability flux from p_0 to p_t , denoted by $\Phi(p_0 \rightarrow p_t)$, is equal to $\Phi(-p_t \rightarrow -p_0)$ the probability flux from $-p_t$ to $-p_0$:

$$\begin{aligned} \Phi(p_0 \rightarrow p_t) &= \left| \sqrt{\frac{\beta}{2\pi}} M^{-\frac{1}{2}} \right| \exp\left[-\frac{\beta}{2} p_0^T M^{-1} p_0\right] \times \left| \frac{1}{\sqrt{2\pi}} \Sigma_t^{-1} \right| \exp\left[-\frac{1}{2} G^T \Sigma_t^{-2} G\right] = \\ & \left| \sqrt{\frac{\beta}{2\pi}} M^{-\frac{1}{2}} \right| \exp\left[-\frac{\beta}{2} (-p_t)^T M^{-1} (-p_t)\right] \times \left| \frac{1}{\sqrt{2\pi}} \Sigma_t^{-1} \right| \exp\left[-\frac{1}{2} \tilde{G}^T \Sigma_t^{-2} \tilde{G}\right] = \Phi(-p_t \rightarrow -p_0). \end{aligned} \quad (4.6)$$

where $|A|$ denotes the determinant of a matrix A and \tilde{G} is the Gaussian noise obtained after reversal of time and momenta in the original OU process. The reversed process is the OU process mapping $-p_t$ back to $-p_0 = -p_t \exp(-\gamma t) + \tilde{G}$. The OU process is said to be *reversible* in the sense that it obeys the form of detailed balance above.

4.2.5 Discretization scheme for Langevin dynamics

The discretization scheme obtained via Trotter-Strang splitting (4.5) associated with evolution equation (4.2) then reads

$$\left\{ \begin{array}{ll} p_{\ell+1/4} &= p_\ell \exp(-\gamma\tau/2) + G_0, & G_0 \sim \mathcal{N}\left(0, \Sigma_{\tau/2}^2\right), \\ p_{\ell+1/2} &= p_{\ell+1/4} - \frac{\tau}{2} \nabla_q U(\lambda_\ell, q_\ell), & \lambda_\ell = \text{Cell}(\zeta_\ell), \\ \begin{bmatrix} q_{\ell+1} \\ \zeta_{\ell+1} \end{bmatrix} &= \begin{bmatrix} q_\ell \\ \zeta_\ell \end{bmatrix} + \begin{bmatrix} \tau M^{-1} p_{\ell+1/2} \\ \tau\varphi + R \end{bmatrix}, & R \sim \mathcal{N}_d\left(0, \frac{\tau}{2}\bar{\sigma}^2\right), \\ p_{\ell+3/4} &= p_{\ell+1/2} - \frac{\tau}{2} \nabla_q U(\lambda_{\ell+1}, q_{\ell+1}), & \lambda_{\ell+1} = \text{Cell}(\zeta_{\ell+1}), \\ p_{\ell+1} &= p_{\ell+3/4} \exp(-\gamma\tau/2) + G_1, & G_1 \sim \mathcal{N}\left(0, \Sigma_{\tau/2}^2\right), \end{array} \right. \quad (4.7)$$

where $U(\lambda, q)$ stands for $U_\lambda(q)$ for clarity. We assume that the rates ϕ_ℓ and $\phi_{\ell+1}$ governing the evolution of λ correspond to a purely external forcing (meaning that $\bar{\sigma} = 0$ in Eq. 4.4). See Ref. [66] for an example of steered Langevin dynamics for which the external parameter evolves stochastically coupled to a high temperature heat bath, i.e $\bar{\beta} \ll \beta$ and $\bar{\sigma} > 0$ in (4.4).

Note that the standard velocity-Verlet scheme (VV) for Hamiltonian dynamics [14] is recovered from scheme (4.7) by setting ϕ , σ and $\bar{\sigma}$ to 0, which entails that γ and $\Sigma_{\tau/2}$ are also equal to 0 in (4.7). The VV scheme is *symmetric*, *reversible* and *symplectic* (see Refs. [47] or [15]).

4.2.6 Time-reverse trajectory, detailed deviation and heat exchanged with thermostat

The Langevin dynamics will be used as a sampling device. For such applications, matrix σ will simply be diagonal positive and so will be the friction matrix γ . The mass matrix will also be diagonal. The difficulty in constructing estimators for evaluating equilibrium thermodynamic averages is that the external forcing steers the dynamics out of equilibrium. Hopefully, such deviations from detailed balance can be measured by reversing the dynamics with respect to the arrow of time. Let us reverse the forward map (4.2) by inverting the order of the indexes:

$$\left\{ \begin{array}{l} -p_{\ell+3/4} = -p_{\ell+1} \exp(-\gamma \frac{\tau}{2}) + \tilde{G}_1, \\ -p_{\ell+1/2} = -p_{\ell+3/4} - \frac{\tau}{2} \nabla_q U(\lambda_{\ell+1}, q_{\ell+1}), \\ \begin{bmatrix} q_\ell \\ \zeta_\ell \end{bmatrix} = \begin{bmatrix} q_{\ell+1} \\ \zeta_{\ell+1} \end{bmatrix} - \begin{bmatrix} \tau M^{-1} p_{\ell+1/2} \\ \tau \varphi + R \end{bmatrix}, \\ -p_{\ell+1/4} = -p_{\ell+1/2} - \frac{\tau}{2} \nabla_q U(\lambda_\ell, q_\ell), \\ -p_\ell = -p_{\ell+1/4} \exp(-\gamma \frac{\tau}{2}) + \tilde{G}_0, \end{array} \right. \quad \begin{array}{l} \tilde{G}_1 \sim \mathcal{N}(0, \Sigma_{\tau/2}^2), \\ \lambda_{\ell+1} = \text{Cell}(\zeta_{\ell+1}), \\ R \sim \mathcal{N}_d(0, \frac{\tau}{2} \bar{\sigma}^2), \\ \lambda_\ell = \text{Cell}(\zeta_\ell), \\ \tilde{G}_0 \sim \mathcal{N}(0, \Sigma_{\tau/2}^2). \end{array} \quad (4.8)$$

In absence of coupling between λ and the thermostat ($\bar{\sigma} = 0$), the probability to transition from λ_ℓ to $\lambda_{\ell+1}$ is equal to the transition probability for the reverse move from $\lambda_{\ell+1}$ to λ_ℓ . The probability of transitioning from $(\lambda, p, q)_\ell$ to $(\lambda, p, q)_{\ell+1}$ is thus given by

$$\mathcal{T}[(\lambda, p, q)_\ell \rightarrow (\lambda, p, q)_{\ell+1}] = \left| \frac{1}{2\pi} \Sigma_{\tau/2}^{-2} \right| \exp \left[- \left(\frac{1}{2} G_0^T \Sigma_{\tau/2}^{-2} G_0 + G_1^T \Sigma_{\tau/2}^{-2} G_1 \right) \right].$$

The overall probability of transitioning from $(\lambda, -p, q)_{\ell+1}$ to $(\lambda, p, q)_{\ell+1}$ in the reverse updating scheme (4.8) is given by

$$\mathcal{T}[(\lambda, -p, q)_\ell \leftarrow (\lambda, -p, q)_{\ell+1}] = \left| \frac{1}{2\pi} \Sigma_{\tau/2}^{-2} \right| \exp \left[- \left(\frac{1}{2} \tilde{G}_0^T \Sigma_{\tau/2}^{-2} \tilde{G}_0 + \tilde{G}_1^T \Sigma_{\tau/2}^{-2} \tilde{G}_1 \right) \right].$$

Resorting to the detailed balance condition (4.6) and denoting the reduced kinetic energy βK by \mathcal{K} , the logarithmic ratio of the transitioning probabilities can be expressed as

$$\ln \frac{\mathcal{T}[(\lambda, -p, q)_\ell \leftarrow (\lambda, -p, q)_{\ell+1}]}{\mathcal{T}[(\lambda, p, q)_\ell \rightarrow (\lambda, p, q)_{\ell+1}]} = \mathcal{K}(p_{\ell+1}) - \mathcal{K}(p_{\ell+3/4}) + \mathcal{K}(p_{\ell+1/4}) - \mathcal{K}(p_\ell) = \mathcal{Q}^{\ell \rightarrow \ell+1},$$

where the quantity $\mathcal{Q}^{\ell \rightarrow \ell+1}$ corresponds to the heat exchanged with the thermostat during the two half-step OU processes. The heat exchanged during L iterations (4.7) starting from $\ell = 0$ reads

$$\begin{aligned} \mathcal{Q}^{0 \rightarrow L} &= \sum_{\ell=0}^{L-1} \mathcal{Q}^{\ell \rightarrow \ell+1} \\ &= \mathcal{K}(p_L) - \mathcal{K}(p_0) + \frac{1}{2} \sum_{\ell=0}^{L-1} (p_{\ell+1/4} - p_{\ell+3/4})^T M^{-1} (p_{\ell+1/4} + p_{\ell+3/4}) \\ &= \mathcal{K}(p_L) - \mathcal{K}(p_0) + \frac{1}{2} \sum_{\ell=0}^{L-1} (q_{\ell+1} - q_\ell)^T [\nabla_q \mathcal{U}(\lambda_{\ell+1}, q_{\ell+1}) + \nabla_q \mathcal{U}(\lambda_\ell, q_\ell)] + \mathcal{C}^{0 \rightarrow L} \end{aligned} \quad (4.9)$$

where the last quantity is a second order term in τ

$$\mathcal{C}^{0 \rightarrow L} = \frac{\tau^2}{8} [\nabla_q \mathcal{U}(\lambda_L, q_L)^T M^{-1} \nabla_q \mathcal{U}(\lambda_L, q_L) - \nabla_q \mathcal{U}(\lambda_0, q_0)^T M^{-1} \nabla_q \mathcal{U}(\lambda_0, q_0)].$$

4.2.7 Work done on the extended system

The work done by the external forces on the extended system is defined from the first law of thermodynamics. It therefore equals the variation of mechanical energy of the extended particle system and of heat in the thermal reservoirs which the coordinates are coupled to. The energy variation of the extended system is the Hamiltonian difference $\mathcal{H}(\lambda_L, p_L, q_L) - \mathcal{H}(\lambda_0, p_0, q_0)$. The energy variation of the thermostat is $-\mathcal{Q}^{0 \rightarrow L}$, the heat flowing

from the particle system into the thermal reservoir. Thus, defining the work from the first law yields

$$\mathcal{W}^{0 \rightarrow L} = \mathcal{H}(\lambda_L, p_L, q_L) - \mathcal{H}(\lambda_0, p_0, q_0) - \mathcal{Q}^{0 \rightarrow L}. \quad (4.10)$$

A work quantity $\mathcal{W}^{\ell \rightarrow \ell+1}$ can similarly be defined for a single iteration of the Langevin scheme, i.e. for a transition from $(\lambda_\ell, p_\ell, q_\ell)$ to $(\lambda_{\ell+1}, p_{\ell+1}, q_{\ell+1})$, as illustrated in Fig. 4.1. The work done on the system arises from the external forcing on λ and from the discretization errors associated with the splitting of the evolution operator [45, 63, 66]. To explain this, let us express the potential energy difference as an integral of the total gradient $\nabla_{\lambda, q}$ along a trajectory Γ that is continuous, piecewise and linear between the consecutive points $(\lambda_\ell, p_\ell, q_\ell)$ and $(\lambda_{\ell+1}, p_{\ell+1}, q_{\ell+1})$ of the discretized trajectory ($0 \leq \ell \leq L-1$). We obtain

$$\mathcal{U}(\lambda_L, q_L) - \mathcal{U}(\lambda_0, q_0) = \int_{\Gamma} [\partial_\lambda \mathcal{U}(\lambda_t, q_t) d\lambda_t + \nabla_q \mathcal{U}(\lambda_t, q_t) dq_t].$$

Similarly, we have $\mathcal{K}(p_L) - \mathcal{K}(p_0) = \int_{\Gamma} \nabla_p \mathcal{K}(p_t) dp_t$. The work and heat along Γ thus write

$$\mathcal{W}_{\Gamma}^{0 \rightarrow L\tau} = \int_{\Gamma} \partial_\lambda \mathcal{U}(\lambda_t, q_t) d\lambda_t dt, \quad (4.11a)$$

$$\mathcal{Q}_{\Gamma}^{0 \rightarrow L\tau} = \mathcal{K}(p_L) - \mathcal{K}(p_0) + \int_{\Gamma} \nabla_q \mathcal{U}(\lambda_t, q_t) dq_t. \quad (4.11b)$$

These two quantities obviously satisfy a conservation equation similar to (4.10), that is

$$\mathcal{W}_{\Gamma}^{0 \rightarrow L\tau} = \mathcal{H}(\lambda_L, p_L, q_L) - \mathcal{H}(\lambda_0, p_0, q_0) - \mathcal{Q}_{\Gamma}^{0 \rightarrow L\tau}. \quad (4.12)$$

They correspond to the exact work and heat along the piecewise linear trajectory. The difference with the work and heat previously defined stem from discretization errors. Indeed, approximating the integral associated with the heat in (4.11b) by numerical quadrature based on trapezoidal rule yields

$$\begin{aligned} \int_{\Gamma} \nabla_q \mathcal{U}(\lambda_t, q_t) \frac{q_t}{dt} dt &\approx \frac{1}{2} \sum_{\ell=0}^{L-1} (q_{\ell+1} - q_\ell)^T [\nabla_q \mathcal{U}(\lambda_{\ell+1}, q_{\ell+1}) + \nabla_q \mathcal{U}(\lambda_\ell, q_\ell)], \\ &\approx \mathcal{Q}^{0 \rightarrow L} - \mathcal{K}(p_L) + \mathcal{K}(p_0) \end{aligned} \quad (4.13)$$

where we plugged relation (4.9) in the second line (4.13) and neglected the second order term $\mathcal{C}^{0 \rightarrow L}$. Plugging relation (4.13) into relation (4.11b) and then comparing the two conservation equations (4.10) and (4.12) yield the following pair of approximations

$$\mathcal{Q}^{0 \rightarrow L} \approx \mathcal{Q}_{\Gamma}^{0 \rightarrow L\tau} \quad \text{and} \quad \mathcal{W}^{0 \rightarrow L} \approx \mathcal{W}_{\Gamma}^{0 \rightarrow L\tau}.$$

The work $\mathcal{W}_{\Gamma}^{0 \rightarrow L\tau}$ in (4.11a) corresponds to the work done by the external force that is exerted along the λ -component of the extended system for compensating the internal force $-\partial_\lambda \mathcal{U}$ and thus displacing λ . This quantity is exactly zero when the external forcing on λ is suppressed by holding the external parameter at a constant value. At variance, the effective work functional $z \mapsto \mathcal{W}^{0 \rightarrow L}$ is non zero in this particular equilibrium case. The effective work can be either positive or negative, but its expected value is always a strictly positive quantity corresponding to an energy irreversibly dissipated toward the thermostat(s). The dissipation of the work done on the system is often referred to as an entropy production since the overall entropy of the thermostats is increased by the heats flowing into them. The produced entropy is due to both time stepping and external forcing [45]. Its strict positiveness is a simple consequence of the fluctuation relation derived hereafter and satisfied by the effective work $\mathcal{W}^{0 \rightarrow L}$ and heat $\mathcal{Q}^{0 \rightarrow L}$. These quantities are precisely to be used in the construction of sampling algorithms and estimators because of the fluctuation relation.

4.2.8 Path statistics and heat fluctuation relation

We define a path z as a sequence of $L+1$ extended states $z = \{(\lambda_0, x_0), \dots, (\lambda_\ell, x_\ell), \dots, (\lambda_L, x_L)\}$ where $x = (p, q)$ and denote the path space by \mathcal{Z} . In practice, paths will be constructed by applying L iterations of the steered langevin dynamics forward or backward starting from an index $\ell \in \llbracket 0, L \rrbracket$. Because of the external steering and time-stepping, detailed balance is violated and the probability to generate a path z depends on

$$\begin{array}{ccc}
\mathcal{W}^{\ell \rightarrow \ell+1} = \mathcal{H}(\lambda_{\ell+1}, p_{\ell+1}, q_{\ell+1}) - \mathcal{H}(\lambda_{\ell}, p_{\ell}, q_{\ell}) - \mathcal{Q}^{\ell \rightarrow \ell+1} & & \\
(\lambda_{\ell}, p_{\ell}, q_{\ell}) & & (\lambda_{\ell+1}, p_{\ell+1}, q_{\ell+1}) \\
\downarrow & \mathcal{Q}^{\ell \rightarrow \ell+1} = \ln \frac{\mathcal{T}[\ell \leftarrow \ell+1]}{\mathcal{T}[\ell \rightarrow \ell+1]} & \uparrow \\
(\lambda_{\ell}, p_{\ell+1/2}, q_{\ell}) & \text{-----} \rightarrow & (\lambda_{\ell+1}, p_{\ell+1/2}, q_{\ell+1})
\end{array}$$

Figure 4.1: The quantity $\mathcal{W}^{\ell \rightarrow \ell+1}$ is the work done on the system by application of a single Langevin iteration with the external parameter forced to move from λ_{ℓ} to $\lambda_{\ell+1}$. It relates to the exchanged with the thermostat, $\mathcal{Q}^{\ell \rightarrow \ell+1}$, through the energy conservation equation which also includes the Hamiltonian variation. The dashed arrow represents the updating of the external and internal coordinates (λ, q) performed at constant momentum p resorting to scheme (4.7).

the starting index ℓ . The conditional probability to generate the indexed path (z, ℓ) given (λ, x) is

$$\mathbb{P}(z, \ell | \lambda, x) = \mathbb{P}_{\text{gen}}^{\ell \rightarrow L}(z) \mathbb{P}_{\text{gen}}^{0 \leftarrow \ell}(z) \mathbf{1}_{\lambda}(\lambda_{\ell}), \delta_x(x_{\ell}) \quad (4.14)$$

where the partial generating probabilities are defined by

$$\mathbb{P}_{\text{gen}}^{\ell \rightarrow L}(z) = \begin{cases} \prod_{l=\ell}^{L-1} \mathcal{T}[(\lambda, p, q)_l \rightarrow (\lambda, p, q)_{l+1}] & \text{if } 0 \leq \ell < L, \\ 1 & \text{if } \ell = L, \end{cases}$$

$$\mathbb{P}_{\text{gen}}^{0 \leftarrow \ell}(z) = \begin{cases} 1 & \text{if } \ell = 0, \\ \prod_{l=0}^{\ell-1} \mathcal{T}[(\lambda, -p, q)_{\ell-l} \rightarrow (\lambda, -p, q)_{\ell-l-1}] & \text{if } 0 < \ell \leq L. \end{cases}$$

A useful identity due to Crooks [4] relates the ratio of path generating probabilities to the heat exchanged with the thermostat. We have

$$\frac{\mathbb{P}(z, \ell | \lambda_{\ell}, x_{\ell})}{\mathbb{P}(z, 0 | \lambda_0, x_0)} = \frac{\mathbb{P}_{\text{gen}}^{0 \leftarrow \ell}(z)}{\mathbb{P}_{\text{gen}}^{0 \rightarrow \ell}(z)} = \exp[\mathcal{Q}^{0 \rightarrow \ell}(z)]. \quad (4.15)$$

We refer to this identity as the heat fluctuation relation. This relation can be generalized to any thermostated dynamics and also plays a crucial role in nonequilibrium steady states. The more general identity is referred to as entropy production fluctuation theorem [4].

4.3 Nonequilibrium path ensemble

4.3.1 Path reweighting estimator

Here, we are concerned with the Hamiltonian-switching schedule introduced by Jarzynski [62]: the external parameter is viewed as a thermodynamic force that is varied during a transient regime from $\lambda_{\text{ref}} = \lambda^0$ to $\lambda_{\text{targ}} = \lambda^L$. For all path $z \in \mathcal{Z}$, the scheduling of the external parameter is imposed by $\lambda_{\ell} = \lambda^{\ell}$ where $\Lambda = (\lambda^0, \dots, \lambda^{\ell}, \dots, \lambda^L)$ is a given sequence of strictly increasing or decreasing values. In this transient nonequilibrium framework, trajectories are generated from the equilibrium distribution $\pi(x | \lambda^0)$ using the forward Langevin scheme (4.7). However, resorting to the reverse map (4.8), it is possible to consider trajectories initiated from any distribution $\pi(x | \lambda)$ with $\lambda \in \Lambda$. We define the conditional path probability given λ from the law of total probability with respect to $x \in \mathcal{X}$

$$\mathbb{P}(z | \lambda) = \sum_{l=0}^L \int_{\mathcal{X}} \mathbb{P}(z, l | \lambda, x) \pi(x | \lambda) dx = \sum_{l=0}^L \mathbb{P}(z, l | \lambda, x_l) \pi(x_l | \lambda).$$

We thus have $\mathbb{P}(z | \lambda)$ equal to 0 if $\lambda \notin \Lambda$, otherwise $\exists \ell \in \llbracket 0, L \rrbracket$ such that $\lambda = \lambda^{\ell}$ and we have:

$$\mathbb{P}(z | \lambda^{\ell}) = \mathbb{P}_{\text{gen}}^{0 \leftarrow \ell}(z) \mathbb{P}_{\text{gen}}^{\ell \rightarrow L}(z) \pi(x_{\ell} | \lambda^{\ell}). \quad (4.16)$$

We define the conditional path expectation of observable \mathcal{O} given $\lambda = \lambda^\ell$ as:

$$\begin{aligned}\mathbb{E}^{\mathcal{Z}} [\mathcal{O}|\lambda^\ell] &= \int_{\mathcal{Z}} \mathcal{O}(\lambda^\ell, x_\ell) \mathbb{P}(z|\lambda^\ell) \mathcal{D}z \\ &= \int_{\mathcal{X}} \int_{\mathcal{Z}} \mathcal{O}(\lambda^\ell, x) \pi(x|\lambda^\ell) \mathcal{D}z \mathbb{P}(z|\lambda^\ell) \mathbb{P}_{\text{gen}}^{0 \leftarrow \ell}(z) \mathbb{P}_{\text{gen}}^{\ell \rightarrow L}(z) \delta_x(x_\ell) \mathcal{D}z dx \\ &= \int_{\mathcal{X}} \mathcal{O}(\lambda^\ell, x) \pi(x|\lambda^\ell) dx = \mathbb{E} [\mathcal{O}|\lambda^\ell]\end{aligned}$$

The path expectation $\mathbb{E}^{\mathcal{Z}} [\mathcal{O}|\lambda^\ell]$ can be expressed as a function of expected values given λ^0 , resorting to the free energy perturbation technique. This requires to specify the form of the conditional probability of x given λ . We write $\pi(x|\lambda) = \exp[\mathfrak{F}(\lambda) - \mathcal{H}(\lambda, x)]$ where the normalizing constant writes $\mathfrak{F}(\lambda) = -\ln \int_{\mathcal{X}} \exp[-\mathcal{H}(\lambda, x)] dx$ and corresponds to the absolute free energy defined in Eq. (1.1). Note that the relative free energy $\mathfrak{A}(\lambda) = \mathfrak{F}(\lambda) + \Psi_0^A$ is more convenient to manipulate in the context of expanded ensembles and was used for this reason in Chapter 2 and 3. The conditional path probability ratio writes

$$\frac{\mathbb{P}(z|\lambda^\ell)}{\mathbb{P}(z|\lambda^0)} = \frac{\mathbb{P}_{\text{gen}}^{0 \leftarrow \ell}(z) \pi(x_\ell|\lambda^\ell)}{\mathbb{P}_{\text{gen}}^{0 \rightarrow \ell}(z) \pi(x_0|\lambda^0)} = \exp[\mathcal{Q}^{0 \rightarrow \ell}] \frac{\exp[\mathfrak{F}(\lambda^\ell) - \mathcal{H}(\lambda^\ell, x_\ell)]}{\exp[\mathfrak{F}(\lambda^0) - \mathcal{H}(\lambda^0, x_0)]}. \quad (4.17)$$

Plugging the effective work quantity $\mathcal{W}^{0 \rightarrow \ell}(z) = \mathcal{H}(\lambda^\ell, x_\ell) - \mathcal{H}(\lambda^0, x_0) - \mathcal{Q}^{0 \rightarrow \ell}$ deduced from the conservation equation (4.10) for the total energy between time $t = 0$ and time $t = \tau\ell$ into ratio (4.17) provides us with the following work fluctuation identity

$$\frac{\mathbb{P}(z|\lambda^\ell)}{\mathbb{P}(z|\lambda^0)} = \exp[\mathfrak{F}(\lambda^\ell) - \mathfrak{F}(\lambda^0) - \mathcal{W}^{0 \rightarrow \ell}(z)].$$

This identity allows us to formulate the following nonequilibrium path average [5]

$$\begin{aligned}\mathbb{E}^{\mathcal{Z}} [\mathcal{O}|\lambda^\ell] &= \mathbb{E}^{\mathcal{Z}} \left[\frac{\mathbb{P}(z|\lambda^\ell)}{\mathbb{P}(z|\lambda^0)} \mathcal{O}(\lambda^\ell, x_\ell) \Big| \lambda^0 \right] \\ &= \mathbb{E}^{\mathcal{Z}} \left[\exp[\mathfrak{F}(\lambda^\ell) - \mathfrak{F}(\lambda^0) - \mathcal{W}^{0 \rightarrow \ell}] \mathcal{O}(\lambda^\ell, x_\ell) \Big| \lambda^0 \right].\end{aligned} \quad (4.18)$$

The two free energies being unknown, they are estimated by setting $\mathcal{O}(\lambda^\ell, x)$ to 1 in (4.18) and solving. The free energy difference exhibits the form:

$$\exp[-(\mathfrak{F}(\lambda^\ell) - \mathfrak{F}(\lambda^0))] = \mathbb{E}^{\mathcal{Z}} \left[\exp(-\mathcal{W}^{0 \rightarrow \ell}) \Big| \lambda^0 \right]. \quad (4.19)$$

The identity above is known as Jarzynski's nonequilibrium work (NW) identity. Plugging the NW identity in the path expectation (4.18) yields

$$\mathbb{E} [\mathcal{O}|\lambda^\ell] = \frac{\mathbb{E}^{\mathcal{Z}} \left[\exp[-\mathcal{W}^{0 \rightarrow \ell}] \mathcal{O}(\lambda^\ell, x_\ell) \Big| \lambda^0 \right]}{\mathbb{E}^{\mathcal{Z}} \left[\exp[-\mathcal{W}^{0 \rightarrow \ell}] \Big| \lambda^0 \right]}. \quad (4.20)$$

The NW identity (4.19) and the NW expectation (4.20) correspond to free energy perturbation and umbrella sampling within a path ensemble, respectively. These two relations tell us how to reweight the information contained in a sample of short nonequilibrium trajectories so as to recover equilibrium expectations. Let us denote the generated sample of trajectories by $\{z_m\}_{0 \leq m \leq M}$. Each trajectory consists of a sequence of states, $z_m = \{\lambda^\ell, x_{m\ell}\}_{0 \leq \ell \leq L}$, initiated from the equilibrium distribution $\pi(x|\lambda^0)$ and driven out of equilibrium using a given *switching* protocol A acting on the external parameter λ . The work for path z_m writes

$$\mathcal{W}_m^{0 \rightarrow \ell} = \mathcal{H}(\lambda^\ell, x_{m\ell}) - \mathcal{H}(\lambda_0, x_{m0}) - \mathcal{Q}_m^{\ell \rightarrow \ell+1}.$$

An estimate of $\mathbb{E}[\mathcal{O}|\lambda^\ell]$ can be obtained from the path sample using the following path reweighting (PR) estimator

$$\Upsilon_{\text{PR}}^{M,L}(\mathcal{O}|\lambda^\ell) = \frac{\frac{1}{M} \sum_{m=1}^M \mathcal{O}(\lambda^\ell, x_{m\ell}) \exp[-\beta \mathcal{W}_m^{0 \rightarrow \ell}]}{\frac{1}{M} \sum_{m=1}^M \exp[-\beta \mathcal{W}_m^{0 \rightarrow \ell}]} \quad (4.21)$$

The denominator in the fraction corresponds to an estimate of the exponential of the free energy difference based on Jarzynski's NW identity.

4.3.2 Illustration on a complex high-dimensional energy landscape

We report an application of the PR estimator (4.21) from Ref. [63]. The goal is to estimate the free energies associated with the low structure the 38-atoms Lennard-Jones system of Chapter 3. The external parameter corresponds to a reduced inverse temperature, the potential energy is $E(q) \equiv \mathcal{V}_{\text{LJ}}(q)$, and the Hamiltonian reads

$$\mathcal{H}(\lambda, x) = \frac{1}{T_{\text{max}}} [K(p) - B \circ Q_4(q)] + \mathcal{V}_{\text{LJ}}(q) \left[\frac{\lambda}{T_{\text{min}}} + \frac{1-\lambda}{T_{\text{max}}} \right]$$

where $B \circ Q_4$ is an additional biasing potential that is introduced to ensure homogeneous sampling along Q_4 at high temperature. We set $\lambda^\ell = \ell/L$. Paths are initiated from distribution $\pi(x|0)$, which corresponds to the high temperature thermodynamic state. The targeted thermodynamic states are the ones at lower temperatures. The Landau free energy $\Lambda(Q_4, E)$ at given temperature T^ℓ relates to the cologarithm of the biased probability $\mathbb{E}[\mathbf{1}_{Q_4, E}|\lambda^\ell]$. Removing the bias $B(Q_4)$ leads to the relation

$$\Lambda(Q_4, E|T^\ell) = B(Q_4) - \ln \mathbb{E}[\mathbf{1}_{Q_4, E}|\lambda^\ell] + c_0$$

where c_0 is an additive constant. The conditionally expected value of the indicator function is estimated using the PR estimator:

$$\Upsilon_{\text{PR}}^{ML}(\mathbf{1}_{Q_4, E}|\lambda^\ell) = \frac{\frac{1}{M} \sum_{m=1}^M \mathbf{1}_{Q_4, E}(Q_{4m\ell}, E_{m\ell}) \exp[-\beta \mathcal{W}_m^{0 \rightarrow \ell}]}{\frac{1}{M} \sum_{m=1}^M \exp[-\beta \mathcal{W}_m^{0 \rightarrow \ell}]} \quad (4.22)$$

where $Q_{4m\ell} = Q_4(q_{m\ell})$ and $E_{m\ell} = E(q_{m\ell})$ correspond to the sampled values of the order parameter and potential energy.

Contour plot of the Landau free energy as obtained from the path sampling⁴ and the path reweighting estimator (4.22) are displayed in Fig. 4.2. The path sampling approach is able to explore the icosahedral and octahedral structures at the lowest temperature, as well as other defected structures around $Q_4 \approx 0.12$. The defected structures, displayed in Fig. 4.3, are missed using parallel tempering or Wang-Landau sampling [63].

4.3.3 Comparison with Harmonic Superposition Approximation

The harmonic superposition approximation (HSA) described in Appendix B.3 is used for comparison with path sampling and reweighting. HSA consists of superposing the harmonic contributions to the free energy of a collection of low energy minima. In figure 4.4 are shown the probabilities to find the defective octahedral structure obtained as a function of temperature using either path-sampling or the harmonic superposition approximation. The two methods agree to a very good extent. Some discontinuities are more clearly visible on the Landau free energy; they result from pollutions arising in the octahedral basin. Conversely, the results of parallel tempering and Wang-Landau sampling, also shown in this figure, significantly disagree (even though they agree with each other). In other terms, their relative probability is much too small, as precisely seen in Fig. 4.4(a).

4.3.4 Advantages and limitations of path sampling and reweighting

The accuracy in the estimations is improved in the low-temperature thermodynamic states despite the severe metastability resulting from the high free energy barriers between the various basins of attraction at low temperatures. By gradually decreasing the temperature starting from an ergodic sample of states generated at

⁴All reported calculations have been carried out with the following parameters: $L = 2 \times 10^5$ with $M = 34650$ or $L = 2 \times 10^7$ with $M = 5818$ paths, respectively. These calculations were performed in parallel and took a total of 360 hours and 600 hours on fifteen 2 GHz Xeon processors, respectively.

high temperature, the path sampling procedure provides a biased sample of states spanning over the different basins of attractions at lower temperatures. The path reweighting estimator (4.22) makes it possible to recover accurate estimates of the free energy associated with the various basins of attraction. The obtained results compare well with those obtained using the superposition harmonic approximations [42].

The present path reweighting approach has two main limitations. A first drawback is that a considerable amount of information is lost: the observable values of the states generated at high temperature are not taken into account in the low temperature average. A second drawback is that barrier regions at low temperatures are poorly sampled because trajectories are attracted to the low energy structures as the effective temperature is decreased (though increasing λ). To circumvent these two limitations, Hummer and Szabo [67] proposed (i) to generate the nonequilibrium paths employing the harmonic coupling setup so as to pull the reaction coordinate over free energy barriers and (ii) to post-process all the information contained in the generated paths by implementing the self-consistent reweighting estimator WHAM. In next Section, we present a more direct approach based on a pathwise conditioning technique within an expanded path ensemble.

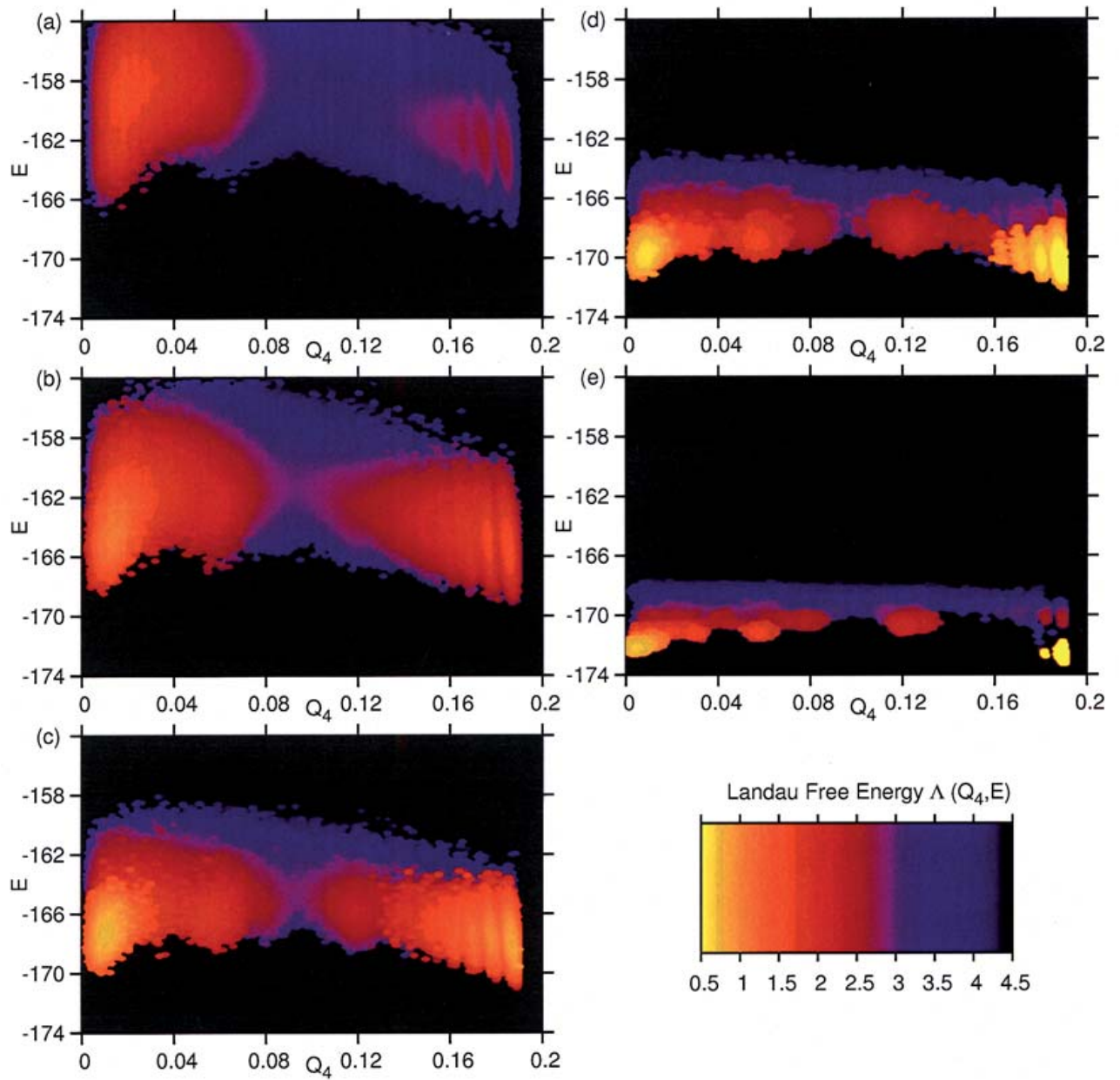


Figure 4.2: Contour plot of the Landau free energy $\Lambda(Q_4, E|T)$ for five temperatures (a) $T = 0.19$, (b) $T = 0.147$, (c) $T = 0.105$, (d) $T = 0.062$, (e) $T = 0.021$.

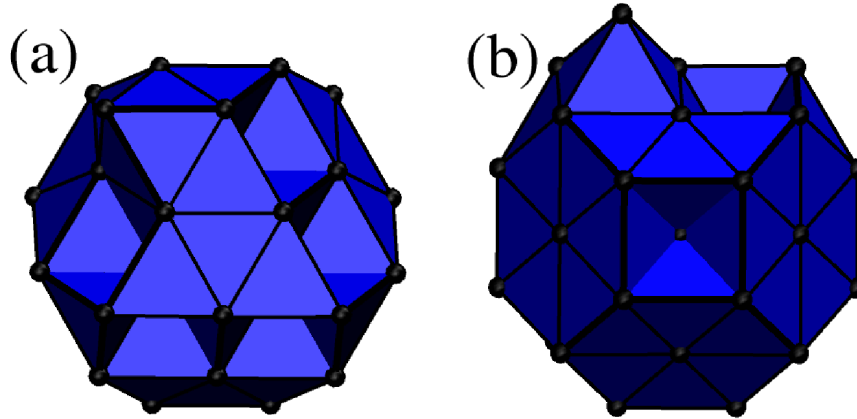


Figure 4.3: Structures of the 38-atom defected octahedral cluster. Its minimum energy is -171.8560 and its order parameter is $Q_4 = 0.121$. View (a) emphasizes the stacking fault while view (b) shows the atom that has been expelled from the outer shell.

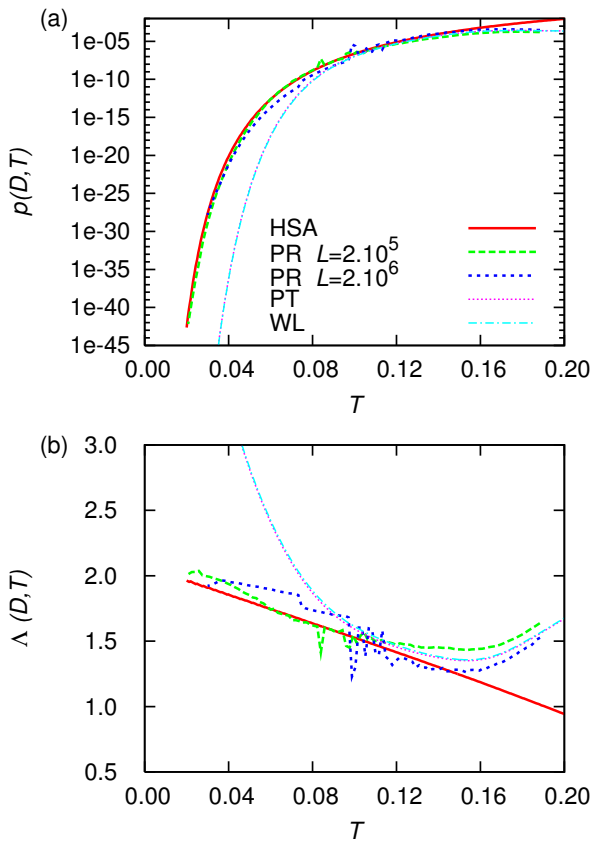


Figure 4.4: (a) Occurrence probability and (b) Landau free energy of the defective truncated octahedral cluster as a function of temperature. The results of two path-sampling calculations are shown for two different switching rates. The dotted line corresponds to the harmonic superposition approximation.

4.4 Expanded path ensemble

The expanded path ensemble is built upon the expanded ensemble resorting to two probability distributions: the joint probability distribution of extended states (ζ, \bar{x}) , denoted by $p_a(\zeta, \bar{x})$ and introduced in (1.13), and the conditional probability distribution of path (z, ℓ) given state (ζ, \bar{x}) denoted by $P(z, \ell | \zeta, \bar{x})$ defined previously in (4.14).

4.4.1 Path probability and total expectations

The path probability of expanded path (z, ℓ) is defined resorting to the following law of total probability

$$P_a(z, \ell) = \sum_{\zeta \in \Lambda} \int_{\mathcal{X}} P(z, \ell | \zeta, \bar{x}) p_a(\zeta, \bar{x}) d\bar{x} = P(z, \ell | \lambda_\ell, x_\ell) p_a(\lambda_\ell, x_\ell) \quad (4.23)$$

where (λ_ℓ, x_ℓ) is the ℓ th extended state of z . The total expectation of a state observable $\mathcal{O}^*(\zeta, \bar{x})$ in the path ensemble is defined as

$$\mathbb{E}_a^{\mathcal{Z}} [\mathcal{O}^*] = \sum_{l=0}^L \int_{\mathcal{Z}} \mathcal{O}^*(\lambda_l, x_l) P_a(z, l) \mathcal{D}z. \quad (4.24)$$

Note that the expectation $\mathbb{E}_a^{\mathcal{Z}} [\cdot]$ can also be applied to path observables, as will be done in the transition path sampling simulations of Section 4.6. Plugging the law of total probability (4.23) into the path expectation (4.24) leads to the following simplification:

$$\mathbb{E}_a^{\mathcal{Z}} [\mathcal{O}^*] = \sum_{\zeta \in \Lambda} \sum_{l=0}^L \int_{\mathcal{Z}, \mathcal{X}} \mathcal{O}^*(\zeta, \bar{x}) P(z, l | \zeta, \bar{x}) p_a(\zeta, \bar{x}) \mathcal{D}z d\bar{x} = \sum_{\zeta \in \Lambda} \int_{\mathcal{Q}} \mathcal{O}^*(\zeta, \bar{x}) p_a(\zeta, \bar{x}) d\bar{x} = \mathbb{E}_a [\mathcal{O}^*].$$

The last equality means that the biased expectation of a state observable with respect to the expanded path distribution coincides with the biased expectation in the expanded ensemble of states. This property suggests one to perform pathwise conditioning over the path indexes with respect to the given path coordinates. Resorting to the law of total expectation yields

$$\mathbb{E}_a^{\mathcal{Z}} [\mathcal{O}^*] = \mathbb{E}_a^{\mathcal{Z}} [\mathbb{E}_a^{\mathcal{Z}} [\mathcal{O}^* | z]] = \mathbb{E}_a^{\mathcal{Z}} \left[\sum_{l=0}^L \mathcal{O}^*(\lambda_l, x_l) P_a(l | z) \right] \quad (4.25)$$

where $P_a(l | z)$ denotes the conditional probability of index l given the path z . It is equal to the conditionally expected value of path index l given z :

$$P_a(l | z) = \mathbb{E}_a^{\mathcal{Z}} [\mathbf{1}_\ell | z] = \frac{P_a(z, \ell)}{\sum_{l=0}^L P_a(z, l)}. \quad (4.26)$$

where $\mathbf{1}_\ell(l) \equiv \delta_{l\ell}$ is the indicator function associated with the index l of expanded path (z, l) . Variance reduction for conditioned estimators based on expectation (4.25) is guaranteed by the law of total variance

$$\mathbb{V}_a^{\mathcal{Z}} [\mathbb{E}_a^{\mathcal{Z}} [\mathcal{O}^* | z]] = \mathbb{V}_a^{\mathcal{Z}} [\mathcal{O}^* | z] - \mathbb{E}_a^{\mathcal{Z}} [\mathbb{V}_a^{\mathcal{Z}} [\mathcal{O}^* | z]].$$

We recall that with the expanded path ensemble approach, neither the reference Hamiltonian nor the reference distribution are modified by the external forcing upon λ coordinate. As a result, the ratio of backward to forward path probabilities differs from Crooks's probability ratio (4.17) in that the free energy is replaced by the auxiliary potential:

$$\frac{P_a(z, \ell)}{P_a(z, 0)} = \frac{P(z, \ell | \lambda_\ell, x_\ell) p_a(\lambda_\ell, x_\ell)}{P(z, 0 | \lambda_0, x_0) p_a(\lambda_0, x_0)} = \exp[\mathcal{Q}_{0 \rightarrow \ell}] \frac{\exp[\mathbf{a}(\lambda_\ell) - \mathcal{H}(\lambda_\ell, x_\ell)]}{\exp[\mathbf{a}(\lambda_0) - \mathcal{H}(\lambda_0, x_0)]},$$

where we plugged the heat fluctuation theorem (4.15). Resorting to the energy conservation equation (4.10)

yields the following relation

$$\frac{P_a(z, \ell)}{P_a(z, 0)} = \exp [\alpha(\lambda_\ell) - \alpha(\lambda_0) - \mathcal{W}^{0 \rightarrow \ell}(z)] \triangleq \exp [-\mathcal{W}_a^{0 \rightarrow \ell}(z)]. \quad (4.27)$$

where $\mathcal{W}_a^{0 \rightarrow \ell}$ represents the work done on the expanded system by the external forcing. It includes the term $-\alpha(\lambda_\ell) + \alpha(\lambda_0)$ that is the opposite of the auxiliary biasing potential variation. In absence of auxiliary biasing potential, the fluctuation identity (4.27) is similar to the Bochkov and Kuzovlev fluctuation identity [68, 69, 70, 64]. Plugging the fluctuation identity (4.27) into (4.26) yields the index probability as a function of the given path coordinates

$$P_a(\ell|z) = \frac{\exp [\alpha(\lambda_\ell) - \mathcal{W}^{0 \rightarrow \ell}(z)]}{\sum_{l=0}^L \exp [\alpha(\lambda_l) - \mathcal{W}^{0 \rightarrow l}(z)]},$$

which is obtained after simplifying by $\alpha(\lambda_0)$. Choosing index 0 as the origin for calculating the work is arbitrary. It will prove computationally more convenient to express the conditional probability of index ℓ as a function of the index from which the path is originally generated. For any index $i \in \llbracket 0, L \rrbracket$, we have

$$P_a(\ell|z) = \frac{\exp [-\mathcal{W}_a^{i \rightarrow \ell}(z)]}{\sum_{l=0}^L \exp [-\mathcal{W}_a^{i \rightarrow l}(z)]}.$$

Owing to pathwise conditioning, any expectation can in principle be estimated from a collection of trajectories sampled from the expanded path distribution by including the information relative to all the generated states. Prior to explaining how this is done, we first detail the path-sampling scheme allowing ergodic sampling of path ensembles.

4.4.2 Path sampling: shooting and indexing moves

The path-sampling scheme for nonequilibrium trajectories is decomposed into two types of Monte Carlo moves, namely, *shooting moves* and *indexing moves*, which reflect the two steps of the Metropolis-type algorithm:

Shooting moves are used to generate a new path $(z, i) \equiv (z_{m+1}, i)$ starting from the current path $(\bar{z}, \ell) \equiv (z_m, \ell)$. The shooting move detailed below requires a state-sampling algorithm whose transition probabilities T are detailed balance with respect to the expanded probability $p_a(\lambda, x)$ and a symmetric law to sample new index i of the shot path. The new path coordinates $z \equiv z_{m+1}$ are generated from the probability distribution $P(z, i|\lambda_i, x_i)$ that is defined in (4.14). By construction, the shooting move from (z, ℓ) to (z, i) obeys the following detailed balance condition

$$P(z, i|\lambda_i, x_i) T(\lambda_i, x_i \leftarrow \bar{\lambda}_\ell, \bar{x}_\ell) \alpha^{i \leftarrow \ell} P_a(\bar{z}, \ell) = P(\bar{z}, \ell|\bar{\lambda}_\ell, \bar{x}_\ell) T(\bar{\lambda}_\ell, \bar{x}_\ell \leftarrow \lambda_i, x_i) \alpha^{\ell \leftarrow i} P_a(z, i),$$

where the two index transition probabilities $\alpha^{i \leftarrow \ell}$ and $\alpha^{\ell \leftarrow i}$ both equal each other. This balance equation is easily verified by substituting $P(\bar{z}, \ell|\bar{\lambda}_\ell, \bar{x}_\ell) p_a(\bar{\lambda}_\ell, \bar{x}_\ell)$ and $P(z, i|\lambda_i, x_i) p_a(\lambda_i, x_i)$ for $P_a(\bar{z}, \ell)$ and $P_a(z, i)$, respectively.

Indexing moves are used to sample a new index for a shot path. One selects l_{m+1} from the probability distribution $\ell \mapsto P_a(\ell|z)$ where $z \equiv z_{m+1}$. It satisfy the detailed balance condition

$$P_a(l_{m+1}|z_{m+1}) P_a(z, i) = P_a(i|z) P_a(z_{m+1}, i).$$

Hence, the combination of shooting and indexing moves allows the ergodic sampling of the expanded path ensemble with probability $P_a(z, l)$. To avoid storing the entire path coordinates, the next path index l_{m+1} is chosen iteratively during the path construction. The conditioned observable $\mathbb{E}_a^{\mathcal{Z}}[\mathcal{O}^*|z_{m+1}]$ is similarly constructed on the fly. These two tricks are implemented in Algorithm 8 detailed page 116 in Appendix B. As explained in Ref. [66], the combination of shooting and indexing can be seen as implementing a Metropolis-like Monte Carlo algorithm generating multiple trial configurations (the proposals) in the expanded state ensemble. Pathwise conditioning thus amounts to conditioning on the multi-proposal. Thus, algorithm 8 is an exact instance of waste-recycling Monte Carlo. Nevertheless, pathwise conditioning is in principle more flexible than waste-recycling because it might be employed in combination with any algorithm that samples the expanded path probability $P_a(z, \ell)$ or the marginal path probability $P_a(z) = \sum_{\ell=0}^L P_a(z, \ell)$.

4.4.3 Conditional and total expectations

We show here how to perform the conditioning on both the states contained in the paths and on the external parameter λ to estimate total and conditional expectations of the form $\mathbb{E}[\mathcal{O}]$ and $\mathbb{E}[\mathcal{O}|\lambda]$ where $\mathcal{O}(\lambda, x)$ is an observable. As for the latter expectation, we replace \mathcal{O}^* by $\pi_a^\lambda(\cdot)\mathcal{O}(\lambda, \cdot)$ and π_a^λ and form the following ratio

$$\mathbb{E}[\mathcal{O}|\lambda] = \frac{\mathbb{E}_a^{\mathcal{Z}} [\pi_a^\lambda(\cdot)\mathcal{O}(\lambda, \cdot)]}{\mathbb{E}_a^{\mathcal{Z}} [\pi_a^\lambda]}. \quad (4.28)$$

Plugging the law of total expectation into the two total expectations of (4.28) allows the conditional expectation $\mathbb{E}[\mathcal{O}|\lambda]$ to be expressed as a function of $\mathbb{P}_a(l|z)$

$$\mathbb{E}[\mathcal{O}|\lambda] = \frac{\mathbb{E}_a^{\mathcal{Z}} [\mathbb{E}_a^{\mathcal{Z}} [\pi_a^\lambda(\cdot)\mathcal{O}(\lambda, \cdot)|z]]}{\mathbb{E}_a^{\mathcal{Z}} [\mathbb{E}_a^{\mathcal{Z}} [\pi_a(\cdot)|z]]} = \frac{\mathbb{E}_a^{\mathcal{Z}} \left[\sum_{l=0}^L \mathbb{P}_a(l|z) \pi_a^\lambda(x_l) \mathcal{O}(\lambda, x_l) \right]}{\mathbb{E}_a^{\mathcal{Z}} \left[\sum_{l=0}^L \mathbb{P}_a(l|z) \pi_a^\lambda(x_l) \right]}.$$

Let now $\{(z_m, l_m)\}_{1 \neq M}$ denote the Markov chain of paths generated according to probability $\mathbb{P}_a(z, l)$. The estimator with pathwise conditioning writes

$$\Upsilon_{\text{PC}}^{M,L}(\mathcal{O}|\lambda) = \frac{\frac{1}{M} \sum_{m=1}^M \sum_{l=0}^L \mathbb{P}_a(l|z_m) \pi_a^\lambda(x_{lm}) \mathcal{O}(\lambda, x_{lm})}{\frac{1}{M} \sum_{m=1}^M \sum_{l=0}^L \mathbb{P}_a(l|z_m) \pi_a^\lambda(x_{lm})}.$$

The total expectation of $\mathcal{O}(\lambda, x)$ is conditioned by replacing π_a^λ by π_a^λ and summing over $\lambda \in \Lambda$:

$$\mathbb{E}[\mathcal{O}] = \frac{\mathbb{E}_a^{\mathcal{Z}} [\mathbb{E}_a^{\mathcal{Z}} [\sum_{\lambda \in \Lambda} \pi_a^\lambda(\cdot)\mathcal{O}(\lambda, \cdot)|z]]}{\mathbb{E}_a^{\mathcal{Z}} [\mathbb{E}_a^{\mathcal{Z}} [\pi_a(\cdot)|z]]} = \frac{\mathbb{E}_a^{\mathcal{Z}} \left[\sum_{l=0}^L \mathbb{P}_a(l|z) \sum_{\lambda \in \Lambda} \pi_a^\lambda(x_l) \mathcal{O}(\lambda, x_l) \right]}{\mathbb{E}_a^{\mathcal{Z}} \left[\sum_{l=0}^L \mathbb{P}_a(l|z) \pi_a(x_l) \right]}.$$

The estimator of $\mathbb{E}[\mathcal{O}]$ with pathwise conditioning then reads

$$\Upsilon_{\text{PC}}^{M,L}(\mathcal{O}) = \frac{\frac{1}{M} \sum_{m=1}^M \sum_{l=0}^L \mathbb{P}_a(l|z_m) \sum_{\lambda \in \Lambda} \pi_a^\lambda(x_{lm}) \mathcal{O}(\lambda, x_{lm})}{\frac{1}{M} \sum_{m=1}^M \sum_{l=0}^L \mathbb{P}_a(l|z_m) \pi_a(x_{lm})}. \quad (4.29)$$

As an example, we consider the LJ-38 atom cluster and the estimator for obtaining the histogram $\widehat{\mathbb{P}}_{Q_4, E}$ associated with the indicator function $\mathbf{1}_{\xi^*} \equiv \mathbf{1}_{Q_4, E}$. The coupling is harmonic and λ is a two-dimensional external parameter. Resorting to the effective biasing potential

$$\mathcal{B}^a(\xi^*) = \ln \sum_{\lambda \in \Lambda} \exp [\alpha(\lambda) - \|\lambda - \xi^*\|^2 + \varepsilon(\xi^*)] \quad (4.30)$$

with $\xi^* = (Q_4, E)^T$ and ε such that $\mathcal{B}^0 = 0$, the PC estimator of $\mathbf{1}_{Q_4, E}$ writes

$$\Upsilon_{\text{PC}}^{M,L}(\mathbf{1}_{Q_4, E}) = \frac{\frac{1}{M} \sum_{m=1}^M \frac{\sum_{l=0}^L \exp [\alpha(\lambda_{lm}) - \mathcal{W}_{lm} - \mathcal{B}_{lm}^a] \mathbf{1}_{Q_4, E}(Q_{4lm}, E_{lm})}{\sum_{l=0}^L \exp [\alpha(\lambda_{lm}) - \mathcal{W}_{lm}]}}{\frac{1}{M} \sum_{m=1}^M \frac{\sum_{l=0}^L \exp [\alpha(\lambda_{lm}) - \mathcal{W}_{lm} - \mathcal{B}_{lm}^a]}{\sum_{l=0}^L \exp [\alpha(\lambda_{lm}) - \mathcal{W}_{lm}]}}. \quad (4.31)$$

A slightly different estimator is used in Ref. [66] where sampling is performed with respect to the state probability $p_f(\lambda, x)$ instead of $p_a(\lambda, x)$, in which the auxiliary potential $\alpha(\lambda)$ is replaced by a biasing potential whose form $f(\xi)$ is invariant under the transformation (4.30). The invariance stems from $\mathcal{B}^f(\xi^*) = \ln \sum_{\lambda \in \Lambda} \exp [f(\xi^*) - \|\lambda - \xi^*\|^2 + \varepsilon(\xi^*)] = f(\xi^*)$. This replacement yields the following variant pathwise condi-

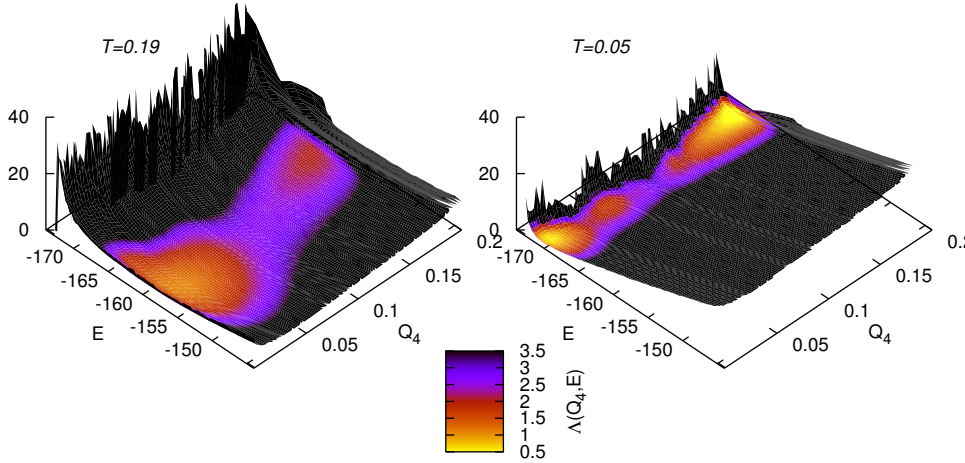


Figure 4.5: Free energy $F(Q_4, E)$ as a function of Q_4 and E . Left panel is the actual measurement at $T = 0.19$, while the right panel represents the free energy reconstruction for temperature $T = 0.05$ as obtained through Legendre transforms of the log-probabilities (or Laplace transforms of the probabilities).

tioning (VPC) estimator [66]

$$\Upsilon_{\text{VPC}}^{M,L}(\mathbf{1}_{Q_4,E}) = \frac{\frac{1}{M} \sum_{m=1}^M \frac{\sum_{l=0}^L \exp[-\mathcal{W}_{lm}] \mathbf{1}_{Q_4,E}(Q_{4lm}, E_{lm})}{\sum_{l=0}^L \exp[f_{lm} - \mathcal{W}_{lm}]}{\frac{1}{M} \sum_{m=1}^M \frac{\sum_{l=0}^L \exp[-\mathcal{W}_{lm}]}{\sum_{l=0}^L \exp[f_{lm} - \mathcal{W}_{lm}]}}. \quad (4.32)$$

A series of 5 path-sampling simulations of LJ_{38} have been carried out at the temperature $T = 0.19$, using the iterative ABP procedure introduced by Coluzza and Frenkel [71]: the free energy estimate $-\ln \hat{P}_{Q_4,E}$ obtained using estimator (4.32) are used as a next biasing potential. Path sampling simulations generate $M = 10^5$ trajectories of $L = 2.5 \cdot 10^5$ steps at each iteration. We refer the reader to Ref. [66] for details concerning other simulation parameters. The estimated histograms $\hat{P}_{Q_4,E}$ of the last iteration are displayed in Fig. 4.5.

The estimated free energies along Q_4 are reported in Fig. 4.6 for comparison with those obtained with other standard methods [63, 66]. We observe that the free energy profile Q_4 at the lowest temperature is lowest with PC except in the range $\in 0.03 - 0.05$ where the PR approach is better. The improved accuracy is attributed to the pathwise conditioning procedure. The loss of accuracy is attributed to the form of the biasing potential and to the different λ -scheduling that is less appropriate. Furthermore, adapting an auxiliary biasing force $a'(\lambda)$ directly based on the PC estimator (4.31) could prove to be more efficient. This new approach should be tested.

4.4.4 Free energy barrier for vacancy migration in α -Fe

When a one-dimensional free energy barrier between equi-probable structures needs to be calculated, the path sampling scheme can be simplified. In this situation, the auxiliary biasing potential can be removed and the scheduling of the external parameter can be determined in such a way to ensure transitions between the coexisting structures. This point is illustrated with simulations of the migration of a single vacancy on a lattice in α -Fe, a crystalline phase of iron with body-centered cubic (BCC) structure. The migration corresponds to the jump of an atom in the [111] direction into a nearest neighbor vacant site. The length of the jump is $a_0\sqrt{3}/2$, where a_0 is the edge of the BCC cube. The cell contains 1023 atoms. Atomic interactions of this atomic system are described by an embedded atom model potential [72]. We use harmonic coupling to the reaction coordinate that is the jumping atom coordinate along [111] direction. The velocity ϕ associated with the external forcing acting on ζ is small enough to ensure that the two equiprobable structures are sampled. We thus generated $M = 10^2$ paths of length $L = 10^5$ with $\lambda_0 = -a/10$ and $\lambda_L = 11a/10$ (where $a = 2.4728\text{\AA}$ is the nearest neighbour distance). With this parameter set, approximately 40% of indexing moves cross the free energy barrier. We calculated the histogram along ξ using the following simplified pathwise conditioned (SPC)

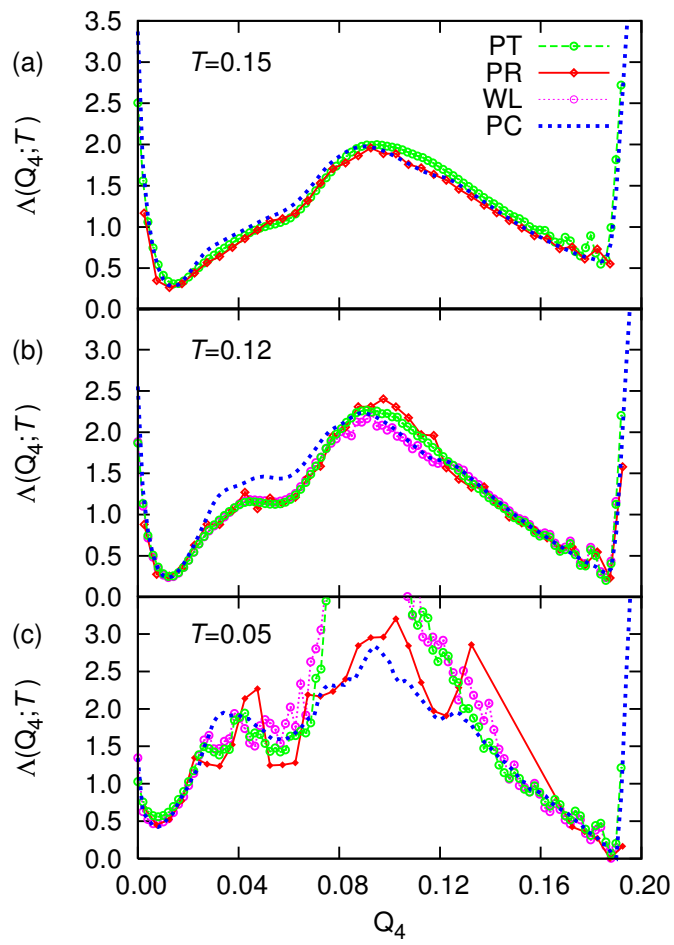


Figure 4.6: Free energy profiles of LJ_{38} as a function of Q_4 obtained with parallel tempering (PT), path reweighting (PR), Wang-Landau (WL), pathwise conditioning (PC). (a) $T = 0.15$; (b) $T = 0.12$; (c) $T = 0.05$.

Figure 4.7: Free energy $\Lambda(\xi; T)$ as a function of ξ and T .

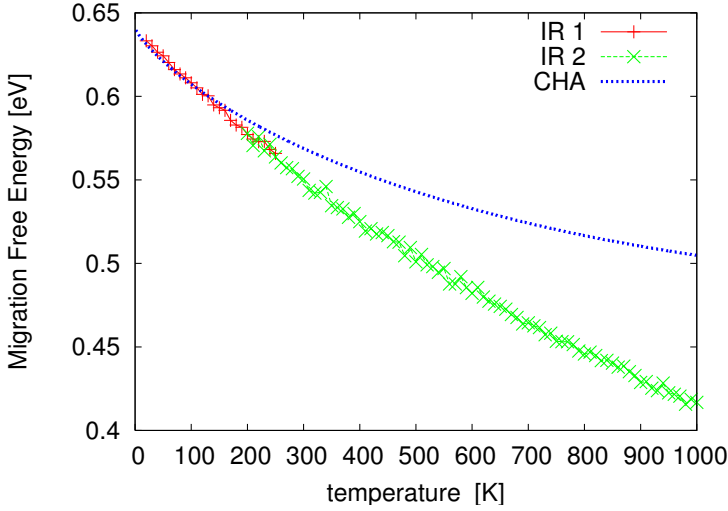
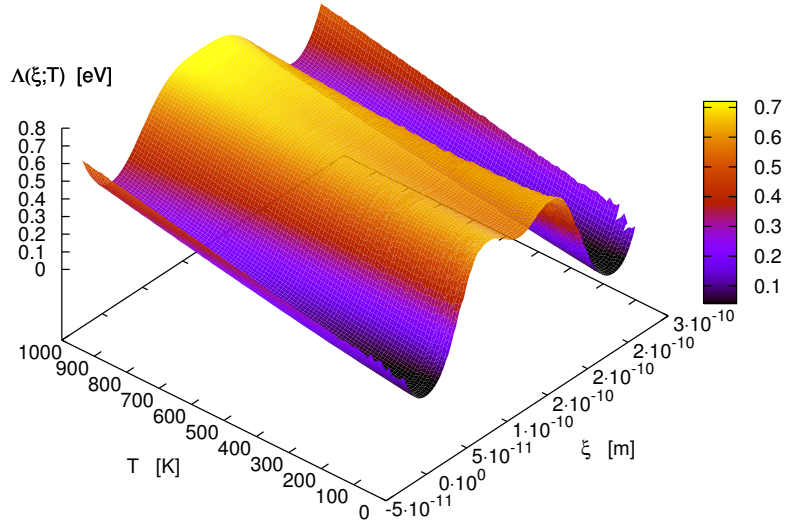


Figure 4.8: Migration free energy as a function of temperature. IR1 and IR2 refer to two values of κ (see text). The dotted line are the results of classical harmonic approximation.

estimator

$$\Upsilon_{\text{SPC}}^{M,L}(\mathbf{1}_{\xi^*}) = \frac{1}{M} \sum_{m=1}^M \frac{\sum_{l=0}^L \exp[-\mathcal{W}_{lm}] \mathbf{1}_{\xi^*}(\xi_{lm})}{\sum_{l=0}^L \exp[-\mathcal{W}_{lm}]}.$$

The SPC estimator is obtained from the PC estimator (4.31) by setting the biasing potential to 0. As a result, the denominator of (4.31) becomes equal to one. The method was found to yield reproducible estimates of the free energy $\Lambda(\xi; T) = -\ln \Upsilon_{\text{SPC}}^{M,L}(\mathbf{1}_{\xi^*})$ down to the temperature T of 20K. Two series of simulations were carried out. From 20K to 250K, we used $\kappa = 10^5 \text{J m}^{-2}$ (IR1) and from 200K to 1000K we used $\kappa = 0.5 \times 10^5 \text{J m}^{-2}$ (IR2). Results are represented by the free energy landscape of Fig. 4.7. We observe that the intermediate free-energy minimum is more pronounced at the lower temperatures and completely disappears at temperatures higher than 700K. The migration free energies are deduced from the relative barrier heights along ξ -axis of Fig. 4.7. They are plotted as a function of temperature in Fig. 4.8 together with the prediction of classical harmonic approximation (CHA) considering one of the two symmetric energy minima and saddle configurations. As expected, Monte Carlo simulations and CHA calculations agree at low temperatures ($T < 200\text{K}$) where anharmonic effects are negligible, confirming the exactness of our simulation method. At temperatures higher than 200K, we observe a substantial deviation between MC simulations and CHA, attesting to strong anharmonicity. Note that the extent of anharmonicity is in quantitative agreement with the one previously reported in the literature [73] for the vacancy migration free energy.

4.5 Calculating rates of thermally activated events

Transition state theory (TST) relates the free energy barrier $\Delta F^{A \rightarrow B}$ from basin A to basin B to the transitioning frequency or rate [74]:

$$k_{\text{TST}}^{A \rightarrow B} = \frac{N^c k_B T}{h} \exp\left(-\frac{\Delta F^{A \rightarrow B}}{k_B T}\right) \quad (4.33)$$

where h is Planck's constant and N^c , the coordination number of BCC structure, accounts for the 8 possible vacancy jumps. Even when the barrier is accurately calculated by Monte Carlo simulations, the transition rate given by TST and the reaction coordinate may significantly differ from the true transition rate that would be estimated from the number of transitions in very long MD simulations. The discrepancy essentially arises from the inability of the reaction coordinate to accurately capture the transition, in particular in the vicinity of the top of the free energy barrier. To explain more specifically, let ξ^\ddagger denote the value of the reaction coordinate at the top of the barrier. The surface $\Sigma^\ddagger = \{q : \xi(q) = \xi^\ddagger\}$ may not coincide with the isocommitor surface (the true dividing surface) and may for instance contain much more configurations from one basin of attraction than from the other. In this situation, the free energy at ξ^\ddagger is lower than the free energy of the isocommitor surface that contains configurations with higher energies in average. In practice, a transmission coefficient, first introduced by Eyring [74], should be included in (4.33). This coefficient yields the probability to ultimately reach basin B starting from ξ^* with momenta distributed from the Boltzmann-Maxwell distribution. It is estimated from the fraction of trajectories initiated from the top of the barrier and committing to basin B first [14, 41]. More advanced techniques for calculating the transmission coefficient have been proposed by Vanden-Eijnden and Tal [75] and Erp and Bolhuis [76].

Transition path sampling (TPS) is a more direct approach [6, 7] aiming at estimating the probability $\mathcal{C}(t)$ that a trajectory initiated in basin A at time 0 reaches basin B at time t . The method has been schematically described in Sec. 2.3. We recall that the probability to compute a state-to-state time correlation function is

$$\mathcal{C}(t) = \frac{\mathbb{E}^* [\chi_A(x_0) \chi_B(x_t)]}{\mathbb{E}^* [\chi_A(x_0)]} \quad (4.34)$$

where χ_A and χ_B denotes the characteristic functions of basins A and B, and symbol \mathbb{E}^* stands for time averaging over the appropriate dynamics. The asymptotic limit of the derivative of the correlation function yields the phenomenological rate constant

$$k^{A \rightarrow B} = \lim_{t \rightarrow \infty} \frac{d\mathcal{C}(t)}{dt}.$$

The difficulty with estimating state-to-state time correlation functions is that the involved transitions are rare. A biasing path functional is thus introduced so as to artificially enhance the occurrence of transitions by gradually confining or tilting the trajectory endpoints to the product state B [7, 47].

Estimating the state-to-state correlation functions in TPS method requires to extract the free energy difference associated with the transformation of a trajectory ensemble into a perturbed ensemble wherein the rare reactive trajectories have become frequent. This task is traditionally achieved using self-consistent estimators (MBAR or WHAM) using a series of independent Markov chains, in which the strength of the biasing path functional favoring the occurrence of reactive trajectories is gradually increased. TPS is therefore an ideal case study to apply the twofold conditioning approach for estimating observable expectations associated with rare events. This first requires to define the appropriate expanded transition path ensemble.

4.6 Expanded transition path ensemble

Following Ref. [8], we show how to construct an overlapping marginal distribution containing both reactive and typical paths and further derive an efficient estimator for the time-correlation function $\mathcal{C}(t)$ with conditioning both on the trial paths and the external parameter.

4.6.1 Path probability

The external parameter λ of the extended Hamiltonian is held at constant value λ_{ref} defining the temperature of the system. We define short and long paths and denote their respective path spaces by \mathcal{Y} and \mathcal{Z} . A path $y \in \mathcal{Y}$ consists of a sequence of $I + 1$ states $y = \{x_0, \dots, x_\ell, \dots, x_I\}$, while a path $z \in \mathcal{Z}$ consists of $L + 1$ states. The dynamical correlations will be measured based on samples of short paths that are extracted from the long paths. The external parameter is denoted by θ to avoid confusion with λ . Herein, θ acts on the entire path $y \in \mathcal{Y}$ via linear coupling to a path functional $\mathcal{L}(y)$. The set of external parameter values is denoted by Θ . The path probability in the expanded transition path ensemble is defined by

$$p_a(\theta, y) = \exp [\alpha(\theta) - \mathcal{S}(\theta, y) - \Psi_a^\Theta] \quad (4.35)$$

where Ψ_a^Θ is the normalizing constant and the path action, the analog of Hamiltonian for paths, is defined by

$$\mathcal{S}(\theta, y) = \mathcal{H}(\lambda_{\text{ref}}, x_0) - \ln [\chi_A(x_0) \mathbf{P}_{\text{gen}}^{0 \rightarrow L}(y)] + \theta \mathcal{L}(y).$$

By convention, the expanded path probability (4.35) is zero if either the characteristic function $\chi_A(x_0)$ or the path generating probability $\mathbf{P}_{\text{gen}}^{0 \rightarrow L}(\chi)$ is zero. In analogy with the marginal probability introduced in Chapters 2 and 3 for states or configurations, we define the marginal path probability as

$$p_a^\Theta(y) = \sum_{\theta \in \Theta} p_a(\theta, y). \quad (4.36)$$

The conditional probability given θ writes

$$\pi_a^\theta(y) = \frac{\exp [\alpha(\theta) - \theta \mathcal{L}(y)]}{\sum_{\vartheta \in \Theta} \exp [\alpha(\vartheta) - \vartheta \mathcal{L}(y)]} = \exp [\alpha(\theta) - \theta \mathcal{L}(\theta) - \mathcal{B}_a(\theta)]$$

where we have defined

$$\mathcal{B}_a(\theta) = \ln \sum_{\vartheta \in \Theta} \exp [\alpha(\vartheta) - \vartheta \mathcal{L}(\vartheta)].$$

From any long path $z = \{x_0, \dots, x_L\}$, $L - I$ sub-paths of length I (of duration τI) can be defined. We denote these sub-paths by $\tilde{z}_l = \{x_l, \dots, x_{l+I}\}$ with $l \in \llbracket 0, L - I \rrbracket$. We define the conditional probability of (z, ℓ) given $\ell \in \llbracket 0, L - I \rrbracket$ and $y = \tilde{z}_\ell$ by

$$\mathbf{P}(z, \ell | y) = \delta_y(\tilde{z}_\ell) \mathbf{P}_{\text{gen}}^{0 \leftarrow \ell}(z) \mathbf{P}_{\text{gen}}^{\ell+I \rightarrow L}(z)$$

and the long-path probability is given by the law of total probability

$$\mathbf{P}_a^\Theta(z, \ell) = \int_{\mathcal{Y}} \mathbf{P}(z, \ell | y) p_a^\Theta(y) \mathcal{D}y = \mathbf{P}(z, \ell | \tilde{z}_\ell) p_a^\Theta(\tilde{z}_\ell).$$

We denote the (total) expectation of path-observable $y \mapsto f(y)$ in the expanded transition path ensemble \mathcal{Y} with respect to marginal probability $p_a^\Theta(y)$ as

$$\mathbb{E}_a^{\mathcal{Y}}[f] = \int_{\mathcal{Y}} f(y) p_a^\Theta(y) \mathcal{D}y.$$

The same expectation can be expressed in the long-path ensemble as follows:

$$\mathbb{E}_a^{\mathcal{Z}}[f] = \sum_{l=0}^L \int_{\mathcal{Z}} f(\tilde{z}_l) \mathbf{P}_a^\Theta(z, l) \mathcal{D}z.$$

To show that these two path expectations coincide, we plug the law of total probability inside the path-integral above and simplify:

$$\mathbb{E}_a^{\mathcal{Z}}[f] = \sum_{l=0}^L \int_{\mathcal{Y}\mathcal{Z}} f(y) \mathbf{P}(z, \ell | y) p_a^\Theta(y) \mathcal{D}y \mathcal{D}z = \int_{\mathcal{Y}} f^\theta(y) p_a^\Theta(y) \mathcal{D}y = \mathbb{E}_a^{\mathcal{Y}}[f].$$

Setting $f(y)$ to $\pi_a^\theta(y)\mathcal{O}(\theta, y)$ and $\pi_a^\theta(y)$ enables one to cast the conditional expectation of $\mathcal{O}(\theta, y)$ given θ as the following expectation ratio

$$\mathbb{E}^{\mathcal{Y}}[\mathcal{O}|\theta] = \frac{\mathbb{E}_a^{\mathcal{Z}}[\pi_a^\theta(\cdot)\mathcal{O}(\theta, \cdot)]}{\mathbb{E}_a^{\mathcal{Z}}[\pi_a^\theta]} = \frac{\mathbb{E}_a^{\mathcal{Z}}[\mathbb{E}_a^{\mathcal{Z}}[\pi_a^\theta(\tilde{z}_l)\mathcal{O}(\theta, \tilde{z}_l)|z]]}{\mathbb{E}_a^{\mathcal{Z}}[\mathbb{E}_a^{\mathcal{Z}}[\pi_a^\theta(\tilde{z}_l)|z]]}.$$

In the rhs ratio, conditioning is performed on the index with respect to the path coordinates z . As done previously in Section 4.4, the conditioned expectation of the index determines the conditional probability of the index given path z :

$$P_a(\ell|z) = \mathbb{E}_a^{\mathcal{Z}}[\mathbf{1}_\ell|z] = \frac{P_a(z, \ell)}{\sum_{l=0}^{L-I} P_a(z, l)} = \frac{P_a^\Theta(\tilde{z}_\ell)}{\sum_{l=0}^{L-I} P_a^\Theta(\tilde{z}_l)}.$$

The r.h.s ratio simplifies because the dynamics is assumed to be exactly detailed balance. Plugging expression (4.36) for the marginal probabilities yields

$$P_a(\ell|z) = \frac{\chi_A(x_\ell) \exp[\mathcal{B}_a(\tilde{z}_\ell)]}{\sum_{l=0}^{L-I} \chi_A(x_l) \exp[\mathcal{B}_a(\tilde{z}_l)]}.$$

The conditional expectation given θ can therefore be cast in the conditioned form

$$\mathbb{E}^{\mathcal{Y}}[\mathcal{O}|\theta] = \frac{\mathbb{E}_a^{\mathcal{Z}}\left[\frac{\sum_{l=0}^{L-I} \exp[\mathbf{a}(\theta) - \theta\mathcal{L}(\tilde{z}_l)] \chi_A(x_l) \mathcal{O}(\theta, \tilde{z}_l)}{\sum_{l=0}^{L-I} \exp[\mathcal{B}_a(\tilde{z}_l)] \chi_A(x_l)}\right]}{\mathbb{E}_a^{\mathcal{Z}}\left[\frac{\sum_{l=0}^{L-I} \exp[\mathbf{a}(\theta) - \theta\mathcal{L}(\tilde{z}_l)] \chi_A(x_l)}{\sum_{l=0}^{L-I} \exp[\mathcal{B}_a(\tilde{z}_l)] \chi_A(x_l)}\right]} \quad (4.37)$$

As an example of application, let us estimate the state-to-state correlation function $\mathcal{C}(\ell\tau)$ defined in (4.34). We define the path observable as $\mathcal{O}(0, y) = \chi_B(x_\ell)$ with $\ell \in \llbracket 0, I \rrbracket$ and plug it into (4.37) with $\theta = 0$ to obtain

$$\mathcal{C}(\ell\tau) = \mathbb{E}^{\mathcal{Y}}[\mathbf{1}_B(x_\ell)] = \frac{\mathbb{E}_a^{\mathcal{Z}}\left[\frac{\sum_{l=0}^{L-I} \chi_A(x_l) \chi_B(x_{l+\ell})}{\sum_{l=0}^{L-I} \exp[\mathcal{B}_a(\tilde{z}_l)] \chi_A(x_l)}\right]}{\mathbb{E}_a^{\mathcal{Z}}\left[\frac{\sum_{l=0}^{L-I} \chi_A(x_l)}{\sum_{l=0}^{L-I} \exp[\mathcal{B}_a(\tilde{z}_l)] \chi_A(x_l)}\right]}.$$

The estimator is therefore

$$\Upsilon_{\text{TPC}}^{M,L}(\chi_B(x_\ell)) = \frac{\frac{1}{M} \sum_{m=1}^M \frac{\sum_{l=0}^{L-I} \chi_A(x_{lm}) \chi_B(x_{(l+\ell)m})}{\sum_{l=0}^{L-I} \exp[\mathcal{B}_a(\tilde{z}_l)] \chi_A(x_l)}}{\frac{1}{M} \sum_{m=1}^M \frac{\sum_{l=0}^{L-I} \chi_A(x_{lm})}{\sum_{l=0}^{L-I} \exp[\mathcal{B}_a(\tilde{z}_{lm})] \chi_A(x_{lm})}}. \quad (4.38)$$

4.6.2 Biasing path functional

Motivated by the ability of eigenvalue-following [77, 78, 79, 80, 81] and Lyapunov-weighting [82, 83, 84, 85, 86, 87, 88, 89] methods to locate saddle points in complex systems based on the topology of their energy surfaces, it was proposed [47] to perform TPS simulations using the lowest eigenvalues of the Jacobian along the trajectory as a biasing functional. We show next that this way of proceeding does not confine the trajectory endpoints to a reactive state, unlike original TPS.

4.6.3 Case study: vacancy migration in α -Fe

We now demonstrate the efficiency of the approach in simulations of the migration of a single vacancy on a lattice in α -Fe at the temperature of 500 K. At this temperature, the number of hopping events during a typical simulation is small. Reference values for the free energy barrier associated with the vacancy migration has been calculated [66] and are reported in Section 4.4.4 where this testbed model is described. Reference values for

migration rates are available as well and are given in Ref. [47]. They were obtained using a combination of transition path sampling and the multistate Bennett acceptance ratio method for postprocessing.

Computational set-up Basin A and B are defined with respect to the underlying perfect lattice whose sites are the atomic positions of the structure at 0 K without the vacancy. The lattice parameter is $a_0 = 2.8553\text{\AA}$. The indicator function χ_A is equal to 1 if all atoms are located within a distance of 0.45\AA from their lattice site, and to 0 otherwise. The indicator function χ_B is 1 if one atom is located beyond a distance of $a_0\sqrt{3}/4$ from its lattice site, otherwise it is 0. Path sampling consists of shooting and indexing moves as detailed in the Sections 4.4 and 4.6. Trajectories contain $L = 150$ steps with time-step $\tau = 2fs$. A position-Verlet scheme [47] is used to construct $x_{\ell+1}$ from x_ℓ , meaning that the gradient of the potential energy is evaluated at $q_{\ell+1/2} = q_\ell + p_\ell\tau/2$. The Jacobian matrix associated with the MD transformation exhibits eigenvalues that are either complex numbers located on the unit circle or real positive numbers. Let us denote by $\mu_{\ell+1/2}$ the logarithm of the smallest eigenvalue modulus. Its value is characterized by the eigenvalue spectrum of the Hessian matrix associated with the potential energy at $q_{\ell+1/2}$. Details on the connection between the Hessian and Jacobian matrices are given in Ref. [47]. The value of $\mu_{\ell+1/2}$ is strictly negative when the lowest eigenvalue of the Hessian matrix is strictly negative, in which case the energy surface is negatively curved along the direction generated by the corresponding eigenvector. The biasing path functional is set to

$$\mathcal{L}(z) = \max \left[\mathcal{L}_{\min}, \sum_{\ell=0}^{L-1} \mu_{\ell+1/2} \right] \leq 0$$

The cut-off parameter \mathcal{L}_{\min} is set to the value -9 . It is used to prevent from exploring regions containing second order saddles and thus to save computational time, trajectories leading to such regions corresponding to non-reactive rare events. The lowest eigenvalues of the Hessian is computed using the Lanczos algorithm [90], as in the activation-relaxation technique [77, 78]. Details about the numerical implementation are given in Ref. [81, 91].

Construction of the auxiliary potential Simulations are performed on a parallel computer architecture where many replicas of the system can be propagated simultaneously and independently while periodically adapting the common biasing force, as was done in ABF simulations of Sec. 3.4. We set $\theta_{\min} = 0$ and $\theta_{\max} = 2.1$. In the following, a simulation run utilizes $K = 480$ replicas and consists of $M = 10^4$ Monte Carlo cycles. Each replica is allocated to a distinct processor. A cycle consists of performing a shooting move followed by an indexing move for each replica. The two procedures are detailed in Section 4.4.

Two consecutive series of 5 independent simulation runs are performed. The first five runs aim at constructing the auxiliary biasing potential using an ABF scheme (see Eq. 18 of Ref. [8] and refer to Chapter 3 for a general exposition of ABF method). Then, freezing the previously obtained biasing potentials, 5 subsequent (production) runs are performed to estimate the expectations associated with the time-correlation function using the estimator (4.38). Figure 4.9 displays the estimates of $P_{\mathcal{A}}(\theta)$, $\mathcal{A}(\theta)$ and $\mathbb{E}(\mathcal{L}|\theta)$ as a function of θ and averaged over the 5 runs. The standard errors are evaluated from the 5 estimates and are indicated by error bars for the three quantities in Fig. 4.9. We observe that a flat histogram is obtained for the marginal probability of θ . Reproducible data are obtained for the mean force and its potential. Furthermore, the difference between the adaptive and production runs is insignificant, final averages could have been taken after the adaptation run.

The standard errors are small and not clearly visible on the graphs in Fig. 4.9, except on the curve displaying the marginal probability of θ . We observe that the standard errors associated with $P_{\mathcal{A}}(\theta)$ increase with θ and become substantial at large θ values. To explain this trend, let us examine $\bar{\rho}(\mathcal{L})$, the probability distributions of the sampled \mathcal{L} values. We observe in Fig. 4.10 that this distribution is bimodal. The large peak at 0 corresponds to typical trajectories that are non reactive. The smaller peak in the range from -7 to -4 contains both reactive trajectories and active trajectories returning to a . The presence of two peaks means that metastability is not completely suppressed through path-sampling, even though the fraction of reactive trajectories is enhanced by several orders of magnitude compared with the one associated with the unbiased distribution $\rho(\mathcal{L}|0)$. Concerning the biased distribution $\rho(\mathcal{L}|\theta_{\max})$, the peak containing the reactive trajectories is higher and more pronounced than that of the sampled distribution. This feature explaining the substantial statistical fluctuations observed in the measurement of $P_{\mathcal{A}}^{\ominus}(\theta)$ when θ is large. Note that the θ_c value for which the two peaks of the bimodal distribution $\rho(\mathcal{L}|\theta_c)$ have equal weights occurs in the range $2.2 - 2.4$ and decreases with the path length [47]. Here, θ_c would correspond to the inflexion of the $\mathbb{E}(\mathcal{L}|\theta)$ curve, outside the plot in Fig. 4.9.c. As reported in

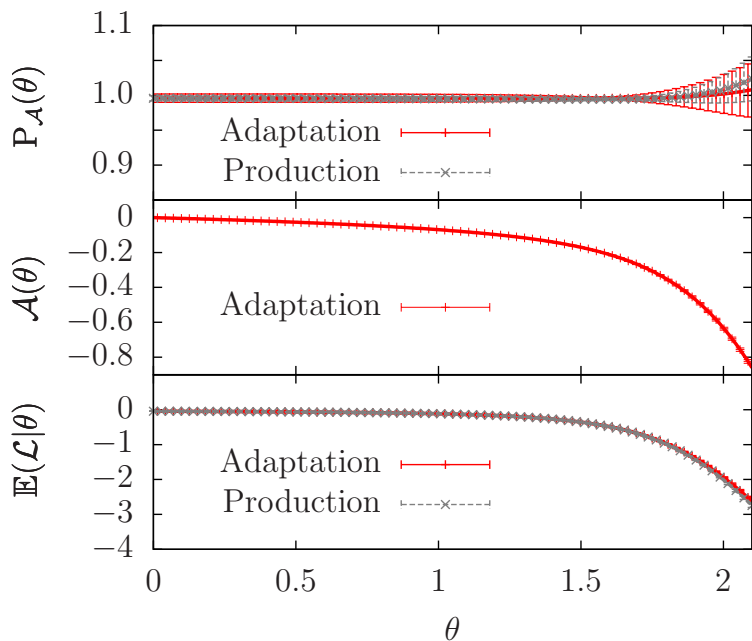


Figure 4.9: Marginal probability of θ ($P_A^\ominus(\theta)$ scaled by $\|\Theta\|$), potential of mean force and mean force as a function of θ .

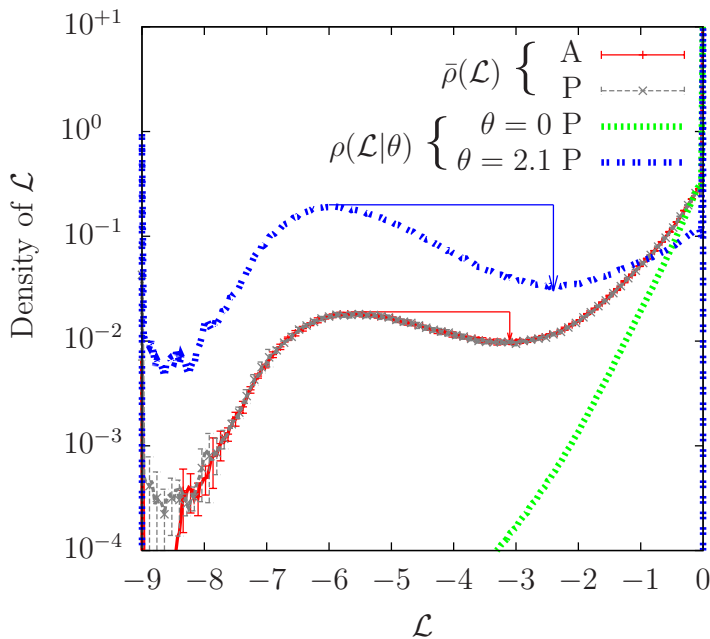


Figure 4.10: Distributions of \mathcal{L} : $\bar{\rho}(\mathcal{L})$ and $\rho(\mathcal{L}|\theta)$ denote the probabilities that $\mathcal{L}(z)$ takes value \mathcal{L} with respect to path distributions $\bar{P}_A(z)$ and $\pi(z|\theta)$, respectively.

Ref. [47], the restricted sampling of the conditional distribution $\pi(z|\theta)$ becomes very difficult when $\theta > \theta_c$, the measured autocorrelation function of \mathcal{L} increases drastically. Important autocorrelations are also observed in the sampling of $\bar{P}_A(z)$ distribution when θ_{\max} is set to a value larger than θ_c . However, the extent of metastability is smaller with a scheme sampling the marginal probability rather than the conditional probabilities. We speculate that this trend results from the smaller barrier height for trajectory deactivation for $\bar{\rho}(\mathcal{L})$ distribution than for $\rho(\mathcal{L}|\theta)$ distribution, as indicated in Fig. 4.10 by the red and blue downward arrows, respectively.

The sampled path distributions with $\theta_{\max} < \theta_c$ contain high enough a fraction of reactive trajectories so as to accurately estimate the A-to-B correlation function. Figure 4.11 represents the time correlation function and its time derivative as obtained after the 5 adaptation runs and the 5 production runs. The phenomenological transition rate corresponds to the plateau value, which is in perfect agreement with the value calculated in Ref. [47] using the self-consistent reweighting estimator MBAR and a set of 40 independent simulations with increasing θ -values. Note that a significant smoothing effect of conditioning on the shifted trial paths is reported in this study for the evaluation of the derivative of the time-correlation function $\mathcal{C}(t)$.

Besides, the proposed biasing path functional based on the curvature of the potential energy surface makes

it possible to explore the multiple reaction channels corresponding to the 8 possible atomic jumps into the vacancy. This is a clear advantage compared with other rare event approaches such as transition interface sampling [76], and forward flux sampling [92] that may confine trajectories into separate transition channels in some circumstances. However, the twofold conditioning approach can be used in combination with path functional that confines trajectories interfaces and may prove useful in studying dislocation motion in crystals.

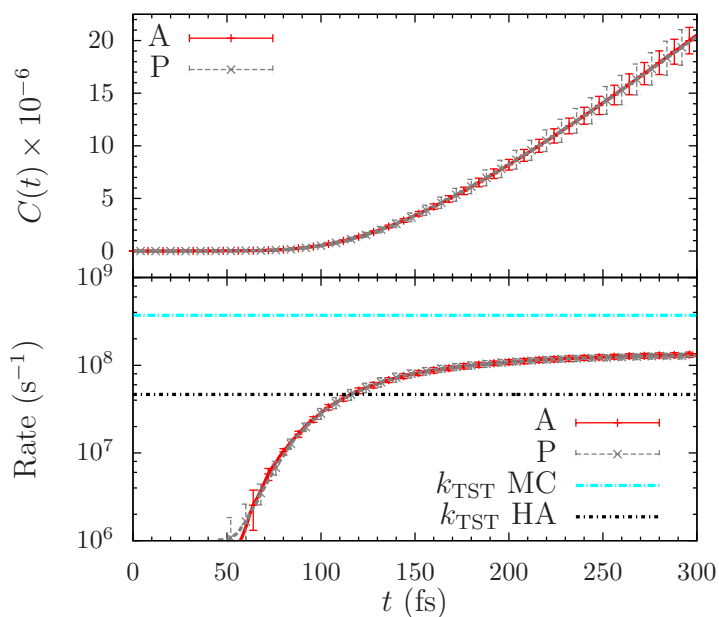


Figure 4.11: Time correlation function and its derivative as a function of the time $t = \ell\tau$, where ℓ is the index of the trajectory states. The horizontal lines corresponds to the values [47] obtained using transition state theory [74] in which the free energy barrier is evaluated using either Monte Carlo simulations (MC) or the classical harmonic approximation (HA).

4.7 Summary

In this Chapter, we presented path sampling schemes to achieve improved accuracy in difficult free-energy and rare-event problems. In the path ensemble framework, conditioning is performed both on the trial paths and on the external parameters for estimating expectations associated with rare-event probabilities and multi-dimensional free energy surfaces. The twofold conditioning approach can straightforwardly be implemented in combination with an auxiliary biasing potential on the external parameters and with biasing path functionals. For the latter case in particular, it makes it possible to estimate the state-to-state time correlation function from a single transition path sampling simulation.

Concerning the calculation of free energy surfaces, the difficulty involves the presence of residual metastability or hidden barriers along the order-parameter coordinates which are often unable to capture the transition state unlike (good) reaction coordinates. The crossing of these hidden barriers is facilitated by the steering schedules on the extended Hamiltonian. As a result, better sampling ergodicity is achieved. Furthermore, pathwise conditioning offers a unifying framework for performing expanded ensemble simulations while taking advantage of the nonequilibrium work identity. In this context, additional studies should investigate to which extent pathwise conditioning accelerate the convergence of the adaptive biasing forces. However, the overall simplicity and flexibility of the twofold conditioning approach place it in good position to further extend the range of applicability of both transition path sampling and expanded ensemble simulations.

In next Chapter, we consider the estimation of free energy differences based on path reweighting in a work-biased path ensemble. Simulations in this ensemble can be performed without the help of any auxiliary biasing forces or potentials, which avoids the task of adapting them. We show how conditioning on the trial paths can be further exploited to improve the estimator by optimally including information relative to the rejected proposals.

5 | Waste recycling and conditioning

In this Chapter, we discuss in greater details the waste-recycling Monte Carlo (WRMC) method introduced by Frenkel [2, 38] and further developed by Delmas and Jourdain [9]. We illustrate the method on calculations of Chromium solubility limits in α -iron.

5.1 Conditioning on Monte Carlo proposals

The WRMC method is a Markov chain Monte Carlo technique that (i) implements a Metropolis-type procedure to accept or reject trial configurations, the proposals, and (ii) performs a conditioning on the outcome of the acceptance/rejection procedure within the estimator. The goal is to reduce the estimator variance by including information about the proposals. The weight of any proposal is equal to its acceptance probability and the weight of the old configuration is the probability to reject the proposal, or all the proposals when multiple proposals are generated in the Monte Carlo trial. The two types of conditioning encountered so far are related to WRMC method. Conditioning on the external parameter λ coincides with waste-recycling when the conditional probabilities involved in the conditioning procedure are also used in the sampling scheme. This is the case when a Gibbs sampling scheme [37] is used in an expanded ensemble to sample λ and perform a conditioning on λ at the same time, as discussed in Section 1.11 of Chapter 1. The path sampling scheme involving indexing moves and pathwise conditioning, which has been discussed in Subsection 4.4.3 of Chapter 4, can also be formulated as an instance of WRMC algorithm. In both cases, multiple proposals are generated and only one is selected using Barker or Boltzmann acceptance rule.

Trial states in multi-proposal schemes are not necessarily generated along a path initiated from the current configuration. In its most general formulation, a WRMC algorithm possibly generates the multiple proposals independently from each others, as done in Ref. [93, 2, 94, 48, 95]. The set of proposals form ramified structures called Markov webs [94]. The important prescription is that the next state of the Markov chain of configurations is selected with a probability that obeys detailed balance. Such multi-proposal Monte Carlo algorithms will not be discussed here and we refer the reader to the cited references.

In the WRMC set-up, the statistical variance of the plain waste-recycling estimator reduction can be further reduced [9]. To achieve this additional variance reduction, Delmas and Jourdain [9] first introduce a family of estimators that are a linear combination of the plain WRMC and MC estimators and then showed how to practically determine the optimal combination in term of variance reduction. This way of proceeding amounts to formulating and solving a control variate problem.

Outline of the Chapter In Sec. 5.2, we give a heuristic derivation of the Delmas-Jourdain optimal waste-recycling estimator. A rigorous justification based on a martingale approach can be found in Ref. [9]. For the ease of exposition, we formulate the problem in the single-proposal framework and keep the notations of previous Chapter. In Sec. 5.3, we describe the transmutation ensemble in which the estimator will be tested in combination with work-biased particle transmutations. We then apply the approach to the calculation of solubility limits in iron alloys in Sec. 5.4.

5.2 Control variate approach to waste-recycling Monte Carlo

The WRMC approach will be applied to free-energy calculations based on the fluctuation theorem, i.e. to free energy perturbation in path space. We thus consider a path ensemble of space \mathcal{Z} in which the expectation of

observable $f(z)$ is

$$\mathbb{E}_\theta [f] = \int_{\mathcal{Z}} \mathbb{P}_\theta(z) f(z) \mathcal{D}z$$

where θ is an external parameter controlling the path probability $\mathbb{P}_\theta(z)$.

5.2.1 Barker selection rule

We consider herein that the sampling scheme is based on Barker selection rule. The probability to accept the proposal \tilde{z} from z is

$$\mathbb{P}(1|z, \tilde{z}) = \frac{\mathbb{P}(z, \tilde{z}|1) \mathbb{P}_\theta(\tilde{z})}{\mathbb{P}(z, \tilde{z}|0) \mathbb{P}_\theta(z) + \mathbb{P}(z, \tilde{z}|1) \mathbb{P}_\theta(\tilde{z})}$$

where $\mathbb{P}(z, \tilde{z}|0)$ is the probability to generate the proposal \tilde{z} from z and, similarly, $\mathbb{P}(z, \tilde{z}|1)$ is the probability to generate proposal z from \tilde{z} in the reverse Monte Carlo move. The proposal probabilities are described in Section 5.4. The probability to reject the proposal is equal to the probability to select the old configuration z

$$\mathbb{P}(0|z, \tilde{z}) = 1 - \mathbb{P}(1|z, \tilde{z}) = \frac{\mathbb{P}(z, \tilde{z}|0) \mathbb{P}_\theta(z)}{\mathbb{P}(z, \tilde{z}|0) \mathbb{P}_\theta(z) + \mathbb{P}(z, \tilde{z}|1) \mathbb{P}_\theta(\tilde{z})}$$

It can easily be verified that any algorithm based on Barker generates a Markov chain $\{z_0, z_1, \dots, z_m\}$ that is ergodic with respect to the probability $\mathbb{P}_\theta(z)$. We denote by $\mathbb{E}[f(z_1)|z_0, \tilde{z}_0]$ the conditional expectation of $f(z_1)$ where z_1 is generated by the sampling process given current path z_0 and trial path \tilde{z}_0 . We have $\mathbb{E}[f(z_1)] = \mathbb{E}_\theta[f]$. With Barker selection rule, we have

$$\mathbb{E}[f(z_1)|z_0, \tilde{z}_0] = f(z_0) \mathbb{P}(0|z_0, \tilde{z}_0) + f(\tilde{z}_0) \mathbb{P}(1|z_0, \tilde{z}_0).$$

5.2.2 A family of estimator

Let g denote the following function taking input values in \mathcal{Z}^3

$$g(z, \tilde{z}, z_s) = f(z) \mathbb{P}(0|z, \tilde{z}) + f(\tilde{z}) \mathbb{P}(1|z, \tilde{z}) - f(z_s).$$

Since the function is based on Barker selection probabilities, we have for any successive points z_m and z_{m+1} in the Markov chain

$$g(z_m, \tilde{z}_m, z_{m+1}) = \mathbb{E}[f(z_{m+1})|z_m, \tilde{z}_m] - f(z_{m+1}),$$

where \tilde{z}_m is the proposal from z_m . The conditional expectation of $g(z_0, \tilde{z}_0, z_1)$ given (z_0, \tilde{z}_0) is obviously zero:

$$\mathbb{E}[g(z_m, \tilde{z}_m, z_{m+1})|z_m, \tilde{z}_m] = 0. \tag{5.1}$$

However, the total expectation of g is always zero:

$$\mathbb{E}[g(z_m, \tilde{z}_m, z_{m+1})] = \mathbb{E}[\mathbb{E}[f(z_{m+1})|z_m, \tilde{z}_m] - \mathbb{E}[f(z_{m+1})]] = 0.$$

Hence, a family of valid and unbiased estimators of $\mathbb{E}_\theta[f]$ is given by

$$\mathbb{I}^M(f + bg) = \frac{1}{M} \sum_{m=0}^{M-1} f(z_{m+1}) + bg(z_m, \tilde{z}_m, z_{m+1}) \triangleq \mathbb{J}_b^M(f), \tag{5.2}$$

where $b \in \mathbb{R}$. At first sight, the parameterized estimator seems useless as it yields estimates of f that contains additional errors. The idea is to tune the value of the control variate b so as to improve the accuracy in the estimation of f by taking advantage of the measurable correlations between f and g . The sign of the correlations will determine the sign of the optimal control variate b_* . If f and g are uncorrelated, we don't expect any possible variance reduction and thus b_* should be equal to 0. These qualitative statements are justified more formally in next Subsection below. In the WRMC context, the correlation between f and g arises from the statistical covariance of the generated sample of f values, as shown by Delmas and Jourdain [9].

$$\mathbf{I}^M(g) = \frac{1}{M} \sum_{m=0}^{M-1} \mathbb{E}[f|z_m, \tilde{z}_m] - f(z_{m+1})$$

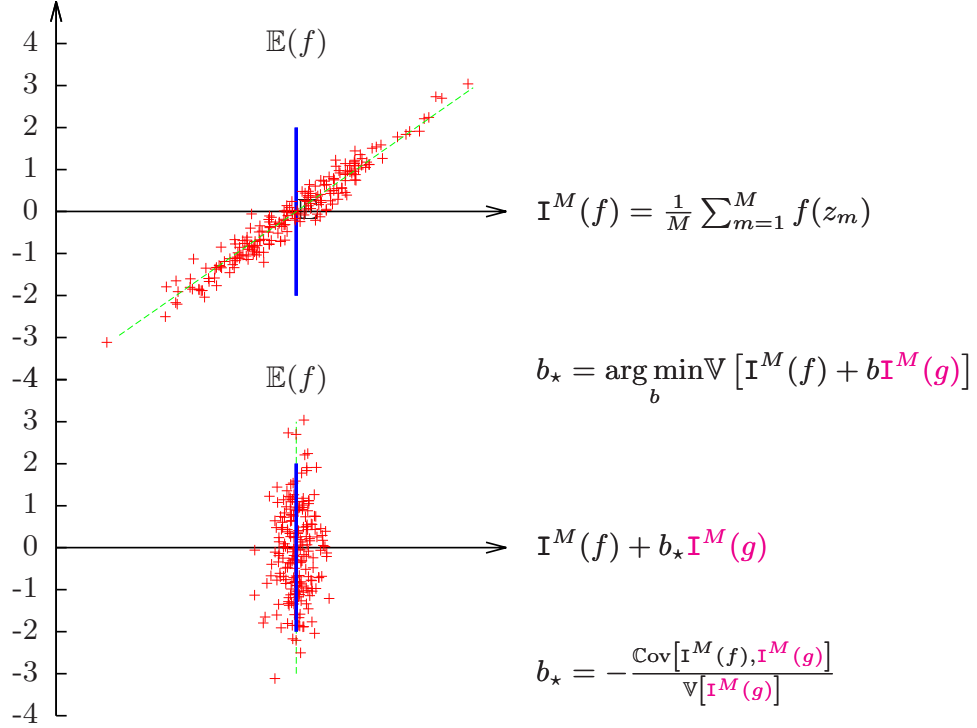


Figure 5.1: The two clouds of + symbols represent two samples of estimate pairs $\{\mathbf{I}^M(f), \mathbf{I}^M(g)\}$ and $\{\mathbf{I}^M(f + b_*g), \mathbf{I}^M(g)\}$. The optimal control variate may be deduced directly from the variance and covariance properties of a large sample of $\mathbf{I}^M(f)$ and $\mathbf{I}^M(g)$ estimates.

5.2.3 Control variate problem

The asymptotic variance of estimator $\mathbf{I}^M(f + bg)$ and the asymptotic covariance of estimators $\mathbf{I}^M(f)$ and $\mathbf{I}^M(g)$ are denoted by $\sigma^2(f + bg)$ and $\kappa(f, g)$, respectively. The value b_* of b minimizing the asymptotic variance $\sigma^2(f + bg)$ is given by

$$b_* = -\frac{\kappa(f, g)}{\sigma^2(g)} \quad (5.3)$$

where $\sigma^2(g)$ denotes the asymptotic variance of g . The optimal value b_* corresponds to the minimum of the following quadratic function

$$\sigma^2(f + bg) = \sigma^2(f) + 2b\kappa(f, g) + b^2\sigma^2(g),$$

a relation obtained by exploiting the scalar product properties of the covariance and the definition of the variance: $\sigma^2(f + bg) = \kappa(f + bg, f + bg)$ and $\sigma^2(g) = \kappa(g, g)$. The improved estimation through the use of a control variate is illustrated in figure 5.1. Besides, the asymptotic variance of the optimal estimator can be expressed as a function of the asymptotic correlation function $\rho(f, g) = \kappa(f, g) / [\sigma(f)\sigma(g)]$:

$$\sigma^2(f + b_*g) = \sigma^2(f) [1 - \rho^2(f, g)].$$

We next cast the two involved covariances into computationally tractable forms and show that the optimal control variate can be accurately estimated in the course of a single simulation. Let h denote a generic function taking values in \mathcal{Z}^3 and define $\mathbf{I}^M(h) = \frac{1}{M} \sum_{m=0}^{M-1} h(z_m, \tilde{z}_m, z_{m+1})$. The function h will later be set to g or

simply f . The asymptotic covariance of $\mathbf{I}^M(h)$ and $\mathbf{I}^M(g)$ is defined by

$$\begin{aligned}
\kappa(h, g) &= \lim_{M \rightarrow +\infty} \frac{1}{M} \sum_{n=0}^{M-1} \sum_{m=0}^{M-1} \text{Cov} [h(z_n, \tilde{z}_n, z_{n+1}), g(z_m, \tilde{z}_m, z_{m+1})] \\
&= \sum_{m=-\infty}^{\infty} \mathbb{E} [h(z_0, \tilde{z}_0, z_1) g(z_m, \tilde{z}_m, z_{m+1})] \\
&= \sum_{m=-\infty}^0 \mathbb{E} [h(z_0, \tilde{z}_0, z_1) g(z_m, \tilde{z}_m, z_{m+1})] + \sum_{m=1}^{\infty} \mathbb{E} [h(z_0, \tilde{z}_0, z_1) \mathbb{E} [g(z_m, \tilde{z}_m, z_{m+1}) | z_m, \tilde{z}_m]] \\
&= \sum_{m=-\infty}^{-1} \mathbb{E} [h(z_0, \tilde{z}_0, z_1) g(z_m, \tilde{z}_m, z_{m+1})] + \mathbb{E} [h(z_0, \tilde{z}_0, z_1) g(z_0, \tilde{z}_0, z_1)]
\end{aligned}$$

where the summation from $m = 1$ to ∞ cancels owing to relation (5.1). To simplify the remaining sum over the negative values of m , let consider that the Markov process is generated backward and let modify the labels of the Markov chain accordingly. We substitute \tilde{z}_{m+1}^\dagger for \tilde{z}_m or z_m depending on whether the proposal is accepted or rejected, in which cases z_{m+1} is equal to \tilde{z}_m or z_m , respectively. The point \tilde{z}_{m+1}^\dagger is precisely the proposal for the reverse sampling scheme. Noticing that $g(z_m, \tilde{z}_m, z_{m+1})$ is equal to $f(z_m) - f(z_{m+1}) + g(z_{m+1}, \tilde{z}_{m+1}^\dagger, z_m)$, the asymptotic covariance therefore simplifies to

$$\begin{aligned}
\kappa(h, g) &= \sum_{m=-\infty}^{-1} \mathbb{E} \left[h(z_0, \tilde{z}_0, z_1) \left\{ f(z_m) - f(z_{m+1}) + g(z_{m+1}, \tilde{z}_{m+1}^\dagger, z_m) \right\} \right] + \mathbb{E} [h(z_0, \tilde{z}_0, z_1) g(z_0, \tilde{z}_0, z_1)] \\
&= \mathbb{E} [h(z_0, \tilde{z}_0, z_1) \{ \mathbb{E}_\theta(f) - f(z_0) \}] + \sum_{m=-\infty}^{-1} \mathbb{E} \left[\mathbb{E} \left[h(z_0, \tilde{z}_0, z_1) g(z_{m+1}, \tilde{z}_{m+1}^\dagger, z_m) | z_{m+1}, \tilde{z}_{m+1}^\dagger \right] \right] \\
&\quad + \mathbb{E} [h(z_0, \tilde{z}_0, z_1) g(z_0, \tilde{z}_0, z_1)]. \tag{5.4}
\end{aligned}$$

where we simplified the telescopic series involving the difference $f(z_m) - f(z_{m+1})$ in the last term. The expectation $\mathbb{E}_\theta[f]$ arises from the fact that z_M and z_0 become independently distributed in the limit $M \rightarrow -\infty$ and thus $\mathbb{E}[f(z_M)] \rightarrow \mathbb{E}_\theta[f]$. Besides, the conditional expectation of $g(z_{m+1}, \tilde{z}_{m+1}^\dagger, z_m)$ given $(z_{m+1}, \tilde{z}_{m+1}^\dagger)$ cancels because the sampling algorithm is reversible (i.e. obeys detailed balance). This entails the equality

$$\mathbb{E} \left[h(z_0, \tilde{z}_0, z_1) g(z_{m+1}, \tilde{z}_{m+1}^\dagger, z_m) | z_{m+1}, \tilde{z}_{m+1}^\dagger \right] = 0, \tag{5.5}$$

for $m \leq -1$. As a result, equality (5.5) leads to the overall cancellation of the series involving these expectations in (5.4). The covariance therefore writes

$$\kappa(h, g) = \mathbb{E} [h(z_0, \tilde{z}_0, z_1) \{ \mathbb{E}_\theta(f) - f(z_0) + g(z_0, \tilde{z}_0, z_1) \}].$$

The interested reader is referred to the study of Delmas and Jourdain [9] for a rigorous mathematical analysis of WRMC based on martingale theory and filtration. The present derivation aims at facilitating an intuitive understanding of the origin for the remarkably simple form of the optimal control variate. We next exhibit this remarkable form. Setting $h(z_0, \tilde{z}_0, z_1)$ to $f(z_0)$ yields

$$\kappa(f, g) = \mathbb{E} [f(z_0) (\mathbb{E}_\theta(f) - f(z_0) + g(z_0, \tilde{z}_0, z_1))] = \mathbb{E} [f(z_0) \{ \mathbb{E}_\theta[f] - f(z_0) \}] = -\mathbb{V}_\theta(f). \tag{5.6}$$

Setting $h(z_0, \tilde{z}_0, z_1)$ to $g(z_0, \tilde{z}_0, z_1)$ yields

$$\kappa(g, g) = \mathbb{E} [g(z_0, \tilde{z}_0, z_1)^2],$$

where we noticed that

$$\mathbb{E} [g(z_0, \tilde{z}_0, z_1) (\mathbb{E}_\theta[f] - f(z_0))] = \mathbb{E} [\mathbb{E} [g(z_0, \tilde{z}_0, z_1) | z_0, \tilde{z}_0] (\mathbb{E}_\theta[f] - f(z_0))] = 0,$$

wherein plugging the law of total expectation with respect to (z_0, \tilde{z}_0) and resorting to equality (5.1) leads to

the overall cancellation.

5.2.4 Various equivalent expressions of the optimal control variate

We next derive in parallel several pairs of expressions for the asymptotic variance of g which are instructive from the point of view of conditioning:

$$\kappa(g, g) = \begin{cases} \mathbb{E} \left[\left(f(z_1) - \mathbb{E} [f(z_1) | z_0, \tilde{z}_0] \right)^2 \right], \\ \mathbb{E} \left[\left(f(z_1) - \mathbb{E} [f(z_0) | z_1, \tilde{z}_1^\dagger] \right)^2 \right], \end{cases}$$

where in the second case above, we resorted to the symmetry of Barker rule and to the Markov process reversibility. Rearranging both cases considered above leads to

$$\kappa(g, g) = \begin{cases} \mathbb{E} \left[\mathbb{E} \left[\left(f(z_1) - f(z_0) - \mathbb{E} [f(z_1) - f(z_0) | z_0, \tilde{z}_0] \right)^2 | z_0, \tilde{z}_0 \right] \right], \\ \mathbb{E} \left[\mathbb{E} [f(z_1) - f(z_0) | z_0, \tilde{z}_0]^2 \right], \end{cases} \quad (5.7)$$

where we reversed back the Markov process in the second case. Subtracting the two null terms

$$0 = \begin{cases} \mathbb{E} \left[\mathbb{E} [f(z_1) - f(z_0) - \mathbb{E} [f(z_1) - f(z_0) | z_0, \tilde{z}_0] | z_0, \tilde{z}_0]^2 \right], \\ \mathbb{E} \left[\mathbb{E} [f(z_1) - f(z_0) | z_0, \tilde{z}_0]^2 \right], \end{cases}$$

to the two cases of Eq. (5.7) helps identifying the conditional variance of $f(z_1) - f(z_0)$ given (z_0, \tilde{z}_0) and the total variance of the conditional expectation of $f(z_1) - f(z_0)$ given (z_0, \tilde{z}_0) :

$$\kappa(g, g) = \begin{cases} \mathbb{E} [\mathbb{V} [f(z_1) - f(z_0) | z_0, \tilde{z}_0]], \\ \mathbb{V} [\mathbb{E} [f(z_1) - f(z_0) | z_0, \tilde{z}_0]]. \end{cases} \quad (5.8)$$

The expressions above will enable us to compare the asymptotic variances of f and the asymptotic covariances of f and g , by yielding a lower bound to the optimal control variate (5.3). Owing to translational invariance of the conditional variances of $f(z_1) - f(z_0)$ given (z_0, \tilde{z}_0) , the first expression for the asymptotic variance of g in system (5.8) can be cast into the following form:

$$\kappa(g, g) = \mathbb{E} [\mathbb{V} [f(z_1) | z_0, \tilde{z}_0]] = \mathbb{V} [f(z_1)] - \mathbb{V} [\mathbb{E} [f(z_1) | z_0, \tilde{z}_0]]. \quad (5.9)$$

where the second equality stems from the law of total variance for $f(z_1)$. One deduces from (5.6) and (5.9) that the optimal control variate (5.3) is strictly larger than one

$$b_\star = \frac{\mathbb{V} [f(z_1)]}{\mathbb{V} [f(z_1)] - \mathbb{V} [\mathbb{E} [f(z_1) | z_0, \tilde{z}_0]]} > 1, \quad (5.10)$$

provided that $\mathbb{V} [f(z_1)] = \mathbb{V}_\theta [f] > 0$. From a dynamical view point, the optimal control variate depends on the correlation between consecutive sampled points. Indeed, taking the half-sum of the two terms of (5.8) leads to

$$\kappa(g, g) = \frac{1}{2} \mathbb{V} [f(z_1) - f(z_0)] = \frac{1}{2} \mathbb{E} \left[\left(f(z_1) - f(z_0) \right)^2 \right] = \mathbb{E}_\theta [f^2] - \mathbb{E} [f(z_1)f(z_0)]. \quad (5.11)$$

Then, substituting expression (5.11) for the denominator of (5.10) yields the following identity:

$$b_\star = \frac{\mathbb{E}_\theta [f^2] - \mathbb{E}_\theta [f]^2}{\frac{1}{2} \mathbb{E} \left[\left(f(z_1) - f(z_0) \right)^2 \right]} = \frac{\mathbb{E}_\theta [f^2] - \mathbb{E}_\theta [f]^2}{\mathbb{E}_\theta [f^2] - \mathbb{E} [f(z_1)f(z_0)]}. \quad (5.12)$$

Interestingly, the expression of the optimal control variate is the same when multiple proposals are used with WRMC, as shown by Delmas and Jourdain [9]. From expression (5.12), it is clear that the optimal control variate depends on the statistical covariance of the sampled points in the generated Markov chain. If the sampled points of the Markov chain were independently distributed, then one would get $\mathbb{E} [f(z_1)f(z_0)] = \mathbb{E}_\theta [f]^2$, entailing

that the optimal control variate would be one. This would entails that conditioning on the proposals provide optimal variance reduction. However, the iid condition is rarely met in practical applications. Even though the proposals be drawn from a constant distribution independently from the current point, the fact of occasionally selecting the old point introduces statistical correlations in the generated Markov chain. From expression (5.12) and inequality (5.10), one easily deduces that the correlation coefficient within pairs of successive values of f along the Markov chain is strictly positive:

$$\text{corr}[f(z_1), f(z_0)] = \frac{\mathbb{E}[f(z_1)f(z_0)] - \mathbb{E}[f(z_1)]\mathbb{E}[f(z_0)]}{\sqrt{\mathbb{V}[f(z_1)]\mathbb{V}[f(z_0)]}} = 1 - b_\star^{-1} > 0.$$

This property stems from the use of a sampling algorithm based on Barker acceptance rule. If the Metropolis rule is used instead, the inequality is not satisfied in general. The standard way [9, 10, 96] of estimating b_\star is deduced from the form (5.12) and the ergodic theorem. It consists In evaluating the quantity

$$\hat{b}_{\text{NC}}^M = \frac{\mathbb{I}^M(f^2) - [\mathbb{I}^M(f)]^2}{\frac{1}{2M} \sum_{m=0}^{M-1} [f(z_{m+1}) - f(z_m)]^2}, \quad (5.13)$$

where f_m and f_{m+1} stands for $f(z_m)$ and $f(z_{m+1})$ to simplify the notations. Subscript NC stands for *no conditioning*. We now show that more accurate estimators of b_\star can be constructed through conditioning.

5.2.5 Estimating the control variate through conditioning

Among the various expressions derived previously for the asymptotic variance of g , we distinguish three levels of conditioning which are evidenced by the following total expectations

$$\kappa(g, g) = \frac{1}{2} \mathbb{V}[f_1 - f_0] = \begin{cases} \mathbb{E}\left[\frac{1}{2}(f_1 - f_0)^2\right] & \implies \text{NC} \\ \mathbb{E}\left[\mathbb{E}\left[\frac{1}{2}(f_1 - f_0)^2 \mid w_0\right]\right] & \implies \text{SC} \\ \mathbb{E}\left[\mathbb{E}\left[\mathbb{E}\left[\frac{1}{2}(f_1 - f_0^\dagger)^2 \mid w_1^\dagger\right] \mid w_0\right]\right] & \implies \text{DC.} \end{cases}$$

where w_0 and w_1^\dagger stand for (z_0, \tilde{z}_0) and $(z_1, \tilde{z}_1^\dagger)$ to further simplify the notations. SC and DC refer to *single conditioning* and *double conditioning*, respectively.

The estimator of b_\star that consists of performing a single conditioning writes

$$\hat{b}_{\text{SC}}^M = \frac{\mathbb{J}_1^M(f^2) - \mathbb{J}_1^M(f)^2}{\frac{1}{2M} \sum_{m=0}^{M-1} \mathbb{P}(1|z_m, \tilde{z}_m) [f(\tilde{z}_m) - f(z_m)]^2}. \quad (5.14)$$

where the denominator is equal to the arithmetic mean of $\frac{1}{2} \mathbb{E}\left[(f(z_{m+1}) - f(z_m))^2 \mid z_m, \tilde{z}_m\right]$. Resorting the reversibility property of the Markov, $\mathbb{E}\left[g_0^\dagger | w_1^\dagger\right] = \mathbb{E}[g_1 | w_0]$ and setting g to f or f^2 , the double conditioning writes

$$\mathbb{E}\left[\mathbb{E}\left[\frac{1}{2}(f_1 - f_0^\dagger)^2 \mid w_1^\dagger\right] \mid w_0\right] = \mathbb{E}\left[\frac{1}{2}f_1^2 - f_1 \mathbb{E}\left[f_0^\dagger \mid w_1^\dagger\right] + \frac{1}{2}\mathbb{E}\left[\left(f_0^\dagger\right)^2 \mid w_1\right] \mid w_0\right] = \mathbb{V}[f_1 - f_0 | w_0].$$

As a result, the doubly conditioned estimator of b_\star writes

$$\hat{b}_{\text{DC}}^M = \frac{\mathbb{J}_1^M(f^2) - \mathbb{J}_1^M(f)^2}{\frac{1}{M} \sum_{m=0}^{M-1} \mathbb{P}(0|z_m, \tilde{z}_m) \mathbb{P}(1|z_m, \tilde{z}_m) [f(\tilde{z}_m) - f(z_m)]^2}. \quad (5.15)$$

The denominator in (5.15) corresponds to the conditional variance of $f(z_{m+1})$ given (z_m, \tilde{z}_m) , written as a function of the two involved conditional probabilities

$$\mathbb{V}[f(z_{m+1}) - f(z_m) | z_m, \tilde{z}_m] = \mathbb{P}(0|z_m, \tilde{z}_m) \mathbb{P}(1|z_m, \tilde{z}_m) [f(\tilde{z}_m) - f(z_m)]^2.$$

The three estimates can easily be evaluated numerically during a simulation. The SC estimator has been proposed and tested in Ref. [10]. It amounts to evaluating the optimal control variate based on waste-recycling.

It was found to be more accurate in practice than NC estimator (5.13). This observation can be rationalized mathematically by noticing the two following inequalities

$$\mathbb{V} \left[\frac{1}{2}(f_1 - f_0)^2 \right] > \mathbb{V} \left[\frac{1}{2} \mathbb{E} [(f_1 - f_0)^2 | w_0] \right] > \mathbb{V} \left[\mathbb{E} \left[\mathbb{E} \left[\frac{1}{2}(f_1 - f_0)^2 | w_1^\dagger \right] | w_0 \right] \right].$$

These inequalities are easily obtained by application of the law of total variance to observable $\frac{1}{2}(f_1 - f_0)^2$. This entails that the NC estimator of the optimal control variate in Eq. (5.13) is less accurate than the estimator based on the singly conditioned expectation. Similarly, the latter estimator is also less accurate than the doubly conditioned estimator, which can be shown resorting to the delta method. We show with a practical example that this double inequality is observed in Sec. 5.4. The testbed application involves estimating the difference of free energies associated with the transmutation of an A atom into a B atom in an AB binary alloy. This free energy difference corresponds to the difference of chemical potentials of the two species. Simulations will be carried out in a work-biased path ensemble [45, 10] that is introduced in Sec. 5.3 below.

5.3 Work-biased path ensemble

5.3.1 Work as a biasing path functional

This ensemble is a variant of the nonequilibrium path ensemble of Section 4.3 in which the work serves as a biasing path functional. The bias aims at improving the convergence of the associated free energy perturbation technique owing to enhanced overlaps between the sampled distribution and the target distributions (see Ref. [46] and also subsection 2.4.2 for the connection with the rare event problem). As in the expanded transition path ensemble of previous section, an external parameter θ couples linearly to the biasing path functional so as to control its strength. It results that paths are most conveniently sampled using a MCMC algorithm in which trial paths are generated either forward or backward. It sounds natural to include the rejected paths in the free energy estimator.

5.3.2 Path probability and expectation

Herein, a path consists of a sequence of extended states: $z = \{(\lambda^0, x_0), \dots, (\lambda^\ell, x_\ell), \dots, (\lambda^L, x_L)\}$ wherein the scheduling of the external parameter is imposed. The Hamiltonian is gradually switched from $\mathcal{H}(\lambda^0, \cdot)$ to $\mathcal{H}(\lambda^L, \cdot)$. Path will be generated by a Monte Carlo process or by a steered Langevin dynamics. The biasing path functional is the work defined from the Hamiltonian variation and the heat via the first law of thermodynamics (4.10)

$$\mathcal{W}^{0 \rightarrow L}(z) = \mathcal{H}(\lambda^L, x_L) - \mathcal{H}(\lambda^0, x_0) - \mathcal{Q}^{0 \rightarrow \ell}(z) \quad (5.16)$$

Besides, the work relates to the path generating probabilities through the work fluctuation relation (4.17):

$$\mathcal{W}^{0 \rightarrow L}(z) = \mathcal{H}(\lambda^L, x_L) - \mathcal{H}(\lambda^0, x_0) - \ln \frac{\mathbb{P}(z | \lambda^L, x_L)}{\mathbb{P}(z | \lambda^0, x_0)}$$

where we plugged the heat fluctuation theorem (4.15) to substitute the heat in (5.16) for the conditional probability ratio. Expressing the two Hamiltonians as a function of the conditional log-probabilities of x_0 given λ^0 and of x_L given λ^L provides us with a useful expression for the work

$$\mathcal{W}(z) \equiv \mathcal{W}^{0 \rightarrow L}(z) = \mathfrak{F}(\lambda^L) - \mathfrak{F}(\lambda^0) - \ln \frac{\mathbb{P}(z | \lambda^L)}{\mathbb{P}(z | \lambda^0)},$$

recalling that $\mathfrak{F}(\lambda)$ denotes the absolute free energy of the system (see relations (4.16)). The biased probability of path z exhibits the following form

$$\mathbb{P}_\theta(z) = n_\theta \mathbb{P}(z | \lambda^L)^\theta \mathbb{P}(z | \lambda^0)^{1-\theta} = n_\theta \exp \{ \theta [\mathfrak{F}(\lambda^L) - \mathfrak{F}(\lambda^0) - \mathcal{W}(z)] \} \mathbb{P}(z | \lambda^0),$$

where n_θ is the normalizing constant. Noticing that $n_1 = n_0 = 1$, the nonequilibrium work relation (4.19) with ℓ set to L is recast into the following form [45]

$$\exp[-\mathfrak{F}(\lambda^L) + \mathfrak{F}(\lambda^0)] = \frac{\mathbb{E}_\theta^{\mathcal{Z}}[\exp[(\theta - 1)\mathcal{W}]]}{\mathbb{E}_\theta^{\mathcal{Z}}[\exp[-\theta\mathcal{W}]]}.$$

The standard nonequilibrium work relation (4.19) is recovered when θ is set to 0, since $\mathbb{E}_{\theta=0}^{\mathcal{Z}}[\exp[-\mathcal{W}]]$ is equivalent to $\mathbb{E}^{\mathcal{Z}}[\exp[-\mathcal{W}^{0 \rightarrow L}] | \lambda^0]$. The work-biased path ensemble is sampled by performing the specific shooting moves described in Refs. [46] and [10] which are variants of the shooting moves described in Chapter 4.

The judicious choice of $\theta \in [0, 1]$ will be discussed page 86. The enhanced bridging properties of the sampled distribution $P_\theta(z)$ for intermediate θ values usually enable better overall efficiency than when θ is set equal to 0 or 1. Compared to expanded path ensemble methods, the absence of auxiliary biasing potential in the present approach obviates the need of running an adaptive process.

We next apply the waste-recycling Monte Carlo with the optimal estimator to our system of interest, binary alloys of varying composition.

5.4 Applications

5.4.1 Binary alloys

The performance of the optimal estimator is first assessed by comparing with that of traditional estimators in a generic but realistic binary system with A and B atoms interacting on a rigid lattice in Sec. 5.4.2. The possibilities of the methodology are then illustrated by performing off-lattice simulations of a model FeCr alloy in Sec. 5.4.3.

The computational cell contains N atoms. In the reference state at $t = 0$, we have $N = N_A + N_B$ or $N = N_{\text{Fe}} + N_{\text{Cr}}$ atoms where N_X refers to the atom number of type X. In the target state at $t = \tau$, the cells still contains N atoms, but an A or Fe atom has been transmuted into a B or Cr atom, respectively. Paths thus consist of artificially switching the potential energy of a selected atom. The switching will be performed instantaneously in the AB alloy (Sec. 5.4.2), or gradually using constant-pressure Langevin dynamics [46] in the FeCr alloy (Sec. 5.4.3).

The infinitely-fast transmutions of Sec. 5.4.2 are carried out without changing the atomic masses. Hence, the ratio of the reverse conditional probability, $P(z|\chi_\tau) = (N_B + 1)^{-1}$, to the forward one, $P(z|\chi_0) = (N - N_B)^{-1}$, relates to the exponential of the ideal chemical potential difference

$$\frac{P(z|\lambda^L, x_L)}{P(z|\lambda^0, x_0)} = \frac{N_B + 1}{N - N_B} = \exp[\beta\Delta\mu^{\text{id}}], \quad (5.17)$$

where A and B are assumed to have identical masses. The ideal chemical potential difference in Eq. (5.17) acts as a heat transferred from a reservoir of A and B atoms into the system. Hence, the dimensionless work \mathcal{W} carried out on the system for transmuting an A atom into a B atom to the Hamiltonian variation can be deduced from the first law:

$$\mathcal{W}(z) = \mathcal{H}(\lambda^L, x_L) - \mathcal{H}(\lambda^0, x_0) - \beta\Delta\mu^{\text{id}}$$

where x_L only differs from x_0 by the transmuted atom. When transmuting a B into an A atom, the quantity $-\mathcal{W}(z)$ must be considered instead. In contrast, the transmutions of Sec. 5.4.3 are performed gradually using constant-pressure Langevin dynamics [46] and linear Hamiltonian switching. As a result, the probability ratio Eq. (5.17) becomes

$$\frac{P(z|\lambda^L, x_L)}{P(z|\lambda^0, x_0)} = \exp[\beta\Delta\mu^{\text{id}} + \beta\mathcal{Q}(z)]$$

where $\mathcal{Q}(z)$ is the *excess* heat transferred from the thermostat and barostat to the particle system [46], in addition to the heat $\Delta\mu^{\text{id}}$ transferred from the atomic reservoir. We thus have

$$\mathcal{W}(z) = \mathcal{H}(\lambda^L, x_L) - \mathcal{H}(\lambda^0, x_0) - \beta\Delta\mu^{\text{id}} - \mathcal{Q}(z)$$

In both set-ups, sampling forward and backward transmutions is sufficient to explore the phase spaces of the alloy. Accepting several paths amounts to exchanging the allocation of atoms on the underlying lattice of the reference and target systems.

Simulations aim at extracting differences of chemical potentials $\Delta\mu$ between both species as a function of the alloy composition. We have either $\Delta\mu = \mu_B - \mu_A$ or $\Delta\mu = \mu_{Cr} - \mu_{Fe}$ depending on the involved alloy system. Both quantities indeed correspond to the difference of Gibbs free energy between the target and reference states

$$\Delta\mu = \beta^{-1} [\mathfrak{F}(\lambda^L) - \mathfrak{F}(\lambda^0)].$$

The generic estimator will be

$$\mathcal{J}_b^M(\Delta\mu) = -\beta^{-1} \ln \frac{J_b^M(\exp[(\theta - 1)\mathcal{W}])}{J_b^M(\exp[\theta\mathcal{W}])} \quad (5.18)$$

where the estimator J_b^M is defined in (5.2) for path function f . Let $c = N_B/N$ or $c = N_{Cr}/N$ denote the alloy concentration in B or Cr. A change in the monotonicity of the function $c \rightarrow \Delta\mu(c)$ is a signature of phase coexistence. The conditions of phase equilibria can then be determined via the equal-area construction with respect to $\Delta\mu(c)$, or equivalently, via the common-tangent construction with respect to the Gibbs free energy

$$G(c) = \int_0^c \Delta\mu(c') dc'. \quad (5.19)$$

measured per atom.

5.4.2 AB system with constant pair interactions

In our simplified binary alloy lattice model, the rigid lattice is body centered cubic. The cell contains $N = 2^{12}$ sites with N_B atoms of type B at $t = 0$. The site function $\eta_B(i)$ is 1 or 0 depending on whether site i is occupied by a B atom or not. Interaction energies are taken as pair interactions ϵ_{XY} between nearest-neighbor sites, where X and Y may equal A or B. The ordering enthalpy $\epsilon = \epsilon_{AA} + \epsilon_{BB} - 2\epsilon_{AB}$ plays a key role as it entirely determines the thermodynamics of the system [97]. Without loss of generality, we can choose $\epsilon_{AA} = \epsilon_{AB} = 0$ and set $\epsilon = -30$ meV. With a negative ordering energy, the system exhibits a miscibility gap below which the solid solution decomposes into A-rich and B-rich phases. The unmixing transition is of first-order except for the $A_{0.5}B_{0.5}$ composition where it is second-order [97] and where the critical temperature is $T_c \approx -\epsilon/(k \times 0.62)$ [98].

The extended Hamiltonian reads

$$\mathcal{H}(\lambda, x) = \beta\epsilon \left[\lambda \sum_{j \in \mathcal{N}(k)} \eta_B(j) + \sum_{i \neq k} \sum_{j \in \mathcal{N}(i)} \eta_B(i)\eta_B(j) \right]$$

where index k denotes the lattice site of the hybrid atom, index i in the second summation runs over lattice sites except site k and index j runs over the sets of nearest neighbor pairs of the involved site (k or i). We first check the Delmas-Jourdain prediction that the asymptotic variance $\sigma(f, bf)^2$ of $J_b^M(f)$ is minimal at $b = b_*$ when the Barker sampler is used. Since $\lim_{M \rightarrow \infty} M\mathbb{W}[J_b^M(f)] = \sigma(f + bg)^2$ where $\mathbb{W}[J_b^M(f)]$ is the statistical variance of $J_b^M(f)$, we evaluate $\mathbb{W}[J_b^M(f)]$ as a function of b for large enough M and confirm whether its minimum occurs close to estimated values of b_* . Note that the real function $b \rightarrow \mathbb{W}[J_b^M(f)]$ is a positive quadratic form regardless of the value of M .

We set temperature to 348 K, the simulation parameter θ to 1/2, and B concentration to 50at.%. The two ensemble averages $\mathbb{E}_\theta[\exp(\pm \frac{1}{2}\beta\mathcal{W})]$ have been evaluated using estimators $J_b^M(f)$ given in Eq. (5.2) with $f = \exp(\pm \frac{1}{2}\beta\mathcal{W})$ and $0 \leq b \leq 20$. The statistical variances $\mathbb{W}[J_b^M(f)]$ have been computed from $K = 10^7$ estimates generated using distinct random seeds. Each estimate consists of $M = 2 \cdot 10^3$ transmutations, from A into B and from B into A alternatively. For each estimation, we also record the estimated value of b_* using estimator \hat{b}_{NC}^M given in Eq. (5.13), estimator \hat{b}_{SC}^M given in Eq. (5.14) and estimator \hat{b}_{DC}^M given in Eq. (5.15), and additionally construct their histograms yielding the probabilities that an estimate of b_* is equal to b .

As shown in Fig. 5.2, the quadratic form $\mathbb{W}[J_b^M(f)]$ is indeed minimum at the value corresponding to the best b_* -estimate indicated by the vertical double-dotted segment, obtained by combining the MK available data from either \hat{b}_{NC}^{MK} , \hat{b}_{SC}^{MK} or \hat{b}_{DC}^{MK} . The minimum is also very close to the horizontal line labeled $\mathbb{W}[J_{b_*}^M(f)]$ corresponding to the variance obtained from the K estimates $J_{b_*}^M(f)$ after substituting the corresponding estimate \hat{b}_{NC}^M for b_* in each run. Substituting \hat{b}_{SC}^M for b_* further decreases the variance by 0.24%, an amount not visible on the graph. A more noticeable benefit to conditioning for estimating b_* can be seen from the three histograms of b_*

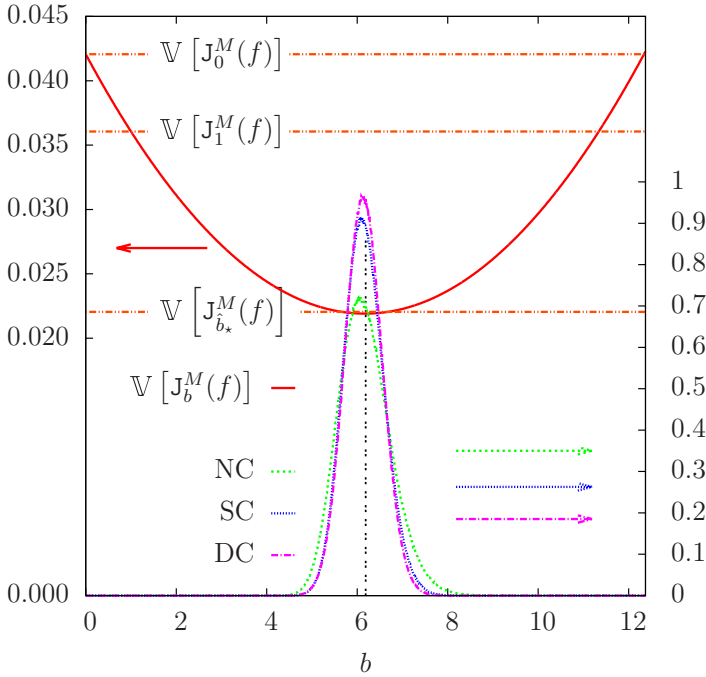


Figure 5.2: (left ordinate) $\mathbb{V} [J_b^M(f)]$ is the statistical variance of $J_b(e^{-\beta W/2})$ and is evaluated from 10^7 estimates. Note that $\mathbb{V} [J_0^M(f)]$ and $\mathbb{V} [J_1^M(f)]$ corresponds to the variances of $\mathbb{I}(e^{-\beta W/2})$ and $J_1(e^{-\beta W/2})$. The optimized variance $\mathbb{V} [J_{b_*}^M(f)]$ is defined in the text; (right ordinate) histograms of the estimated optimal parameters b_* , obtained without conditioning (NC) with single conditioning (SC) and double conditioning (DC). The histograms are obtained by averaging the indicator function $h_b(\hat{b}_*)$ where \hat{b}_* is one of the 10^7 estimated control variate.

displayed in Fig. 5.2. The histogram obtained with double conditioning is slightly narrower than the histogram obtained with single conditioning that is itself slightly narrower than the one obtained without conditioning.

Choice of the external parameter θ . In the series of simulations presented above, θ was set equal to $1/2$. This symmetric setting is often used in practice [44, 45, 46, 99] because the work distribution associated with $P_{1/2}$ exhibits sufficient overlaps with those associated with both P_0 and P_1 , ensuring a fast convergence of the involved exponential averages [46]. However, the optimal external parameter value θ^* that minimizes the total variance in the estimates of $\Delta\mu$ from Eq. (5.18) is not known in general. A series of simulations with varying the value of θ in the range $[0,1]$ has been carried out in Ref. [10] so as to locate the optimal value θ^* with respect to the evaluation of $\Delta\mu$ at the asymmetric composition $c = 10at.\% B$ by calculating the statistical variance of estimator (5.18) with b set to \hat{b}_{SC}^M . The value θ^* was found to be closed to $1/2$. Besides, the optimal value seems to be exactly $1/2$ at the symmetric composition of the (symmetric) Ising system.

Choice of the acceptance rule In the present simulations, the sampling algorithm is suboptimal because the acceptance probabilities with the Barker rule are always lower than those of the Metropolis rule. When the sampling scheme is based on Metropolis selection rule and when the Metropolis acceptance and rejection probabilities are used in the estimator, then it may happen that the waste-recycling estimator exhibits an increased statistical variance in some circumstances. This feature was predicted theoretically and illustrated practically on a toy model by Delmas and Jourdain [9]. However, when Barker acceptance probabilities are included in the estimator, while still using the Metropolis selection rule in the sampling, the procedure amounts to a conditioning with respect to a well-defined probability distribution, performed independently from the transition probabilities associated with the sampling process. As a result, variance reduction is guaranteed by the law of total variance. This implementation corresponds to a particular instance of the virtual-move Monte Carlo (VMMC) method [38]. The question of whether the combination of the optimal Metropolis sampler and the suboptimal estimators J_0^M or J_1^M may achieve better efficiency than the combination of the suboptimal Barker sampler and the optimal estimator $J_{b_*}^M$ is not answered by theory [9]. Hence, it is instructive to address this numerically. The statistical variances of the $\Delta\mu$ -estimates obtained using the biased estimator of Eq. (5.18) have been calculated and plotted as a function of B concentration in Fig. 5.3. We observe that it is always more efficient to implement the optimized estimator $J_{b_*}^M$ with the suboptimal sampler than estimators J_0^M or J_1^M with Metropolis sampling. Note that $J_{b_*}^M$ is still a valid and unbiased estimator when combined with the Metropolis sampler (but is not optimal anymore). Here, the combination was found slightly more efficient, with variance further decreased by 4.7% for $A_{0.5}B_{0.5}$ compared to Barker sampling and $J_{b_*}^M$. However, variance reduction is

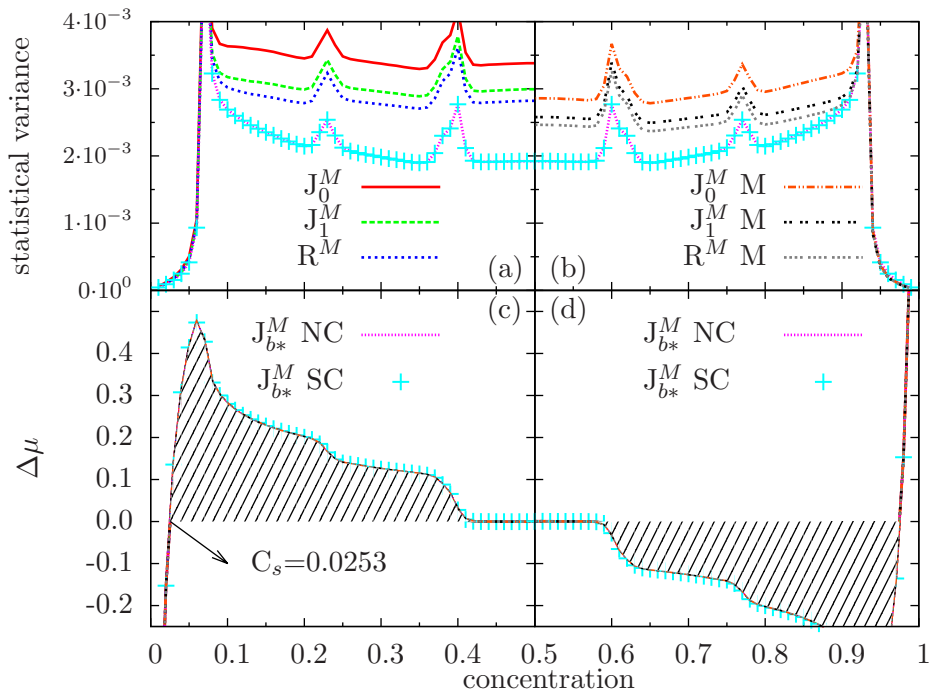


Figure 5.3: (a,b) statistical variances of estimated differences of excess chemical potentials [displayed in (c,d)] as a function of concentration. Used estimators are indicated in the legends. The symmetry of this Ising system with respect to $C_B = 50\%$ explains the equality between chemical potentials ($\Delta\mu = 0$) at the solubility limit C_s .

not always guaranteed mathematically. A solution would be to extract b_* corresponding to the minimum variance by postprocessing.

5.4.3 Fe-Cr system with EAM interactions

We now test our estimators on a more difficult model whose inter-atomic potentials are based on the embedded atom method (EAM). We have implemented the EAM potentials of Olsson *et al.* [100] developed to model the α and α' phases of the FeCr binary system. This EAM potential correctly reproduces the BCC structure of Iron and Chromium. Furthermore, the lowest energy states found for the Iron-rich and Chromium-rich compositions have negative formation energies of -10.08 meV at 6.67%Cr and -8.18 meV at 93.33%Cr, respectively [101]. The lowest formation energy in the intermediate composition range (found by probing many candidate intermetallic BCC structures based on the theory of the convex polyhedron in the correlation function space [97]) is -8.51 meV at 50%Cr [102], above the corresponding value of -9.13 meV associated with the convex hull. Phase separation should therefore be favoured over formation of intermetallics with intermediate compositions. The expected miscibility gap of FeCr alloy was indeed observed in Monte Carlo simulations carried out on a rigid lattice with the interaction energies directly deduced from the EAM potential [100]. Here, the rigid-lattice assumption is entirely released in the construction of the phase diagram. We perform path-sampling simulations to compute the chemical potential difference with varying concentration and temperature. Transmutations are now performed gradually in 10^2 steps with linear Hamiltonian switching and constant-pressure Langevin dynamics [46] in a computational cell containing 432 atoms. Equilibration proceeds in 20 transmutations per atom, starting from a random distribution of the atoms on 6^3 unit cells of the BCC structure. Simulations have been carried out with temperature ranging from 300 to 1700 K in step of 25 K. Examination of the simulated microstructures show evidence of phase separation at low enough temperatures. Figure 5.4 displays the snapshot of a typical phase separated microstructure for alloy $\text{Fe}_{0.8}\text{Cr}_{0.2}$ at 300 K.

Figure 5.5 displays the statistical variances obtained for the various estimators obtained with $M = 400$ transmutations (per estimate) and $K = 200$ estimates at $T=500$ K. The aforementioned hierarchy still holds in the present case for all concentrations. Because the amount of transmutations per estimate is much smaller than previously, it is more relevant to estimate b_* using conditioning (SC) than without (NC). The former variant further decreases the variance associated with the estimation of b_* by 20 % on average over the latter

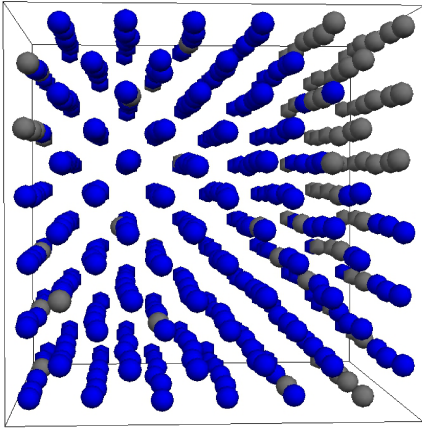


Figure 5.4: Snapshot of a simulated microstructure containing 20% at. Cr obtained at $T = 300\text{K}$. Fe and Cr atoms are displayed in blue and gray, respectively.

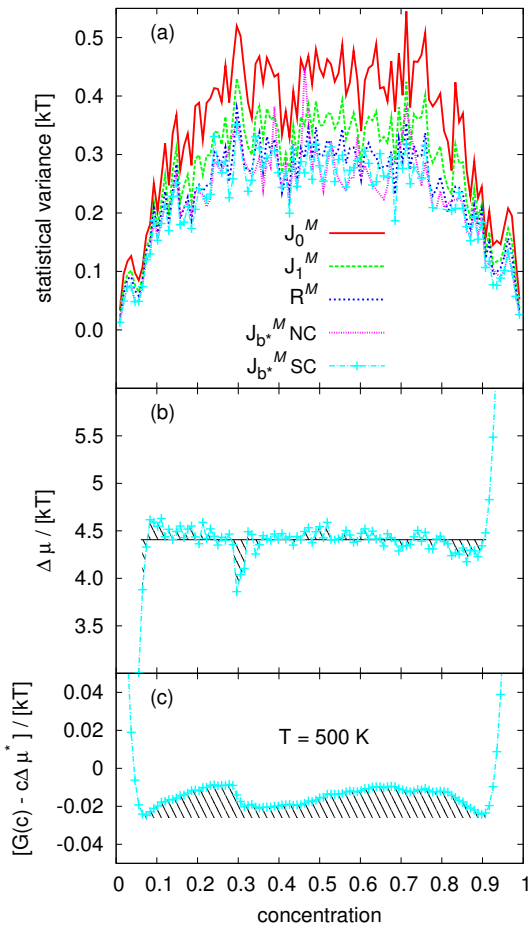


Figure 5.5: (a) statistical variances of estimated differences of excess chemical potentials [displayed in (b)];(c) solubility limits displayed in the concentration-temperature plane as obtained from Maxwell equal-area construction at $T = 500\text{K}$. Used estimators are indicated in the legend.

one. Averaging over all temperatures, estimator $\mathcal{J}_{b_*}^M$ -SC decreases the variance by a factor of 2 to 5/2 compared to \mathcal{J}_0^M and by 20 to 30 % compared to $\mathcal{J}_{b_*}^M$ with NC. The $\Delta\mu$ -values displayed in Fig. 5.5b correspond to a single estimate obtained from the $8 \cdot 10^4 = M \times K$ transmutations used to evaluate the statistical variance. Figures 5.5b and 5.5c illustrate the equal-area or common-tangent constructions of Maxwell and corroborate the occurrence of phase coexistence.

The reconstructed Gibbs free energy surface G is less fluctuating because it is based on a self-averaging integral Eq. (5.19). The potential quantity $\Delta\mu_*(T)$ in Fig. 5.5c is such that the occurrence probabilities of the Fe-rich and Cr-rich phases are equal. The occurrence probability is $P^*(c, T) = Z^{-1} e^{N\beta[c\Delta\mu^* - G(c)]}$ where $Z = \int_0^1 e^{N\beta[c'\Delta\mu^* - G(c')]} dc'$ is the semigrand canonical partition function [14] associated with the finite computational cell. The potential function $\Delta\mu^*(T)$ exactly coincides with the slope of the common-tangent at coexistence and in the thermodynamic limit only. Within finite computational cells, $\Delta\mu^*(T)$ is defined even when there is no common tangent, is always easy to determine and fluctuates less than the slope of the common-tangent when there exists one. The transformed Gibbs free energy surfaces $G(c) - c\Delta\mu^*$ are displayed in Fig. 5.6. The contour plot in the temperature-concentration plane of the bottom panel clearly visualizes the miscibility gap in the composition range going approximately from $\text{Fe}_{0.1}\text{Cr}_{0.9}$ to $\text{Fe}_{0.9}\text{Cr}_{0.1}$.

The coexistence lines (solubility limits) associated with the gap end around 500 K both in the iron-rich or chromium-rich sides and are indicated by the solid white curve in Fig. 5.6b. Above 525 K, we observe that free energy profiles becomes lower for intermediate composition which indicates the presence of a stability field for these intermediate compositions and of two immiscibility fields for the Fe-rich and Cr-rich compositions. Solubility limits on the Fe-rich and Cr-rich sides associated with the two immiscibility fields are indicated by the dashed white curves in Fig. 5.6b. However, examination of snapshots of the simulated systems within the expected stability field still shows unmixed microstructures with a tendency to phase separation decreasing with increasing temperature from 525 K to 1700 K. This is attributed to the fact that the correlation length diverges at the critical temperature T_c where the thermodynamic transition is second order. Given that the computational cell contains only 2×6^3 atoms and that atomic interactions up to 7th nearest neighbors were shown to play an important role [101], strong finite-size effects are expected. The low temperature of 500 K measured for the present closure of the miscibility gap should therefore not be interpreted as an estimate of the critical temperature T_c whose experimental value is expected to lie around 900 K [102]. A finite-size scaling analysis [103] should therefore be carried out, which entails performing simulations with much larger computational cells. To achieve this task, the overall computation time has to be reduced considerably, possibly by evaluating the interatomic potential and forces on parallel computer architectures [96]. While the preliminary results presented here show that a direct and accurate construction of the equilibrium phase diagram of FeCr alloy is achievable in principle, they also emphasize the need for more extensive free energy calculations in this system.

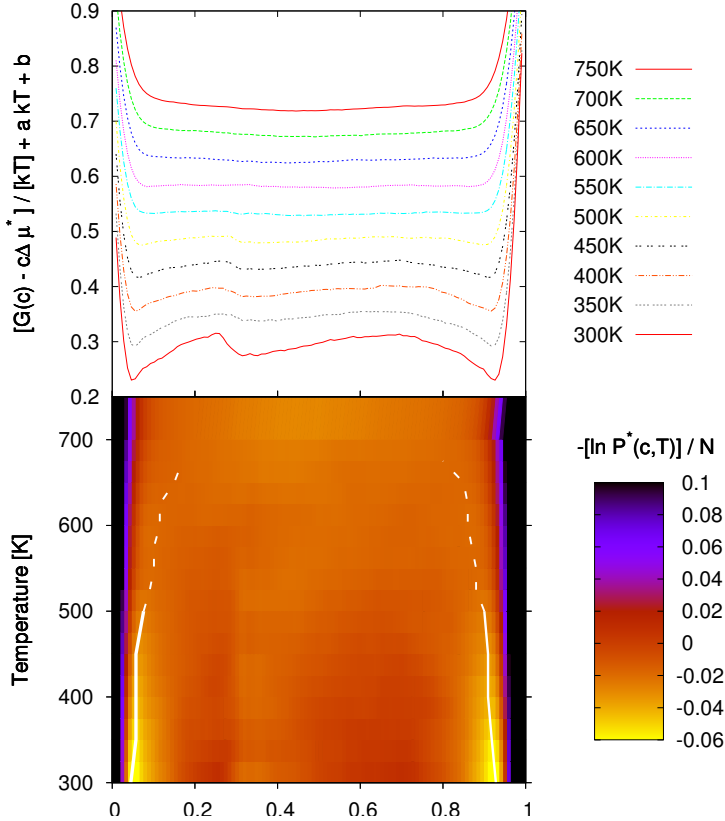


Figure 5.6: Top are the Gibbs free energies transformed for better visualization ($a = 10^{-3}$ and $b = \ln Z/N$) as a function of concentration for various temperatures; bright regions on the bottom contour plot correspond to stability fields, the Fe and Cr solubility limits of the Fe-rich and Cr-rich phases are schematized by the two white lines.

5.5 Summary

The optimal estimator proposed by Delmas and Jourdain for waste-recycling Monte Carlo has been assessed numerically. As a testbed, we simulated two alloy systems via the work-biased path ensemble and simultaneously estimated the free energy differences from the nonequilibrium works measured along the transmutations. We find that the estimator indeed achieves variance reduction compared to the other Monte Carlo estimators that are compatible with the present sampling approach. Furthermore, the maximal reduction of the statistical variance that is predicted by the theory is attained for relatively short simulations ($2 \cdot 10^3$ sampled paths).

Concerning the investigated examples of binary alloys, we point out that achieving numerical ergodicity in the reference and target thermodynamic states entails exchanging the allocation of atoms of distinct types on the underlying lattice (which amounts to performing pairs of simultaneous transmutations with opposite direction) with a high enough frequency. With path-sampling, exchanges of atom allocation are automatically achieved when trial paths are successively accepted within the transmutation ensemble. It turns out that the phase space exploration is considerably facilitated. Resorting to such a path-sampling scheme was found particularly advantageous in the FeCr alloy system which presents a large magnetic misfit. Direct exchange moves sampled using a standard scheme in the reference and target system would have been extremely infrequent and thus computationally expensive compared to the gradual transmutations considered here. The approach might work as well in the numerous alloy systems exhibiting large atomic misfits.

Overall, the Delmas-Jourdain estimator is unbiased and optimal in terms of asymptotic variance with respect to a simple control variate b_* that can be accurately estimated from the correlations in the collected data. One substantial benefit to employing this optimal estimator is the flexibility in the choice of the sampler, allowing us to couple waste recycling Monte Carlo with a work-biased transmutation path ensemble ideally formulated to study the phase coexistence of binary alloys. Since information associated with trial switching processes is optimally included in the free-energy estimates for any sampler, this one is to be chosen so as to facilitate the phase space exploration. In other scenarios, another Monte Carlo sampling scheme might be better posed, yet the optimal estimator of Delmas and Jourdain would still be applied quite similarly. As an example, the free energy barriers associated with the migration of small molecules inside zeolites have been estimated by combining a multi-proposal sampling scheme to the same control variate structure [96].

6 | A matter of time evolution: kinetic pathways and deconditioning

This Chapter focuses on the kinetic Monte Carlo (kMC) method. Herein, conditioning aims at accelerating the kMC simulations by enabling each mobile defect to perform entire sequences of hops at once. Deconditioning then serves to synchronize defects evolving in parallel.

6.1 Kinetic Monte Carlo and master equation

The kMC method [104, 105, 106] is extensively used to simulate the time evolution of many physical systems described by discrete master equations (ME), i.e. sets of ordinary differential equations for the time-dependent vector of state probabilities [107, 108]. Statistically equivalent to the (most often unknown) solution of the ME, kMC finds a growing number of applications in natural and engineering sciences. However, still wider applicability of kMC is severely limited by the notorious kinetic trapping where the stochastic trajectory repeatedly visits a subset of states, a trapping basin, connected to each other by high-rate transitions while transitions out of the trapping basin are infrequent and take great many kMC steps to observe.

We herein present an efficient method for sampling stochastic trajectories escaping from the trapping basins. Unlike recent transition path sampling methods that focus on short portions of the full kinetic path directly leading to the escapes and/or require equilibration over a path ensemble [7, 109, 110, 111, 112, 113, 114], our method constructs an entire stochastic trajectory within the trapping basin including the typically large numbers of repeated visits to each trapping state as well as the eventual escape. Referred hereafter as kinetic Path Sampling (kPS), the proposed algorithm is statistically equivalent to the standard kMC simulation and entails (i) factorization of paths inside a trapping basin via conditioning over probabilities of repeated visits, (ii) sampling a single exit state within the basin's perimeter and (iii) generating a first-passage path and an exit time to the selected perimeter state through an exact deconditioning procedure (randomization). The kPS algorithm does not require any advance knowledge of the trapping basin nor does it entail matrix diagonalization.

Outline of the chapter We describe the of kPS method in Sec. 6.2 and demonstrate its accuracy and efficiency on two models: diffusion on a random energy landscape specifically designed to yield a wide and continuous spectrum of time scales (Sec. 6.3), and kinetics of phase separation in super-saturated solid solutions of copper in iron (Sec. 6.3).

6.2 Conditioning and deconditioning

The evolution operator, obtained formally from solutions of the ME, can be expressed as an exponential of the time-independent transition rate matrix ¹

$$\mathbf{P}(t, t + \tau) = \exp \left(\int_t^{t+\tau} \mathbf{M} ds \right) = \exp(\tau \mathbf{M}), \quad (6.1)$$

where $P_{\beta\gamma}(t, t + \tau)$ is the probability to find the system in state γ at $t + \tau$ given that it was in state β at time t , $M_{\beta\gamma}$ is the rate of transitions from state β to state γ (off-diagonal elements only) and the standard convention

¹The evolution operator is obtained by integrating the ME $\dot{\mathbf{v}}^T(t) = \mathbf{v}^T(t)\mathbf{M}$ from t to $t + \tau$ and identifying the formal solution with $\mathbf{v}^T(t + \tau) = \mathbf{v}^T(t)\mathbf{P}(t, t + \tau)$ where $\mathbf{v}^T(t)$ is the state-probability (row) vector at t .

is used to define the diagonal elements as $M_{\beta\beta} = -\sum_{\beta \neq \nu} M_{\beta\nu}$. As defined, the evolution operator belongs to the class of stochastic matrices such that $\sum_{\nu} P_{\beta\nu} = 1$ and $P_{\beta\gamma} \geq 0$ for any β, γ, t and τ . If known, the evolution operator can be used to sample transitions between any two states ² and over arbitrary time intervals τ . In particular, substantial simulation speed-ups can be achieved by sampling transitions to distant states on an absorbing perimeter of a trapping basin. Two main deficiencies of the existing implementations of this idea [115, 116, 117, 118] is that states within the trapping basin are expected to be known *a priori* and that computing the evolution operator requires a partial eigenvalue decomposition of \mathbf{M} entailing high computational cost [119].

Consider the linearized evolution operator

$$\mathbf{P}^{(0)}(t, t + \tau) = \mathbf{I} + \tau\mathbf{M}, \quad (6.2)$$

where $\mathbf{I} = \mathbf{P}^{(0)}(t, t)$ is the identity matrix. Assuming that $\tau \leq \min\{-(M_{\beta\beta})^{-1} : \forall\beta\}$, $\mathbf{P}^{(0)}$ is a proper stochastic matrix that can be used to generate stochastic sequences of states from the ensemble of paths defined by matrix \mathbf{M} . The diagonal elements of $\mathbf{P}^{(0)}$ define the probabilities of round-trip transitions after which the system remains in the same state. To correct for the linearization of the evolution operator in (6.2), the time elapsed before any transition takes place is regarded as a stochastic variable and sampled from an exponential distribution $t \rightarrow \tau^{-1} \exp(-t/\tau)$ [120]. This simple time randomization obviates the need for exponentiating the transition rate matrix in (6.1).

The mean residence time of a transition from β based on $\mathbf{P}^{(0)}$ is simply τ :

$$\mathcal{T}_{\beta}^{(0)} = \mathbb{E}^{(0)}[t] = \int_0^{\infty} \frac{t}{\tau} \exp\left[-\frac{t}{\tau}\right] dt = \tau.$$

Drawing the elapsed time in the exponentially decaying distribution aims at correctly synchronizing mobile defects evolving in parallel. This task is a crucial aspect of KMC simulations, especially in models describing alloys under irradiation [104, 121] in which many interacting defects evolves in parallel. The advantage of employing the mean residence times [122, 123] is that the procedure can be generalized through conditioning, making it possible to perform accelerated kMC simulations. We next describe the conditioning procedure.

Noticing that the probability $1 - P_{\beta\beta}^{(0)}$ to exit from β is equal to $\tau M_{\beta\beta}$, the mean first-passage time for exiting state β is obtained from the law of total expectation, either *explicitly*:

$$\mathcal{T}_{\beta}^{(1)} = \mathbb{E}^{(1)}\left[\mathbb{E}^{(1)}\left[\tau(1+n)\mathcal{T}_{\beta}^{(1)}|n\right]\right] = \sum_{n=0}^{\infty} (1+n)\tau \left[P_{\beta\beta}^{(0)}\right]^n (1 - P_{\beta\beta}^{(0)}) = (M_{\beta\beta})^{-1},$$

with n the number of $\beta \rightarrow \beta$ round-trips of probability $P_{\beta\beta}^{(0)}$, or *implicitly*:

$$\mathcal{T}_{\beta}^{(1)} = \mathbb{E}^{(1)}\left[\mathbb{E}^{(1)}\left[\tau + \mathcal{T}_{\beta}^{(1)}|\beta \rightarrow \beta\right]\right] = \tau + \mathcal{T}_{\beta}^{(1)} P_{\beta\beta}^{(0)}.$$

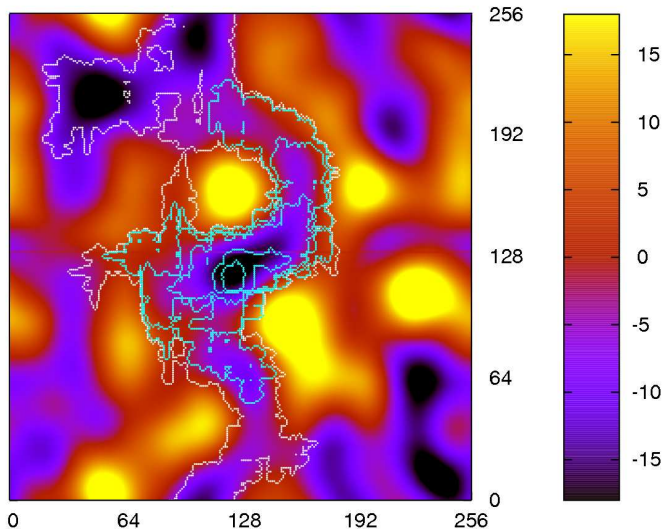
The implicit relation can be immediately generalized to trapping basins \mathcal{E}^N consisting of N states and provides with a linear system in which the unknown quantities are the mean first-passage times from any states $\beta \in \mathcal{E}^N$:

$$\mathcal{T}_{\beta}^{(N)} = \mathbb{E}^{(N)}\left[\mathbb{E}^{(N)}\left[\tau + \mathcal{T}_{\gamma}^{(N)}|\beta \rightarrow \gamma\right]\right] = \tau + \sum_{\gamma} \mathcal{T}_{\gamma}^{(N)} P_{\beta\gamma}^{(0)},$$

where $\mathcal{T}_{\gamma}^{(N)}$ is zero if $\gamma \notin \mathcal{E}^N$. The linear system of equations can be solved using various methods, for instance by inverting the transition rate matrix $\mathbf{M} = \tau^{-1}\mathbf{P}^{(0)} - \mathbf{I}$ inside the trapping basin using the Gauss-Jordan pivot elimination method [124]. This matrix factorization technique yields not only the mean first-passage times, but also the exit probabilities $\mathbf{P}^{(N)}$ from the trapping basin \mathcal{E}^N . With this factorization [125, 124], the mean first-passage times and exit probabilities are obtained *explicitly* by subsuming all possible transitions involving the eliminated states in the trapping basin \mathcal{E}^N . This remarkable path interpretation [122, 125] makes it possible to construct a detailed escape trajectory statistically equivalent to the standard kMC without ever performing an inefficient kMC simulation that accounts for all transitions within \mathcal{E}^N , reverting back to transition matrix

²If the system is in β at a given time, then the state-probability vector at a later time τ is $\mathbf{v}_{\beta}^T(\tau) = \mathbf{1}_{\beta}^T \mathbf{P}(0, \tau)$ where $\mathbf{1}_{\beta}^T$ denotes the row vector whose β th entry is one and the other ones are zero. The entries of $\mathbf{v}_{\beta}^T(\tau)$ are $P_{\beta\gamma}(0, \tau)$ and can be used as transition probabilities for kMC moves from β .

Figure 6.1: Energy surface of the saddle points. The color scale is in the units of ϵ . Artificial smoothing is used for better visualization.



$\mathbf{P}^{(0)}$. This deconditioning procedure [124] entails a statistically exact randomization. In practice, escape paths are constructed by drawing random deviates from the Gamma, binomial and negative binomial distributions whose shape parameters are contained in the path factorization.

In brief, kPS detects kinetic trapping on the fly, charts the trapping basin sequentially, state by state, achieves high computational efficiency by eliminating the most trapping states owing to the ongoing path factorization [122, 126, 125] and generates statistically correct exit times from the charted basins. A description of the kPS algorithm is given in Ref. [124] and its supplemental materials.

6.3 Application to diffusion in a disordered substrate

We first apply kPS to simulations of a random walker on a disordered energy landscape (substrate) [127]. The substrate is a periodically replicated 256×256 fragment of the square lattice on which the walker hops to its four nearest-neighbour (NN) sites with transition rates

$$M_{\beta\gamma} = \exp \left[(E_{\beta} - E_{\beta\gamma}^s) / T \right],$$

where T is the temperature, E_{β} the site energy and $E_{\beta\gamma}^s$ the saddle energy between sites β and γ . The energy landscape is purposefully constructed to contain trapping basins of widely distributed sizes and depths (see the Supplemental Material [124] for details) and is centered around the walker's initial position next to the lowest energy saddle (Fig. 6.1).

When performed at temperature $T = 2.5$, standard kMC simulations (with hops only to the NN sites) are efficient enabling the walker to explore the entire substrate. However at $T = 1$, the walker remains trapped near its initial position repeatedly visiting states within a trapping basin. To chart a basin set \mathcal{E} for subsequent kPS simulations, the initial state 1 is eliminated at the very first iteration followed in sequence by the “most absorbing states” for which $P_{1\gamma}^{(n)}$ is found to be largest at the n -th iteration ($2 \leq n \leq N$). The expanding contours shown in Fig. 6.1 depict the absorbing boundary $\partial\mathcal{A}$ (perimeter of the basin) obtained after eliminating 2^7 , 2^9 , 2^{11} , 2^{12} , 2^{13} and 2^{14} states. The perimeter contour $\partial\mathcal{A}$ consists of all states γ for which $P_{1\gamma}^{(N)}$ is nonzero.

To demonstrate correctness of kPS, we generated 10^4 paths starting from state $(127, 127)$ and ending at the absorbing boundary $\partial\mathcal{A}$ of the basin containing $N = 2^{13}$ states, using both kPS and kMC at $T = 2.5$. The perfect match between the two estimated distributions of exit times is shown in Fig. 6.2.a. The mean times of exit to $\partial\mathcal{A}$ are plotted as a function of the number of eliminated states at $T = 2.5$ and $T = 1.0$ in Fig. 6.2.b, while the costs of both methods are compared in Fig. 6.2.c. At $T = 1.0$, kMC trajectories are trapped and never reach $\partial\mathcal{A}$: in this case we plot the expectation value for the number of kMC hops required to exit \mathcal{E} which is always available

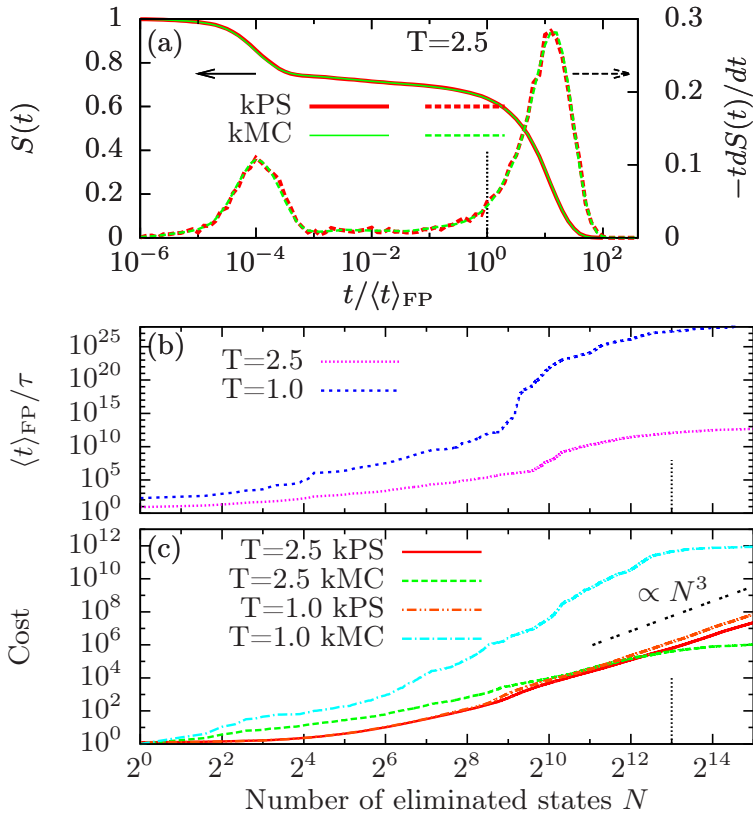


Figure 6.2: (a) The probability $S(t)$ for the walker to remain within a trapping basin containing $N = 2^{13}$ states (solid line) and the distribution of times of escape out of the same basin (dashed lines) using a log scale for the bins; (b) The mean first-passage time $\langle t \rangle_{\text{FP}}$ as a function of the number of states N included in the trapping basin; (c) Computational cost of kMC and kPS simulations as a function of N at two different temperatures (in the units of a single kMC hop).

after path factorization [125]. We observe that the kPS cost scales as N^3 , as expected for this factorization, and exceeds that of kMC for $N > 2^{12}$ at $T=2.5$. However, at $T=1$ trapping becomes severe rendering the standard kMC inefficient and the wall clock speedup achieved by kPS is four orders of magnitude for $N = 2^{15}$. We observe that in kPS the net cost of generating an exit trajectory is nearly independent of the temperature but grows exponentially with the decreasing temperature in kMC. At the same time, an accurate measure of the relative efficiency of kPS and kMC is always available in path factorization, allowing one to revert to the standard kMC whenever it is relatively more efficient. Thus, when performed correctly, a stochastic simulation combining kPS and kMC should always be more efficient than kMC alone.

6.4 Application to phase separation kinetics in FeCu

As a second illustration, we apply kPS to simulate the kinetics of copper precipitation in iron within a lattice model parameterized using electronic structure calculations [128]. The simulation volume is a periodically replicated fragment of the body centered cubic lattice with $128 \times 128 \times 128$ sites on which 28,163 Cu atoms are initially randomly dispersed. Fe atoms occupy all the remaining lattice sites except one that is left vacant allowing atom diffusion to occur by vacancy (V) hopping to one of its NN lattice sites. Its formation energy being substantially lower in Cu than in Fe, the vacancy is readily trapped in Cu precipitates rendering kMC grossly inefficient below 550 K [128]. Whenever the vacancy is observed to attach to a Cu cluster, we perform kPS over a pre-charted set \mathcal{E} containing N trapping states that correspond to all possible vacancy positions inside the VCu_{N-1} cluster containing $N - 1$ Cu atoms: the shape of the trapping cluster is fixed at the instant when the vacancy first attaches. The fully factored matrix $\mathbf{P}^{(N)}$ is then used to propagate the vacancy to a lattice site just outside the fixed cluster shape which is often followed by vacancy returning to the same cluster. If the newly formed trapping cluster has the same shape as before, the factorized matrix is used again to sample yet another escape. However a new path factorization (kPS cycle) is performed whenever the vacancy re-attaches to the same Cu cluster but in a different cluster shape or attaches to another Cu cluster (see the Supplementary Material for additional simulation details [124]).

We simulated copper precipitation in iron at three different temperatures $T_0 = 273$ K, $T_1 = 373$ K and $T_2 = 473$ K for which the atomic fraction of Cu atoms used in our simulations significantly exceeds copper

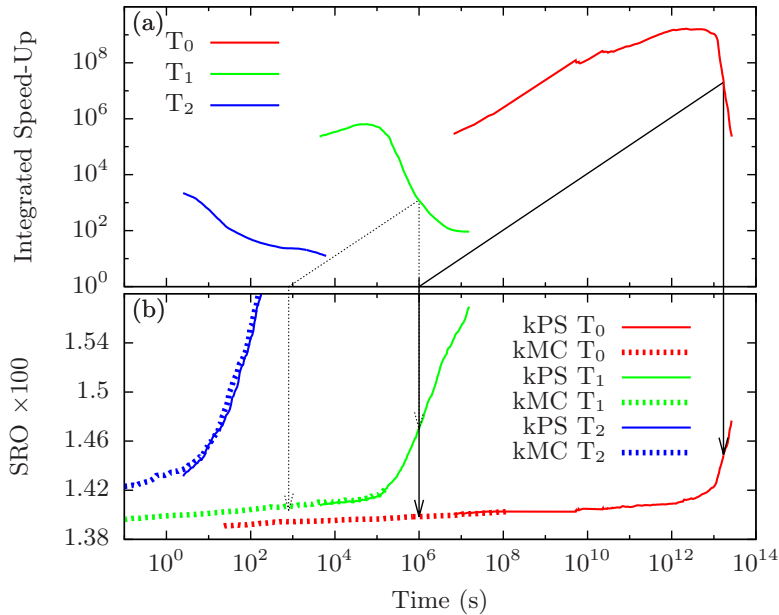


Figure 6.3: (a) Integrated speed-up plotted as a function of the physical time simulated by kPS; (b) Time evolution of the averaged SRO in kPS and kMC simulations at three different temperatures.

solubility limits in iron. Defined as the ratio of physical time simulated by kPS to that reached in kMC simulations over the same wall clock time, the integrated speed-up is plotted in Fig. 6.3.a. as a function of the physical time simulated by kPS (averaged over 41 simulations for each method and at each temperature).

The precipitation kinetics are monitored through the evolution of the volume-averaged Warren-Cowley short-range order (SRO) parameter [98] shown in Fig. 6.3.b both for kPS and kMC simulations. At T_0 and T_1 the kinetics proceed through a distinct incubation stage reminiscent to a time lag associated with repeated re-dissolution of subcritical nuclei prior to reaching the critical size in the classical nucleation theory [129]. However, “incubation” observed here is of a distinctly different nature since all our simulated solid solutions are thermodynamically unstable and even the smallest of Cu clusters, once formed, never dissolve. At all three temperatures the growth of VCu_{N-1} clusters is observed to proceed not through the attachment of mobile V-Cu dimers but primarily through the cluster’s own diffusion and sweeping of neighboring immobile Cu monomers [124]. This is consistent with an earlier study that also suggested that, rather counter-intuitively, the diffusivity of VCu_{N-1} clusters should increase with the increasing N before tapering off at $N = 30 \div 100$ (see Fig. 9 of Ref. [128]). We further observe that at T_0 the cross-over from the slow initial “incubation” to faster “agglomeration” growth seen on 6.3.b occurs concomitantly with the largest cluster growing to 15-16 Cu atoms [124]. Individual realizations of the stochastic precipitation kinetics reveal that, in addition to $N = 15$, cluster growth slows down again once the cluster reaches $N = 23, 27, 35$ and so on (see figure S4 in the Supplementary Materials). Leaving precise characterization of these transitions to future work, we speculate that the observed “magic numbers” correspond to compact clusters with fully filled nearest-neighbor shells in which vacancy trapping is particularly strong reducing the rate of shape-modifying vacancy escapes required for cluster diffusion.

Numerically, as expected, the integrated speed-up rapidly increases with the decreasing temperature as vacancy trapping becomes more severe. Two line segments of unit slope and two pairs of vertical arrows are drawn in Fig. 6.3 to compare evolution stages achievable within kPS and kMC over the same wall clock time. As marked by the pair of two solid vertical arrows on the right, the integrated speed-up exceeds seven orders of magnitude at T_0 . Subsequent reduction in the speed-up coincides with the transition into the agglomeration regime where increasingly large VCu clusters repeatedly visit increasingly large number of distinct shapes. To understand the origin of the efficiency decrease, we have monitored the number of distinct shapes of the vacancy-copper cluster. For a V-Cu₃₀ cluster, we found that, over the 10^3 last factorizations that have been performed, there are only 21 different cluster shapes and that the 5 most frequent shapes occur with a frequency of about 60%. Indeed, the efficiency of kPS simulations for this particular model can be improved by indexing distinct cluster shapes for each cluster size and storing the path factorizations to allow for their repeated use during

the simulations [130, 131]. In any case, given its built-in awareness of the relative cost measured in kMC hops, kPS is certain to enable more efficient simulations of diffusive phase transformations in various technologically important materials. In particular, it is tempting to relate an anomalously long incubation stage observed in aluminium alloys with Mg, Si and Se additions [132] to possible trapping of vacancies on Se, similar to the retarding effect of Cu on the ageing kinetics reported here for the Fe-Cu alloys.

6.5 Summary

A kinetic Path Sampling algorithm suitable for simulating the evolution of systems prone to kinetic trapping is developed. Unlike most other algorithms dealing with this numerical bottleneck [115, 116, 117, 133, 134, 130], kPS does not require any *a priori* knowledge of the properties of the trapping basin. It relies on an iterative path factorization of the evolution operator to chart possible escapes, measures its own relative cost and reverts to standard kMC if the added efficiency no longer offsets its computational overhead. At the same time, the kPS algorithm is exact and samples stochastic trajectories from the same statistical ensemble as the standard kMC algorithms. The proposed method is less sensible to kinetic trapping and performs well under simulation conditions where the standard kMC simulations slows down to a crawl. In particular, it reaches later stages of phase separation in the Fe-Cu system and captures a qualitatively new kinetics and mechanism of copper precipitation. The kPS method is well positioned to extend the range of applicability of stochastic simulations beyond their current limits.

Perspectives kPS should be combined with spatial protection [121] and synchronous or asynchronous algorithms to enable efficient parallel simulations of a still wider class of large-scale stochastic models [135, 136, 137]. A synchronization issue occurs when, at a given time, a mobile defect enters a trapping basin already containing a defect. The location of the latter defect needs to be known. This requires solving the (restricted) master equation governing the evolution of the latter defect conditioned by the fact that it did not reach the absorbing boundary. Remarkably, removing the absorbing boundaries will suppress the sources of irreversibility and will make it possible to symmetrize the evolution operator via similarity transformation based on detailed balance condition satisfied for intra-basin transitions. The subsequent eigenvalue decomposition should be greatly facilitated by this symmetrization.

Conclusion and perspectives

Molecular simulations methods usually requires to vary the value of an external parameter λ within a specified range A . In such problems, enhanced ergodicity is achieved if simulations are performed in an expanded ensemble wherein the external parameter behaves like an additional coordinate subject to an auxiliary biasing force. The various methods of computing thermodynamic expectations and free energies which can be used in the expanded ensemble framework are reviewed below

- (a) *Thermodynamic integration* to estimate the derivative of the free energy along λ and then to obtain the free energy through integration by numerical quadrature. This approach resorts to a binning estimator and is used in combination with adaptive biasing force method to construct an auxiliary biasing potential that converges towards the free energy.
- (b) *Thermodynamic occupation* to directly extract the free energy from occupation probabilities. This approach is based on a binning estimator and may also be employed to adapt the biasing potential directly on the free energy along λ .
- (c) *Free energy perturbation* to extract the free energies from partition function ratios using a simple standard reweighting estimator. This approach requires substantial overlaps between the various λ -samples and has been rarely used.
- (d) Post-treatment procedures such as the *self-consistent reweighting* estimator based on Bennett acceptance ratio method (STWHAM) or the *histogram reweighting* estimator based on thermodynamic integration along the reaction coordinate (CZAR). The goal is to estimate the desired thermodynamic property more accurately than with estimators (a-c). The latter procedure is employed to compute the free energy along reaction coordinates using mechanical restraints.

Remarkably, conditioning over the external parameter in the expanded ensemble provides us with a unifying methodology: once conditioned, the various estimators associated with methods (a-d) become equivalent and exhibit systematically reduced statistical variances. In practice, simulations performed with the conditioned estimators are facilitated by the fact that the external parameter need not being sampled. Characterizing the structural transition temperature in LJ₃₈ has been shown to be a simple task.

Furthermore, the proposed unifying approach is amenable to path sampling simulations involving the estimation of rate constants in rare-event problems or the calculation of free energies in difficult problem presenting spurious metastability.

The avenue for future research on the conditioned estimators will involve formulating and constructing biasing potentials that allow optimal variance reduction for estimating thermodynamic expectations within a given set of external parameter values. The feasibility of the biasing potential optimization is demonstrated in Appendix C where an optimal biasing potential is constructed adaptively using a partial biasing technique [138]. Preliminary results are promising. This optimization approach compare favorably with the one that would be developed for the replica exchange method (see Sec. 1.6), for which optimally allocating the replicas along the external parameter is a difficult task, especially if a self-consistent estimator is used to postprocess the harvested data.

The advocated conditioning approaches are well positioned to further extend the range of applicability of Monte Carlo and molecular dynamics techniques to the calculation of free energies and thermodynamic properties in condensed matter systems. From a broad perspective, we enumerate below several possible extensions of the conditioning approach to expanded ensembles together with applicability domains of materials science:

1. developing a method for performing simulations in a semi-grand expanded ensemble wherein the difference of chemical potentials is the external parameter. The goal is to estimate isotherms of both the canonical

and semi-grand canonical ensembles in a single run owing to conditioning. Specific applications would involve calculating solubility limits of Ni, Si, Mn, Cu impurities in α -iron;

2. enabling the expanded transition path sampling method to extract free energy barriers along some collective variables concomitantly with the time correlation function. Combining with the activation-relaxation technique to focus the efforts in the vicinity of saddle states. Application would involve the migration and transformation of extended defects and impurities in alloys;
3. calculating the rate of vacancy emission from multi-component clusters by combining adaptively biased sampling techniques and a time rescaling technique based on the quasi-equilibrium assumption [139]; applications would involve the numerous high-dimensional problems that are intractable to path factorization due to combinatorial explosion;
4. monitoring the Gibbs statistical entropy of a supercooled liquid through its jamming transition, using adaptively biased simulations performed in an expanded nonequilibrium path ensemble [95]. The goal is to investigate from a fundamental viewpoint the behavior of the statistical entropy when a glass forms from a metastable liquid assumed to be in a local equilibrium. Gibbs entropy, which can not be measured experimentally out of equilibrium, is a measure of the phase space volume of the system that coincides with Boltzmann's entropy at equilibrium.

Bibliography

- [1] D. Brillinger. “The calculation of cumulants via conditioning”. In: *Annals of the Institute of Statistical Mathematics* 21.1 (1969), pp. 215–218 (cit. on pp. v, 108).
- [2] D. Frenkel. “Speed-up of Monte Carlo simulations by sampling of rejected states”. In: *Proceedings of the National Academy of Sciences of the United States of America* 101.51 (2004), pp. 17571–17575 (cit. on pp. v, 17, 77).
- [3] B. Jourdain. *Probabilités et statistique*. <http://cermics.enpc.fr/~jourdain/probostat/poly.pdf>. 2013 (cit. on pp. vi, 108, 109).
- [4] G. E. Crooks. “Entropy production fluctuation theorem and the nonequilibrium work relation for free energy differences”. In: *Phys. Rev. E* 60 (3 1999), pp. 2721–2726 (cit. on pp. vi, 51, 57).
- [5] G. E. Crooks. “Path-ensemble averages in systems driven far from equilibrium”. In: *Phys. Rev. E* 61 (3 2000), pp. 2361–2366 (cit. on pp. vi, 51, 58).
- [6] C. Dellago, P. G. Bolhuis, F. S. Csajka, and D. Chandler. “Transition path sampling and the calculation of rate constants”. In: *The Journal of Chemical Physics* 108.5 (1998), pp. 1964–1977 (cit. on pp. vii, 22, 69).
- [7] P. G. Bolhuis, D. Chandler, C. Dellago, and P. L. Geissler. “TRANSITION PATH SAMPLING: Throwing Ropes Over Rough Mountain Passes, in the Dark”. In: *Annual Review of Physical Chemistry* 53.1 (2002). PMID: 11972010, pp. 291–318 (cit. on pp. vii, 22, 32, 51, 69, 91).
- [8] P. Terrier, M.-C. Marinica, and M. Athènes. “Using Bayes formula to estimate rates of rare events in transition path sampling simulations”. In: *The Journal of Chemical Physics* 143.13, 134121 (2015) (cit. on pp. vii, 12, 14, 29, 30, 69, 72).
- [9] J.-F. Delmas and B. Jourdain. “Does waste recycling really improve the multi-proposal Metropolis–Hastings algorithm? An analysis based on control variates”. In: *J. Appl. Probab.* 46.4 (Dec. 2009), pp. 938–959 (cit. on pp. vii, 17, 77, 78, 80–82, 86).
- [10] G. Adjanor, M. Athènes, and J. Rodgers. “Waste-recycling Monte Carlo with optimal estimates: Application to free energy calculations in alloys”. In: *The Journal of Chemical Physics* 135.4, 044127 (2011), pp. – (cit. on pp. vii, 82–84, 86).
- [11] M. Dufflo. *Random Iterative Models*. Vol. 34. Applications of Mathematics. Berlin Heidelberg: Springer-Verlag, 1997 (cit. on p. 3).
- [12] G. Torrie and J. Valleau. “Nonphysical sampling distributions in Monte Carlo free-energy estimation: Umbrella sampling”. In: *Journal of Computational Physics* 23.2 (1977), pp. 187–199 (cit. on pp. 5, 14, 25).
- [13] R. W. Zwanzig. “High-Temperature Equation of State by a Perturbation Method. I. Nonpolar Gases”. In: *The Journal of Chemical Physics* 22.8 (1954), pp. 1420–1426 (cit. on pp. 6, 14, 24).
- [14] D. Frenkel and B. Smit. *Understanding molecular simulation: from algorithms to applications*. Academic Press, 2001 (cit. on pp. 6, 14, 21, 24, 40, 52, 54, 69, 89).
- [15] T. Lelièvre, M. Rousset, and G. Stoltz. *Free energy computations: a mathematical perspective*. London: Imperial College Press, 2010 (cit. on pp. 6, 7, 11, 14, 42, 43, 52, 54).
- [16] C. H. Bennett. “Efficient estimation of free energy differences from Monte Carlo data”. In: *Journal of Computational Physics* 22.2 (1976), pp. 245–268 (cit. on pp. 6, 7, 32, 34).
- [17] A. M. Ferrenberg and R. H. Swendsen. “Optimized Monte Carlo data analysis”. In: *Phys. Rev. Lett.* 63 (12 1989), pp. 1195–1198 (cit. on p. 6).
- [18] M. R. Shirts and J. D. Chodera. “Statistically optimal analysis of samples from multiple equilibrium states”. In: *The Journal of Chemical Physics* 129.12, 124105 (2008), p. 124105 (cit. on pp. 6, 7, 9, 19).
- [19] R. H. Swendsen and J.-S. Wang. “Replica Monte Carlo Simulation of Spin-Glasses”. In: *Phys. Rev. Lett.* 57 (21 1986), pp. 2607–2609 (cit. on pp. 6, 7).

- [20] C. Geyer. *Estimating Normalizing Constants and Reweighting Mixtures*. Technical Report 568. School of Statistics University of Minnesota, 1994 (cit. on p. 6).
- [21] A. Gelman and X.-L. Meng. “Simulating normalizing constants: from importance sampling to bridge sampling to path sampling”. In: *Statist. Sci.* 13.2 (May 1998), pp. 163–185 (cit. on p. 6).
- [22] Z. Tan, E. Gallicchio, M. Lapelosa, and R. M. Levy. “Theory of binless multi-state free energy estimation with applications to protein-ligand binding”. In: *The Journal of Chemical Physics* 136.14 (2012), p. 144102 (cit. on pp. 6, 19).
- [23] A. Kong, P. McCullagh, X.-L. Meng, D. Nicolae, and Z. Tan. “A theory of statistical models for Monte Carlo integration”. In: *Journal of the Royal Statistical Society: Series B (Statistical Methodology)* 65.3 (2003), pp. 585–604 (cit. on p. 6).
- [24] Z. Tan. “On a likelihood approach for Monte-Carlo integration”. In: *Journal of the American Statistical Association* 99 (2004), pp. 1027–1037 (cit. on pp. 6, 7).
- [25] Y. Sugita and Y. Okamoto. “Replica-exchange molecular dynamics method for protein folding”. In: *Chemical Physics Letters* 314.1–2 (1999), pp. 141–151 (cit. on p. 7).
- [26] T. T. Pham and M. R. Shirts. “Optimal pairwise and non-pairwise alchemical pathways for free energy calculations of molecular transformation in solution phase”. In: *The Journal of Chemical Physics* 136.12 (2012), p. 124120 (cit. on p. 7).
- [27] A. P. Lyubartsev, A. A. Martsinovski, S. V. Shevkunov, and P. N. Vorontsov-Velyaminov. “New approach to Monte Carlo calculation of the free energy: Method of expanded ensembles”. In: *The Journal of Chemical Physics* 96.3 (1992), pp. 1776–1783 (cit. on pp. 9, 14).
- [28] P. J. Steinhardt, D. R. Nelson, and M. Ronchetti. “Bond-orientational order in liquids and glasses”. In: *Phys. Rev. B* 28 (2 1983), pp. 784–805 (cit. on pp. 10, 38, 45, 49).
- [29] S. Park and V. S. Pande. “Choosing weights for simulated tempering”. In: *Phys. Rev. E* 76 (1 2007), p. 016703 (cit. on p. 10).
- [30] E. Darve and A. Pohorille. “Calculating free energies using average force”. In: *The Journal of Chemical Physics* 115.20 (2001), pp. 9169–9183 (cit. on pp. 11, 45, 115).
- [31] E. Darve, D. Rodríguez-Gómez, and A. Pohorille. “Adaptive biasing force method for scalar and vector free energy calculations”. In: *The Journal of Chemical Physics* 128.14, 144120 (2008), p. 144120 (cit. on pp. 11, 45, 115).
- [32] T. Lelièvre, M. Rousset, and G. Stoltz. “Long-time convergence of an adaptive biasing force method”. In: *Non-linearity* 21.6 (2008), p. 1155 (cit. on pp. 11, 42, 43).
- [33] A. V. Brukhno, T. V. Kuznetsova, A. P. Lyubartsev, and P. Vorontsov-Vel’yaminov. “Calculation of the Free Energy of Polymers Within the Framework of Lattice and Continuum Models by Molecular Simulation Methods Using Expanded Statistical Ensembles”. In: *Vysokomolekuliarnye soedineniia. Seriya A i Seriya B* 38.1 (1996), pp. 77–83 (cit. on pp. 11, 42, 114).
- [34] L. Cao, G. Stoltz, T. Lelièvre, M.-C. Marinica, and M. Athènes. “Free energy calculations from adaptive molecular dynamics simulations with adiabatic reweighting”. In: *The Journal of Chemical Physics* 140.10, 104108 (2014), p. 104108 (cit. on pp. 12, 25, 43–45, 49, 115, 122).
- [35] J. D. Chodera, W. C. Swope, J. W. Pitera, C. Seok, and K. A. Dill. “Use of the Weighted Histogram Analysis Method for the Analysis of Simulated and Parallel Tempering Simulations”. In: *Journal of Chemical Theory and Computation* 3.1 (2007), pp. 26–41 (cit. on pp. 14, 19, 111).
- [36] J. Lidmar. “Improving the efficiency of extended ensemble simulations: The accelerated weight histogram method”. In: *Phys. Rev. E* 85 (5 2012), p. 056708 (cit. on p. 17).
- [37] J. D. Chodera and M. R. Shirts. “Replica exchange and expanded ensemble simulations as Gibbs sampling: Simple improvements for enhanced mixing”. In: *The Journal of Chemical Physics* 135.19, 194110 (2011), p. 194110 (cit. on pp. 17, 77).
- [38] D. Frenkel. “Waste-Recycling Monte Carlo”. In: *Computer Simulations in Condensed Matter Systems: From Materials to Chemical Biology Volume 1*. Berlin, Heidelberg: Springer Berlin Heidelberg, 2006, pp. 127–137 (cit. on pp. 18, 77, 86).
- [39] D. Chandler. “Statistical mechanics of isomerization dynamics in liquids and the transition state approximation”. In: *The Journal of Chemical Physics* 68.6 (1978), pp. 2959–2970 (cit. on p. 21).
- [40] A. Lesage, T. Lelièvre, G. Stoltz, and J. Hémin. “Smoothed Biasing Forces Yield Unbiased Free Energies with the Extended-System Adaptive Biasing Force Method”. In: *The Journal of Physical Chemistry B* 121.15 (2017), pp. 3676–3685 (cit. on pp. 23, 25, 44).

- [41] D. Chandler. *Introduction to modern statistical mechanics*. Oxford University Press, 1987 (cit. on pp. 24, 69).
- [42] D. Wales. *Energy Landscapes*. Cambridge Molecular Science. Cambridge, UK: Cambridge University Press, 2003 (cit. on pp. 24, 45, 60, 117, 122).
- [43] J. G. Kirkwood. “Statistical Mechanics of Fluid Mixtures”. In: *The Journal of Chemical Physics* 3.5 (1935), pp. 300–313 (cit. on p. 24).
- [44] M. Athènes. “Computation of a chemical potential using a residence weight algorithm”. In: *Phys. Rev. E* 66 (4 2002), p. 046705 (cit. on pp. 29, 40, 41, 51, 86).
- [45] M. Athènes. “A path-sampling scheme for computing thermodynamic properties of a many-body system in a generalized ensemble”. English. In: *The European Physical Journal B - Condensed Matter and Complex Systems* 38.4 (2004), pp. 651–663 (cit. on pp. 29, 51, 53, 56, 83, 84, 86).
- [46] G. Adjanor and M. Athènes. “Gibbs free-energy estimates from direct path-sampling computations”. In: *The Journal of Chemical Physics* 123.23, 234104 (2005) (cit. on pp. 29, 51, 83, 84, 86, 87).
- [47] M. Athènes, M.-C. Marinica, and T. Jourdan. “Estimating time-correlation functions by sampling and unbiasing dynamically activated events”. In: *The Journal of Chemical Physics* 137.19, 194107 (2012), pp. – (cit. on pp. 32, 54, 69, 71–74).
- [48] M. Athènes. “Web ensemble averages for retrieving relevant information from rejected Monte Carlo moves”. English. In: *The European Physical Journal B* 58.1 (2007), pp. 83–95 (cit. on pp. 32, 77).
- [49] W. Li and A. Ma. “Recent developments in methods for identifying reaction coordinates”. In: *Molecular Simulation* 40.10-11 (2014), pp. 784–793 (cit. on p. 40).
- [50] S. Marsili, A. Barducci, R. Chelli, P. Procacci, and V. Schettino. “Self-healing Umbrella Sampling: A Non-equilibrium Approach for Quantitative Free Energy Calculations”. In: *The Journal of Physical Chemistry B* 110.29 (2006). PMID: 16854090, pp. 14011–14013 (cit. on p. 42).
- [51] A. Laio and M. Parrinello. “Escaping free-energy minima”. In: *Proceedings of the National Academy of Sciences* 99.20 (2002), pp. 12562–12566 (cit. on pp. 42, 43).
- [52] G. Fort, B. Jourdain, E. Kuhn, T. Lelièvre, and G. Stoltz. “Convergence of the Wang-Landau algorithm”. In: *AMRX Appl.Math.Res.Express* 2014 (2014), pp. 275–311 (cit. on p. 42).
- [53] M. A. Cuendet and M. E. Tuckerman. “Free Energy Reconstruction from Metadynamics or Adiabatic Free Energy Dynamics Simulations”. In: *Journal of Chemical Theory and Computation* 10.8 (2014). PMID: 26588271, pp. 2975–2986 (cit. on p. 43).
- [54] M. Iannuzzi, A. Laio, and M. Parrinello. “Efficient Exploration of Reactive Potential Energy Surfaces Using Car-Parrinello Molecular Dynamics”. In: *Phys. Rev. Lett.* 90 (23 2003), p. 238302 (cit. on p. 43).
- [55] A. Laio and F. L. Gervasio. “Metadynamics: a method to simulate rare events and reconstruct the free energy in biophysics, chemistry and material science”. In: *Reports on Progress in Physics* 71.12 (2008), p. 126601 (cit. on p. 43).
- [56] V. Lindahl, J. Lidmar, and B. Hess. “Accelerated weight histogram method for exploring free energy landscapes”. In: *The Journal of Chemical Physics* 141.4 (2014), p. 044110 (cit. on p. 44).
- [57] J. P. Neirotti, F. Calvo, D. L. Freeman, and J. D. Doll. “Phase changes in 38-atom Lennard-Jones clusters. I. A parallel tempering study in the canonical ensemble”. In: *The Journal of Chemical Physics* 112.23 (2000), pp. 10340–10349 (cit. on p. 45).
- [58] F. Calvo, J. P. Neirotti, D. L. Freeman, and J. D. Doll. “Phase changes in 38-atom Lennard-Jones clusters. II. A parallel tempering study of equilibrium and dynamic properties in the molecular dynamics and microcanonical ensembles”. In: *The Journal of Chemical Physics* 112.23 (2000), pp. 10350–10357 (cit. on p. 45).
- [59] J. Comer, J. C. Gumbart, J. Hénin, T. Lelièvre, A. Pohorille, and C. Chipot. “The Adaptive Biasing Force Method: Everything You Always Wanted To Know but Were Afraid To Ask”. In: *The Journal of Physical Chemistry B* 119.3 (2015). PMID: 25247823, pp. 1129–1151 (cit. on p. 45).
- [60] Z. Tan. “Optimally adjusted mixture sampling and locally weighted histogram analysis”. In: *Journal of Computational and Graphical Statistics*.ja (2015) (cit. on p. 49).
- [61] C. Dellago and G. Hummer. “Computing Equilibrium Free Energies Using Non-Equilibrium Molecular Dynamics”. In: *Entropy* 16.1 (2014), pp. 41–61 (cit. on p. 51).
- [62] C. Jarzynski. “Nonequilibrium Equality for Free Energy Differences”. In: *Phys. Rev. Lett.* 78 (14 1997), pp. 2690–2693 (cit. on pp. 51, 52, 54, 57).
- [63] G. Adjanor, M. Athènes, and F. Calvo. “Free energy landscape from path-sampling: application to the structural transition in LJ38”. English. In: *The European Physical Journal B - Condensed Matter and Complex Systems* 53.1 (2006), pp. 47–60 (cit. on pp. 51, 53, 56, 59, 66).

- [64] C. Jarzynski. “Nonequilibrium work relations: foundations and applications”. In: *The European Physical Journal B* 64.3 (2008), pp. 331–340 (cit. on pp. 52, 64).
- [65] L. Maragliano and E. Vanden-Eijnden. “A temperature accelerated method for sampling free energy and determining reaction pathways in rare events simulations”. In: *Chemical Physics Letters* 426.1–3 (2006), pp. 168–175 (cit. on p. 53).
- [66] M. Athènes and M.-C. Marinica. “Free energy reconstruction from steered dynamics without post-processing”. In: *Journal of Computational Physics* 229.19 (2010), pp. 7129–7146 (cit. on pp. 53, 54, 56, 64–66, 71, 116).
- [67] G. Hummer and A. Szabo. “Free energy reconstruction from nonequilibrium single-molecule pulling experiments”. In: *Proceedings of the National Academy of Sciences* 98.7 (2001), pp. 3658–3661 (cit. on p. 60).
- [68] G. N. Bochkov and Y. E. Kuzovlev. “Contribution to general theory of thermal fluctuations in nonlinear-systems”. In: *Journal of Experimental and Theoretical Physics* 72 (1977), 238–247 (cit. on p. 64).
- [69] G. N. Bochkov and Y. E. Kuzovlev. “Nonlinear fluctuation-dissipation relations and stochastic models in nonequilibrium thermodynamics. I. Generalized fluctuation-dissipation theorem”. In: *Physica A Statistical Mechanics and its Applications* 106 (Apr. 1981), pp. 443–479 (cit. on p. 64).
- [70] J. Horowitz and C. Jarzynski. “Comparison of work fluctuation relations”. In: *Journal of Statistical Mechanics: Theory and Experiment* 2007.11 (2007), P11002 (cit. on p. 64).
- [71] I. Coluzza and D. Frenkel. “Virtual-Move Parallel Tempering”. In: *ChemPhysChem* 6.9 (2005), pp. 1779–1783 (cit. on p. 66).
- [72] G. J. Ackland, M. I. Mendeleev, D. J. Srolovitz, S. Han, and A. V. Barashev. “Development of an interatomic potential for phosphorus impurities in α -iron”. In: *Journal of Physics: Condensed Matter* 16.27 (2004), S2629 (cit. on p. 66).
- [73] M. Marchese, G. De Lorenzi, G. Jacucci, and C. P. Flynn. “Jump dynamics and the isotope effect in solid-state diffusion”. In: *Phys. Rev. Lett.* 57 (26 1986), pp. 3280–3283 (cit. on p. 68).
- [74] P. Hänggi, P. Talkner, and M. Borkovec. “Reaction-rate theory: fifty years after Kramers”. In: *Rev. Mod. Phys.* 62 (2 1990), pp. 251–341 (cit. on pp. 69, 74).
- [75] E. Vanden-Eijnden and F. A. Tal. “Transition state theory: Variational formulation, dynamical corrections, and error estimates”. In: *The Journal of Chemical Physics* 123.18 (2005), p. 184103 (cit. on p. 69).
- [76] T. S. van Erp and P. G. Bolhuis. “Elaborating transition interface sampling methods”. In: *Journal of Computational Physics* 205.1 (2005), pp. 157–181 (cit. on pp. 69, 74).
- [77] G. T. Barkema and N. Mousseau. “Event-Based Relaxation of Continuous Disordered Systems”. In: *Phys. Rev. Lett.* 77 (21 1996), pp. 4358–4361 (cit. on pp. 71, 72).
- [78] N. Mousseau and G. T. Barkema. “Traveling through potential energy landscapes of disordered materials: The activation-relaxation technique”. In: *Phys. Rev. E* 57 (2 1998), pp. 2419–2424 (cit. on pp. 71, 72).
- [79] L. J. Munro and D. J. Wales. “Defect migration in crystalline silicon”. In: *Phys. Rev. B* 59 (6 1999), pp. 3969–3980 (cit. on p. 71).
- [80] G. Henkelman and H. Jónsson. “A dimer method for finding saddle points on high dimensional potential surfaces using only first derivatives”. In: *The Journal of Chemical Physics* 111.15 (1999), pp. 7010–7022 (cit. on p. 71).
- [81] E. Cancès, F. Legoll, M.-C. Marinica, K. Minoukadeh, and F. Willaime. “Some improvements of the activation-relaxation technique method for finding transition pathways on potential energy surfaces”. In: *The Journal of Chemical Physics* 130.11 (2009), p. 114711 (cit. on pp. 71, 72).
- [82] R. J. Hinde, R. S. Berry, and D. J. Wales. “Chaos in small clusters of inert gas atoms”. In: *The Journal of Chemical Physics* 96.2 (1992), pp. 1376–1390 (cit. on p. 71).
- [83] C. Amtrano and R. S. Berry. “Probability distributions of local Liapunov exponents for small clusters”. In: *Phys. Rev. Lett.* 68 (6 1992), pp. 729–732 (cit. on p. 71).
- [84] Z. Sándor, B. Érdi, A. Széll, and B. Funk. “The Relative Lyapunov Indicator: An Efficient Method of Chaos Detection”. In: *Celestial Mechanics and Dynamical Astronomy* 90.1 (2004), pp. 127–138 (cit. on p. 71).
- [85] J. Tailleur and J. Kurchan. “Probing rare physical trajectories with Lyapunov weighted dynamics”. In: *Nature Physics* 3 (2007), pp. 203–207 (cit. on p. 71).
- [86] F. Calvo. “Chaos and dynamical coexistence in Lennard-Jones clusters”. In: *The Journal of Chemical Physics* 108.16 (1998), pp. 6861–6867 (cit. on p. 71).
- [87] P. Geiger and C. Dellago. “Identifying rare chaotic and regular trajectories in dynamical systems with Lyapunov weighted path sampling”. In: *Chemical Physics* 375.2 (2010). Stochastic processes in Physics and Chemistry (in honor of Peter Hänggi), pp. 309–315 (cit. on p. 71).

- [88] C. Giardina, J. Kurchan, V. Lecomte, and J. Tailleur. “Simulating Rare Events in Dynamical Processes”. In: *Journal of Statistical Physics* 145.4 (2011), pp. 787–811 (cit. on p. 71).
- [89] M. Picciani, M. Athènes, J. Kurchan, and J. Tailleur. “Simulating structural transitions by direct transition current sampling: The example of LJ(38)”. In: *Journal of Chemical Physics* 135.3 (2011) (cit. on p. 71).
- [90] C. Lanczos. *Applied Analysis*. Prentice Hall, 1961 (cit. on p. 72).
- [91] M.-C. Marinica, F. Willaime, and N. Mousseau. “Energy landscape of small clusters of self-interstitial dumbbells in iron”. In: *Phys. Rev. B* 83 (9 2011), p. 094119 (cit. on p. 72).
- [92] R. J. Allen, D. Frenkel, and P. R. ten Wolde. “Forward flux sampling-type schemes for simulating rare events: Efficiency analysis”. In: *The Journal of Chemical Physics* 124.19, 194111 (2006), pp. – (cit. on p. 74).
- [93] M. Athènes. “Parallel Monte Carlo simulations using a residence weight algorithm”. In: *Phys. Rev. E* 66 (1 2002), p. 016701 (cit. on p. 77).
- [94] G. C. Boulougouris and D. Frenkel. “Monte Carlo Sampling of a Markov Web”. In: *Journal of Chemical Theory and Computation* 1.3 (2005). PMID: 26641505, pp. 389–393 (cit. on p. 77).
- [95] M. Athènes and F. Calvo. “Multiple-Replica Exchange with Information Retrieval”. In: *ChemPhysChem* 9.16 (2008), pp. 2332–2339 (cit. on pp. 77, 98).
- [96] J. Kim, J. Rodgers, M. Athènes, and B. Smit. “Molecular Monte Carlo Simulations Using Graphics Processing Units: To Waste Recycle or Not?” In: *Journal of Chemical Theory and Computation* 7.10 (2011), 3208–3222 (cit. on pp. 82, 89, 90).
- [97] F. Ducastelle. *Order and phase stability in alloys*. English. Includes bibliographical references and indexes. Amsterdam ; New York : North-Holland ; New York, NY, USA : Sole distributors for the USA and Canada, Elsevier Science Pub. Co, 1991 (cit. on pp. 85, 87).
- [98] M. Athènes, P. Bellon, and G. Martin. “Effects of atomic mobilities on phase separation kinetics: a Monte-Carlo study”. In: *Acta Materialia* 48.10 (2000), pp. 2675–2688 (cit. on pp. 85, 95).
- [99] F. M. Ytreberg, R. H. Swendsen, and D. M. Zuckerman. “Comparison of free energy methods for molecular systems”. In: *The Journal of Chemical Physics* 125.18 (2006), p. 184114 (cit. on p. 86).
- [100] P. Olsson, J. Wallenius, C. Domain, K. Nordlund, and L. Malerba. “Two-band modeling of α -prime phase formation in Fe-Cr”. In: *Phys. Rev. B* 72 (21 2005), p. 214119 (cit. on p. 87).
- [101] C. Pareige, C. Domain, and P. Olsson. “Short- and long-range orders in Fe-Cr: A Monte Carlo study”. In: *Journal of Applied Physics* 106.10 (2009), p. 104906 (cit. on pp. 87, 89).
- [102] G. Bonny, R. Pasianot, L. Malerba, A. Caro, P. Olsson, and M. Lavrentiev. “Numerical prediction of thermodynamic properties of iron-chromium alloys using semi-empirical cohesive models: The state of the art”. In: *Journal of Nuclear Materials* 385.2 (2009). Nuclear Materials III, pp. 268–277 (cit. on pp. 87, 89).
- [103] D. Landau and K. Binder. *A Guide to Monte Carlo Simulations in Statistical Physics*. New York, NY, USA: Cambridge University Press, 2005 (cit. on p. 89).
- [104] J.-M. Lanore. “Simulation de l’évolution des défauts dans un réseau par le méthode de monte-carlo”. In: *Radiation Effects* 22.3 (1974), pp. 153–162 (cit. on pp. 91, 92).
- [105] A. Bortz, M. Kalos, and J. Lebowitz. “A new algorithm for Monte Carlo simulation of Ising spin systems”. In: *Journal of Computational Physics* 17.1 (1975), pp. 10–18 (cit. on p. 91).
- [106] D. T. Gillespie. “Exact stochastic simulation of coupled chemical reactions”. In: *The Journal of Physical Chemistry* 81.25 (1977), pp. 2340–2361 (cit. on p. 91).
- [107] N. G. Van Kampen. *Stochastic Processes in Physics and Chemistry*. Third Edition. Amsterdam: Elsevier, 2007, pp. iii – (cit. on p. 91).
- [108] S. Redner. *A guide to first-passage processes*. Cambridge: Cambridge University Press, 2001 (cit. on p. 91).
- [109] S. X. Sun. “Path Summation Formulation of the Master Equation”. In: *Phys. Rev. Lett.* 96 (21 2006), p. 210602 (cit. on p. 91).
- [110] B. Harland and S. X. Sun. “Path ensembles and path sampling in nonequilibrium stochastic systems”. In: *The Journal of Chemical Physics* 127.10 (2007), p. 104103 (cit. on p. 91).
- [111] C. D. V. Sical. “Stochastic method for accommodation of equilibrating basins in kinetic Monte Carlo simulations”. In: *Journal of Physics: Condensed Matter* 19.7 (2007), p. 072201 (cit. on p. 91).
- [112] N. Eidelson and B. Peters. “Transition path sampling for discrete master equations with absorbing states”. In: *The Journal of Chemical Physics* 137.9 (2012), p. 094106 (cit. on p. 91).
- [113] T. Mora, A. M. Walczak, and F. Zamponi. “Transition path sampling algorithm for discrete many-body systems”. In: *Phys. Rev. E* 85 (3 2012), p. 036710 (cit. on p. 91).

- [114] M. Manhart and A. V. Morozov. “Path-Based Approach to Random Walks on Networks Characterizes How Proteins Evolve New Functions”. In: *Phys. Rev. Lett.* 111 (8 2013), p. 088102 (cit. on p. 91).
- [115] M. A. Novotny. “Monte Carlo Algorithms with Absorbing Markov Chains: Fast Local Algorithms for Slow Dynamics”. In: *Phys. Rev. Lett.* 74 (1 1995), pp. 1–5 (cit. on pp. 92, 96).
- [116] G. C. Boulougouris and D. N. Theodorou. “Dynamical integration of a Markovian web: A first passage time approach”. In: *The Journal of Chemical Physics* 127.8 (2007), p. 084903 (cit. on pp. 92, 96).
- [117] M. Barrio, A. Leier, and T. T. Marquez-Lago. “Reduction of chemical reaction networks through delay distributions”. In: *The Journal of Chemical Physics* 138.10 (2013), p. 104114 (cit. on pp. 92, 96).
- [118] G. Nandipati, Y. Shim, and J. G. Amar. “First-passage time approach to kinetic Monte Carlo simulations of metal (100) growth”. In: *Phys. Rev. B* 81 (23 2010), p. 235415 (cit. on p. 92).
- [119] C. Moler and C. V. Loan. “Nineteen Dubious Ways to Compute the Exponential of a Matrix, Twenty-Five Years Later”. In: *SIAM Review* 45.1 (2003), pp. 3–49 (cit. on p. 92).
- [120] S. A. Serebrinsky. “Physical time scale in kinetic Monte Carlo simulations of continuous-time Markov chains”. In: *Phys. Rev. E* 83 (3 2011), p. 037701 (cit. on p. 92).
- [121] T. Opplestrup, V. V. Bulatov, G. H. Gilmer, M. H. Kalos, and B. Sadigh. “First-Passage Monte Carlo Algorithm: Diffusion without All the Hops”. In: *Phys. Rev. Lett.* 97 (23 2006), p. 230602 (cit. on pp. 92, 96).
- [122] M. Athènes, P. Bellon, and G. Martin. “Identification of novel diffusion cycles in B2 ordered phases by Monte Carlo simulation”. In: *Philosophical Magazine A* 76.3 (1997), pp. 565–585 (cit. on pp. 92, 93).
- [123] M. Athènes and P. Bellon. “Antisite-assisted diffusion in the L12 ordered structure studied by Monte Carlo simulations”. In: *Philosophical Magazine A* 79.9 (1999), pp. 2243–2257 (cit. on p. 92).
- [124] M. Athènes and V. V. Bulatov. “Path factorization approach to stochastic simulations”. In: *Physical Review Letters* 113 (23 2014), p. 230601 (cit. on pp. 92–95).
- [125] D. J. Wales. “Calculating rate constants and committor probabilities for transition networks by graph transformation”. In: *The Journal of Chemical Physics* 130.20 (2009), p. 204111 (cit. on pp. 92–94).
- [126] S. A. Trygubenko and D. J. Wales. “Graph transformation method for calculating waiting times in Markov chains”. In: *The Journal of Chemical Physics* 124.23 (2006), p. 234110 (cit. on p. 93).
- [127] Y. Limoge and J. L. Bocquet. “Temperature behavior of tracer diffusion in amorphous materials: A random-walk approach”. In: *Phys. Rev. Lett.* 65 (1 1990), pp. 60–63 (cit. on p. 93).
- [128] F. Soisson and C.-C. Fu. “Cu-precipitation kinetics in α -Fe from atomistic simulations: Vacancy-trapping effects and Cu-cluster mobility”. In: *Phys. Rev. B* 76 (21 2007), p. 214102 (cit. on pp. 94, 95).
- [129] E. Clouet. “Modeling of Nucleation Processes”. In: *Fundamentals of Modeling for Metals Processing*. Ed. by D. Furrer and S. Semiatin. ASM International. Vol. 22A. ASM Handbook. 2010, pp. 203–219 (cit. on p. 95).
- [130] L. K. Béland, P. Brommer, F. El-Mellouhi, J.-F. m. c. Joly, and N. Mousseau. “Kinetic activation-relaxation technique”. In: *Phys. Rev. E* 84 (4 2011), p. 046704 (cit. on p. 96).
- [131] T. Vanacker. “Improvement of an advanced kinetic Monte Carlo algorithm through storing and recycling factorized transition matrices”. MA thesis. Ecole Centrale Paris and KTH, 2017 (cit. on p. 96).
- [132] S. Pogatscher, H. Antrekowitsch, M. Werinos, F. Moszner, S. S. A. Gerstl, M. F. Francis, W. A. Curtin, J. F. Löffler, and P. J. Uggowitzer. “Diffusion on Demand to Control Precipitation Aging: Application to Al-Mg-Si Alloys”. In: *Phys. Rev. Lett.* 112 (22 2014), p. 225701 (cit. on p. 96).
- [133] D. Mason, R. Rudd, and A. Sutton. “Stochastic kinetic Monte Carlo algorithms for long-range Hamiltonians”. In: *Computer Physics Communications* 160.2 (2004), pp. 140–157 (cit. on p. 96).
- [134] B. Puchala, M. L. Falk, and K. Garikipati. “An energy basin finding algorithm for kinetic Monte Carlo acceleration”. In: *The Journal of Chemical Physics* 132.13 (2010), p. 134104 (cit. on p. 96).
- [135] Y. Shim and J. G. Amar. “Rigorous synchronous relaxation algorithm for parallel kinetic Monte Carlo simulations of thin film growth”. In: *Phys. Rev. B* 71 (11 2005), p. 115436 (cit. on p. 96).
- [136] M. Merrick and K. A. Fichthorn. “Synchronous relaxation algorithm for parallel kinetic Monte Carlo simulations of thin film growth”. In: *Phys. Rev. E* 75 (1 2007), p. 011606 (cit. on p. 96).
- [137] E. Martínez, P. Monasterio, and J. Marian. “Billion-atom synchronous parallel kinetic Monte Carlo simulations of critical 3D Ising systems”. In: *Journal of Computational Physics* 230.4 (2011), pp. 1359–1369 (cit. on p. 96).
- [138] G. Fort, B. Jourdain, T. Lelièvre, and G. Stoltz. “Convergence and efficiency of adaptive importance sampling techniques with partial biasing”. In: *ArXiv e-prints* (Oct. 2016) (cit. on pp. 97, 121, 123, 124).
- [139] A. F. Voter. “Hyperdynamics: Accelerated Molecular Dynamics of Infrequent Events”. In: *Phys. Rev. Lett.* 78 (20 1997), pp. 3908–3911 (cit. on p. 98).

- [140] F. Wang and D. P. Landau. “Efficient, Multiple-Range Random Walk Algorithm to Calculate the Density of States”. In: *Phys. Rev. Lett.* 86 (10 2001), pp. 2050–2053 (cit. on p. 114).
- [141] M. Athènes and P. Terrier. “Estimating thermodynamic expectations and free energies in expanded ensemble simulations: Systematic variance reduction through conditioning”. In: *The Journal of Chemical Physics* 146.19 (2017), p. 194101 (cit. on p. 115).
- [142] F. H. Stillinger. “Exponential multiplicity of inherent structures”. In: *Phys. Rev. E* 59 (1 1999), pp. 48–51 (cit. on p. 117).
- [143] F. Calvo, J. P. K. Doye, and D. J. Wales. “Characterization of anharmonicities on complex potential energy surfaces: Perturbation theory and simulation”. In: *The Journal of Chemical Physics* 115.21 (2001), pp. 9627–9636 (cit. on p. 117).
- [144] J. P. K. Doye, M. A. Miller, and D. J. Wales. “The double-funnel energy landscape of the 38-atom Lennard-Jones cluster”. In: *The Journal of Chemical Physics* 110.14 (1999), pp. 6896–6906 (cit. on p. 117).

A | Asymptotic variances of estimators

A.1 Elementary laws of probability theory and statistics

We review here the elementary laws of probability theory that are systematically applied within the expanded ensemble framework. Let us consider the joint probability $p_a(\zeta, \bar{q})$ defined over an extended space $\Lambda \times \mathcal{Q}$. Set Λ denotes the discrete space of the external parameter ζ or λ . The set \mathcal{Q} denotes the position space for the coordinates \bar{q} or q of the particles. The total expectation associated with observable $\mathcal{G}(\zeta, \bar{q})$ is defined by:

$$\mathbb{E}_a[\mathcal{G}] = \sum_{\zeta \in \Lambda} \int_{\mathcal{Q}} \mathcal{G}(\zeta, \bar{q}) p_a(\zeta, \bar{q}) d\bar{q}.$$

The marginal probabilities of $\lambda \in \Lambda$ and $q \in \mathcal{Q}$ can be expressed as expected values of the indicator function $\mathbf{1}_\lambda$ and of the delta function $\delta_q(\bar{q})$, respectively:

$$p_a^\Lambda(\lambda) = \int_{\mathcal{Q}} p_a(\lambda, \bar{q}) d\bar{q} = \mathbb{E}_a[\mathbf{1}_\lambda], \quad \text{and} \quad p_a^\mathcal{Q}(q) = \sum_{\zeta \in \Lambda} p_a(\zeta, q) = \mathbb{E}_a[\delta_q].$$

Let denote the expectations defined with respect to the marginal probabilities p_a^Λ and $p_a^\mathcal{Q}$ by \mathbb{E}_a^Λ and $\mathbb{E}_a^\mathcal{Q}$, respectively. These expectations are useful for expressing the following two laws of total expectation, with conditioning done on λ or q :

$$\mathbb{E}_a[\mathcal{G}] = \begin{cases} \mathbb{E}_a^\Lambda[\mathbb{E}_a[\mathcal{G}(\lambda, \cdot)|\lambda]] & = \sum_{\lambda \in \Lambda} \mathbb{E}_a[\mathcal{G}(\lambda, \cdot)|\lambda] p_a^\Lambda(\lambda), \\ \mathbb{E}_a^\mathcal{Q}[\mathbb{E}_a[\mathcal{G}(\cdot, q)|q]] & = \int_{\mathcal{Q}} \mathbb{E}_a[\mathcal{G}(\cdot, q)|q] p_a^\mathcal{Q}(q) dq. \end{cases} \quad (\text{A.1})$$

Noticing that the conditional probability of q (λ) given λ (q) is the conditionally expected value of the dirac (indicator) function,

$$\pi(q|\lambda) = \mathbb{E}_a[\delta_q|\lambda], \quad \text{and} \quad \pi_a(\lambda|q) = \mathbb{E}_a[\mathbf{1}_\lambda|q],$$

allows us to derive the laws of the total probabilities of q and λ from the laws of total expectations for the dirac and indicator functions, respectively

$$p_a^\mathcal{Q}(q) = \mathbb{E}_a^\Lambda[\mathbb{E}_a[\delta_q|\lambda]] = \sum_{\lambda \in \Lambda} \pi(q|\lambda) p_a^\Lambda(\lambda), \quad \text{and} \quad p_a^\Lambda(\lambda) = \mathbb{E}_a^\mathcal{Q}[\mathbb{E}_a[\mathbf{1}_\lambda|q]] = \int_{\mathcal{Q}} \pi_a(\lambda, q) p_a^\mathcal{Q}(q) dq.$$

We eventually formulate the law of total variance on q , which states that the total variance of \mathcal{G} is equal to the sum of two terms, the expectation of the conditional variances of \mathcal{G} given q and the variance of the conditionally expected value of \mathcal{G} given q :

$$\mathbb{V}_a[\mathcal{G}] = \mathbb{E}_a^\mathcal{Q}[\mathbb{V}_a[\mathcal{G}(\cdot, q)|q]] + \mathbb{V}_a^\mathcal{Q}[\mathbb{E}_a(\mathcal{G}(\cdot, q)|q)]. \quad (\text{A.2})$$

This identity is easily verified by expressing the involved variances as functions of their expectation:

$$\mathbb{V}_a[\mathcal{G}] = \mathbb{E}_a[\mathcal{G}^2] - \mathbb{E}_a[\mathcal{G}]^2, \quad \text{and} \quad \mathbb{V}_a[\mathcal{G}|q] = \mathbb{E}_a[\mathcal{G}^2|q] - \mathbb{E}_a[\mathcal{G}|q]^2. \quad (\text{A.3})$$

We similarly define $\mathbb{V}_a^\mathcal{Q}$, the variance with respect to probability $p_a^\mathcal{Q}$, by replacing expectations \mathbb{E}_a by expectations $\mathbb{E}_a^\mathcal{Q}$ in Eq. (A.3). The law of total variance (A.2) is used in Sec. 1.11 for proving variance reduction through conditioning of various estimators with the delta method described next.

The law of total probability, the law of total expectation, and the law of total variance, which are extensively applied throughout this thesis, can be generalized into the law of total cumulance [1] in probability theory and statistics.

A.2 Delta method

Since expectations are considered with respect to the expanded ensemble, we write the dependence on the biasing potential $\alpha(\lambda)$ explicitly when needed and use the notation \mathbb{V}_α adopted throughout the article for the variance. The lemma below establishes a general and useful property of covariance matrices

Lemma A.2.1. *Let Γ be the covariance matrix of a random vector Y taking its values in \mathbb{R}^d and $u \in \mathbb{R}^d$ be a constant vector. Then, we have*

$$u^T \Gamma u = \mathbb{V}_\alpha [u^T Y].$$

Proof. Let write $Y = (Y^i)_{1 \leq i \leq d}$ and $u = (u^i)_{1 \leq i \leq d}$. By definition, element Γ_{ij} of covariance matrix Γ is equal to $\text{Cov}_\alpha(Y^i, Y^j)$ the covariance of the one-dimensional random variables Y^i and Y^j , defined by

$$\text{Cov}_\alpha[Y^i, Y^j] = \mathbb{E}_\alpha [Y^i Y^j] - \mathbb{E}_\alpha [Y^i] \mathbb{E}_\alpha [Y^j].$$

Since the covariance has scalar product properties, we have the following sequence of equalities

$$u^T \Gamma u = \sum_{i=1}^d \sum_{j=1}^d u^i \text{Cov}_\alpha(Y^i, Y^j) u^j = \text{Cov}_\alpha(u^T Y, u^T Y) = \mathbb{V}_\alpha(u^T Y).$$

□

The delta method will allow us to characterize the asymptotic variance of all aforementioned estimators. It consists of applying the generalized central limit theorem that follows:

Theorem A.2.2. *Let $\{Y_m\}_{m \geq 1}$ be a sequence of independent, identically distributed and square integrable random vectors taking their values in \mathbb{R}^d . Let μ and Γ respectively denote the expected vector and the covariance matrix of the Y_m and $\bar{Y}^M = \frac{1}{M} \sum_{m=1}^M Y_m$. Let $g : \mathbb{R}^d \mapsto \mathbb{R}$ be a function that is differentiable at μ . Then, we have the following convergence in law*

$$\sqrt{M} \left(g(\bar{Y}^M) - g(\mu) \right) \xrightarrow[M \rightarrow +\infty]{\mathcal{L}} \mathcal{N}(0, \nabla g(\mu)^T \Gamma \nabla g(\mu)).$$

Proof. Let define $r_{y\mu} : [0, 1] \mapsto \mathbb{R}^d$ such that

$$r_{y\mu}(\alpha) = \alpha y + (1 - \alpha)\mu.$$

We have

$$g(y) - g(\mu) = \int_0^1 \frac{\partial}{\partial \alpha} (g \circ r_{y\mu}(\alpha)) d\alpha = \int_0^1 r'_{y\mu}(\alpha) \nabla g \circ r_{y\mu}(\alpha) d\alpha = \int_0^1 \nabla g \circ r_{y\mu}(\alpha) d\alpha \cdot (y - \mu)$$

Setting y to \bar{Y}_M , we obtain

$$\sqrt{M} (g(\bar{Y}_M) - g(\mu)) = \int_0^1 \nabla g(\alpha \bar{Y}_M + (1 - \alpha)\mu) d\alpha \cdot \sqrt{M} (\bar{Y}_M - \mu).$$

Besides, from the law of large numbers (Theorem 5.2.2, page 72 in ref [3]) and the fact that the Y_M 's are iid and integrable, then \bar{Y}_M converges almost surely (a.s.) to μ as M tends to infinity. As a consequence, we have

$$\forall \alpha \in [0, 1], \quad \alpha \bar{Y}_M + (1 - \alpha)\mu \xrightarrow[M \rightarrow +\infty]{\text{a.s.}} \mu,$$

and by continuity of ∇g

$$D_M = \int_0^1 \nabla g(\alpha \bar{Y}_M + (1 - \alpha)\mu) d\alpha \xrightarrow[M \rightarrow +\infty]{\text{a.s.}} \nabla g(\mu).$$

From the multi-dimensional central limit theorem (see Theorem 6.2.8 page 94 of ref [3]) the random variable $\sqrt{M}(\bar{Y}_M - \mu)$ converges in law to a centered random gaussian vector with covariance matrix Γ when M tends to infinity

$$G_M = \sqrt{M}(\bar{Y}_M - \mu) \xrightarrow[M \rightarrow +\infty]{\mathcal{L}} G \sim \mathcal{N}(0, \Gamma).$$

Since D_M converges almost surely to the constant $\nabla g(\mu)$ and G_M converges in law to $\mathcal{N}(0, \Gamma)$, one can apply Slutsky's theorem (see ref [3], Theorem 5.3.12, page 79) and conclude that the product converges in law to a gaussian random variable of mean zero and variance $\nabla g(\mu)^T \Gamma \nabla g(\mu)$

$$D_M G_M \xrightarrow[M \rightarrow +\infty]{\mathcal{L}} \mathcal{N}(0, \nabla g(\mu)^T \Gamma \nabla g(\mu)).$$

□

The variance of the gaussian variable above corresponds to the asymptotic variance of random variable $g(Y)$. Below, the asymptotic variances of all estimators considered throughout this report are deduced from the variance of random variable $\nabla g(\mu)^T Y$ expressed using eq A.2.1, i.e, by applying Theorem A.2.2 while taking advantage of relation

$$\nabla g(\mu)^T \Gamma \nabla g(\mu) = \mathbb{V}_a (\nabla g(\mu)^T Y). \quad (\text{A.4})$$

A.3 Estimation of conditional expectations

For the generic $\Upsilon_G^M(\mathcal{O}|\lambda)$ estimator given in Eq. 1.26 and conditioned in subsection 1.11.3, we set $Y_m = (g_a^\lambda(\zeta_m, \bar{q}_m) \mathcal{O}(\lambda, \bar{q}_m), g_a^\lambda(\zeta_m, \bar{q}_m))^T \in \mathbb{R}^2$, $g(r, s) = r/s$. We have $\mu = (\mathbb{E}_a [g_a^\lambda(\cdot, \cdot) \mathcal{O}(\lambda, \cdot)], \mathbb{E}_a [g_a^\lambda])^T$ and

$$\nabla g(\mu) = \begin{pmatrix} 1/\mathbb{E}_a [g_a^\lambda] \\ -\mathbb{E}_a [g_a^\lambda(\cdot, \cdot) \mathcal{O}(\lambda, \cdot)] / \mathbb{E}_a [g_a^\lambda]^2 \end{pmatrix} = \frac{1}{\mathbb{E}_a [g_a^\lambda]} \begin{pmatrix} 1 \\ 1 - \mathbb{E}[\mathcal{O}|\lambda] \end{pmatrix}.$$

Resorting to Eq. (A.4), the asymptotic variance $\nabla g(\mu)^T \Gamma \nabla g(\mu)$ is therefore

$$\sigma_a^2 [\Upsilon_G^M(\mathcal{O}|\lambda)] = \frac{1}{\mathbb{E}_a [g_a^\lambda]^2} \mathbb{V}_a \left[\begin{pmatrix} 1 \\ -\mathbb{E}[\mathcal{O}|\lambda] \end{pmatrix}^T \begin{pmatrix} g_a^\lambda(\cdot, \cdot) \mathcal{O}(\lambda, \cdot) \\ g_a^\lambda(\cdot, \cdot) \end{pmatrix} \right] = \frac{\mathbb{V}_a [g_a^\lambda \mathcal{O}^\lambda]}{p_a^A(\lambda)^2},$$

recalling that $\mathcal{O}^\lambda(q) = \mathcal{O}(\lambda, q) - \mathbb{E}[\mathcal{O}|\lambda]$ and that $\mathbb{E}_a [g_a^\lambda] = p_a^A(\lambda)$. The square root of the asymptotic variance of $\Upsilon_G^M(\mathcal{O}|\lambda)$ estimator is given in Eq. 1.35. Along the same line of reasoning, the asymptotic variance of adiabatic reweighting estimator $\Upsilon_{\Pi}^M(\mathcal{O}|\lambda)$ can be deduced after substituting π_a^λ for g_a^λ .

A.4 Estimation of total expectations

For the generic estimator $\Upsilon_G^M(\mathcal{O})$ of total expectation $\mathbb{E}[\mathcal{O}]$ that is given in Eq. (2.6), we set $g(r, s) = r/s$ together with

$$Y = \begin{pmatrix} \sum_{\lambda \in \Lambda} \mathcal{O}(\lambda, \bar{q}) \mathfrak{g}_a^\lambda(\zeta, \bar{q}) \\ \mathfrak{g}_a(\zeta, \bar{q}) \end{pmatrix},$$

$$\mathbb{E}_a[Y] = \begin{pmatrix} \mathbb{E}_a [\sum_{\lambda \in \Lambda} \mathcal{O}(\lambda, \cdot) \mathfrak{g}_a^\lambda(\cdot, \cdot)] \\ \mathbb{E}_a [\mathfrak{g}_a] \end{pmatrix},$$

$$\nabla g(\mathbb{E}_a[Y]) = \frac{1}{\mathbb{E}_a [\mathfrak{g}_a]} \begin{pmatrix} 1 \\ -\mathbb{E}[\mathcal{O}] \end{pmatrix},$$

where $g_a^\lambda(\zeta, \bar{q}) = \exp[-\alpha(\lambda)]g_a^\lambda(\zeta, \bar{q})$ and $g_a = \sum_{\lambda \in \Lambda} g_a^\lambda$. The scalar product of the first and third vectors above is

$$Y^T \nabla g(\mathbb{E}_a[Y]) = \sum_{\lambda \in \Lambda} \mathcal{O}(\lambda, \bar{q}) \frac{g_a^\lambda(\zeta, \bar{q})}{\mathbb{E}_a[g_a]} - \mathbb{E}[\mathcal{O}] \frac{g_a(\zeta, \bar{q})}{\mathbb{E}_a[g_a]}.$$

This expression enables one to obtain the asymptotic variance of the estimator by application of Lemma A.2.1 and Theorem A.2.2

$$\sigma_a^2[\Upsilon_G^\infty(\mathcal{O})] = \mathbb{V}_a \left[\sum_{\lambda \in \Lambda} \mathcal{O}(\lambda, \cdot) \frac{g_a^\lambda(\cdot, \cdot)}{\mathbb{E}_a[g_a]} - \mathbb{E}[\mathcal{O}] \frac{g_a(\cdot, \cdot)}{\mathbb{E}_a[g_a]} \right].$$

The asymptotic variance of adiabatic reweighting estimator $\Upsilon_{\Pi}^M(\mathcal{O})$ can be deduced by substituting, $\Pi_a^\lambda = \mathbb{E}_a[g_a^\lambda|q]$ for g_a^λ , Π_a for g_a and following the same line of reasoning:

$$\sigma_a^2[\Upsilon_{\Pi}^\infty(\mathcal{O})] = \mathbb{V}_a \left[\sum_{\lambda \in \Lambda} \mathcal{O}(\lambda, \cdot) \frac{\Pi_a^\lambda(\cdot)}{\mathbb{E}_a[\Pi_a]} - \mathbb{E}[\mathcal{O}] \frac{\Pi_a(\cdot)}{\mathbb{E}_a[\Pi_a]} \right].$$

When the observable is an indicator function $\mathbf{1}_{\xi^*} \circ \xi(q)$ associated with a reaction coordinate $\xi(q)$ that is independent of the external parameter, the asymptotic variance simplifies into

$$\sigma_a^2[\Upsilon_{\Pi}^\infty(\mathbf{1}_{\xi^*} \circ \xi)] = \mathbb{V}_a \left[\mathbf{1}_{\xi^*}^A \circ \xi \frac{\Pi_a}{\mathbb{E}_a[\Pi_a]} \right],$$

where $\mathbf{1}_{\xi^*}^A \circ \xi(q) = \mathbf{1}_{\xi^*} \circ \xi(q) - \mathbb{E}[\mathbf{1}_{\xi^*} \circ \xi]$. The formulation of estimator Υ_G^M for observables that are dependent on the external parameter is useful in the free energy context below.

A.5 Estimation of free energies along λ

As for the generic estimator of the free energy $\mathcal{A}(\lambda)$ considered in subsection 2.2.2, the asymptotic variance can be obtained by noticing that the free energy corresponds to the co-logarithm of the total expectation of observable $\mathbf{1}_\lambda$. Here, one applies theorem A.2.2 with function g set to the co-logarithm function and \bar{Y}^M set to $\Upsilon_G^M(\mathbf{1}_\lambda)$, where G corresponds to R (standard reweighting) and H (binning) for the FEP and TO methods, respectively. This yields the following expression for the asymptotic variance of the corresponding free energy method

$$\sigma_a^2 \left[\widehat{\mathcal{A}(\lambda)}_{\text{FEP/TO}}^\infty \right] = \frac{\sigma_a^2[\Upsilon_G^\infty(\mathbf{1}_\lambda)]}{p_0^A(\lambda)^2} = \mathbb{V}_a \left[\frac{g_a^\lambda}{p_0^A(\lambda)\mathbb{E}_a[g_a]} - \frac{\mathbb{E}[\mathbf{1}_\lambda]}{p_0^A(\lambda)} \frac{g_a}{\mathbb{E}_a[g_a]} \right].$$

Noticing that $\mathbb{E}[\mathbf{1}_\lambda]$ is $p_0^A(\lambda)$ and that $p_0^A(\lambda)\mathbb{E}_a[g_a]$ is $\mathbb{E}_a[g_a^\lambda]$, one eventually obtain the desired asymptotic variance in a more compact form

$$\sigma_a^2 \left[\widehat{\mathcal{A}(\lambda)}_{\text{FEP/TO}}^\infty \right] = \mathbb{V}_a \left[\frac{g_a^\lambda}{\mathbb{E}_a[g_a^\lambda]} - \frac{g_a}{\mathbb{E}_a[g_a]} \right]. \quad (\text{A.5})$$

The asymptotic variance of the AR method similarly writes

$$\sigma_a^2 \left[\widehat{\mathcal{A}(\lambda)}_{\text{AR}}^\infty \right] = \mathbb{V}_a^{\mathcal{Q}} \left[\frac{\mathbb{E}_a[g_a^\lambda(\cdot, q)|q]}{\mathbb{E}_a[g_a^\lambda]} - \frac{\mathbb{E}_a[g_a(\cdot, q)|q]}{\mathbb{E}_a[g_a]} \right] = \mathbb{V}_a \left[\frac{\Pi_a^\lambda}{\mathbb{E}_a[\Pi_a^\lambda]} - \frac{\Pi_a}{\mathbb{E}_a[\Pi_a]} \right]. \quad (\text{A.6})$$

A.6 Variance reduction through conditioning of self-consistent reweighting

We prove here variance reduction when conditioning is done within self-consistent reweighting. Let first assume the state space \mathcal{Q} be enumerable and introduce the indicator functions $H_q(\bar{q})$ and $Y_{\lambda, q}(\zeta, \bar{q}) = \mathbf{1}_\lambda(\zeta)H_q(\bar{q})$. We define the corresponding multi-dimensional vectors as $H = \{H_q\}_{q \in \mathcal{Q}}$ and $Y = \{Y_{\lambda, q}\}_{\lambda \in \Lambda, q \in \mathcal{Q}}$. The averaged vector $\bar{Y}^M = \frac{1}{M} \sum_{m=1}^M Y_m$ constructed from the Markov chain $\{\zeta_m, \bar{q}_m\}_{1 \leq m \leq M}$ encodes all the information that is necessary to evaluate any observable estimate through self-consistent reweighting (1.38). It contains in

particular the information that is required to solve the associated set of self-consistent equations (1.39) wherein $M_\lambda = \bar{\mathbf{1}}_\lambda^M$. Since the Markov chain is generated according the $p_a(\zeta, \bar{q})$ distribution, we have for all $\lambda \in \Lambda$

$$\mathbb{E}_a \left[\bar{\mathbf{1}}_\lambda^\infty | \bar{H}^\infty \right] = \bar{\mathbf{1}}_\lambda^\infty = \mathbb{E}_a [\mathbf{1}_\lambda] = p_a^A(\lambda)$$

and, more generally

$$\mathbb{E}_a \left[\bar{Y}^\infty | \bar{H}^\infty \right] = \bar{Y}^\infty = \mathbb{E}_a [Y]. \quad (\text{A.7})$$

The law of total covariance allows us to decompose the covariance matrix of Y into the following sum

$$\Gamma [Y] = \mathbb{E}_a [\Gamma [Y|H]] + \Gamma [\mathbb{E}_a [Y|H]] \quad (\text{A.8})$$

where $\Gamma [Y|H]$ is the conditional covariance of Y given H and $\Gamma [\mathbb{E}_a [Y|H]]$ is the covariance of the conditionally expected value of Y given H . Covariance matrices are semidefinite. Herein, we consider that the three covariance matrices are definite positive, otherwise the problem would be degenerate and sampling might not be necessary. The following strict inequality thus holds

$$\nabla g(\bar{Y}^\infty)^T \mathbb{E}_a [\Gamma [Y|H]] \nabla g(\bar{Y}^\infty) > 0, \quad (\text{A.9})$$

where g denote the smooth function $\bar{Y}^M \mapsto \Upsilon_{\text{SC}}^M(\mathcal{O}|\lambda)$, i.e. the (unknown) function returning the estimate from the given data \bar{Y}^M . The estimate being unique, $\nabla g(\bar{Y}^\infty)$ is a non zero vector. The asymptotic variance of the self-consistent reweighting estimator writes

$$\sigma_a^2 [\Upsilon_{\text{SC}}^\infty(\mathcal{O}|\lambda)] = \nabla g(\bar{Y}^\infty)^T \Gamma [Y] \nabla g(\bar{Y}^\infty).$$

As a result of (A.7), (A.8) and (A.9), the asymptotic variance of the conditioned self-consistent reweighting estimator is systematically lowered

$$\nabla g(\bar{Y}^\infty)^T \Gamma [\mathbb{E}_a [Y|H]] \nabla g(\bar{Y}^\infty) = \sigma_a^2 [\Upsilon_{\text{H}}^\infty(\mathcal{O}|\lambda)] < \sigma_a^2 [\Upsilon_{\text{SC}}^\infty(\mathcal{O}|\lambda)].$$

When the state space \mathcal{Q} is not enumerable, we may first approximate the observable expectation using appropriate histograms of the energies $H_{\lambda,u}$ and of the observable values $H_{\lambda,u,\mathcal{O}}$ (see Section 2.6 in Ref. [35]), perform the conditioning, compare the asymptotic limit and eventually consider the small bin-width limit to conclude that variance reduction still holds.

B | Algorithms

B.1 Metropolis algorithms

Algorithm 1 used in Sec. 3.2 is a Metropolis algorithm in a biased ensemble. The standard deviation σ for the coordinate moves was fitted so that the mean acceptance rate is 20 – 50% and was set to 0.1.

```

1: for  $m = 1$  to  $M$  do
2:   generate gaussian deviate  $g$  of standard deviation  $\sigma$ 
3:   draw integer deviate  $i$  uniformly in  $\llbracket 1, N \rrbracket$ 
4:   construct trial configuration  $\bar{q} = (\bar{q}_1, \dots, \bar{q}_N)$  from current configuration  $q_{m-1} = (q_1, \dots, q_N)$  by setting  $\bar{q}_i = q_i + g$  and  $\bar{q}_j = q_j$  for  $j \neq i$ 
5:   draw real number  $r$  randomly and uniformly in  $[0, 1[$ 
6:   if  $r \leq \exp[f \circ \xi(\bar{q}) - \mathcal{U}_0(\bar{q}) - f \circ \xi(q_{m-1}) + \mathcal{U}_0(q_{m-1})]$  then ▷ Metropolis test
7:      $q_m \leftarrow \bar{q}$ 
8:   else
9:      $q_m \leftarrow q_{m-1}$ 
10:  end if
11: end for

```

Algorithm 2 is used in Sec. 3.2 and referred to as **Work-bias Monte Carlo algorithm**. We set σ to 0.1. We define $\mathcal{U}_f(\lambda, q) = \mathcal{U}(\lambda, q) - f \circ \xi(q)$.

```

1: for  $m = 1$  to  $M$  do
2:    $\lambda^0 \leftarrow \lambda_{m-1}$ 
3:    $\mathcal{W}_f^{0 \rightarrow 0} \leftarrow 0$  ▷ or resample  $\lambda^0$  from  $(\lambda_{m-1}, q_{m-1})$ 
4:    $q^0 \leftarrow q_{m-1}$ 
5:   sample  $\lambda^L \propto \mathcal{N}(2.5 + \lambda^0, 3\sigma)$ 
6:   for  $\ell = 0$  to  $L - 1$  do
7:     set  $\lambda^{\ell+1} = \lambda^0 + \frac{\ell+1}{L}(\lambda^L - \lambda^0)$  and compute  $\mathcal{W}^{\ell \rightarrow \ell+1} = \mathcal{U}_f(\lambda^{\ell+1}, q^\ell) - \mathcal{U}_f(\lambda^\ell, q^\ell) + \mathcal{W}^{0 \rightarrow \ell}$ 
8:     draw integer deviate  $i$  uniformly in  $\llbracket 1, N \rrbracket$ 
9:     construct trial configuration  $\bar{q} = (\bar{q}_1, \dots, \bar{q}_N)$  from current configuration  $q^\ell = (q_1, \dots, q_N)$  by setting  $\bar{q}_j = q_j$  for  $j \neq i$  and sampling  $\bar{q}_i \propto \mathcal{N}(q_i, \sigma)$ 
10:    draw random real  $r$  uniformly in  $[0, 1[$ 
11:     $\tilde{\mathcal{Q}}^{\ell \rightarrow \ell+1} = \mathcal{U}_f(\lambda^{\ell+1}, \bar{q}) - \mathcal{U}_f(\lambda^{\ell+1}, q^\ell)$ 
12:    if  $r \leq \exp[-\tilde{\mathcal{Q}}^{\ell \rightarrow \ell+1}]$  then ▷ local Metropolis test
13:       $q^{\ell+1} \leftarrow \bar{q}$  and  $\mathcal{Q}_f^{\ell \rightarrow \ell+1} = \tilde{\mathcal{Q}}^{\ell \rightarrow \ell+1}$ 
14:    else
15:       $q^{\ell+1} \leftarrow q^\ell$  and  $\mathcal{Q}_f^{\ell \rightarrow \ell+1} = 0$ 
16:    end if
17:     $\mathcal{Q}_f^{0 \rightarrow \ell+1} = \mathcal{Q}_f^{0 \rightarrow \ell} + \mathcal{Q}_f^{\ell \rightarrow \ell+1}$ 
18:     $\mathcal{W}_f^{0 \rightarrow \ell+1} = \mathcal{W}_f^{0 \rightarrow \ell} + \mathcal{W}_f^{\ell \rightarrow \ell+1}$ 
19:  end for
20:  draw real number  $r$  randomly and uniformly in  $[0, 1[$ 
21:  if  $r \leq \exp[-\mathcal{W}_f^{0 \rightarrow L}]$  then ▷ global Metropolis test
22:     $q_m \leftarrow q^L$  ▷ acceptance of global move
23:  else
24:     $q_m \leftarrow q_{m-1}$  ▷ rejection of global move
25:  end if
26: end for

```

B.2 Adaptively biased sampling algorithms

Algorithm 3 is discussed in Sec. 3.3.1. It corresponds to a Generic ABP algorithm. Setting γ_i equal to μ_i and choosing $\mu_i \gg 1$ allow recovering the updating scheme proposed in [33] for observable $\widehat{\mathcal{O}}(q)$.

```

1: for  $i = 0$  to  $I$  do
2:   for  $m = 1$  to  $\mu_i$  do
3:     construct trial configuration  $\bar{q}$  from current configuration  $q_{m-1}^i$ 
4:     draw real number  $r$  randomly and uniformly in  $[0, 1[$ 
5:     if  $r \leq \exp[f_i \circ \xi(\bar{q}) - \mathcal{U}_0(\bar{q}) - f_i \circ \xi(q_{m-1}^i) + \mathcal{U}_0(q_{m-1}^i)]$  then ▷ Metropolis test
6:        $q_m^i \leftarrow \bar{q}$    else    $q_m^i \leftarrow q_{m-1}^i$ 
7:     end if
8:   end for
9:   if  $i \leq I - 1$  then
10:    for  $\xi^* \in \Xi$  do ▷ auxiliary biasing potential update
11:       $f_{i+1}(\xi^*) = f_i(\xi^*) - \ln \left[ 1 + \frac{\gamma_i}{\mu_i} \sum_{m=1}^{\mu_i} \mathbf{1}_{\xi^*}(\xi(q_m^i)) \right] + \ln \left[ 1 + \frac{\gamma_i}{\mu_i} \sum_{m=1}^{\mu_i} \exp(-f_i \circ \xi(q_m^i)) \right]$ 
12:    end for
13:     $q_0^{i+1} \leftarrow q_{\mu_i}^i$ 
14:    else ▷ estimation on last iteration
15:     $\widehat{\mathcal{O}} = \frac{\sum_{m=1}^{\mu_i} \exp[-f_i \circ \xi(q_m^i)] \widehat{\mathcal{O}}(q_m^i)}{\sum_{m=1}^{\mu_i} \exp[-f_i \circ \xi(q_m^i)]}$ 
16:  end if
17: end for

```

Algorithm 4 ABP algorithm based on the updating scheme [140]

```

1: for  $i = 0$  to  $I$  do
2:   construct trial configuration  $\bar{q}$  from current configuration  $q^i$ 
3:   draw real number  $r$  randomly and uniformly in  $[0, 1[$ 
4:   if  $r \leq \exp[f_i \circ \xi(\bar{q}) - \mathcal{U}_0(\bar{q}) - f_i \circ \xi(q^i) + \mathcal{U}_0(q^i)]$  then ▷ Metropolis test
5:      $q^{i+1} \leftarrow \bar{q}$ 
6:   else
7:      $q^{i+1} \leftarrow q^i$ 
8:   end if
9:   for  $\xi^* \in \Xi$  do ▷ auxiliary potential update
10:     $f_{i+1}(\xi^*) = f_i(\xi^*) - \ln [1 + \gamma_i \mathbf{1}_{\xi^*}(\xi(q^{i+1}))] + \ln [1 + \gamma_i \exp(-f_i \circ \xi(q^{i+1}))]$ 
11:  end for
12: end for

```

Algorithm 5 ABF algorithm [30, 31] described in Sec. 3.3.2.

```

1: for  $\xi^* \in \Xi$  do
2:    $C(\xi^*) \leftarrow 0, D(\xi^*) \leftarrow 0$ 
3: end for
4: for  $m = 1$  to  $M$  do
5:   for  $k = 1$  to  $K$  do
6:     construct trial configuration  $\bar{q}^k$  from current configuration  $q_{m-1}^k$ 
7:     draw real number  $r$  randomly and uniformly in  $[0, 1[$ 
8:     if  $r \leq \exp[f_{m-1} \circ \xi(\bar{q}^k) - \mathcal{U}_0(\bar{q}^k) - f_{m-1} \circ \xi(q_{m-1}^k) + \mathcal{U}_0(q_{m-1}^k)]$  then ▷ Metropolis test
9:        $q_m^k \leftarrow \bar{q}^k$ 
10:    else
11:       $q_m^k \leftarrow q_{m-1}^k$ 
12:    end if
13:  end for
14:  for  $\xi^* \in \Xi$  do ▷ adaptation
15:     $C(\xi^*) \leftarrow C(\xi^*) + \sum_{k=1}^K \frac{d\mathcal{U}_0}{d\xi}(q_m^k) \mathbf{1}_{\xi^*}(\xi(q_m^k))$ 
16:     $D(\xi^*) \leftarrow D(\xi^*) + \sum_{k=1}^K \mathbf{1}_{\xi^*}(\xi(q_m^k))$ 
17:     $f'_m(\xi^*) = \frac{C(\xi^*)}{D(\xi^*)}$  ▷ biasing force update
18:     $f_m(\xi^*) = \int_{\xi_0}^{\xi^*} f'_m(d\tilde{\xi})$  ▷ integration of biasing force
19:     $f_m(\xi^*) \leftarrow f_m(\xi^*) + \ln \int_{\Xi} \exp[-f_m(\tilde{\xi})] d\tilde{\xi}$  ▷ normalization
20:  end for
21: end for

```

Algorithm 6 ABF algorithm used in Sec. 3.4 for expanded ensemble simulations [34, 141] with conditioning on $\lambda \in \Lambda$. The K replicas of the system shares the same biasing force. Either a Metropolis Monte Carlo algorithm or a Langevin dynamics scheme can be used to propagate the replicas.

```

1: for  $\lambda \in \Lambda$  do
2:    $C(\lambda) \leftarrow 0, D(\lambda) \leftarrow 0$ 
3: end for
4: for  $m = 1$  to  $M$  do
5:   for  $k = 1$  to  $K$  do
6:      $\bar{q}^k = q_{m-1}^k + \sqrt{2\tau} G_m^k$  with  $G_m^k \sim \mathcal{N}(0, 1)$  ▷ Apply diffusion to current configuration
7:     if Metropolis algorithm then
8:        $r \sim \mathbb{U}_{[0,1]}$  ▷  $r$  is drawn uniformly in  $[0, 1[$ 
9:       if  $r \leq \frac{\sum_{\lambda \in \Lambda} \exp[a_{m-1}(\lambda) - \mathcal{U}(\lambda, \bar{q}^k)]}{\sum_{\lambda \in \Lambda} \exp[a_{m-1}(\lambda) - \mathcal{U}(\lambda, q_{m-1}^k)]}$  then ▷ Metropolis test
10:         $q_m^k \leftarrow \bar{q}^k$ 
11:       else
12:         $q_m^k \leftarrow q_{m-1}^k$ 
13:       end if
14:     else if Overdamped Langevin dynamics then
15:        $q_m^k = \bar{q}^k + \tau \nabla_q \ln \sum_{\lambda \in \Lambda} \exp[a_{m-1}(\lambda) - \mathcal{U}(\lambda, \bar{q}^k)]$ 
16:     end if
17:   end for
18:   for  $\lambda \in \Lambda$  do
19:      $\bar{\pi}_{a_{m-1}}(\lambda|q_m^k) = \exp[a_{m-1}(\lambda) - \mathcal{U}(\lambda, \bar{q}^k)] / \left\{ \sum_{\zeta \in \Lambda} \exp[a_{m-1}(\zeta) - \mathcal{U}(\zeta, \bar{q}^k)] \right\}$ 
20:      $C(\lambda) \leftarrow C(\lambda) + \sum_{k=1}^K \partial_\lambda \mathcal{U}(\lambda, q_m^k) \bar{\pi}_{a_{m-1}}(\lambda|q_m^k)$ 
21:      $D(\lambda) \leftarrow D(\lambda) + \sum_{k=1}^K \bar{\pi}_{a_{m-1}}(\lambda|q_m^k)$ 
22:      $a'_m(\lambda) = \frac{C(\lambda)}{D(\lambda)}$  ▷ biasing force update
23:      $a_m(\lambda) \leftarrow \int_{\lambda_0}^{\lambda} a'_m(\zeta) d\zeta$  ▷ the symbolic integration of biasing force is performed by numerical quadrature based on trapezoidal rule
24:      $a_m(\lambda) \leftarrow a_m(\lambda) + \ln \sum_{\zeta \in \Lambda} \exp[-a_m(\zeta)]$  ▷ normalization
25:   end for
26: end for

```

Algorithm 7 Conditioning and sampling schemes for estimating the conditional expectation of $\mathcal{O}(\lambda, q)$ observable and the total expectation of $\tilde{\mathcal{O}}(q)$ observable, with time-homogeneous biasing potential $\hat{\mathcal{A}}(\lambda)$.

```

1:  $\tilde{C} \leftarrow 0, \tilde{D} \leftarrow 0$ 
2: for  $\lambda \in \Lambda$  do
3:    $C(\lambda) \leftarrow 0, D(\lambda) \leftarrow 0$ 
4: end for
5: for  $m = 1$  to  $M$  do
6:   for  $k = 1$  to  $K$  do
7:      $\bar{q}^k = q_{m-1}^k + \sqrt{2\tau}G_m^k$  with  $G_m^k \sim \mathcal{N}(0, 1)$ 
8:     if Metropolis algorithm then
9:        $r \sim U_{[0,1]}$ 
10:      if  $r \leq \frac{\sum_{\lambda \in \Lambda} \exp[\hat{\mathcal{A}}(\lambda) - u(\lambda, \bar{q}^k)]}{\sum_{\lambda \in \Lambda} \Lambda \exp[\hat{\mathcal{A}}(\lambda) - u(\lambda, q_{m-1}^k)]}$  then ▷ Metropolis test
11:         $q_m^k \leftarrow \bar{q}^k$ 
12:      else
13:         $q_m^k \leftarrow q_{m-1}^k$ 
14:      end if
15:      else if Overdamped Langevin dynamics then
16:         $q_m^k = \bar{q}^k + \tau \nabla_q \ln \sum_{\lambda \in \Lambda} \exp[\hat{\mathcal{A}}(\lambda) - u(\lambda, \bar{q}^k)]$ 
17:      end if
18:    end for
19:    for  $\lambda \in \Lambda$  do
20:       $\bar{\pi}_{\hat{\mathcal{A}}}(\lambda|q_m^k) = \exp[\hat{\mathcal{A}}(\lambda) - u(\lambda, q_m^k)] / \left\{ \sum_{\zeta \in \Lambda} \exp[\hat{\mathcal{A}}_{m-1}(\zeta) - u(\zeta, q_m^k)] \right\}$ 
21:       $C(\lambda) \leftarrow C(\lambda) + \sum_{k=1}^K \mathcal{O}(q_m^k) \bar{\pi}_{\hat{\mathcal{A}}}(\lambda|q_m^k)$ 
22:       $D(\lambda) \leftarrow D(\lambda) + \sum_{k=1}^K \bar{\pi}_{\hat{\mathcal{A}}}(\lambda|q_m^k)$ 
23:    end for
24:     $\varpi_{\hat{\mathcal{A}}}(q_m^k) = \sum_{\lambda \in \Lambda} \exp[-\hat{\mathcal{A}}(\lambda)] \bar{\pi}_{\hat{\mathcal{A}}}(\lambda|q_m^k)$ 
25:     $\tilde{C} \leftarrow \tilde{C} + \sum_{k=1}^K \mathbb{1}_{\hat{\mathcal{A}}}(q_m^k) \tilde{\mathcal{O}}(q_m^k)$ 
26:     $\tilde{D} \leftarrow \tilde{D} + \sum_{k=1}^K \mathbb{1}_{\hat{\mathcal{A}}}(q_m^k)$ 
27:  end for
28:  for  $\lambda \in \Lambda$  do
29:     $\Upsilon_{\Pi}^M(\mathcal{O}|\lambda) = C(\lambda)/D(\lambda)$  ▷ Estimate of conditional expectation
30:  end for
31:   $\Upsilon_{\Pi}^M(\tilde{\mathcal{O}}) = \tilde{C}/\tilde{D}$  ▷ Estimate of total expectation

```

Algorithm 8 is used in Sec. 4.4 for sampling the expanded path ensemble. The proof that the next index l_{m+1} is selected with probability $\mathbb{P}_a(l|z_{m+1})$ is given in Ref. [66].

Start from indexed path (z_0, l_0) :

for $m = 0$ to $M - 1$ **do**

Draw i randomly from l_m using $\alpha^{i \rightarrow l_m}$ transition probability matrix; Set l_{m+1} to i ;

Move to state (λ_i, x_i) from state $(\bar{\lambda}, \bar{x}) = (\lambda_{l_m}, x_{l_m})$ of the current path (z_m, l_m) using the state-sampling algorithm;

Set ℓ to i ;

while $\ell < L$ **do**

Apply the forward Langevin scheme; Evaluate $\mathcal{W}_a^{i \rightarrow \ell+1} = \mathcal{W}_a^{i \rightarrow \ell} + \mathcal{W}_a^{\ell \rightarrow \ell+1}$;

Increment \mathcal{N} by $\mathcal{O}^*(\lambda_{\ell+1}, x_{\ell+1}) \exp[-\mathcal{W}_a^{i \rightarrow \ell+1}]$

Increment \mathcal{D} by $\exp[-\mathcal{W}_a^{i \rightarrow \ell+1}]$;

Increment ℓ by 1;

Change l_{m+1} to ℓ with probability $\exp[-\mathcal{W}_a^{i \rightarrow \ell+1}] / \mathcal{P}$

end while

set ℓ to i ;

while $\ell > 0$ **do**

Apply the backward Langevin scheme; Evaluate $\mathcal{W}_a^{i \rightarrow \ell-1} = \mathcal{W}_a^{i \rightarrow \ell} + \mathcal{W}_a^{\ell \rightarrow \ell-1}$;

Increment \mathcal{N} by $\mathcal{O}^*(\lambda_{\ell}, x_{\ell}) \exp[-\mathcal{W}_a^{i \rightarrow \ell-1}]$

Increment \mathcal{D} by $\exp[-\mathcal{W}_a^{i \rightarrow \ell-1}]$;

Decrement ℓ by 1;

Change l_{m+1} to $\ell + 1$ with probability $\exp[-\mathcal{W}_a^{i \rightarrow \ell-1}] / \mathcal{D}$;

end while

Evaluate $\mathbb{E}_a^{\mathcal{Z}}[\mathcal{O}^*|z_{m+1}] = \mathcal{N}/\mathcal{D}$,

...

end for

B.3 Harmonic superposition approximation

Equilibrium properties of clusters, including the free energy itself, can be formally expressed from the contributions of the basins of attraction (or inherent structures) rather than configurations [42]. The relative probability p_α of visiting isomer α is calculated as a function of temperature. The isomers are therefore sorted according to their value of Q_4 , denoted as $Q_4^{(\alpha)}$ for isomer α , and neglecting the variations of $Q_4^{(\alpha)}$ with temperature. Again, this approximation will be satisfied only at low temperatures, below T_{ss} . Note that the superposition approximation can provide accurate thermodynamics observables over broad temperature ranges, if anharmonic contributions are included, and if the minima of the potential energy surface are correctly sampled. For small systems such as LJ₁₃, a nearly complete enumeration of the minima can be performed [42]. However, the number of isomers is likely to grow at least exponentially with the number of degrees of freedom [142], and reweighting schemes are needed for large systems. Anharmonic corrections to the free energies have been proposed from systematic perturbation expansions [143]. Such methods, which aim at characterizing the global thermodynamics of the system over broad temperature ranges, will not be considered here, as we only use the superposition approximation at low temperatures to get an estimate of the relative probabilities of some specific low-energy isomers, particularly the defective truncated octahedra.

Quenches from parallel tempering Monte Carlo simulations provided 6837 different structures (identified by Doye *et al.* [144]), which were gathered into classes depending on their value of Q_4 . The first class $O = \{\alpha | Q_4^\alpha > 0.18\}$ corresponds to the truncated octahedral global minimum, as well as a few defective cubic isomers. The second class, $D = \{\alpha | 0.09 \leq Q_4^\alpha \leq 0.12\}$, contains about half a dozen of defective cubic structures presenting stacking faults. Finally, the third class I consists of all remaining isomers, including icosahedral and disordered structures. Because we will not use any reweighting scheme, the free energies calculated this way will not correctly represent the disordered phase, and should not be expected to compare with parallel tempering or Wang-Landau sampling above the melting temperature.

C | Perspectives

C.1 Optimal biasing potential for estimating conditional expectation through standard binning

When estimating conditional expectations of an observable $q \mapsto \mathcal{O}(\lambda, q)$ given $\lambda \in \Lambda$, the biasing potential should ideally be chosen such that it minimizes the sum of the asymptotic variances over $\lambda \in \Lambda$, assuming all estimates to be equally important. It appears that an analytical form of the optimal biasing potential can be exhibited for the binning estimator $\Upsilon_{\mathbb{H}}^M(\mathcal{O}|\lambda)$. Let consider that λ takes values in a discrete set $\Lambda = \{\lambda^j\}_{0 \leq j \leq J}$ with for instance $\lambda^j = j/J$ or $\lambda^j = \lambda_{\min} + j\lambda_{\max}/J$ depending on the set-up. Then, the sum of asymptotic variances to minimize is

$$\sigma_{\mathbb{H}}^2(\mathcal{O}) = \sum_{\lambda \in \Lambda} \sigma^2 [\Upsilon_{\mathbb{H}}^{+\infty}(\mathcal{O}|\lambda)] = \sum_{\lambda \in \Lambda} \frac{\mathbb{E}_{\alpha} \left[\mathbf{1}_{\lambda}(\zeta) (\mathcal{O}(\lambda, q) - \mathbb{E}[\mathcal{O}(\lambda, q)|\lambda])^2 \right]}{p_{\alpha}^{\Lambda}(\lambda)^2} = \sum_{\lambda \in \Lambda} \frac{v^{\lambda}}{p_{\alpha}^{\Lambda}(\lambda)}. \quad (\text{C.1})$$

where we introduced

$$v^{\lambda} = \frac{1}{p_{\alpha}^{\Lambda}(\lambda)} \mathbb{E}_{\alpha} \left[\mathbf{1}_{\lambda}(\zeta) (\mathcal{O}(\lambda, q) - \mathbb{E}[\mathcal{O}(\lambda, q)|\lambda])^2 \right] = \text{var}(\mathcal{O}(\lambda, q)|\lambda).$$

The expression (C.1) is obtained from (1.35) by substituting $\mathbf{1}_{\lambda}(\zeta)$ for $g_{\alpha}^{\lambda}(\zeta, q)$ and simplifying. The nice feature is that the variances of the numerators do not depend on the biasing potential α as they are conditioned on λ . Given the conditional variances v^{λ} , the auxiliary potential minimizing $\sigma_{\mathbb{H}}^2(\mathcal{O})$ subject to the equality constraint

$$\sum_{\lambda \in \Lambda} p_{\alpha}^{\Lambda}(\lambda) = 1 \quad (\text{C.2})$$

can be obtained through the method of Lagrange's multipliers. The discrete biases $a^{\lambda} = \mathbf{a}(\lambda)$ being determined up to a common additive constant, we can assume that $a^{\lambda} = \ln p_{\alpha}^{\Lambda}(\lambda) + \mathcal{A}(\lambda)$. Denoting by α the multiplier associated with the constraint, the Lagrangian function to minimize is therefore

$$\mathcal{L}(\alpha, \mathbf{a}) = \alpha \left(-1 + \sum_{\lambda \in \Lambda} \exp [a^{\lambda} - \mathcal{A}(\lambda)] \right) + \sum_{\lambda \in \Lambda} \exp [-a^{\lambda} + \mathcal{A}(\lambda) + \ln v^{\lambda}]$$

where $\mathbf{a} = \{a^{\lambda}\}_{\lambda \in \Lambda}$. The stationary points of the cost function must satisfy the following conditions

$$\begin{cases} \frac{\partial \mathcal{L}}{\partial \alpha}(\alpha, \mathbf{a}) = 0, \\ \frac{\partial \mathcal{L}}{\partial a^{\lambda}}(\alpha, \mathbf{a}) = 0, \quad \lambda \in \Lambda \end{cases} \iff \begin{cases} \alpha = \left(\sum_{\zeta \in \Lambda} \sqrt{v^{\zeta}} \right)^2 \\ a^{\lambda} = \mathcal{A}(\lambda) + \ln \sqrt{v^{\lambda}} - \ln \left(\sum_{\zeta \in \Lambda} \sqrt{v^{\zeta}} \right), \quad \lambda \in \Lambda. \end{cases}$$

The solution, denoted by (α_c, \mathbf{a}_c) , corresponds to a minimum with respect to the coordinates $\{a^\lambda\}_{\lambda \in \Lambda}$ because the associated Hessian matrix is diagonal and because its diagonal entries (the eigenvalues) are strictly positive

$$\frac{\partial^2 \mathcal{L}}{\partial^2 a^\lambda}(\alpha_c, \mathbf{a}_c) = \left(\sqrt{v^\lambda} + 1/\sqrt{v^\lambda} \right) \left(\sum_{\zeta \in \Lambda} \sqrt{v^\zeta} \right) > 0$$

The marginal probability of λ associated with the optimal biasing potential \mathbf{a}_c is therefore

$$p_{a_c}^A(\lambda) = \exp[\mathbf{a}_c(\lambda) - \mathcal{A}(\lambda)] = \frac{\sqrt{\text{var}[\mathcal{O}(\lambda, q)|\lambda]}}{\sum_{\zeta \in \Lambda} \sqrt{\text{var}[\mathcal{O}(\zeta, q)|\zeta]}}$$

Hence, assuming that the sampled states are independently and identically distributed, then the optimal biasing potential for estimating $\mathbb{E}[\mathcal{O}(\lambda, q)|\lambda]$ over Λ is equal to the sum of the free energy and of the half logarithm of the normalized variance of the observable. As shown in Section 1.11, variance reduction is obtained for any auxiliary biasing potential by implementing a conditioning scheme. An additional variance reduction can therefore be obtained in simulations employing the optimal biasing potential associated with the histogramming estimator in particular.

C.2 Optimal biasing potential for the thermodynamic occupation method

Here, we determine the optimal biasing potential for the TO method described in Sec. 2.2.2. We set $\Lambda = \{\lambda^j\}_{0 \leq j \leq J}$ with $\lambda^j = j/J$ and assume that the biasing potential is such that

$$\sum_{j=0}^J \exp[\mathbf{a}(\lambda^j) - \mathcal{A}(\lambda^j)] = 1. \quad (\text{C.3})$$

This entails that $p_a^A(\lambda) = \exp[\mathbf{a}(\lambda) - \mathcal{A}(\lambda)]$ and $\mathbb{E}_a[\mathfrak{g}_a] = 1$. The asymptotic variance of this TO method is therefore

$$\begin{aligned} \sigma^2 \left[\widehat{\mathcal{A}(\lambda)}_{\text{TO}}^\infty \right] &= \mathbb{V}_a \left[\frac{\mathbf{1}_\lambda}{p_a^A(\lambda)} - \sum_{j=0}^J \mathbf{1}_\lambda(\zeta) \exp[-\mathbf{a}(\lambda^j)] \right] \\ &= \exp[-\mathbf{a}(\lambda)] \{ \exp[\mathcal{A}(\lambda)] - 2 \} + \sum_{j=0}^J \exp[-\mathbf{a}(\lambda^j) - \mathcal{A}(\lambda^j)] \end{aligned}$$

where we developed the variance resorting to the equalities $\mathbb{E}_a[\mathbf{1}_\lambda(\zeta)^2] = \mathbb{E}_a[\mathbf{1}_\lambda(\zeta)] = p_a^A(\lambda)$. The summed variance of the TO method is therefore, assuming equal weight for all bins

$$\sigma_{\text{TO}}^2 = \sum_{j=0}^J \exp[-\mathbf{a}(\lambda^j)] \{ \exp[\mathcal{A}(\lambda^j)] - 2 + (1 + J) \exp[-\mathcal{A}(\lambda^j)] \}$$

The summed variance can now be minimized using the method of Lagrange multipliers with constraint (C.3), in a way analogous to what was done in Section C.1 for conditional expectations. The analysis provides us with an optimal biasing potential which, omitting the additive constant used to normalize equation C.3, writes

$$\alpha_{\text{opt}}(\lambda) = \mathcal{A}(\lambda) + \frac{1}{2} \ln [1 - 2 \exp[-\mathcal{A}(\lambda)] + (1 + J) \exp[-2\mathcal{A}(\lambda)]] .$$

The derivative of the optimal bias is approximately equal to the mean force wherever the free energy is substantially larger than $\ln(1 + J)$. This happens for all $\lambda \in \Lambda$ as soon as the number of bins is sufficiently large. The quantity $\exp[-\mathcal{A}(\lambda)]$ scales as J^{-1} with increasing J . Figure C.1 illustrates the convergence as the number of bins increases to 10^3 , a typical value that is used in simulations. The free energy thus corresponds to the

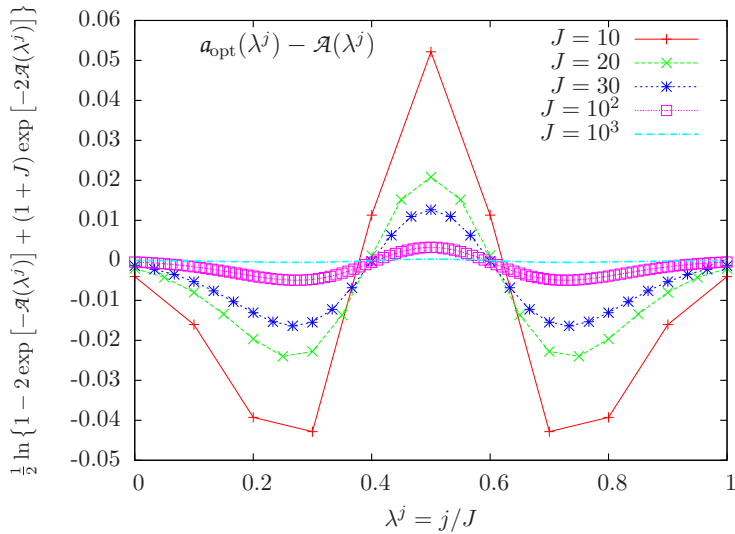


Figure C.1: Difference between the optimal biasing potential and the free energy as a function of $\lambda^j = j/J$ with increasing the bin number J . The free energy is $\mathcal{A}(\lambda) = \omega(\lambda - \frac{1}{2})^2 + \ln \sum_{i=0}^J \exp[-\omega(\lambda^i - \frac{1}{2})^2]$ with $\omega = 16$. Lines are to guide the eyes.

optimal biasing potential in the limit of a large number of bins.

C.3 Optimal biasing potential with conditioned estimators

Unfortunately, the optimal biasing potential associated with the adiabatic reweighting estimator is much more difficult to exhibit because of the occurrence of the auxiliary potential in the involved conditional expectations and variances to minimize. The asymptotic variance of the adiabatic reweighting estimator can be cast in the following form

$$\sigma^2 [\Upsilon_{\Pi}^{\infty}(\mathcal{O}|\lambda)] = \frac{\mathbb{V}_a \left[(\pi_a^\lambda)^2 [\mathcal{O}(\lambda, \cdot) - \mathbb{E}[\mathcal{O}(\lambda, \cdot)|\lambda]]^2 \right]}{p_a^A(\lambda)^2} = \frac{\mathbb{E}_a \left[[\pi_a^\lambda \mathcal{O}^\lambda]^2 \right]}{p_a^A(\lambda)^2}$$

recalling that $\mathcal{O}^\lambda = \mathcal{O} - \mathbb{E}[\mathcal{O}(\lambda, \cdot)|\lambda]$ and $\mathbb{E}_a [\pi_a^\lambda \mathcal{O}^\lambda] = 0$. The quantity that should be minimized is therefore

$$\sigma_{\Pi}^2(\mathcal{O}) = \mathbb{E}_a \left[\sum_{\lambda \in \Lambda} \left[\frac{\pi_a^\lambda \mathcal{O}^\lambda}{p_a^A(\lambda)} \right]^2 \right].$$

Minimizing this summed variance subject to constraint (C.2) leads to

$$p_a^A(\lambda) = \exp[\alpha(\lambda) - \mathcal{A}(\lambda)] = -\frac{\partial}{\partial \alpha^\lambda} \ln \sigma_{\Pi}(\mathcal{O}) = \frac{\mathbb{E}_a \left[\pi_a^\lambda \sum_{\zeta \in \Lambda} \left[\frac{\pi_a^\zeta \mathcal{O}^\zeta}{p_a^A(\zeta)} \right]^2 \right]}{\mathbb{E}_a \left[\sum_{\zeta \in \Lambda} \left[\frac{\pi_a^\zeta \mathcal{O}^\zeta}{p_a^A(\zeta)} \right]^2 \right]} \triangleq \exp[\varphi_a(\lambda)] \quad (\text{C.4})$$

Taking the logarithm, the optimal biasing potential appears as the solution of an implicit equation whose form is

$$\alpha(\lambda) = \mathcal{A}(\lambda) + \varphi_a(\lambda) \quad (\text{C.5})$$

where $\lambda \in \Lambda$ and the quantity φ_a defined in (C.4) depends on the free energy \mathcal{A} , the observable \mathcal{O} and the biasing potential itself. A similar implicit equation is obtained for the estimation of the free energy using the conditioned estimator:

$$\alpha(\lambda) = \mathcal{A}(\lambda) + \Phi_a(\lambda) \quad (\text{C.6})$$

A preliminary study shows that it is possible to adapt the biasing potential in such a way that the implicit equation (C.5) or (C.6) is satisfied for long enough simulations. This is achieved by implementing the adaptive partial biasing algorithm described in Algorithm 9 below and inspired from [138]. To give a practical example, we consider a cluster of 55 Lennard-Jones particles and perform simulation in a range of inverse temperature

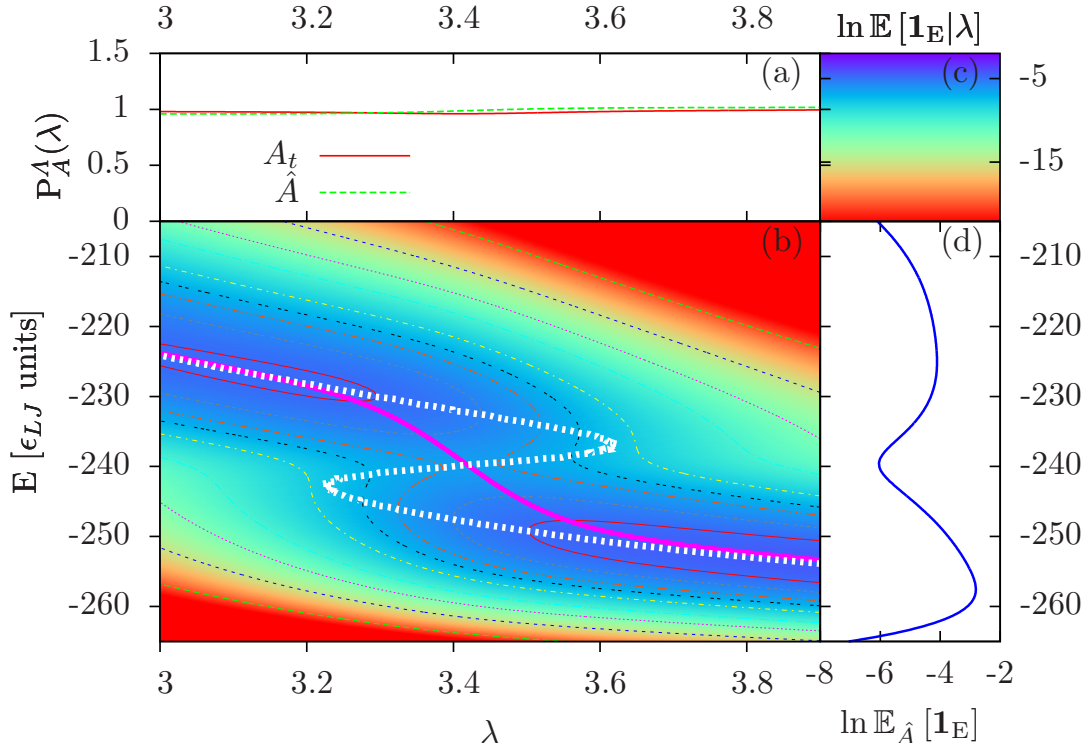


Figure C.2: (a) $P_A^A(\lambda)$ is the scaled marginal probability $\|A\| \times p_A^A(\lambda)$, as estimated in the ABF run (A_t) and production run (\hat{A}); (b) contour map of $\ln \mathbb{E}[\mathbf{1}_E|\lambda]$ with some isolines, and with color-box displayed in (c); the thick magenta solid line and the thick white dashed line represent the two stationary lines, $\{\lambda, \mathcal{A}'(\lambda)\}$ and $\{S'(E), E\}$ curves, respectively, where $S(E)$ is the microcanonical entropy; (d) $\{\ln \mathbb{E}_A[\mathbf{1}_E], E\}$ curve.

around the inverse melting temperature [34] using a variant of the linear coupling setup (1.8):

$$\mathcal{U}(\lambda, q) = \beta \epsilon_{LJ} \lambda E(q)$$

where β , the reference temperature, is set to one. We set the observable to the partial derivative of the extended potential with respect to λ , that is equal to the potential energy in LJ units of energy ϵ_{LJ} : $\mathcal{O} \equiv \epsilon_{LJ} E$ for all $\lambda \in A$. The evolution of the mean potential energy provides relevant information about the finite-size phase transition in this cluster [42]. The results of expanded ensemble simulations [34], performed using the adiabatic ABF algorithm and reported in Fig. C.2, clearly characterize the melting transition with a kind of vander Waals loop for the entropy derivative.

To show the feasibility of constructing optimal biasing potentials, additional expanded ensemble simulations using Algorithm 9 and $M = 10^9$ Langevin steps. We display the simulation results in panels (c-d) of Fig. C.3:

- (c): the biasing potential is constructed through partial biasing based on relation (C.5), so as to optimize the estimation of the mean potential energy (the derivative of the free energy);
- (d): the biasing potential is constructed through partial biasing based on relation (C.6), so as to optimize the estimation of the free energy (the primitive of the mean potential energy);
- (e): tentative construction of the biasing potential through full biasing so as to make the biasing potential equal to the free energy.

The quantity δA is the difference between the biasing potential and the estimated free energy. The fact that $\exp[\delta A]$ becomes equal to the scaled marginal probability $P_A^A(\lambda)$ in simulations (c) and (d) indicates that the biasing potential has converged to its optimal form and that the implicit relation is satisfied. The overall reduction of statistical variance is about a few percents only. However, the main advantage of the approach is that simulations automatically allocate the computational resources in λ -ranges of interest, in the vicinity of the phase transitions and on the edges, regions where the statistical variance is larger. With full biasing, δA is always zero and the estimated marginal probability of λ should be homogeneous. The fact that this is not the

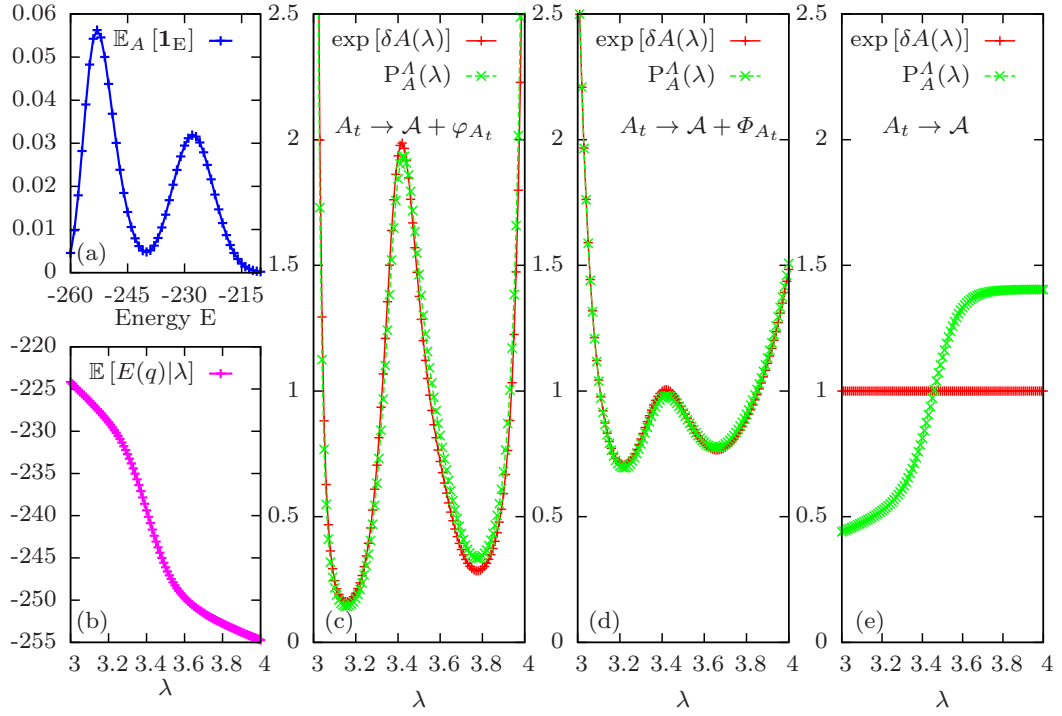


Figure C.3: The displayed quantity δA is the difference between the adaptive biasing potential and the free energy, (a) Histogram of the energies from a converged simulation in the range $\lambda \in [3, 4]$; (b) evolution of mean internal energy as a function of λ , the inflexion point characterizing the melting temperature, (c) adaptation of the biasing potential on $\mathcal{A} + \varphi_A$ (converged simulation); (d) adaptation of the biasing potential on $\mathcal{A} + \Phi_A$ (converged simulation); (e) adaptation of the biasing potential on \mathcal{A} (non converged simulation).

case in the displayed simulation (e) indicates that the biasing potential failed to converge, despite the use of the same updating rate as in simulations (c) and (d). The reason is attributed to the residual metastability that is amplified by the slowly converging biasing potential. The updating rate γ_m is decaying too fast. Variant forms of γ_m are advocated in Ref. [138] in such circumstances.

Algorithm 9 partial biasing algorithm inspired from updating schemes studied by Fort et al. [138] and transposed to expanded ensemble simulations with conditioning. Only a fraction $\varphi_{a_m}(\lambda)^{-1}$ of the conditional probability $\pi_a^\lambda(q)$ is used to adapt the biasing potential. Replacing φ_a by Φ_a allows optimizing the calculations of free energies. Setting φ_a to 1 allows recovering the standard ABP algorithm 4. C is a constant.

```

for  $m = 1$  to  $M$  do
   $q_m = q_{m-1} + \tau \nabla_q \ln \sum_{\lambda \in \Lambda} \exp[a_{m-1}(\lambda) - u(\lambda, \bar{q})] + \sqrt{2\tau} G_m$  with  $G_m \sim \mathcal{N}(0, 1)$  ▷ Langevin dynamics
  for  $\lambda \in \Lambda$  do
    update  $\varphi_{a_m}(\lambda)$  and  $p_{a_m}^\Lambda(\lambda)$  from  $\varphi_{a_{m-1}}(\lambda)$  and  $p_{a_{m-1}}^\Lambda(\lambda)$ 
  end for
   $\gamma_m = \frac{C}{m} [\sum_{\lambda \in \Lambda} \varphi_{a_m}(\lambda)^{-1}]^{-1}$ 
  for  $\lambda \in \Lambda$  do ▷ auxiliary potential update
     $a_m(\lambda) = a_{m-1}(\lambda) - \ln \left[ 1 + \gamma_m \frac{\pi_{a_{m-1}}^\lambda(q_m)}{\varphi_{a_m}(\lambda)} \right] + \ln \left[ 1 + \gamma_m \sum_{\zeta \in \Lambda} \frac{\pi_a^\zeta(q_m)}{\varphi_{a_m}(\zeta)} \right]$ 
  end for
end for

```
